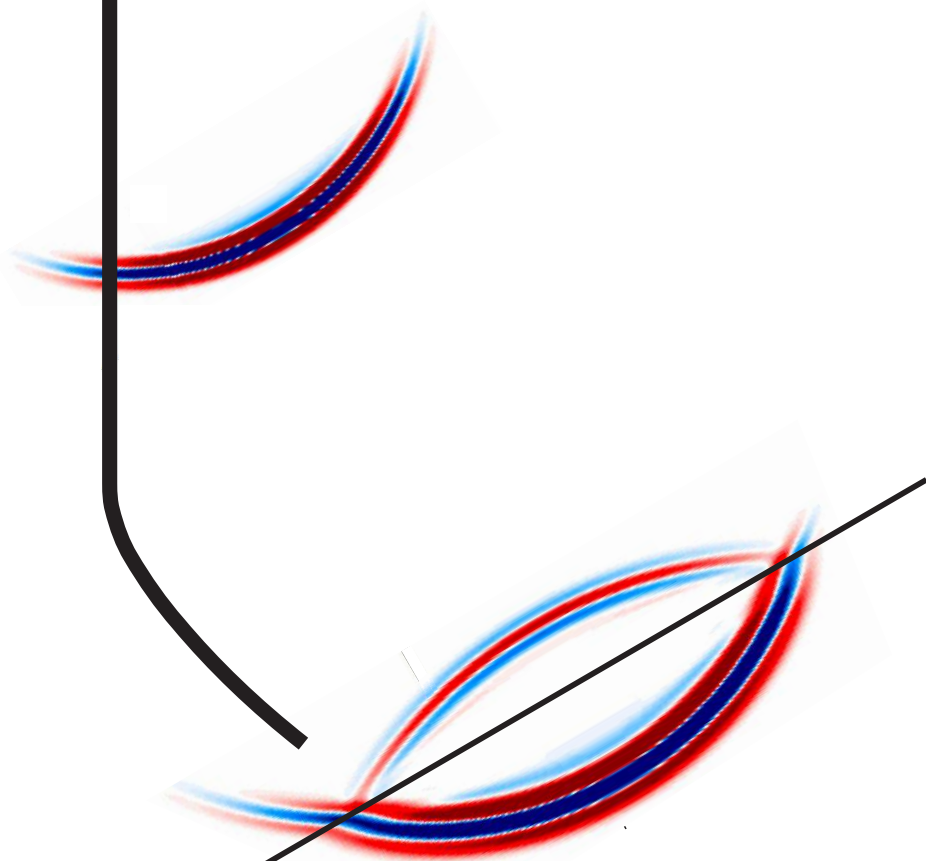# Imaging geothermal reservoirs using vertical seismic profiling

Fabienne Reiser

DISS. ETH NO. 24948

IMAGING GEOTHERMAL RESERVOIRS USING VERTICAL SEISMIC PROFILING

A thesis submitted to attain the degree of

DOCTOR OF SCIENCES of ETH ZURICH

(Dr. sc. ETH Zurich)

presented by

Fabienne Reiser

M.Sc. Geophysics

ETH Zurich

born on March 20, 1985

citizen of Switzerland

accepted on the recommendation of

Prof. Dr. Hansruedi Maurer, examiner

Dr. Cedric Schmelzbach, co-examiner

Prof. Dr. Stewart Greenhalgh, co-examiner

Prof. Dr. Johan O. A. Robertsson, co-examiner

Prof. Dr. Lars Nielsen, co-examiner

2018

Abstract

Renewable resources play an important role in the present energy policies of most nations because of the worldwide rising energy demand as well as the limited availability of oil and gas reserves. Increased public concerns regarding negative environmental impacts of fossil fuels and nuclear power plants require alternative energy resources to produce electricity in a sustainable manner. Geothermal resources provide a promising energy supply and can be used for direct heating systems, space heating, bathing, cooling, aquaculture, greenhouses or electricity production. However, they still play a minor role on the global scale compared to other renewable energy resources like hydropower, solar energy, wind power or biomass energy. Establishing geothermal power plants is still risky and requires high costs. Further research and development is necessary to build economically viable geothermal power plants. It is challenging to identifying suitable geothermal reservoirs with high enough temperatures and sufficient permeability to enable fluid flow.

Seismic exploration can contribute to improved exploration of geothermal sites, better well siting and monitoring during production. However, seismic exploration over geothermal reservoirs is often challenging and, hence, improved exploration techniques are needed. Vertical seismic profiling (VSP) is a promising method to image the subsurface in complex environments. In this thesis, the benefits and limitations of VSP techniques in geothermal environments are critically examined. Advanced seismic imaging methods are tested and seismic acquisition and processing workflows are established for an improved and cost-optimized exploration of geothermal reservoirs.

In the first part of the thesis, an experimental design study on synthetic VSP data was performed for imaging fracture zones within a crystalline basement. 2D and 3D acoustic data are simulated and processed up to the pre-stack depth migration stage to optimize survey layouts for mapping fracture zones of different dip and location. The optimal survey layout strongly depends on the position and dip of the fracture zone and hence stresses the importance of à priori information. We have found that fracture zones located at the same depth range as the receivers but with 300 m lateral offset can be imaged reliably for various dips. More source positions and larger offsets are required for steeper dipping fracture zones. A useful image of the fracture zone can be already obtained using a relatively small number of suitably placed source positions. Adding sources outside the optimal spread did not improve the results, but rather deteriorated the quality of the migrated image in some cases. Hence, the optimization procedure established does not only help to optimally plan future field surveys with a favorable benefit-cost ratio, but also allows the selection of useful data subsets for optimal target-oriented processing.

The second part of the thesis study comprises the analysis of a multi-offset VSP field dataset from a high-temperature geothermal area in Krafla, Iceland. Seismic imaging in volcanic environments is generally very difficult due to intense scattering and absorption of the seismic waves caused by the pronounced heterogeneity. The design of the VSP survey was not optimal due to limited financial resources and entailed only a few source positions. A workflow was established for processing this sparse VSP dataset with a focus on first-arrival traveltime tomography and seismic reflection processing. A multicomponent (vectorial) pre-stack Kirchhoff migration algorithm, which combines

wavefield separation and depth imaging, was applied to obtain separate PP, PS and SS migrated images. This helped to assess the reliability of reflections and to demonstrate the benefits of using 3C geophones. By considering à priori information, such as geological information and hypocenter locations from microseismicity studies, we were able to constrain the processing results which enabled a more reliable interpretation. We conclude that VSP surveying is able to image key lithological boundaries, volcanic stratigraphy, fracture zones, dykes and potentially magma chambers. However, à priori knowledge was essential to constrain the seismic processing and to interpret the migrated images which, due to the paucity of shots, contained significant migration artefacts. Based on this field study we formulated strategies for future VSP acquisition in complex magmatic environments.

In the last part of the thesis, elastic full waveform inversion (FWI) was applied to a multi-offset VSP data set recorded in the geothermal area of Thonex, Switzerland. It turned out that the data acquisition was unsuitable for the application of FWI due to very limited receiver coverage. Consequently, the inversion problem was highly underdetermined and was hampered by a strong trade-off between the velocity model and the source wavelet estimation. Including a far-offset source position led to improved results due the longer receiver array. However, the generally sparse dataset prevented a reliable interpretation of the velocity models. Further field data sets need to be analyzed to assess the potential of FWI in geothermal exploration.

Zusammenfassung

Wegen des weltweiten Anstiegs des Energiebedarfs und der limitierten Verfügbarkeit von Öl- und Gasreserven spielen erneuerbare Energien heutzutage eine wichtige Rolle in der Energiepolitik von diversen Nationen. Die zunehmenden Bedenken der Öffentlichkeit in Bezug auf negative Umwelteinwirkungen von fossilen Brennstoffen und Atomkraftanlagen erfordern alternative Energie Ressourcen, um auf eine nachhaltige Weise elektrischen Strom zu produzieren. Geothermie Ressourcen sind vielversprechend und können für Heizung, Kühlung, Bäder, Aquakultur, Treibhäuser und Stromproduktion verwendet werden. Im Vergleich zu anderen erneuerbaren Energien wie Wasserkraft, Solarenergie, Windkraft oder Energie aus Biomasse, spielt die Geothermie auf globaler Skala jedoch eine kleine Rolle. Ein Geothermie-Kraftwerk zu errichten ist risikoreich und mit hohen Kosten verbunden. Weitere Forschung und Entwicklung sind erforderlich, um ökonomisch realisierbare Geothermie-Kraftwerke zu errichten. Es ist eine grosse Herausforderung, Geothermie Reservoirs zu finden, welche eine genügend hohe Temperatur und Permeabilität aufweisen.

Seismische Erkundungen können dazu beitragen, Geothermie-Standorte besser zu erforschen, passendere Bohrlochstandorte zu finden und die Produktion zu überwachen. Seismische Exploration über Geothermie-Regionen ist jedoch oft mit Herausforderungen verbunden, weshalb verbesserte Erkundungsmethoden erforderlich sind. Vertical seismic profiling (VSP) ist eine vielversprechende Methode, um einen komplexen Untergrund abzubilden. In dieser These werden Nutzen und Limitationen der VSP Technik in Geothermie-Regionen kritisch untersucht. Erweiterte seismische Abbildungsmethoden werden getestet und neue Abläufe und Methoden für die seismische Akquisition und Datenverarbeitung erarbeitet, um eine verbesserte und kosten-optimierte Erkundung von Geothermie-Reservoirs zu erzielen.

Im ersten Teil der These wird anhand von synthetischen Daten die optimale Anordnung von seismischen Quellen studiert, um Bruchzonen innerhalb des kristallinen Untergrunds besser abzubilden. 2D und 3D akustische Daten wurden simuliert und bis zur Tiefenmigration verarbeitet, um die Anordnung der seismischen Quellen für verschiedene Neigungen und Positionen von Bruchzonen zu optimieren. Die optimale Anordnung hängt stark von der Neigung und der Position der Bruchzone ab. Deshalb ist es wichtig, vorhandene Informationen vor der Akquisition in die Planung miteinzubeziehen. Wir haben herausgefunden, dass Bruchzonen, welche sich im Tiefbereich der Geophone mit einem horizontalen Abstand von 300 m vom Bohrloch weg befinden, in verschiedenen Neigungen verlässlich abgebildet werden können. Eine grössere Anzahl seismischer Quellen und grössere Abstände zum Bohrloch sind erforderlich, um steilstehende Strukturen abzubilden. Ein verwertbares Abbild einer Bruchzone kann im Allgemeinen schon mit einer relativ kleinen Anzahl an optimierten Quellpositionen erzielt werden. Quellen ausserhalb des optimalen Bereichs hinzuzufügen verbesserte die Resultate nicht, sondern kann in einigen Fällen das Abbild sogar verschlechtern. Deshalb ist die erarbeitete Optimierungsmethode nicht nur geeignet, um zukünftige kosten-optimierte VSP Akquisitionen zu planen, sondern auch um gemessene Daten optimal und zielorientiert zu verarbeiten.

Der zweite Teil der These umfasst die Analyse eines VSP Datensatzes, welcher in der Geothermie-Region um den Vulkan Krafla, Island, aufgenommen wurde. Das seismische Abbilden von vulka-

nischen Gebieten ist grundsätzlich wegen der erhöhten Streuung und Absorption der seismischen Wellen innerhalb des heterogenen Untergrundes sehr schwierig. Die Akquisition des VSP war nicht optimal und umfasste wegen limitierten finanziellen Mitteln nur eine kleine Anzahl an Quellpositionen. Ein Workflow für die Verarbeitung des VSP Datensatz wurde erarbeitet, wobei der Fokus auf einer Laufzeittomographie und auf dem Abbilden von seismischen Reflektoren lag. Es wurde eine multikomponenten Kirchhoff-Tiefenmigration angewendet, um separate PP, PS und SS Abbildungen zu erhalten. Die Multikomponenten-Analyse der Daten hat geholfen, die Verlässlichkeit von abgebildeten Reflektionen zu beurteilen, und zeigt somit den grossen Nutzen von 3-Komponenten Geophonen für VSP Experimente. Mit der Berücksichtigung bereits bestehender Informationen wie geologischen Angaben und Hypozentren von lokalen Erdbeben, ist es gelungen, die Datenverarbeitung besser einzuschränken und eine verlässlichere Interpretation zu erstellen. Wir schliessen aus unserer Studie, dass VSP wichtige lithologische Grenzen, vulkanische Stratigraphie, Bruchzonen, magmatische Gänge und allenfalls Magmakammern abbilden kann. Wegen auftretenden Migrationsartefakten ist es jedoch nötig, bereits vorhandenes Wissen miteinzubeziehen, um Mehrdeutigkeiten in der Datenverarbeitung und der Interpretation einzuschränken. Auf Grund der Studie haben wir Strategien für zukünftige VSP Akquisitionen in komplexen magmatischen Regionen erarbeitet.

Im letzten Teil der These, wird die elastische Wellenfeld-Inversion auf einen VSP Datensatz angewendet, welcher in der Geothermie-Region von Thonex, Schweiz, aufgenommen wurde. Es stellte sich heraus, dass wegen der limitierten Geophon-Abdeckung die Anwendung der Wellenfeld-Inversion ungeeignet war. Das Inversionsproblem war unterbestimmt und hauptsächlich nur durch die Charakterisierung des Quellsignals bestimmt. Die Inversion einer Schusspunkt-Aufzeichnung mit einer grösseren Geophon-Abdeckung war hingegen erfolgreicher. Auf Grund der limitierten Datenverfügbarkeit war jedoch eine verlässliche Interpretation der Geschwindigkeitsmodelle nicht möglich. Weitere Datensätze müssen analysiert werden, um das Potential der Wellenfeld-Inversion in Geothermie Regionen besser beurteilen zu können.

Contents

1

Introduction

Contents

1.1 Geothermal resources

Geothermal energy is a promising sustainable energy resource with a large potential in electricity generation and district heating systems. Renewable energy resources have gained increased public interest and acceptance in recent years due to climate policies, negative environmental impacts of fossil fuels, and safety concerns in electricity production by nuclear power plants (Shortall et al. (2015)). Global electricity consumption is expected to keep on rising due to population growth, increasing industrialization and modernization, whereas fossil fuel reserves are decreasing and hence creating energy security problems (Bromley et al. (2010); Pazheri et al. (2014)). This clearly shows the need for renewable energy resources, such as hydro power, solar energy, wind power, biomass energy and geothermal energy.

Renewable energy sources covered approximately 16.6% of the global energy consumption in the year 2010 with a continuing increase over recent years (Pazheri et al. (2014)). Geothermal energy still plays a minor role on the global scale compared to other renewable energy sources and shows a low growth rate compared to wind and solar energy (Rybach (2014)). However, electricity production based on geothermal energy is well established in some countries and a significant energy source (e.g., Italy, Iceland). Geothermal energy has wide applications also in direct heating systems, such as space heating, bathing, cooling, aquaculture or greenhouses. Geothermal energy is potentially almost universally available, independent of season/weather, has a low environmental impact with a small footprint for surface facilities, produces low CO2 emissions, and hence shows a high potential for energy exploitation (Bromley et al. (2010)).

The worldwide electrical energy that was produced with geothermal power plants in the year 2015 was 12.7 GWe, with an increase of 1.8 GWe in the period 2010-2015 (Bertani (2016)). The average global growth in geothermal energy shows a linear trend with an increase of around 4% per year (Rybach (2014); Younger (2015)). This is far below the growth rate of other renewable energy sources and hence stresses the need for further research and development to make use of the high potential of geothermal resources. The estimated growth curve of geothermal power plants until 2050 as shown in an IPCC (Intergovernmental Panel on Climate Change) report has an exponential character (Fridleifsson et al. (2008)). Until now, most of the electricity that is based on geothermal energy was produced with hydrothermal systems that require high-temperature fluids present at depths of about 2-4 km. Since these hydrothermal systems are limited to certain geological provinces, the development of hydrothermal systems is not expected to be accelerated more than the linear trend (Rybach (2014)). To meet the exponential demand, development of successful enhanced geothermal system (EGS) pilot plants are required (Rybach (2014)).

Geothermal energy is the energy that is stored in the interior of the earth as a result of residual gravitational heat from planetary core formation and the decay process of radioactive elements of mainly uranium, thorium and potassium within the mantle. The temperatures reach up to about $5800\,°C$ at the center of the Earth and decrease to around $14\,°C$ on average at the Earth's surface (Stober and Bucher (2013)). Due to the resulting geothermal gradient, heat is continuously transported from the interior of the Earth towards the surface (mainly by convection but also conduction), leading to an average global heat flow of $82\,mW/m^2$ at the surface (Lund et al. (2008)). Geothermal heat can

be utilized for electricity generation or direct use such as for example heating or cooling. Due to the enormous amount of heat stored in the interior of the Earth and the global availability, the potential of geothermal energy is very large.

On average, the geothermal gradient is about 3 °C per 100 m depth interval in the upper crust. However, the temperature gradients are not uniform around the globe and strongly depend on the geological setting and the composition of the crust (Stober and Bucher (2013)). Positive heat anomalies, where higher than average subsurface temperatures are observed, are of primary interest in geothermal exploration. These conditions prevail mainly at subduction zones (e.g . Circum-Pacific ring of fire), spreading ridges (e.g. Atlantic mid-ocean ridge, east African continental rift zone) hot spots (e.g. Hawaii) or a combination of spreading ridge-and mantle plume-volcanism (e.g., Iceland). These areas are characterized by active volcanism and hence increased temperatures. Negative anomalies are observed in areas of old continental shields or deep sedimentary basins, although there are some exceptions (e.g. Cooper Basin in Australia).

1.1.1 Hydrothermal systems

Hydrothermal systems are one of two main types of geothermal systems. They are characterized by porous formations or permeable areas like fault zones that allow fluids or vapor to circulate freely in the subsurface. Such geothermal fluids occur naturally at depth and often originate from surface infiltration of precipitation (e.g. Rybach (2014)). The water at several kilometers depth heats up through contact with the warm crustal rocks and can lead to positive geothermal anomalies (Huenges and Ledru (2011)). The concept of a hydrothermal reservoir exploited with a doublet system is shown in Figure 1.1a. One well is used as a production well and the second well as an injection well, where the cooled water is reinjected back into the hydrothermal reservoir. The cold water circulates within the porous formation or permeable fault zone, heats up and can then be extracted for electricity production or district heating purposes. In order to produce electricity with conventional power plants, temperatures above 180° are required (Fridleifsson et al. (2008)). A vapor-dominated system can directly be used to turn a turbine-generator, whereas fluids first need to be converted to steam by lowering the pressure (Lund et al. (2008)). If the temperatures are too low for producing steam, a binary power plant can be used where a secondary working fluid with a lower boiling point is heated that converts to steam and can then be used to spin the turbine (Younger (2015)).

The economic viability of geothermal systems depends on the amount of water that can be extracted and the drilling depth that is necessary to reach the required rock temperature. A geothermal reservoir can exist in various depth ranges, depending on surrounding heat sources, such as magma chambers. High enthalpy systems are mostly related to recent volcanism, show high temperatures at relatively shallow depths and are responsible for the majority of electricity production from geothermal areas. Lardarello in Italy (Brogi et al. (2003); Casini et al. (2010)) and several reservoirs in Iceland (Arnórsson (1995)) are examples for high-enthalpy hydrothermal systems in Europe that successfully produce electricity. To increase the efficiency of production, the Iceland Deep Drilling Project (IDDP) focuses on using supercritical fluids that are located at a depth of about 3.5-5 km with temperatures of 450-600 °C (Fridleifsson and Elders (2005)). Above the critical point (for wa-
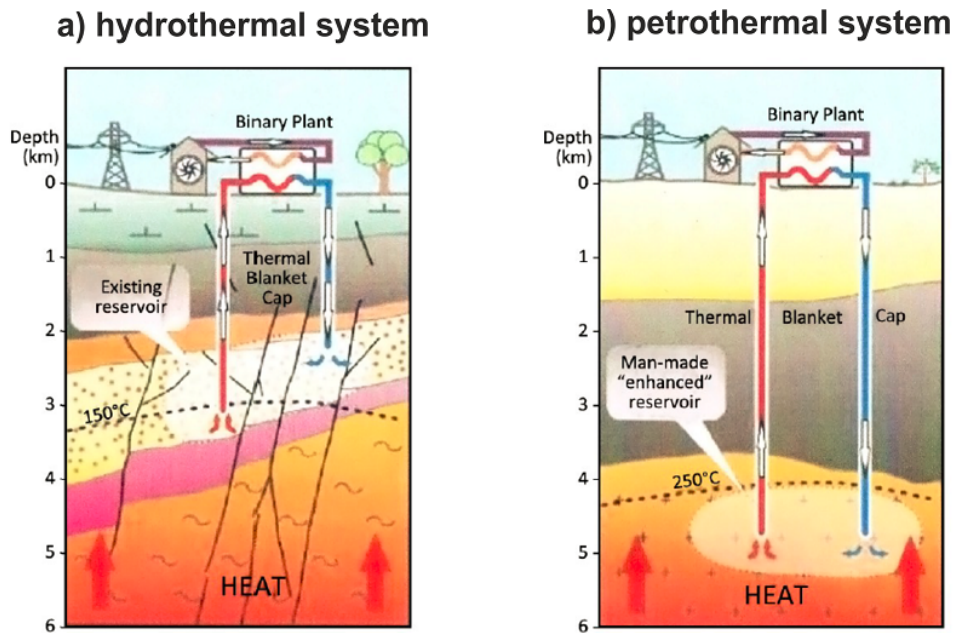
Figure 1.1: The two main types of geothermal systems. a) The concept of a hydrothermal system,
where naturally occurring porous formations or permeable fault structures are used to
circulate water at depth. b) Petrothermal system where an artificially created reservoir
is used to circulate fluid in the hot rocks (modified after Rybach (2014)).

ter at about 221 bars and 374 °C) there are no distinct liquid or gas phases anymore. Instead, only
a single phase, a supercritical fluid, exists that has a higher enthalpy than steam from boiling water
(Friðleifsson et al. (2014)). It is expected that the production from systems with supercritical fluid
can be increased by a factor of 10 compared to conventional high-enthalpy wells. Hence, exploita-
tion of critical fluids provides an efficient power production if the potential can be realized (Younger
(2015)).

However, moderate-temperature geothermal reservoirs can also be used for electricity production.
Examples are the porous sandstone in the Northern German sedimentary basin (Schellschmidt et
al. (2010)), where an aquifer is present that enables the fluid to circulate, or Unterhaching near
Munich, where large fault systems and karstification provide a high hydraulic conductivity. Even
though most of the electricity is produced with hydrothermal systems, the optimal conditions only
prevail in specific geological and hydrological locations, hence making the general usage limited.

1.1.2 Petrothermal systems

Petrothermal systems, which have been recently referred to as enhanced geothermal systems (EGS),
have their maximum potential in crystalline rock at depth of at least a few kilometers, where temper-
atures are high enough (150-200 °C) for electricity generation (Rybach (2014)). Either a pre-existing
fault system or an artificially created fracture network is used to circulate fluid in the hot rocks. The
permeability of a typical reservoir is normally too low, and hence needs to be enhanced by hydraulic
or chemical fracturing (e.g. Barbier (2002)). The concept of an EGS is shown in Figure 1.1b. Once
the permeable man-made reservoir is created, water can be injected in one well, absorb the heat

from the reservoir rock and then be extracted from a second well located several hundred meters away to produce electricity (Tester et al. (2007)).

EGS have great potential, since the concept is not limited to specific geological settings like hydrothermal or magmatic systems, but can be exploited in many places worldwide, where a suitable volume of hot rock is accessible in the upper few kilometers of the Earth's crust (Lund et al. (2008)). Even though the principle is simple, there is still a lack of operational EGS around the world. The main challenge is that several conditions need to be met, in order to produce electricity in an economically viable way. Based on Rybach (2014) the required subsurface properties are a sufficiently high fluid production rate (50-100 kg/s),high fluid temperatures (150-200 °C), total effective heat exchange surface ($>2x106\,m^2$), rock volume ($>2x108\,m^3$), low flow impedance ($<0.1\,Mpa/(kg/s)$), a limited amount of water loss ($<10\%$) and a sufficiently low induced seismicity. Even though several research programs have been developed along with pilot plants, e.g. Tenton Hill in the US (Duchane and Brown (2002)), Soultz-sous-Forêts in France (Genter et al. (2010)), Hijiori and Ogachi in Japan (Kuriyagawa and Tenma (1999); Kaieda et al. (2005)), Cooper Basin in Australia (Chopra and Wyborn (2003)), the realization of these necessary factors at different sites still remains a significant challenge. To date there is still limited EGS experience and hence further research, technology advances and more financial and political support are necessary to establish commercially feasible EGS (Breede et al. (2013)).

1.2 The IMAGE project

The IMAGE (Integrated Methods for Advanced Geothermal Exploration) project started in November 2013, ran for 4 years and was funded by the EU to the tune of 10 Mio Euros. The focus of the project was to address challenges regarding development and assessment of geothermal reservoirs, to maximize the success rate of geothermal power plants and to reduce the risk that is associated with an expensive drilling program. New methods were developed, assessed and tested in sedimentary and crystalline basements and in high-temperature magmatic systems by total consortium of 19 leading European research institutes and industry partners. The interdisciplinary project was based on three general pillars (Figure 1.2):

- The first part focuses on understanding processes and properties that lead to favorable reservoir conditions which control the critical geothermal reservoir parameters at European to local scales. The parameters comprise temperatures, in-situ stresses, fracture permeability and hazard that can be deduced from modeling studies, field analogues, laboratory experiments and public datasets. These parameters help to better understand the reservoir properties. The first part yields a catalogues of rock properties that was the basis for other tasks within the IMAGE project.

- The second part includes the improvement of established exploration techniques for a more comprehensive imaging of the subsurface and to obtain information about critical geothermal reservoir parameters. This includes geophysical methods such as active seismic, ambient seismic noise correlation analysis and magnetotellurics. It also covers fibre-optic downhole logging
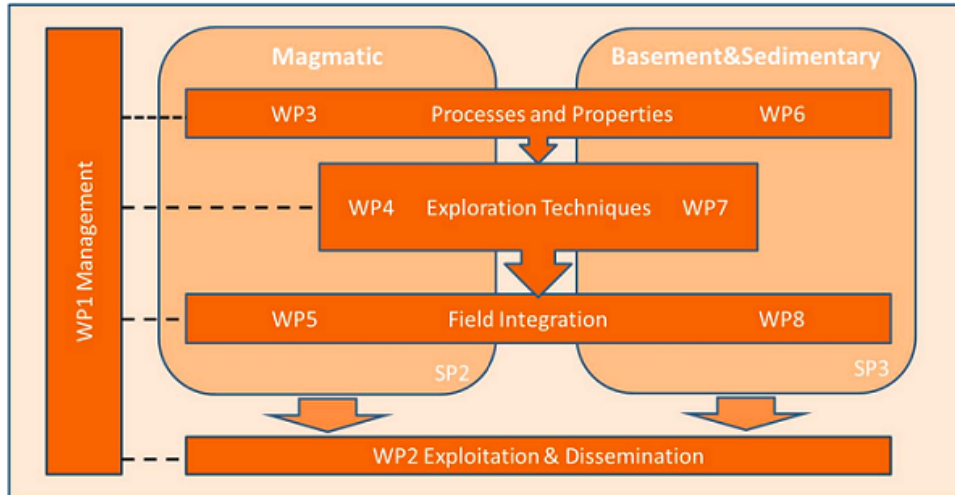
Figure 1.2: Overview of the different aspects/work-packages of the IMAGE project that are divided into magmatic (SP2) and basement/sedimentary (SP3) systems.

     tools to determine physical rock properties and development of new tracers and geothermometers.

- The third pillar uses the added value of the first two parts from established exploration methods, improved rock models and parameters to demonstrate the additionally gained knowledge on actual field datasets for a better site characterization and well-siting.

The different parts are further subdivided into high temperature magmatic systems and basement/deep sedimentary systems, as these two systems differ in characteristics (e.g. heat transport, fluid flow) and hence need separate approaches. Different scales are investigated, such as regional scales where e.g. stress and temperature field measurements were used to constrain the model or local scales where geothermal gradients and heat flow were determined. Several field sites are analyzed. Examples include magmatic sites at Krafla and Reykjanes (Iceland), Lardarello (Italy), Elba Island (Italy), Pico Alto (Azores) and sedimentary/basement sites at Alsace (France), Geneva (Switzerland), Bad Waldsee (Germany) and Luttelgeest (Netherlands). The geothermal field sites are used to validate the developed methods and to provide a direct linkage between research and the demonstration stage.

The IMAGE project comprises several work packages that cover different aspects of magmatic and basement/sedimentary systems within Europe (Figure 1.2). The research performed in this thesis is embedded in WP4, WP5, WP7 and WP8 that focus on developing and testing exploration techniques in both sedimentary and magmatic geothermal systems and applying the techniques to actual geothermal field datasets.

1.3   Status of seismic exploration in hydrocarbons, crystalline rocks and geothermal reservoirs

Seismic exploration in geothermal areas is a relatively new discipline compared to its long history of successful application in the oil and gas industry. Seismic surveying is an important tool to investigate

potential geothermal sites and to reduce the risk that is associated with an expensive drilling program in that it enables more intelligent and selective drilling. Due the large experience in oil and gas exploration as well as mineral search, the geothermal industry can benefit from the large knowledge and practice gained in past decades from these disciplines. Also deep lithospheric studies can yield valuable information for geothermal prospecting, hence seismic exploration over different geological environments are reviewed in more detail in the following sections.

1.3.1 Oil and gas exploration

Many sedimentary basins have been explored by oil companies, and hence a large amount of data exists such as seismic reflection data, well logs, reservoir properties and temperature-depth profiles which could reduce the geothermal exploration risk (Porro et al. (2012)). Geothermal exploration in sedimentary basins (and/or the underlying basement) can benefit from these already available data, well-known exploration, drilling and fracturing techniques in these environments as well as established reservoir characterization in terms of porosity and permeability.

Imaging fracture zones is not only important in geothermal environments, but also in oil and gas reservoirs, since fracture zones control fluid flow and hence the productivity of hydrocarbon reservoirs. Amplitude versus offset analysis (AVO) or amplitude variations with azimuth (AVAz) are used to better image and characterize fracture zones (Rüger (1997); Mallick et al. (1998)). It was shown that P-waves are relatively insensitive in a vertically fractured medium at narrow incidence angles, but can be sensitive at large offsets when the waves travel across the fracture zone; this leads to a decrease in P wave amplitudes (MacBeth et al. (1999); Luo and Evans (2004)). Mallick et al. (1998) have shown that P-wave reflection amplitudes decrease with increasing angle/offset and that the rate of decrease is largest for a fracture zone striking perpendicular to the wave propagation direction. Amplitude analysis can hence be used to determine the main fracture orientation of the medium. They suggest that a 3D survey with at least six source-to-receiver azimuths with a regular offset sampling rate needs to be acquired to properly characterize the fracture orientation.

The development of 3D seismic technology led to a large improvement in imaging capabilities in terms of spatial resolution and accurate positioning of reflectors in three dimensions (Dorn (1998); Cartwright and Huuse (2005)). In particular, improvements could be made in mapping of complex geological structures, such as salt domes and thrust fault systems, where dipping interfaces and lateral velocity variations complicate the seismic imaging. Extensive attribute analysis can be performed based on 3D seismic images and can be used to better characterize fracture zones in reservoirs (Chen and Sidney (1997); Chopra and Marfurt (2005); Ogiesoba and Hart (2009)).

4D seismic monitoring, where 3D seismic data is acquired multiple times at the same location over a certain time period has advanced rapidly in recent years (Lumley (2001)). Time-lapse seismic monitoring provides the possibility of mapping changes in the subsurface over time that can be attributed to fluid flow (water, gas, steam, CO2) in areas that are not covered by wells Lumley (2010). Variations in reservoir properties such as saturation, temperature and pressure during production or injection lead to changes in seismic reflection properties. Based on these changes fluid flow can be monitored within the reservoir and the productivity of the reservoir can be optimized.

Multicomponent seismic surveying enables the recording of polarization information in addition to amplitude and phase information (e.g. Gaiser (2016)). Hence, P-, S- and mode-converted waves can be examined that yield additional imaging possibilities. The value of multicomponent seismic acquisition in fractured reservoirs has been demonstrated by Thomsen (1988), Alford et al. (1989), Stewart et al. (2003), and Hardage et al. (2011). Multicomponent data can be used for an improved fracture mapping, reservoir characterization below and within gas zones, near-surface resolution, lithologic estimation, fluid description and reservoir monitoring (Juhlin (1990); Stewart et al. (2002); Barkved et al. (2004)). Shear wave birefringence is a key diagnostic of anisotropic media such as due to rock fracturing. From the fast shear wave polarization direction and the time delay between the two split shear waves, useful inferences can be made on fracture orientation and density.

1.3.2   Mineral exploration in crystalline rock environments

EGS have their potential in crystalline rock and, hence, it is essential to understand the challenges related to seismic exploration in such environments. Most shallow crustal studies over crystalline rock are connected to mineral exploration, finding suitable underground repositories for nuclear waste and geological mapping.

In mineral seismic exploration it is important to image ore bodies or to map fracture zones and other associated structures that control the mineralization in the subsurface (Drummond et al. (2003); Dehghannejad et al. (2010)). Salisbury et al. (2007) have shown that the impedance contrast of ore bodies and fluid-filled fracture zones in crystalline rock can be large enough to be detected by a seismic reflection experiment. Several studies exist where fracture zones were successfully imaged in crystalline rock environment (Green and Mair (1983); Milkereit et al. (1994); Goleby et al. (1997); Juhlin and Palm (2003); Malehmir et al. (2012)a,b). An example of a migrated section with imaged fault systems within a crystalline environment in Finland is shown in Figure 1.3 (Malehmir et al. (2012)b).

However, there are several challenges encountered when dealing with seismic imaging over crystalline rock described in, for example, Salisbury et al. (2007) and Greenhalgh and Manukyan (2013):

- Relatively small acoustic impedance contrasts, small dimensions and complex shapes of reflectors within the crystalline basement lead to weak reflection amplitudes and hence generally low signal-to-noise ratios.

- A large impedance contrast between the sediment cover (thin layers of unconsolidated recent sediments as well as thick sedimentary units in alpine forelands) and the underlying basement significantly reduce the amount of seismic energy transmitted into the crystalline basement.

- In contrast to sedimentary basins, reflectors in crystalline rocks are normally discontinuous due to deformation processes, complex morphology and lithology.

- Targets may be small and hence difficult to detect.

- The generally high velocities in crystalline rock lead to long seismic wavelengths and therefore a low resolution.

- Crystalline rocks can be heterogeneous on a range of scales which leads to significant scattering, in particular of high-frequency signals.

- Fracture zones attenuate seismic waves and hence lead to a lower signal-to-noise ratio in areas below the fracture zone.

- Fracture zones that are of a primary interest are often steeply dipping and hence difficult to image without large aperture recording arrays.

- Fracture zones and layering introduce anisotropy that leads to complex wave propagation.

As these factors complicate the seismic imaging of features within crystalline basement and need to be considered when planning a seismic experiment. Small source/receiver spacing, high-fold data and good receiver coupling is required to obtain seismic data with a high signal-to-noise ratio in such challenging areas (Bergman et al. (2002)). In order to image steeply dipping structures, such as faults or dykes, large offsets are favorable as well as high frequencies to correctly image these features (Greenhalgh and Manukyan (2013)).

Sophisticated seismic processing is essential with particular focus on refraction statics, noise suppression, DMO corrections, velocity analysis and migration (Eaton et al. (2003); Schmelzbach et al. (2007); Greenhalgh and Manukyan (2013)). Therefore, an effort must be made to preserve (relative) true-amplitudes in order to extract information from AVO analysis. However, due to the generally low signal-to-noise ratio in crystalline rock environments it still remains challenging to image structural features without the application of prestack automatic gain control for amplitude equalization (Malehmir et al. (2012)b).

1.3.3 Deep lithospheric studies

Geothermal exploration can benefit from deep crustal and upper mantle seismic studies due to the developed acquisition and processing techniques for crystalline environments, as well as the geological understanding gained. Additionally, crustal studies can serve as a basis for a smaller study area and further evaluation of potential geothermal sites. Large scale structures of the lithosphere can e.g. yield information about deep magmatism and explain thermal anomalies observed at the surface (Bitri et al. (2010)).

Several seismic surveys have been acquired at regional scale in recent decades on different continents to image the continental crust and lithosphere. Examples include the COCORP program in the USA, Europrobe in Europe and Lithoprobe in Canada (Cook et al. (1979); Juhlin et al. (1998); Clowes et al. (1984)). The seismic experiments were conducted with the goal of obtaining a better understanding of the geology, tectonics and structure of the continental lithosphere. Challenges arise from the low reflectivity of the crust that make the imaging of large scale structures such as the Moho discontinuity or major fault systems difficult (Milkereit and Eaton (1998)).
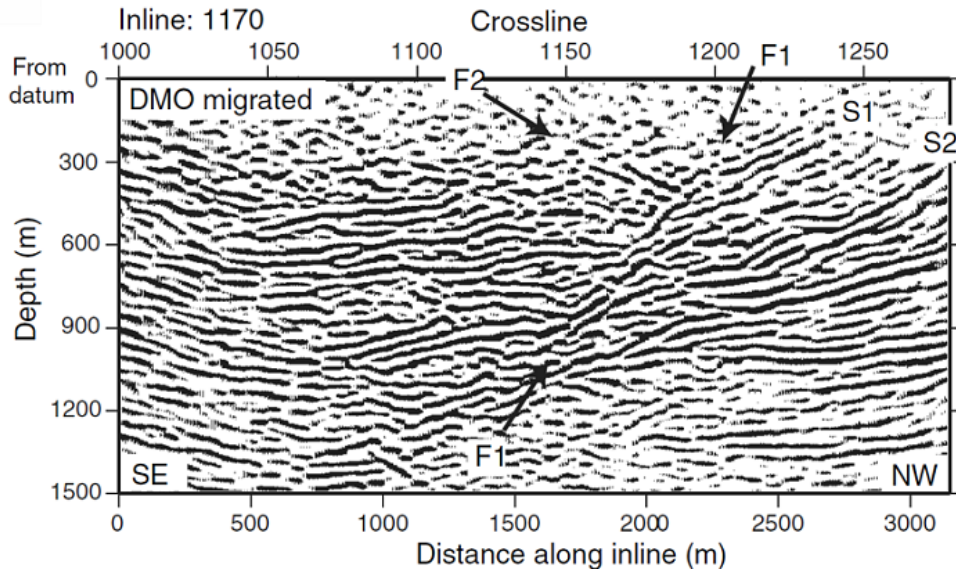
Figure 1.3: Migrated and time-to-depth converted section from a waste disposal site in Finland (taken from Malehmir et al. (2012)b). A large fault system is indicated with F1 and F2.

A crustal study related to geothermal exploration is shown in Brogi et al. (2005) where two deep seismic reflection lines were acquired to better understand the Lardarello geothermal site. Based on the study, the tectonic setting could be better characterized and a regional structural model constructed to identify a magmatic body that could serve as a current heat source of the geothermal site.

1.3.4 Enhanced geothermal systems

Seismic investigations in geothermal areas have only been sparingly applied compared to their prolific use in the oil and gas industry. Seismic exploration of EGS systems focuses mostly on detailed imaging of fault and fracture zones within crystalline environments. The characterization of subsurface structures can be used as a basis for establishing a flow model and to find suitable well positions.

Schneeberg in Germany is one of the rare areas over crystalline rock where 3D surface seismic exploration has been performed to better characterize pre-existing fault systems for geothermal purposes. Lüschen et al. (2015) processed 3D seismic data to test the seismic method as an exploration tool. Steeply dipping and conjugate faults were imaged within the granitic basement. Ahmed et al. (2015) and Hloušek et al. (2015) used advanced seismic imaging techniques to map steeply dipping fault zones between 2-5 km depth for potential geothermal usage (Figure 1.4). Schreiter et al. (2015) further inferred the approximate extent and velocity structure of the fault systems based on the analysis of reflection amplitudes.

Abul Khair et al. (2015) examined deep granitic bodies and faults in the Cooper Basin of South Central Australia, where an EGS pilot power plant was established. The goal was to map faults that provide pathways for circulating fluids. They presented a workflow to better locate potential EGS
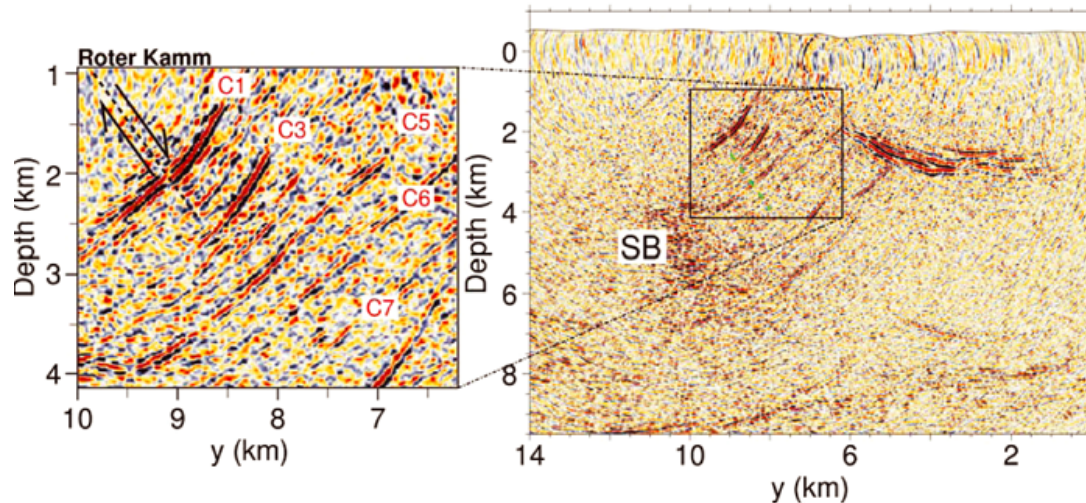
Figure 1.4: Vertical depth slice through a stacked image cube of a geothermal area in Schneeberg, Germany after the application of coherency migration (taken from Hloušek et al. (2015)). The black line marks the Roter Kamm fault and C1-7 conjugate fault systems.

sites based on fault characterization within granitic environments. They used seismic attributes to better locate fault systems that intersect the basement.

1.3.5 Hydrothermal systems

Since hydrothermal systems are naturally occurring, they are only located at specific geographic locations. Hence, a primary focus of seismic exploration is to find them and better characterize the extent of the exploited aquifers, such as a porous layers or fault and fracture networks (Matsushima and Okubo (2003)). Most of the geothermal reservoirs that successfully produce electricity are related to high-enthalpy systems such as several places in Iceland (Arnórsson (1995)) and Lardarello in Italy (Brogi et al. (2003); Casini et al. (2010)). Lardarello developed the first geothermal power plant that successfully produced electricity in 1904. The area is very well examined, also by surface seismic reflection imaging. Brogi et al. (2003) analyzed 2D reflection seismic lines and imaged several shear zones, major fractures and the brittle-ductile transition. Casini et al. (2009) established a geological and structural model of the Lardarello field and mapped fracture zones in the deep geothermal reservoir based on a 3D seismic survey. Riedel et al. (2015) processed two seismic lines and demonstrated that the images can be further improved by the application of Fresnel volume migration that eliminates artefacts.

Another high-enthalpy geothermal field that was examined with seismic reflection imaging is the Kakkonda geothermal field in Japan. Matsushima and Okubo (2003) report that the quality of the seismic data in this area is often poor due to a high noise level and seismic wave attenuation within the hot gas- or fluid-saturated rocks. They show that a seismic section of higher S/N ratio can be obtained by prestack time migration compared to conventional CDP stacking. Matsushima et al. (2004) showed that reservoir changes after shut-in could be detected by repeated seismic measurements and hence demonstrate the possibility of using the time-lapse seismic imaging for geothermal reservoir monitoring.
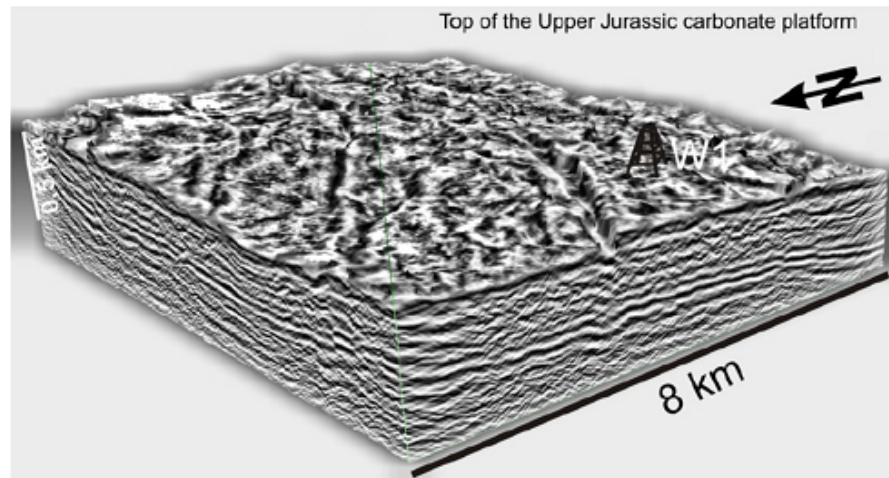
Figure 1.5: Spatial view of a seismic cube with the top horizon representing the Upper Jurassic (taken from von Hartmann et al. (2012)). The uppermost horizon clearly reveals the morphology and intense faulting.

In high-enthalpy geothermal systems it is important to locate steam bearing fracture zones as steam can be used to produce electricity. Steam has the effect of absorbing seismic energy and decreasing the seismic wave speed. It was shown by Wei et al. (2014)a,b that P-waves were strongly attenuated by gas-filled pores whereas S-waves were less affected. Hence, P-SV images could significantly improve the image quality bellow the gas-filled formation.

Moderate-temperature reservoirs can be exploited for direct use (e.g. heating, cooling) or also for electricity production when binary systems are used. Lüschen et al. (2014) characterized a hydrothermal reservoir at the geothermal power plant in Unterhaching (Germany) using a 3D seismic survey covering an area of ~27 km². Based on the analysis of reflection amplitudes indications of fracture orientation could be obtained. They used coherency and dip attributes, as well as spectral decomposition to distinguish different facies within the carbonate formation and improve fracture zone imaging. von Hartmann et al. (2012) showed that attribute analysis can help to identify different carbonate facies in the Southern Germany Molasse Basin. An example of a horizon-based 3D section, where the morphology of the Upper Jurassic is shown, is displayed in Figure 1.5. Pussak et al. (2014) demonstrated on a 3D dataset in the Polish basin that a common-reflection-surface (CRS) stack technique (Jäger et al. (2001)) can improve the S/N ratio and can hence be beneficial for attribute analysis.

1.4 Vertical seismic profiling

Vertical seismic profiling (VSP) is a technique whereby seismic signals are created from a surface source and detected by geophones that are placed at various depths along a borehole (Hardage (2000)). Sources can be fired at different offsets (including at the wellhead) and different azimuths. The concept of a VSP is shown in Figure 1.6 for a simple 2 layer model. Since the geophones are lo-

cated below the surface, they can record downgoing (e.g. direct wave) as well as upgoing wavefields (e.g. reflected wave). The different moveout directions of the direct and reflected wave (Figure 1.6b) allows the separation of these wavefields. More details on VSP data processing can be found in, for example, Hardage (2000), Kuzmiski et al. (2008) and Gaiser (2016).

VSP can be applied to identify reflections and trace them to their points of origin in the subsurface, provide information about their orientation and exact location when they intersect the borehole and tie borehole geology to surface seismic data (Emsley et al. (2007)). Further applications include identification of primary and multiple events, location of fault planes, looking for reflectors ahead of the drill bit, measurement of both P- and S-wave velocities and estimation of P- to S-wave conversion and direct measurement of attenuation and geometric divergence (Hardage (2000); Campbell et al. (2005)). VSP has several advantages compared to surface seismic data (Cosma et al. (2003)):

- Since receivers are located within the well, traveltimes are shorter and hence the VSP data suffer less from attenuation compared to surface seismic data. Since the seismic waves only travel once through the highly absorbing and heterogeneous shallow near surface zone, the data contain normally higher frequencies and hence provide better resolution.

- Since the geophones are placed in the well they are located close to the target zone and thus improve detection and recognition of features of interest.

- Three-component geophones record the full vector wavefield and hence the orientation of reflectors can be retrieved with polarization analysis. In surface seismic data this information is often lost due to the low velocity near surface layer and due to Snell's law of refraction the resultant nearly vertically arriving wavefronts.

- Imaging of dipping reflectors with surface seismic-reflection surveys is difficult, as large offsets are required. VSP provides a suitable geometry for mapping gently to steeply dipping features, especially for multi-offset and multi-azimuth experiments.

- Multiples can often be identified by comparison of the outer corridor stack (dominated by primary reflections) and inner corridor stack (dominated by primary reflections and interbed multiples) (Burton and Lines (1997)).

Due to the numerous advantages of VSP, the method provides the possibility for high-resolution imaging of lithological interfaces and dipping reflectors in the vicinity of a borehole. VSP data contain information on reflectivity, velocity and anisotropy and provide an important link between the lithology in the borehole and seismic data. Detailed velocity-depth profiles can be extracted for time-depth conversion of surface seismic data.

The principal disadvantage of VSP compared to surface seismic reflection surveys is the limited illumination area. Imaging of lithological interfaces and dipping reflectors is primarily restricted to the vicinity of the borehole and the region in the extended depth position of the borehole, depending on the dip of the reflector. Hence, a much smaller area can be covered with VSP.
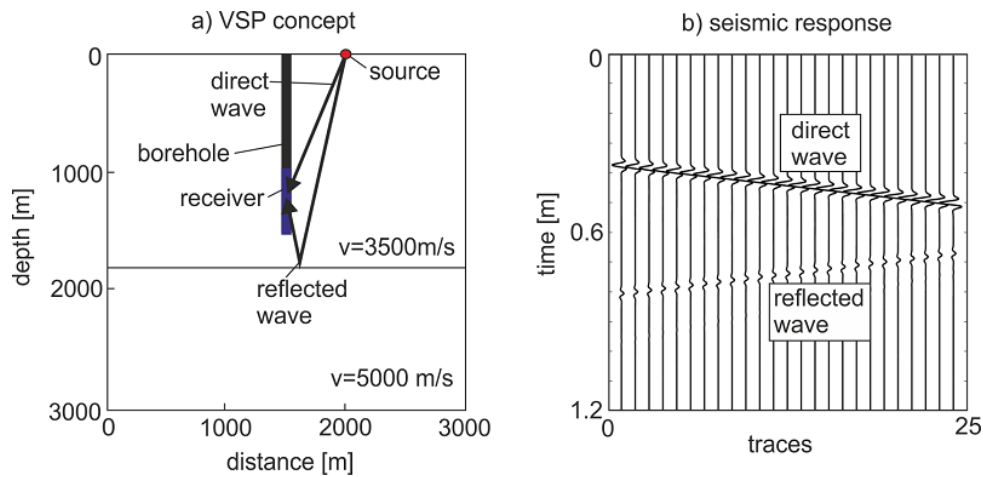
Figure 1.6: Concept of a VSP experiment. a) A source is fired at the surface and the downgoing (direct wave) as well as the upgoing wavefield (reflected wave) is recorded by the geophones located along the borehole. b) Seismic response of the simple two layer case shown in a). Direct and reflected waves show different moveout directions and hence allow the separation of these wavefields.

1.4.1 Hydrocarbon and crystalline rock exploration

VSP has been applied successfully in different contexts, such as in fractured carbonate reservoirs (Emsley et al. (2007)), for better understanding of seismic properties in the crust (Carr et al. (1996); Rabbel et al. (2004)), in mineral exploration (Adam et al. (2003); Perron et al. (2003); Bellefleur et al. (2004)) and in nuclear waste disposal sites (Cosma et al. (2001), (2003)).

VSP has extensively been conducted in oil and gas prospecting, mainly for linking borehole properties to surface seismic data. Campbell et al. (2005) showed on a dataset from Texas that VSP can provide much more than a corridor stack and the possibility for correlation with surface seismic data. They also obtained attenuation (1/Q) values and spherical divergence correction factors, identified interbed multiples and carried out acoustic impedance inversion. Leaney (2008) has analyzed different methods to estimate vertical transverse isotropy with VSP data and demonstrated that walkaway VSP is a suitable method to measure polar anisotropy. The number of 3D VSP surveys has been growing in the recent years, especially where high-resolution 3D seismic images are required such as in areas with complex overburden or below salt (Gulati and Stewart (2013)). Campbell et al. (2013) demonstrated the benefit of a 3D VSP survey since high resolution P-wave images are obtained from an area in British Columbia, Canada. They additionally estimated anisotropy, Q, and fracture orientation by the application of shear-wave splitting as well as being able to identify multiples.

VSP can also be of great value in mineral exploration. Adam et al. (2003) used two VSP surveys to image volcanogenic massive sulfide deposits in northwestern Québec, Canada. Bellefleur et al. (2004) processed P-, S- and converted waves of a VSP experiment in New Brunswick, Canada and imaged massive sulfide lenses in a low-reflectivity host rock. Melanson et al. (2015) analyzed three-component zero-offset VSP data and observed reflections originated from a volcanogenic massive sulfide ore system.

1.4.2 Geothermal exploration

As shown above, VSP offers a suitable method for high resolution imaging of lithologies, structural features or dipping interfaces intersecting, beneath or offset from the well. Therefore, VSP has a considerable potential to characterize geothermal reservoirs and image fracture zones in the vicinity of the well. However, VSP has been applied only rarely in geothermal areas. Some examples are presented in the following.

Majer et al. (1988) processed data from a VSP pilot study in the Geyser steam-bearing geothermal field in northern California and obtained anisotropy information based on velocity differences between the differently polarized shear waves. Cameli et al. (1995) analyzed VSP data from the Lardarello region in Italy. They observed several reflectors that could be related to petrophysical changes and the main fracture zones down to about 4 km depth. Nakagome et al. (1998) studied VSP data from the Kakkonda geothermal field in Japan and mapped relevant faults and fracture zones. They concluded that the VSP data showed more structural details than the surface seismic reflection data. A higher signal-to-noise ratio for the VSP data compared to the surface data was observed in a zero offset and moving source VSP experiment at Unterhaching in Munich (Thomas and Schulz (2007)). Several reflectors could be imaged in the sedimentary hydrothermal reservoir and fault systems interpreted.

Place et al. (2010), (2011) processed VSP data sets from the EGS site in Soultz-sous-Forêts, France, that were acquired in 1988 and 1993. Several fracture zones within the granitic basement could be identified based on reflections from P- and P-to-S mode-converted waves. A migrated image of the VSP data, where steeply dipping fracture zones are mapped, is shown in Figure 1.7. Synthetic modelling was used to explain the observed reflection traveltimes and helped to generate a fracture zone model of the area.
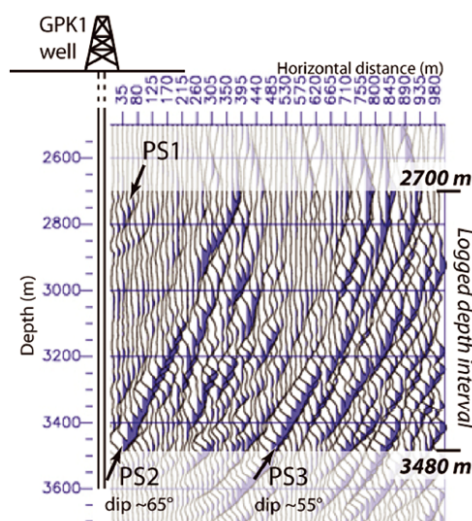
Figure 1.7: Migrated image of VSP data from Soultz-sous-Forêts where steeply dipping reflectors were mapped using P-S converted reflections (taken from Place et al. (2011).)

1.5 Advanced seismic processing techniques

As seismic exploration in the geothermal context is quite challenging due to the complex environment, advanced seismic processing techniques are likely required to extract the maximum information possible out of the dataset. Different techniques were developed in the past few decades by the oil and gas industry and it needs to be tested which of the techniques can be valuable for geothermal exploration and how the techniques need to be adapted in the geothermal context. Some of the techniques that could be beneficial for geothermal exploration are presented in the following sections.

1.5.1 Traveltime and fat ray tomography

The goal of traveltime tomography is to find a subsurface velocity model that explains the first-arrival traveltimes of the observed data. During the inversion, the velocity model is iteratively adjusted and updated until the differences between the observed and calculated first arrivals lie within the picking uncertainty (Lanz et al. (1998); Zelt and Barton (1998); Rawlinson and Sambridge (2003)).

Classical ray-based traveltime tomography is based on the high frequency assumption, where the ray is assumed to be infinitely thin and not affected by diffraction and scattering from the surrounding medium.

Fat ray tomography is a compromise between the classical ray-based tomography and full waveform inversion (FWI) (Vasco et al. (1995); Watanabe et al. (1999); Husen and Kissling (2001)). Fat ray tomography considers the frequency characteristics of the wavefield in that it takes the first Fresnel zone around the central ray into account for the wave propagation. Scattering within the first Fresnel zone leads to constructive interference of the seismic signal. The influence of the Fresnel zone can be described by the sensitivity kernels that are calculated based on source and receiver traveltime fields (Husen and Kissling (2001); Jordi et al. (2016)). The sensitivities are implemented in the Jacobian matrix and are the main difference between classical ray and fat ray tomography.

Fat ray tomography provides an increased coverage and more realistic wave propagation, and hence enhanced imaging of the subsurface is expected (Jordi et al. (2016)). Due to the additional subsurface information, the velocity model can potentially be better constrained which results in improved resolution, and better localization of low velocity zones. Fat ray tomography can provide advanced velocity models that can further be used for migration, statics analysis or as a starting model for FWI.

Geothermal exploration could benefit from fat ray tomography in that enhanced imaging is expected due to the more realistic wave propagation. In geothermal exploration, the financial investments are often considerably smaller compared to the oil and gas exploration and hence datasets are often limited in terms of number of source positions. Especially in the cases of sparsely acquired datasets, fat ray tomography could be beneficial since the velocity models can be better constrained due to the nature of the method.

1.5.2 Full waveform inversion

Full waveform inversion (FWI) is a non-linear imaging method that aims at exploiting the entire seismic wavefield with a minimum of preprocessing to obtain images of the subsurface at sub-wavelength resolution. FWI iteratively minimizes the misfit function between the observed and predicted waveforms with a linearized least-square optimization procedure. Since the whole seismograms are used, rather than just the first arrival time s and/or pulse amplitudes, the most complete representation of the subsurface is expected from FWI. A comparison between traveltime tomography and FWI is shown in Figure 1.8 (Pratt (1999)). Traveltime tomography only resolve the coarse structure, whereas the application of FWI results in a much more detailed subsurface image. FWI tries to reconstruct the physical parameters such as wavespeeds Vp, Vs and density. In addition, attenuation, anisotropy values and impedance can in principle be extracted. FWI takes phases and amplitudes of of all arrivals into account. Hence, the method can potentially provide images of physical parameters with a resolution comparable to migration and diffraction imaging (half of the shortest wavelength).

However, FWI also encounters several challenges. The accurate numerical modelling of the full 3D viscoelastic wave propagation in a complex and arbitrary medium including features like faults, the free surface with arbitrary topography, attenuation and anisotropy is a difficult task and requires enormous computational power. An additional challenge is the non-linearity of the FWI problem. A priori information of the large-scale structures is required to reconstruct the smallest features and compensate for missing low-frequency information in the seismic data. This large-scale information can be obtained by velocity analysis, refraction or reflection tomography and can then be included in the initial model for the FWI.

FWI emerged in the 1980's (Tarantola (1984); Mora (1987)), but was not widely used until recently, mainly due to the lack of computational power (Plessix (2008); Buske et al. (2009)). Reviews of the method are given, for example, by Virieux and Operto (2009) and Fichtner (2011). FWI was initially introduced for 2D acoustic data in the time domain (Tarantola (1984)) and further developed in the frequency domain due to the computational efficiency (e.g. Pratt and Worthington (1990)). The advantage of FWI in the frequency domain is that the inversion only needs to be performed with a few well-chosen frequencies and hence substantially lower computational costs are experienced (e.g. Sirgue and Pratt (2004); Maurer et al. (2009)). Additionally, due to the strong non-linearity of the inverse problem the inversion can be started with low frequencies and higher frequencies can be added as the iterations proceed (Bunks et al. (1995)). This reduces the chance of getting trapped in a local-minimum. Several authors also applied traveltime tomography to wide-angle refraction data to build initial models that can be used for FWI (Operto et al. (2004); Dessa et al. (2004)).

So far, most FWI studies were restricted to 2D problems, but in more recent years, with the improvement of computing facilities, also 3D acoustic and elastic inversions have become feasible and have been applied successfully on marine data sets (Sirgue et al. (2009); Vigh et al. (2014)) as well as on the regional and global scale by using earthquake sources (Fichtner et al. (2008)).

Most of the FWI studies are related to surface-based or ocean-bottom surveys in oil and gas exploration (e.g. Shipp and Singh (2002); Sears et al. (2008); Brossier et al. (2009)) or monitoring of C02 at depth (e.g. Zhang et al. (2013)). Examples of crosswell studies in the context of monitoring
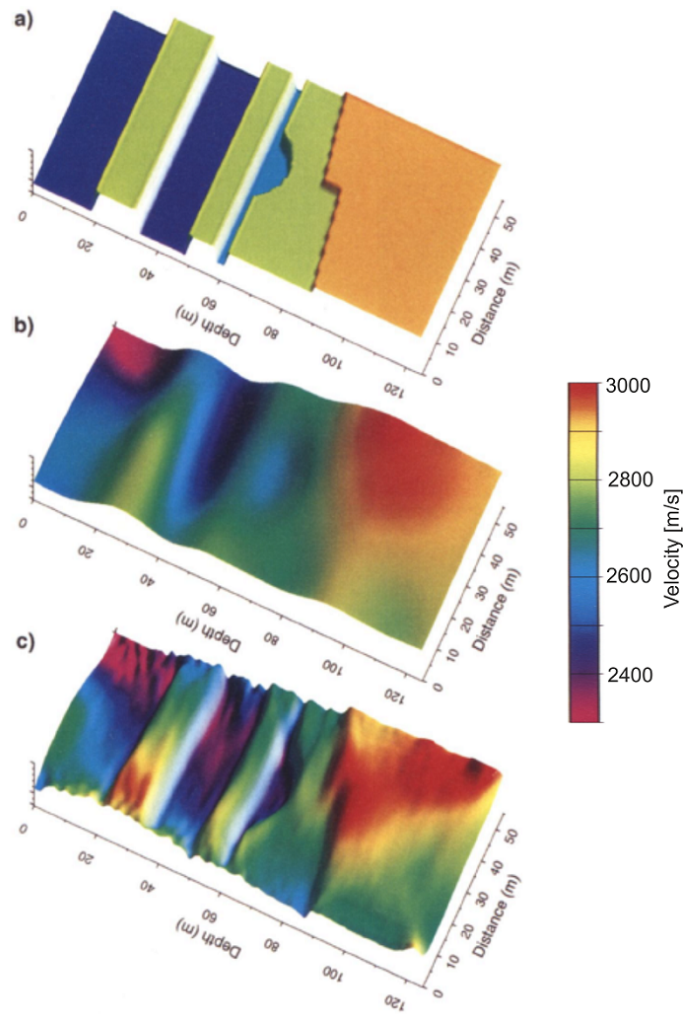
Figure 1.8: Comparison of traveltime tomography and FWI modified after Pratt (1999)). a) True velocity model, b) result from traveltime tomography, c) and FWI. Note the clearly higher imaging resolution of the FWI.

nuclear waste repositories are found in Marelli et al. (2012) and Manukyan et al. (2012). The advantage of transmission configurations (crosshole and VSP experiments) is that the inverse problem is more linear when transmitted (forward-scattered) rather than reflected (back-scattered) waves are used. Additionally, borehole information such as sonic log velocities can be used in crosshole/VSP surveys to obtain a consistent and accurate initial velocity model (Pratt and Goulty (1991)).

To date, FWI has not been applied in the geothermal context (Schmelzbach et al. (2016)b). The exploration depth and surface illumination configurations are similar to oil and gas exploration and hence FWI in geothermal areas can benefit from the studies performed in oil prospecting. However, the same challenges and limitations are encountered, such as high cost of forward modelling, accurate construction of initial velocity and density models, data preprocessing or data transformation for the acoustic case. Although the application of FWI to surface reflection seismic data is challenging, difficulties can be reduced, when FWI is applied to crosshole or VSP data. Accurate velocity models can be obtained by traveltime inversion of the first arrivals or borehole information, such as sonic logs, help to constrain the initial velocity model and stabilize the inversion.

1.5.3 Multicomponent seismic data analysis

Multicomponent seismic data offer many advantages compared to vertical component data because polarization properties can be extracted in addition to amplitude and phase information. Multicomponent geophones record a vector wavefield and hence polarization analysis can be used to locate earthquake epicenters (Magotra et al. (1987)), to suppress ground roll and to separate P- and S-waves (Perelberg and Hornbostel (1994)). P- and S-waves sample the subsurface differently and hence complementary information can be gained by individually processing P- and S-wavefields. S-waves have the advantage to be less affected by absorption in gas bearing fracture zones, yield anisotropy information by studying shear wave splitting, to provide higher resolution images due to the slower velocities and hence shorter wavelength compared to P-waves, to enable a more detailed lithological characterization and to improve fluid description and reservoir monitoring (Crampin (1981), (1985); Alford et al. (1989); Granli et al. (1999); Stewart et al. (2003); Hardage et al. (2011)).

Separating P- and S-waves is challenging and many different techniques were developed to determine the direction of the arriving wave field (Hearn and Hendrick (1999)). Through the analysis of relative amplitudes of the three components within a time window, the azimuth and inclination
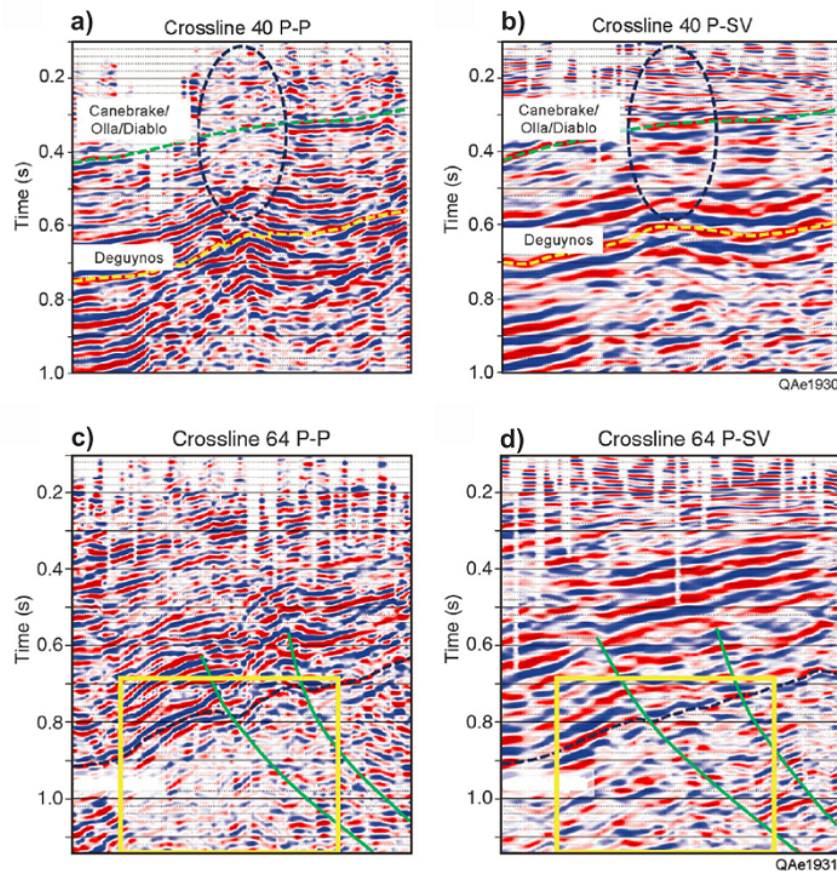
Figure 1.9: Seismic sections of the Wister geothermal fields in California. (a, b) Differences are illustrated between P-P and P-SV stacks within gas clouds marked by black ovals. (c, d) Differences across a region with low saturation of high temperature are indicated with a yellow rectangle, modified after Wei et al. (2014)b.

of an impinging wave can be determined. If seismic data is acquired with geophone lines or spatial arrays, then, the additional moveout information can be used to separate overlapping events with the application of 2D filters such as f-k, median, or τ-p filters (Dankbaar (1985); Greenhalgh et al. (1990)).

A distinct separation of P- and S-waves is also essential when performing scalar migration, since arte-facts from other modes can decrease the quality of processed migration images. Vector migration that incorporates the different components was introduced by Jackson et al. (1991). Sollberger (2013) developed a multicomponent Kirchhoff migration algorithm that includes a wavefield separation step to obtain individual PP, PS and SS migrated images.

In geothermal exploration, it is important to locate steam-bearing fracture zones as steam can be extracted to produce electricity. Steam decreases the seismic velocity and leads to higher absorp-tion of the seismic waves. Wei et al. (2014)a,b demonstrated the benefits of using multicomponent seismic data in the Wister geothermal fields, which is a Cenozoic sedimentary basin in California. The aim of this study was to evaluate potential reservoir units, locate fault and fracture zones and investigate the benefits of multicomponent seismic data. It was shown that Vp/Vs velocity ratios maps were valuable to identify and specify different rock types and that P-SV converted waves were more sensitive to fractures than P-P waves, particularly in hot steam filled sections. They showed that P-waves get strongly attenuated by gas-filled pores and hence P-SV images can significantly improve the image quality within and below the gas filled formation (Figure 1.9).

1.5.4 Other seismic data analysis techniques

Diffraction imaging. The focus of hardrock geothermal exploration is usually in imaging fractures, faults, shear zones and fluid pathways. The velocity contrast of such features is often small, the dips steep and the surface areas of the reflectors small. This results in signal amplitudes that are typically one-fifth or less that of reflections from laterally continuous sedimentary layers in hydro-carbon exploration (Schmelzbach et al. (2016)b). Geothermal targets in a depth of 3-5 km are often of complex shape and the spatial dimensions might be comparable or smaller than the Fresnel zone associated with the dominant frequencies of the seismic data. Subsurface heterogeneities with an extent of the first Fresnel zone or smaller lead to energy scattered in all directions based on Hugyens' secondary source principle. When seismic data is migrated, diffracted energy is projected back to the point of origin and hence information from point diffractors can get lost when the final migrated image is interpreted. However, diffracted and scattered energy can provide useful lithological and structural information, such as indication of mineral deposits (Milkereit et al. (1996); Adam et al. (2003); Malehmir et al. (2009)) or fault and fracture zones (Heincke et al. (2006); Schmelzbach et al. (2008); Schwarz and Gajewski (2017)). Schmelzbach et al. (2008) and Malehmir et al. (2009) have shown that by measuring the similarity along diffraction traveltime curves, the diffractor's point of origin can be located. Place et al. (2010) used diffraction imaging on a VSP dataset to complement the seismic reflection data in the geothermal area of Soultz-sous-Forêts. They retrieved additional structural information by analyzing diffractions. This is an example how diffraction imaging can be used to better characterize the subsurface in geothermal environments.

Seismic attribute analysis is a technique that can be used to extract structural and lithological information on the subsurface from seismic data (Chopra and Marfurt (2005)). Geometrical attributes are normally used in stratigraphic interpretation to enhance geometrical characteristics, such as continuity, unconformities, faults, dip, azimuth and curvature (Taner et al. (1994)). Physical attributes have a direct link to physical parameters in the subsurface and are generally used for characterization of lithology and reservoirs. Dip and azimuth became the basis for many geometrical attributes such as coherence and curvature and very essential attributes for identification of faults and other subtle stratigraphic features. Attribute analysis has also been applied to seismic data in geothermal areas to enhance the visibility of fault and fracture zones. Lüschen et al. (2014) performed attribute analysis on a 3D seismic dataset in Unterhaching, Germany. They could distinguish different facies within the carbonate formation and image fault zones in more detail by using coherency and dip attributes. Pussak et al. (2014) used RMS amplitudes, instantaneous frequencies, coherency and spectral decomposition attributes to characterize a geothermal reservoir and locate fluid-bearing fracture zones the Polish basin. Abul Khair et al. (2015) used the curvature attribute to image fault zones that intersect the basement of the EGS site in Cooper Basin, Australia. Hence, these studies show the improved fracture mapping in geothermal systems by the application of attribute analysis.

Shear wave birefringence is another technique that helps to better characterize fracture zones. S-waves split into a fast and slow S-wave travelling with orthogonal polarization in the same direction as the incident S-wave, whereas a P-wave is less affected by the anisotropy (Crampin (1985); Alford et al. (1989); Hardage et al. (2011)). The polarization of the fast S-wave is oriented parallel to the main fracture direction and the slow S-wave shows particle motion perpendicular to the fracture plane. Hence, if the polarization information can be extracted from the dataset, fracture orientation can be determined (Mueller (1991)). The time difference between the fast and slow S-wave depends on the propagation length and direction, as well as the degree of anisotropy (Li and Mueller (1997)). Since fracture density is mainly responsible for the degree of anisotropy the time delay can give indications on the fracture density (Lewis et al. (1991)). Shear wave birefringence in geothermal fields has so far been analyzed by using natural and induced seismic events. Case studies in the Coso geothermal field in Sierra Nevada Range, the Geysers geothermal site near the San Andreas fault and the Krafla site in northern Iceland demonstrated the benefit of using shear wave splitting, as polarization information and time delays could be used to detect orientation and fracture density (Vlahovic et al. (2003); Rial et al. (2005); Tang et al. (2008)). As the estimation of fracture orientation and fracture density as well as understanding the stress state of the subsurface is of great importance in geothermal exploration, shear wave splitting provides a useful tool to better characterize the subsurface. Shear wave splitting can potentially provide regions with larger hydraulic conductivity and could predict preferred directions of hydraulic fracturing. This would lead to further constraints on the location and design of geothermal wells.

1.6   Current challenges

There is a wide range of risks and challenges involved with the establishment of geothermal power plants. These issues need to be addressed so that economically viable geothermal systems can be built. Key challenges include (Rybach (2014); Adams et al. (2015)):

- Identifying a suitable target at sufficient depth with the required permeability and fluid flow.

- Engineering challenges regarding the well, such as mechanical damage during the well development, corrosion and scaling from geothermal fluids, thermal stress, failure and expansion of entrapped fluids.

- Hydraulic stimulations may induce significant microseismicity.

- Imaging the hydraulic stimulated or enhanced fracture network by monitoring systems is required.

- Public acceptance is generally low due to environmental and microseismicity concerns.

- Risk of pollution of the environment.

- Geothermal projects are perceived as costly and risky.

The engineering tasks are non-trivial, but also the geoscience contributions to locate and identify suitable reservoirs are considerable. To date there is still limited EGS experience and further research is required to demonstrate the usefulness of successfully operating EGS pilot plants. Building an EGS is still risky, involves high costs and hence requires considerable financial support. However, due to the limited success rates and profit, financial investments are often considerably smaller compared to oil and gas exploration. The main contributions that applied geophysics can provide are improved exploration prior to drilling and reservoir monitoring during production. In particular, seismic methods have been developed extensively. High costs arise particularly in the development phase of establishing geothermal power plants (Younger (2015)). Drilling is expensive and hence it is of great importance to reduce the risk that is associated with high drilling costs. The exploration and characterization of geothermal reservoirs is crucial for minimizing these economic risks. Seismic methods can reduce the risk that is associated with an expensive drilling program and help to find suitable well positions. Due to normally small budgets in geothermal projects, seismic datasets from geothermal areas are often limited in terms of number of source positions. Hence, a careful survey planning with target oriented imaging and a favorable benefit-cost ratio is required.

Monitoring the production operations is also very challenging and special time-lapse techniques for more accurate monitoring are needed. Due to the problem of induced seismicity during reservoir stimulation, it is essential to have à priori knowledge about the regional stress field and pre-existing fault systems (Shortall et al. (2015)). Especially in densely populated areas it is essential to keep the microseismicity below a certain threshold to maintain safety and gain public acceptance. Another public concern is related to ground subsidence due to extraction of geothermal fluid from the reservoir, ground uplift due to underground formations such as anhydrite or pollution of ground water

(Stober and Bucher (2013); Shortall et al. (2015)). Identifying aquifers and monitoring changes in the subsurface is hence essential.

1.7 Objectives and Outline of the Thesis

The challenges outlined in section 1.6 stress the importance and necessity for further research and development in geothermal exploration so that geothermal systems can become economically viable energy sources. A focus of seismic exploration is to locate potential geothermal sites and better characterize geothermal reservoirs, especially with regard to mapping critical fault and fracture networks. Seismic imaging of crystalline basement structures is very challenging. VSP can potentially offer a powerful means to image subsurface features intersecting, or being located beneath or offset from a well in complex environments. However, VSP has been applied only rarely in the geothermal context. Therefore, I investigate in this thesis, how VSP can contribute to a better understanding of geothermal reservoirs and what limitations are associated with the method. Sophisticated seismic processing workflows are needed for an improved imaging in complex environments. The overarching goal of my thesis is to *develop seismic processing flows as well as establishing optimal acquisition design workflows for improved imaging of geothermal reservoirs*. In detail, I addressed the following topics in this thesis:

- Improving fracture zone imaging, since fracture zones control the permeability and hence the fluid flow and productivity of geothermal wells;

- Examining whether VSP can contribute to a better reservoir characterization as a tool for imaging of fracture zones, stratigraphy, steam zones, dykes or magmatic bodies;

- Investigating how seismic imaging techniques need to be adapted and applied to geothermal sites;

- Testing advanced seismic imaging methods for a more comprehensive imaging of the subsurface.

To achieve the thesis objectives, an experimental design study on synthetic VSP data was performed for imaging fracture zones within crystalline basement and advanced seismic imaging techniques were tested on VSP field data from two different geothermal sites one in Iceland and the other in Switzerland. Even though the experimental design study was based on the setting of the geothermal site of Soultz-sous-Forêts, France, the methodology is flexible and can be applied to any other subsurface geology and borehole geometry. The case studies address specific problems of the area, however, the developed methodology can be generalized and transferred to other geothermal sites. With the knowledge and experience gained from the analysis of the VSP field datasets, the thesis can serve as a basis for planning future VSP surveys in geothermal areas.

The thesis is subdivided in the following chapters.

In chapter 2, 2D and 3D acoustic synthetic data are simulated and processed to pre-stack depth migration to optimize VSP survey layouts for mapping moderately to steeply dipping fracture zones within possible basement geothermal reservoirs. Imaging fracture zones is a primary focus of geothermal

seismic imaging, and it is important to understand the possibilities and limitations of imaging fracture zones within a complex environment using VSP. The aim of chapter 2 is to provide a methodology that helps to design future field surveys with a favorable benefit-cost ratio in areas with available à priori knowledge. Especially in geothermal projects with normally limited financial resources and hence only a small number of source positions it is critical to minimize the number of sources and thus place the sources only at the most beneficial positions. An additional goal of the methodology is to provide an optimization workflow that can also be valuable for selecting useful subsets of acquired data for optimum target-oriented processing. The work presented in chapter 2 was published in *Journal of Applied Geophysics* (Reiser et al. (2017)).

In chapter 3, results from the first multi-offset VSP experiment over a high-temperature geothermal field in Iceland are presented. The goal of chapter 3 is to test, whether VSP is a suitable method to map volcanic stratigraphy, fractures, dykes, steam zones and magmatic bodies at the Krafla site and for volcanic environments in general. As the data set consists only of a few source positions, the aim is to establish a workflow for processing a sparse VSP dataset using traveltime tomography and seismic reflection processing. An additional goal is to apply advanced seismic imaging techniques to an existing dataset such as fat-ray tomography and multicomponent Kirchhoff migration to obtain separate PP, PS and SS migrated images. Finally, the objective of chapter 3 is to show benefits and limitations of VSP surveys for geothermal prospecting in volcanic areas are formulate strategies for improved data acquisition in volcanic environments. The work introduced in chapter 3 was submitted to Journal of Volcanology and Geothermal Research (Reiser et al. (2018)).

In chapter 4, elastic full waveform inversion (FWI) was applied to a VSP dataset acquired in a geothermal well in Thonex, Switzerland. To date, FWI has not been applied in the geothermal context. Hence, the goal of chapter 4 is to apply FWI to a VSP field dataset and test the potential of imaging geothermal reservoirs using FWI. More specific, it is studied if FWI can provide a detailed velocity model of the subsurface that leads to a better characterization of the subsurface at the geothermal site.

In chapter 5, a synthesis of the results of the previous chapters and perspectives for future research are presented.

In Appendix A, a review of advanced seismic processing and imaging techniques and their potential for geothermal exploration is presented. The work in Appendix A was published in Interpretation (Schmelzbach et al. (2016)). Appendix B and Appendix C contain different conference abstracts.

References

Abul Khair, H., D. Cooke, and M. Hand. 2015. "Seismic mapping and geomechanical analyses of faults within deep hot granites, a workflow for enhanced geothermal system projects". *Geothermics* 53:46–56.

Adam, E., T. Bohlen, and B. Milkereit. 2003. "Vertical seismic profiling at the Bell Allard orebody, Matagami, Quebec". In *Hardrock seismic exploration*, 181–193. Society of Exploration Geophysicists.

Adams, C. A., A. M. Auld, J. G. Gluyas, and S. Hogg. 2015. "Geothermal energy–The global opportunity". *Proceedings of the Institution of Mechanical Engineers, Part A: Journal of Power and Energy* 229 (7): 747–754.

Ahmed, K., B. Schwarz, and D. Gajewski. 2015. "Application of the 3D common-reflection-surface stack workflow in a crystalline rock environment". *Geophysical Prospecting* 63 (4): 990–998.

Alford, R. M., H. B. Lynn, and L. A. Thomsen. 1989. *Seismic surveying technique for the detection of azimuthal variations in the earth's subsurface*. US Patent 4,817,061.

Arnórsson, S. 1995. "Geothermal systems in Iceland: structure and conceptual models—I. High-temperature areas". *Geothermics* 24 (5-6): 561–602.

Barbier, E. 2002. "Geothermal energy technology and current status: an overview". *Renewable and Sustainable Energy Reviews* 6 (1): 3–65.

Barkved, O., B. Bartman, J. Gaiser, R. Van Dok, T. Johns, P. Kristiansen, T. Probert, and M. Thompson. 2004. "The many facets of multicomponent seismic data". *Oilfield Review* 16 (2): 42–56.

Bellefleur, G., C. Müller, D. Snyder, and L. Matthews. 2004. "Downhole seismic imaging of a massive sulfide orebody with mode-converted waves, Halfmile Lake, New Brunswick, Canada". *Geophysics* 69 (2): 318–329.

Bergman, B., C. Juhlin, and H. Palm. 2002. "High-resolution reflection seismic imaging of the upper crust at Laxemar, southeastern Sweden". *Tectonophysics* 355 (1): 201–213.

Bertani, R. 2016. "Geothermal power generation in the world 2010–2014 update report". *Geothermics* 60:31–43.

Bitri, A., J.-P. Brun, D. Gapais, F. Cagnard, C. Gumiaux, J. Chantraine, G. Martelet, and C. Truffert. 2010. "Deep reflection seismic imaging of the internal zone of the South Armorican Hercynian belt (western France)(ARMOR 2/Géofrance 3D Program)". *Comptes Rendus Geoscience* 342 (6): 448–452.

Breede, K., K. Dzebisashvili, X. Liu, and G. Falcone. 2013. "A systematic review of enhanced (or engineered) geothermal systems: past, present and future". *Geothermal Energy* 1 (1): 4.

Brogi, A., A. Lazzarotto, D. Liotta, and G. Ranalli. 2003. "Extensional shear zones as imaged by reflection seismic lines: the Larderello geothermal field (central Italy)". *Tectonophysics* 363 (1): 127–139.

Brogi, A., A. Lazzarotto, D. Liotta, G. Ranalli, C. W. Group, et al. 2005. "Crustal structures in the geothermal areas of southern Tuscany (Italy): insights from the CROP 18 deep seismic reflection lines". *Journal of Volcanology and Geothermal Research* 148 (1): 60–80.

Bromley, C. J., M. Mongillo, B. Goldstein, G. Hiriart, R. Bertani, E. Huenges, H. Muraoka, A. Ragnarsson, J. Tester, and V. Zui. 2010. "Contribution of geothermal energy to climate change mitigation: the IPCC renewable energy report". In *Proceedings World Geothermal Congress 2010*.

Brossier, R., S. Operto, and J. Virieux. 2009. "Seismic imaging of complex onshore structures by 2D elastic frequency-domain full-waveform inversion". *Geophysics* 74 (6): WCC105–WCC118.

Bunks, C., F. M. Saleck, S. Zaleski, and G. Chavent. 1995. "Multiscale seismic waveform inversion". *Geophysics* 60 (5): 1457–1473.

Burton, A., and L. Lines. 1997. "VSP detection of interbed multiples using inside-outside corridor stacking". *Geophysics* 62 (5): 1628–1635.

Buske, S., I. Lecomte, T. Nemeth, S. Operto, and V. Sallares. 2009. *Imaging and inversion—Introduction*. Tech. rep. Society of Exploration Geophysicists.

Cameli, G., F. Batini, I. Dini, J. Lee, R. Gibson Jr, and M. Toksöz. 1995. "Seismic delineation of a geothermal reservoir in the Monteverdi area from VSP data". In *Proceedings of the World Geothermal Congress*, 2:821–826. Florence Italy.

Campbell, A., A. Fryer, and S. Wakeman. 2005. "Vertical seismic profiles—More than just a corridor stack". *The Leading Edge* 24 (7): 694–697.

Campbell, A., S. Leaney, J. Gulati, J. Leslie-Panek, and E. Von Lunen. 2013. "Images, anisotropy, multiples, and more from an unconventional 3D VSP". *The Leading Edge* 32 (10): 1238–1244.

Carr, B., S. Smithson, N. Kareav, A. Ronin, V. Garipov, Y. Kristofferson, P. Digranes, D. Smythe, and C. Gillen. 1996. "Vertical seismic profile results from the Kola Superdeep Borehole, Russia". *Tectonophysics* 264 (1-4): 295–307.

Cartwright, J., and M. Huuse. 2005. "3D seismic technology: the geological 'Hubble'". *Basin Research* 17 (1): 1–20.

Casini, M., S. Ciuffi, A. Fiordelisi, A. Mazzotti, I. Perticone, E. Spinelli, and E. Stucchi. 2009. "3D seismic for the deep exploration of the Travale geothermal field (Italy): I-GET project results". In *Geothermal Resources Council Annual Meeting*.

Casini, M., S. Ciuffi, A. Fiordelisi, A. Mazzotti, and E. Stucchi. 2010. "Results of a 3D seismic survey at the Travale (Italy) test site". *Geothermics* 39 (1): 4–12.

Chen, Q., and S. Sidney. 1997. "Seismic attribute technology for reservoir forecasting and monitoring". *The Leading Edge* 16 (5): 445–448.

Chopra, P., and D. Wyborn. 2003. "Australia's first hot dry rock geothermal energy extraction project is up and running in granite beneath the Cooper Basin, NE South Australia". In *Proceedings of the Ishihara Symposium: Granites and Associated Metallogenesis*, vol. 43.

Chopra, S., and K. Marfurt. 2005. "Seismic attributes—A historical perspective". *Geophysics* 70 (5): 3SO–28SO.

Clowes, R., A. Green, C. Yorath, E. Kanasewich, G. West, and G. Garland. 1984. "LITHOPROBE—a national program for studying the third dimension of geology". *Journal of the Canadian Society of Exploration Geophysicists* 20:23–39.

Cook, F. A., D. S. Albaugh, L. D. Brown, S. Kaufman, J. E. Oliver, and R. D. Hatcher. 1979. "Thin-skinned tectonics in the crystalline southern Appalachians; COCORP seismic-reflection profiling of the Blue Ridge and Piedmont". *Geology* 7 (12): 563–567.

Cosma, C., P. Heikkinen, and J. Keskinen. 2003. "Multiazimuth VSP for rock characterization of deep nuclear waste disposal sites in Finland". In *Hardrock seismic exploration*, 207–226. Society of Exploration Geophysicists.

Cosma, C., O. Olsson, J. Keskinen, and P. Heikkinen. 2001. "Seismic characterization of fracturing at the Äspö Hard Rock Laboratory, Sweden, from the kilometer scale to the meter scale". *International Journal of Rock Mechanics and Mining Sciences* 38 (6): 859–865.

Crampin, S. 1985. "Evaluation of anisotropy by shear-wave splitting". *Geophysics* 50 (1): 142–152.

Crampin, S. 1981. "A review of wave motion in anisotropic and cracked elastic-media". *Wave motion* 3 (4): 343–391.

Dankbaar, J. 1985. "Separation of P-and S-waves". *Geophysical Prospecting* 33 (7): 970–986.

Dehghannejad, M., C. Juhlin, A. Malehmir, P. Skyttä, and P. Weihed. 2010. "Reflection seismic imaging of the upper crust in the Kristineberg mining area, northern Sweden". *Journal of Applied Geophysics* 71 (4): 125–136.

Dessa, J.-X., S. Operto, S. Kodaira, A. Nakanishi, G. Pascal, J. Virieux, and Y. Kaneda. 2004. "Multiscale seismic imaging of the eastern Nankai trough by full waveform inversion". *Geophysical Research Letters* 31 (18).

Dorn, G. A. 1998. "Modern 3-D seismic interpretation". *The Leading Edge* 17 (9): 1262–1262.

Drummond, B., A. Owen, J. Jackson, B. Goleby, and S. Sheard. 2003. "Seismic-Reflection imaging of the environment around the Mount Isa Orebodies, Northern Australia: A case study". In *Hardrock seismic exploration*, 127–138. Society of Exploration Geophysicists.

Duchane, D., and D. Brown. 2002. "Hot dry rock (HDR) geothermal energy research and development at Fenton Hill, New Mexico". *Geo-Heat Centre Quarterly Bulletin* 23 (4): 13–19.

Eaton, D. W., B. Milkereit, and M. H. Salisbury. 2003. *Hardrock seismic exploration*. Society of Exploration Geophysicists.

Emsley, S., P. Shiner, N. Enescu, A. Beccacini, and C. Cosma. 2007. "Using VSP surveys to bridge the scale gap between well and seismic data". *Geological Society, London, Special Publications* 270 (1): 83–91.

Fichtner, A., B. Kennett, H. Igel, and H. Bunge. 2008. "Theoretical background for continental-and global-scale full-waveform inversion in the time–frequency domain". *Geophysical Journal International* 175 (2): 665–685.

Fichtner, A. 2011. "Introduction to Iterative Non-linear Minimisation". In *Full Seismic Waveform Modelling and Inversion*, 113–140. Springer.

Friðleifsson, G., H. Ármannsson, Á. Guðmundsson, K. Árnason, A. Mortensen, B. Pálsson, and G. Einarsson. 2014. "Site selection for the well IDDP-1 at Krafla". *Geothermics* 49:9–15.

Fridleifsson, G. O., and W. A. Elders. 2005. "The Iceland Deep Drilling Project: a search for deep unconventional geothermal resources". *Geothermics* 34 (3): 269–285.

Fridleifsson, I. B., R. Bertani, E. Huenges, J. W. Lund, A. Ragnarsson, L. Rybach, et al. 2008. "The possible role and contribution of geothermal energy to the mitigation of climate change". In *IPCC scoping meeting on renewable energy sources, proceedings, Luebeck, Germany*, 20:59–80. 25. Citeseer.

Gaiser, J. 2016. *3C Seismic and VSP: Converted waves and vector wavefield applications*. Society of Exploration Geophysicists.

Genter, A., K. Evans, N. Cuenot, D. Fritsch, and B. Sanjuan. 2010. "Contribution of the exploration of deep crystalline fractured reservoir of Soultz to the knowledge of enhanced geothermal systems (EGS)". *Comptes Rendus Geoscience* 342 (7): 502–516.

Goleby, B., B. Drummond, A. Owen, A. Yeates, J. Jackson, C. Swager, and P. Upton. 1997. "Structurally controlled mineralization in Australia—How seismic profiling helps finding minerals: Recent case histories". In *Proceedings of Exploration*, 97:409–420.

Granli, J. R., B. Arntsen, A. Sollid, and E. Hilde. 1999. "Imaging through gas-filled sediments using marine shear-wave data". *Geophysics* 64 (3): 668–677.

Green, A., and J. Mair. 1983. "Subhorizontal fractures in a granitic pluton: Their detection and implications for radioactive waste disposal". *Geophysics* 48 (11): 1428–1449.

Greenhalgh, S., I. Mason, E. Lucas, D. Pant, and R. Eames. 1990. "Controlled direction reception filtering of P-and S-waves in τ-p space". *Geophysical Journal International* 100 (2): 221–234.

Greenhalgh, S., and E. Manukyan. 2013. "Seismic reflection for hardrock mineral exploration: Lessons from numerical modeling". *Journal of Environmental and Engineering Geophysics* 18 (4).

Gulati, J. S., and R. R. Stewart. 2013. "Overview and introduction to this special section: 3D VSP". *The Leading Edge* 32 (10): 1234–1236.

Hardage, B. A. 2000. *Vertical seismic profiling*. Handbook of Geophysical Exploration, Seismic Exploration, 14, Pergamon.

Hardage, B. A., M. V. DeAngelo, P. E. Murray, and D. Sava. 2011. *Multicomponent seismic technology*. Society of Exploration Geophysicists.

Hearn, S., and N. Hendrick. 1999. "A review of single-station time-domain polarisation analysis techniques". *Journal of Seismic Exploration* 8 (2): 181–202.

Heincke, B., A. G. Green, J. Van Der Kruk, and H. Willenberg. 2006. "Semblance-based topographic migration (SBTM): A method for identifying fracture zones in 3D georadar data". *Near Surface Geophysics* 4 (2): 79–88.

Hloušek, F., O. Hellwig, and S. Buske. 2015. "Three-dimensional focused seismic imaging for geothermal exploration in crystalline rock near Schneeberg, Germany". *Geophysical Prospecting* 63 (4): 999–1014.

Huenges, E., and P. Ledru. 2011. *Geothermal energy systems: exploration, development, and utilization*. John Wiley & Sons.

Husen, S., and E. Kissling. 2001. "Local earthquake tomography between rays and waves: fat ray tomography". *Physics of the earth and Planetary Interiors* 123 (2): 127–147.

Jackson, G., I. Mason, and D. Lee. 1991. "Multicomponent common-receiver gather migration of single-level walk-away seismic profiles". *Geophysical Prospecting* 39 (8): 1015–1029.

Jäger, R., J. Mann, G. Höcht, and P. Hubral. 2001. "Common-reflection-surface stack: Image and attributes". *Geophysics* 66 (1): 97–109.

Jordi, C., C. Schmelzbach, and S. Greenhalgh. 2016. "Frequency-dependent traveltime tomography using fat rays: Application to near-surface seismic imaging". *Journal of Applied Geophysics* 131:202–213.

Juhlin, C. 1990. "Seismic attenuation, shear wave anisotropy and some aspect of fracturing in the crystalline rock of the Siljan Ring area, central Sweden". PhD thesis, Acta Universitatis Upsaliensis.

Juhlin, C., M. Friberg, H. Echtler, T. Hismatulin, A. Rybalka, A. Green, and J. Ansorge. 1998. "Crustal structure of the Middle Urals: Results from the (ESRU) Europrobe seismic reflection profiling in the Urals experiments". *Tectonics* 17 (5): 710–725.

Juhlin, C., and H. Palm. 2003. "Experiences from Shallow Reflection Seismics over Granitic Rocks in Sweden". In *Hardrock seismic exploration*, 93–109. Society of Exploration Geophysicists.

Kaieda, H., H. Ito, K. Kiho, K. Suzuki, H. Suenaga, and K. Shin. 2005. "Review of the Ogachi HDR project in Japan". In *Proceedings of the world geothermal congress*.

Kuriyagawa, M., and N. Tenma. 1999. "Development of hot dry rock technology at the Hijiori test site". *Geothermics* 28 (4): 627–636.

Kuzmiski, R., R. Charters, and M. Galbraith. 2008. "Processing considerations for 3D VSP". *First Break* 26 (7).

Lanz, E., D. E. Boerner, H. Maurer, and A. Green. 1998. "Landfill delineation and characterization using electrical, electromagnetic and magnetic methods". *Journal of Environmental and Engineering Geophysics* 3 (4): 185–196.

Leaney, W. S. 2008. "Polar anisotropy from walkway VSPs". *The Leading Edge* 27 (10): 1242–1250.

Lewis, C., T. L. Davis, and C. Vuillermoz. 1991. "Three-dimensional multicomponent imaging of reservoir heterogeneity, Silo Field, Wyoming". *Geophysics* 56 (12): 2048–2056.

Li, X.-Y., and M. C. Mueller. 1997. "Case studies of multicomponent seismic data for fracture characterization: Austin Chalk examples". In *Carbonate seismology*, 337–372. Society of Exploration Geophysicists.

Lumley, D. 2001. "Time-lapse seismic reservoir monitoring". *Geophysics* 66 (1): 50–53.

Lumley, D. 2010. "4D seismic monitoring of CO 2 sequestration". *The Leading Edge* 29 (2): 150–155.

Lund, J. W., L. Bjelm, G. Bloomquist, and A. K. Mortensen. 2008. "Characteristics, development and utilization of geothermal resources-a Nordic perspective". *Episodes* 31 (1): 140–147.

Luo, M., and B. J. Evans. 2004. "An amplitude-based multiazimuthal approach to mapping fractures using P-wave 3D seismic data". *Geophysics* 69 (3): 690–698.

Lüschen, E., S. Görne, H. Hartmann, R. Thomas, and R. Schulz. 2015. "3D seismic survey for geothermal exploration in crystalline rocks in Saxony, Germany". *Geophysical Prospecting* 63 (4): 975–989.

Lüschen, E., M. Wolfgramm, T. Fritzer, M. Dussel, R. Thomas, and R. Schulz. 2014. "3D seismic survey explores geothermal targets for reservoir characterization at Unterhaching, Munich, Germany". *Geothermics* 50:167–179.

MacBeth, C., H. Jakubowicz, W. Kirk, K. Li, and F. Ohlsen. 1999. "Fracture-related amplitude variations with offset and azimuth in marine seismic data". *First Break* 17:13–26.

Magotra, N., N. Ahmed, and E. Chael. 1987. "Seismic event detection and source location using single-station (three-component) data". *Bulletin of the Seismological Society of America* 77 (3): 958–971.

Majer, E., T. V. McEvilly, F. Eastwood, and L. Myer. 1988. "Fracture detection using P-wave and S-wave vertical seismic profiling at The Geysers". *Geophysics* 53 (1): 76–84.

Malehmir, A., R. Durrheim, G. Bellefleur, M. Urosevic, C. Juhlin, D. J. White, B. Milkereit, and G. Campbell. 2012a. "Seismic methods in mineral exploration and mine planning: A general overview of past and present case histories and a look into the future". *Geophysics* 77 (5): WC173–WC190.

Malehmir, A., C. Juhlin, C. Wijns, M. Urosevic, P. Valasti, and E. Koivisto. 2012b. "3D reflection seismic imaging for open-pit mine planning and deep exploration in the Kevitsa Ni-Cu-PGE deposit, northern Finland". *Geophysics*.

Malehmir, A., C. Schmelzbach, E. Bongajum, G. Bellefleur, C. Juhlin, and A. Tryggvason. 2009. "3D constraints on a possible deep> 2.5 km massive sulphide mineralization from 2D crooked-line seismic reflection data in the Kristineberg mining area, northern Sweden". *Tectonophysics* 479 (3): 223–240.

Mallick, S., K. L. Craft, L. J. Meister, and R. E. Chambers. 1998. "Determination of the principal directions of azimuthal anisotropy from P-wave seismic data". *Geophysics* 63 (2): 692–706.

Manukyan, E., S. Latzel, H. Maurer, S. Marelli, and S. A. Greenhalgh. 2012. "Exploitation of data-information content in elastic-waveform inversions". *Geophysics* 77 (2): R105–R115.

Marelli, S., H. Maurer, and E. Manukyan. 2012. "Validity of the acoustic approximation in full-waveform seismic crosshole tomography". *Geophysics* 77 (3): R129–R139.

Matsushima, J., and Y. Okubo. 2003. "Rheological implications of the strong seismic reflector in the Kakkonda geothermal field, Japan". *Tectonophysics* 371 (1): 141–152.

Matsushima, J., T. Yokota, Y. Okubo, S. Rokugawa, K. Tanaka, T. Tsuchiya, N. Narita, and K. Tani. 2004. "Repeated seismic reflection measurements in the Kakkonda geothermal field". *Journal of volcanology and geothermal research* 129 (4): 343–356.

Maurer, H., S. Greenhalgh, and S. Latzel. 2009. "Frequency and spatial sampling strategies for crosshole seismic waveform spectral inversion experiments". *Geophysics* 74 (6): WCC79–WCC89.

Melanson, D., D. White, C. Samson, G. Bellefleur, E. Schetselaar, and D. Schmitt. 2015. "Mode-converted volcanogenic massive sulphide ore lens reflections in vertical seismic profiles from Flin Flon, Manitoba, Canada". *Geophysical Prospecting* 63 (4): 849–860.

Milkereit, B., and D. Eaton. 1998. "Imaging and interpreting the shallow crystalline crust". *Tectonophysics* 286 (1): 5–18.

Milkereit, B., D. Eaton, J. Wu, G. Perron, and M. Salisbury. 1996. "Seismic Imaging of Massive Sulfide Deposits: Part II. Reflection Seismic Profiling". *Economic Geology* 91 (1): 829–834.

Milkereit, B., A. Green, J. Wu, D. White, and E. Adam. 1994. "Integrated seismic and borehole geophysical study of the Sudbury Igneous Complex". *Geophysical Research Letters* 21 (10): 931–934.

Mora, P. 1987. "Nonlinear two-dimensional elastic inversion of multioffset seismic data". *Geophysics* 52 (9): 1211–1228.

Mueller, M. C. 1991. "Prediction of lateral variability in fracture intensity using multicomponent shear-wave surface seismic as a precursor to horizontal drilling in the Austin Chalk". *Geophysical Journal International* 107 (3): 409–415.

Nakagome, O., T. Uchida, and T. Horikoshi. 1998. "Seismic reflection and VSP in the Kakkonda geothermal field, Japan: Fractured reservoir characterization". *Geothermics* 27 (5): 535–552.

Ogiesoba, O., and B. Hart. 2009. "Fault imaging in hydrothermal dolomite reservoirs: A case study". *Geophysics* 74 (3): B71–B82.

Operto, S., C. Ravaut, L. Improta, J. Virieux, A. Herrero, and P. Dell'Aversana. 2004. "Quantitative imaging of complex structures from dense wide-aperture seismic data by multiscale traveltime and waveform inversions: a case study". *Geophysical prospecting* 52 (6): 625–651.

Pazheri, F., M. Othman, and N. Malik. 2014. "A review on global renewable electricity scenario". *Renewable and Sustainable Energy Reviews* 31:835–845.

Perelberg, A. I., and S. C. Hornbostel. 1994. "Applications of seismic polarization analysis". *Geophysics* 59 (1): 119–130.

Perron, G., D. Eaton, B. Elliot, and D. Schmitt. 2003. "Application of downhole seismic imaging to map near-vertical structures: Normétal (Abitibi Greenstone Belt), Québec". In *Hardrock seismic exploration*, 194–206. Society of Exploration Geophysicists.

Place, J., M. Diraison, C. Naville, Y. Géraud, M. Schaming, and C. Dezayes. 2010. "Decoupling of deformation in the Upper Rhine Graben sediments. Seismic reflection and diffraction on 3-component Vertical Seismic Profiling (Soultz-sous-Forêts area)". *Comptes Rendus Geoscience* 342 (7): 575–586.

Place, J., J. Sausse, J.-M. Marthelot, M. Diraison, Y. Géraud, and C. Naville. 2011. "3-D mapping of permeable structures affecting a deep granite basement using isotropic 3C VSP data". *Geophysical Journal International* 186 (1): 245–263.

Plessix, R.-E. 2008. "Introduction: Towards a full waveform inversion". *Geophysical Prospecting* 56 (6): 761–763.

Porro, C., A. Esposito, C. Augustine, and B. Roberts. 2012. "An estimate of the geothermal energy resource in the major sedimentary basins in the United States". In *Geothermal Resources Council Transactions, Geothermal Resources Council 2012 Annual Meeting*, 1359–1369.

Pratt, R. G. 1999. "Seismic waveform inversion in the frequency domain, Part 1: Theory and verification in a physical scale model". *Geophysics* 64 (3): 888–901.

Pratt, R. G., and N. R. Goulty. 1991. "Combining wave-equation imaging with traveltime tomography to form high-resolution images from crosshole data". *Geophysics* 56 (2): 208–224.

Pratt, R. G., and M. Worthington. 1990. "Inverse theory applied to multi-source cross-hole tomography. Part 1: Acoustic wave-equation method". *Geophysical prospecting* 38 (3): 287–310.

Pussak, M., K. Bauer, M. Stiller, and W. Bujakowski. 2014. "Improved 3D seismic attribute mapping by CRS stacking instead of NMO stacking: Application to a geothermal reservoir in the Polish Basin". *Journal of Applied Geophysics* 103:186–198.

Rabbel, W., T. Beilecke, T. Bohlen, D. Fischer, A. Frank, J. Hasenclever, G. Borm, J. Kück, K. Bram, G. Druivenga, et al. 2004. "Superdeep vertical seismic profiling at the KTB deep drill hole (Germany): Seismic close-up view of a major thrust zone down to 8.5 km depth". *Journal of Geophysical Research: Solid Earth* 109 (B9).

Rawlinson, N., and M. Sambridge. 2003. "Seismic traveltime tomography of the crust and lithosphere". *Advances in Geophysics* 46:81–199.

Reiser, F., C. Schmelzbach, D. Sollberger, H. Maurer, S. Greenhalgh, S. Planke, F. Kästner, Ó. Flóvenz, R. Giese, S. Halldórsdóttir, and G. Hersir. 2018. *Imaging the high-temperature geothermal field at Krafla using vertical seismic profiling*. Submitted to Journal of Volcanology and Geothermal Research.

Reiser, F., C. Schmelzbach, H. Maurer, S. Greenhalgh, and O. Hellwig. 2017. "Optimizing the design of vertical seismic profiling (VSP) for imaging fracture zones over hardrock basement geothermal environments". *Journal of Applied Geophysics* 139:25–35.

Rial, J. A., M. Elkibbi, and M. Yang. 2005. "Shear-wave splitting as a tool for the characterization of geothermal fractured reservoirs: Lessons learned". *Geothermics* 34 (3): 365–385.

Riedel, M., C. Dutsch, C. Alexandrakis, I. Dini, S. Ciuffi, and S. Buske. 2015. "Seismic depth imaging of a geothermal system in Southern Tuscany". *Geophysical Prospecting* 63 (4): 957–974.

Rüger, A. 1997. "P-wave reflection coefficients for transversely isotropic models with vertical and horizontal axis of symmetry". *Geophysics* 62 (3): 713–722.

Rybach, L. 2014. "Geothermal power growth 1995–2013—A comparison with other renewables". *Energies* 7 (8): 4802–4812.

Salisbury, M. H., C. W. Harvey, and L. Matthews. 2007. "The acoustic properties of ores and host rocks in hardrock terranes". In *Hardrock seismic exploration*, 9–19. Society of Exploration Geophysicists.

Schellschmidt, R., B. Sanner, S. Pester, and R. Schulz. 2010. "Geothermal energy use in Germany In: Proceedings of the World Geothermal Congress". *Bali, Indonesia*.

Schmelzbach, C., S. Greenhalgh, F. Reiser, J.-F. Girard, F. Bretaudeau, L. Capar, and A. Bitri. 2016. "Advanced seismic processing/imaging techniques and their potential for geothermal exploration". *Interpretation* 4 (4): SR1–SR18.

Schmelzbach, C., C. Juhlin, R. Carbonell, and J. F. Simancas. 2007. "Prestack and poststack migration of crooked-line seismic reflection data: A case study from the South Portuguese Zone fold belt, southwestern Iberia". *Geophysics* 72 (2): B9–B18.

Schmelzbach, C., J. F. Simancas, C. Juhlin, and R. Carbonell. 2008. "Seismic reflection imaging over the South Portuguese Zone fold-and-thrust belt, SW Iberia". *Journal of Geophysical Research: Solid Earth* 113 (B8).

Schreiter, L., F. Hloušek, O. Hellwig, and S. Buske. 2015. "Characterization of seismic reflections from faults in a crystalline environment, Schneeberg, Germany". *Geophysical Prospecting* 63 (4): 1015–1032.

Schwarz, B., and D. Gajewski. 2017. "Accessing the diffracted wavefield by coherent subtraction". *Geophysical Journal International* 211 (1): 45–49.

Sears, T. J., S. Singh, and P. Barton. 2008. "Elastic full waveform inversion of multi-component OBC seismic data". *Geophysical Prospecting* 56 (6): 843–862.

Shipp, R., and S. Singh. 2002. "Two-dimensional full wavefield inversion of wide-aperture marine seismic streamer data". *Geophysical Journal International* 151 (2): 325–344.

Shortall, R., B. Davidsdottir, and G. Axelsson. 2015. "Geothermal energy for sustainable development: A review of sustainability impacts and assessment frameworks". *Renewable and sustainable energy reviews* 44:391–406.

Sirgue, L., O. Barkved, J. Van Gestel, O. Askim, and J. Kommedal. 2009. "3D waveform inversion on Valhall wide-azimuth OBC". In *71st EAGE Conference and Exhibition incorporating SPE EUROPEC 2009*.

Sirgue, L., and R. G. Pratt. 2004. "Efficient waveform inversion and imaging: A strategy for selecting temporal frequencies". *Geophysics* 69 (1): 231–248.

Sollberger, D. 2013. *Multicomponent Seismic Processing for Coherent Noise Suppression and Arrival Identification*. Master Thesis, ETH Zurich, Switzerland.

Stewart, R. R., J. E. Gaiser, R. J. Brown, and D. C. Lawton. 2003. "Converted-wave seismic exploration: Applications". *Geophysics* 68 (1): 40–57.

Stewart, R., J. E. Gaiser, R. J. Brown, and D. C. Lawton. 2002. "Converted-wave seismic exploration: Methods". *Geophysics* 67 (5): 1348–1363.

Stober, I., and K. Bucher. 2013. "Geothermal energy". *Germany: Springer-Verlag Berlin Heidelberg. doi* 10:978–3.

Taner, M. T., J. S. Schuelke, R. O'Doherty, and E. Baysal. 1994. "Seismic attributes revisited". In *SEG Technical Program Expanded Abstracts 1994,* 1104–1106. Society of Exploration Geophysicists.

Tang, C., J. A. Rial, and J. M. Lees. 2008. "Seismic imaging of the geothermal field at Krafla, Iceland using shear-wave splitting". *Journal of Volcanology and Geothermal Research* 176 (2): 315–324.

Tarantola, A. 1984. "Inversion of seismic reflection data in the acoustic approximation". *Geophysics* 49 (8): 1259–1266.

Tester, J. W., B. J. Anderson, A. S. Batchelor, D. D. Blackwell, R. DiPippo, E. M. Drake, J. Garnish, B. Livesay, M. C. Moore, K. Nichols, et al. 2007. "Impact of enhanced geothermal systems on US energy supply in the twenty-first century". *Philosophical Transactions of the Royal Society of London A: Mathematical, Physical and Engineering Sciences* 365 (1853): 1057–1094.

Thomas, R., and R. Schulz. 2007. "Facies differentiation of the Malm by interpretation of reflection seismic profiles and a moving source VSP Experiment". In *Proceedings of the European Geothermal Congress*.

Thomsen, L. 1988. "Reflection seismology over azimuthally anisotropic media". *Geophysics* 53 (3): 304–313.

Vasco, D. W., J. E. Peterson Jr, and E. L. Majer. 1995. "Beyond ray tomography: Wavepaths and Fresnel volumes". *Geophysics* 60 (6): 1790–1804.

Vigh, D., K. Jiao, D. Watts, and D. Sun. 2014. "Elastic full-waveform inversion application using multicomponent measurements of seismic data collection". *Geophysics*.

Virieux, J., and S. Operto. 2009. "An overview of full-waveform inversion in exploration geophysics". *Geophysics* 74 (6): WCC1–WCC26.

Vlahovic, G., M. Elkibbi, and J. Rial. 2003. "Shear-wave splitting and reservoir crack characterization: the Coso geothermal field". *Journal of volcanology and geothermal research* 120 (1): 123–140.

Von Hartmann, H., H. Buness, C. M. Krawczyk, and R. Schulz. 2012. "3-D seismic analysis of a carbonate platform in the Molasse Basin-reef distribution and internal separation with seismic attributes". *Tectonophysics* 572:16–25.

Watanabe, T., T. Matsuoka, and Y. Ashida. 1999. "Seismic traveltime tomography using Fresnel volume approach". In *SEG Technical Program Expanded Abstracts 1999,* 1402–1405. Society of Exploration Geophysicists.

Wei, S., M. DeAngelo, and B. Hardage. 2014a. "Interpretation of multicomponent seismic data across Wister geothermal field, Imperial Valley, California". *Interpretation*.

Wei, S., M. V. DeAngelo, and B. A. Hardage. 2014b. "Advantages of joint interpretation of PP and P-SV seismic data in geothermal exploration". *Interpretation*.

Younger, P. L. 2015. *Geothermal energy: delivering on the global potential*.

Zelt, C. A., and P. J. Barton. 1998. "Three-dimensional seismic refraction tomography: A comparison of two methods applied to data from the Faeroe Basin". *Journal of Geophysical Research: Solid Earth* 103 (B4): 7187–7210.

Zhang, F., C. Juhlin, M. Ivandic, and S. Lüth. 2013. "Application of seismic full waveform inversion to monitor CO2 injection: Modelling and a real data example from the Ketzin site, Germany". *Geophysical Prospecting* 61 (s1): 284–299.

<div align="right">

2

</div>

Optimizing the design of vertical seismic profiling (VSP) for imaging fracture zones over hardrock basement geothermal environments

Contents

Abstract

A primary focus of geothermal seismic imaging is to map dipping faults and fracture zones that control rock permeability and fluid flow. Vertical seismic profiling (VSP) is therefore a most valuable means to image the immediate surroundings of an existing borehole to guide, for example, the placing of new boreholes to optimize production from known faults and fractures. We simulated 2D and 3D acoustic synthetic seismic data and processed it through to pre-stack depth migration to optimize VSP survey layouts for mapping moderately to steeply dipping fracture zones within possible basement geothermal reservoirs. Our VSP survey optimization procedure for sequentially selecting source locations to define the area where source points are best located for optimal imaging makes use of a cross-correlation statistic, by which a subset of migrated shot gathers is compared with a target or reference image from a comprehensive set of source gathers. In geothermal exploration at established sites, it is reasonable to assume that sufficient à priori information is available to construct such a target image. We generally obtained good results with a relatively small number of optimally chosen source positions distributed over an ideal source location area for different fracture zone scenarios (different dips, azimuths, and distances from the surveying borehole). Adding further sources outside the optimal source area did not necessarily improve the results, but rather resulted in image distortions. It was found that fracture zones located at borehole-receiver depths and laterally offset from the borehole by 300 m can be imaged reliably for a range of the different dips, but more source positions and large offsets between sources and the borehole are required for imaging steeply dipping interfaces. When such features cross-cut the borehole, they are particularly difficult to image. For fracture zones with different azimuths, 3D effects are observed. Far offset source positions contribute less to the image quality as fracture zone azimuth increases. Our optimization methodology is best suited for designing future field surveys with a favorable benefit-cost ratio in areas with significant à priori knowledge. Moreover, our optimization workflow is valuable for selecting useful subsets of acquired data for optimum target-oriented processing.

2.1 Introduction

Geothermal energy is a promising sustainable energy resource, but it has not yet reached its full potential. Generally, the distinction can be made between two different types of geothermal systems, namely hydrothermal systems and petrothermal systems (the latter being more recently referred to as enhanced geothermal systems or EGS). Hydrothermal systems are characterized by high heat flow at shallow to moderate depth, a naturally occurring permeable layer and an appreciable amount of fluid that can circulate in the subsurface. The water is heated through direct contact as well as by convective transport from the hot crustal rocks and the high enthalpy fluids (liquid and steam) can then be extracted to produce electricity. Examples of operational hydrothermal systems are Lardarello in Italy (Brogi et al. (2003)), several reservoirs in Iceland (Arnórsson (1995)) and Unterhaching in Germany (Wolfgramm et al. (2007)).

In this study we will focus on EGS but our workflow can readily be adopted to hydrothermal systems as well. EGS have their maximum potential in crystalline rock at depths of at least a few kilometers, where temperatures are sufficiently high. Either a pre-existing fault system exists and needs to have its permeability enhanced or a fracture network is created by artificial means (engineered fracking)

to circulate hot fluid that can then be extracted for electricity production (e.g. Barbier (2002)). Therefore, a primary focus in hardrock geothermal exploration is to map faults and fracture zones, which control permeability and fluid flow.

Geophysical exploration of EGS systems often includes magnetotelluric investigations, potential field measurements and local earthquake tomography (Geiermann and Schill (2010), Biasi and Preston (2011)). These methods are suitable for resolving gross structures, but they offer only limited, low resolution information on individual fracture zones. A useful option for obtaining high-resolution images of such features is controlled-source seismic surveying (reflection and refraction imaging), but compared with oil and gas exploration, this has been only sparingly applied for geothermal exploration (e.g., Schmelzbach et al. (2016)).

Controlled-source seismic methods can generally be subdivided according to their recording geometry into three surveying configurations: surface-based, surface-to-borehole and borehole-to-borehole (or crosswell). In recent years, several surface-based seismic studies in geothermal areas have been performed to image and characterize fracture zones over hardrock environments. For example, Ahmed et al. (2015) and Hloušek et al. (2015) investigated the fault system in a hardrock environment near Schneeberg, western Erzgebirge (Germany) with 3D seismic data. They showed that even relatively steeply dipping fracture zones can be imaged with 3D seismic data. Schreiter et al. (2015) further characterized the fault system near Schneeberg by analyzing reflection amplitudes of different faults and inferred the approximate extent and velocity structure of the faults.

Despite some successes, surface-based seismic reflection imaging investigations in crystalline rocks have revealed that the task is a very challenging one for a variety of reasons (e.g. Salisbury et al. (2007)): (1) large impedance contrast between the sediments and the underlying basement, such that little energy can penetrate into the basement; (2) small impedance contrasts between lithological units within the basement and therefore low signal-to-noise ratios; (3) reflectors are of limited lateral extent due to the complex and discontinuous morphology; (4) high velocities in crystalline basement result in a loss of resolution due to relatively long wavelengths; (5) obtaining the required velocity function within basement is problematic; (6) often steeply dipping structures occur which are difficult to image without very large aperture recording arrays.

If the imaging target is spatially confined, improved results can be expected, when the area of interest can be more effectively illuminated, such as by means of crosswell transmission tomography (e.g., Niitsuma et al. (1999)) or surface-to-borehole methods (vertical seismic profiling, VSP; e.g., (Hardage (2000)). VSP data usually contain significantly higher frequencies than surface-based seismic data because receivers are placed downhole whereas shots fired on the surface, and the seismic waves travel only once through the absorbing overburden (near-surface layers), thus suffering less from frequency-dependent attenuation (e.g. Cosma et al. (2003)). Therefore, VSP imaging can be used for high resolution imaging of the lithological and other interfaces, such as fracture zones, either intersecting, beneath or offset from the well. This is especially important for mapping dipping interfaces and is critical for placing additional wells.

VSP surveys have been applied successfully in fractured carbonate reservoirs (Emsley et al. (2007)), as well as in crystalline rock for better understanding of seismic properties in the crust (Carr et al.

(1996); Rabbel et al. (2004)). They have also been used effectively in mineral exploration (Adam et al. (2003); Perron et al. (2003); Bellefleur et al. (2004)) and in siting of potential nuclear waste disposal sites (Cosma et al. (2001); Cosma et al. (2003)). A few examples exist, where VSP has been used to better characterize geothermal sites. For example, Majer et al. (1988) performed a VSP pilot study in the Geyser steam bearing geothermal field in northern California. They obtained fracture anisotropy information by analyzing shear wave splitting on the VSP dataset. In a separate study, Nakagome et al. (1998) analyzed VSP data in the Kakkonda geothermal field in Japan and concluded that the VSP data contained more detailed structural information than the surface-based seismic data. Thomas and Schulz (2007) found from their investigation a much better signal-to-noise ratio of the VSP data compared to the surface seismic data at the Unterhaching geothermal site. Several reflectors and fault systems could be mapped and interpreted in the sedimentary hydrothermal system. Place et al. (2010) and Place et al. (2011) used VSP data acquired in 1988 and 1993 to study the EGS site in Soultz-sous-Forêts. Several reflections resulting from fracture zones within granitic basement were identified in the data. Synthetic modelling was used to compare the observed reflection traveltimes with the calculated traveltimes to generate a fracture zone model of the area.

All of these studies demonstrated that VSP techniques have a considerable potential for characterizing steeply dipping fracture zones associated with EGS reservoirs in crystalline host rocks, but they also showed that it can be quite challenging to process and interpret existing VSP datasets. Tools of optimized experimental design (e.g., Maurer et al. (2010)) may allow designing cost-effective VSP surveys while taking the particularities of seismic geothermal exploration explicitly into account. Successful experimental design critically depends on à priori knowledge. At the stage in geothermal exploration when VSP surveys are considered, it is reasonable to assume that some prior knowledge about the subsurface exists from previous surface-based seismic surveys and/or existing boreholes. For example, optimized experimental design will allow for the cost-effective acquisition of target-oriented VSP's to plan the placing of additional production boreholes at already established geothermal sites.

Here, we describe a novel methodology whereby optimized field layouts can be employed for VSP recording with a favorable benefit-cost ratio. We demonstrate our workflow using realistic synthetic data because a comprehensive field dataset that would be needed to illustrate the (unrealistic) maximum best possible acquisition setup was not available to us. Initially, we employ a 2D setup for demonstrating the possibilities and limitations of the method. By means of a pre-stack depth migration algorithm we examine the fracture zone images that can be obtained using a relatively small number of suitably placed surface source positions. Then, we extend our modelling study to 3D geometries for imaging fracture zones with different azimuths.

2.2 Experimental setup

The basic idea of our experimental design approach is to define a setup including (i) a seismic velocity model that mimics the geology of the host rock, (ii) a set of fracture zones, as they might be found in the investigation area, (iii) the geometry of boreholes available and (iv) receiver positions in the borehole. Furthermore, we define a large number of locations where surface sources could be placed.
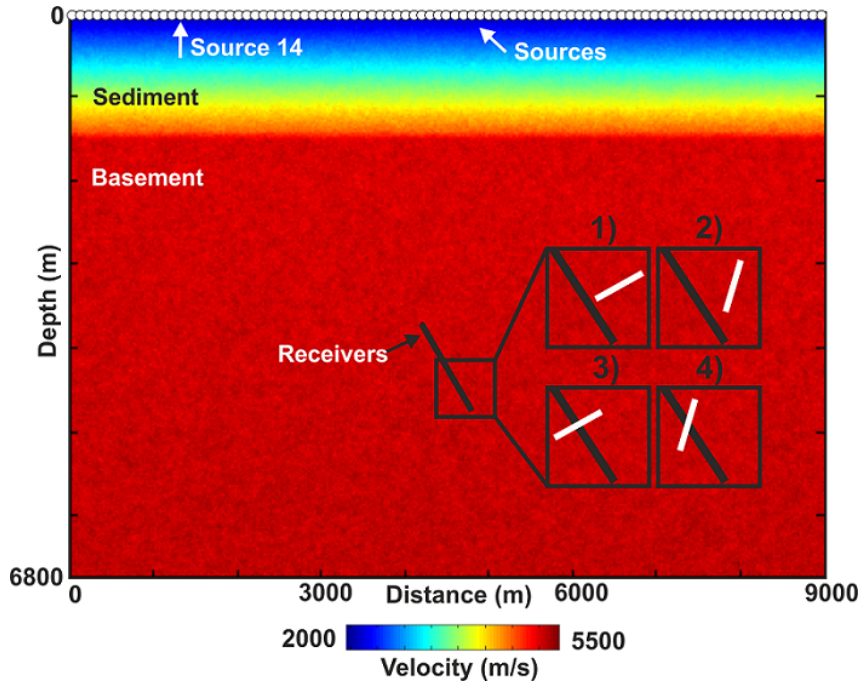
Figure 2.1: Velocity model with receivers (black) and 91 source positions at the surface (white). Insets show the different fracture zone configurations (white) used in this study.

All possible source-receiver combinations constitute a comprehensive dataset. Our experimental design procedure then identifies an optimal subset of source positions that provide subsurface images of comparable quality to those of the comprehensive dataset.

For EGS in the Alpine foreland, faults and fractures of interest will typically be located at a few kilometers depth within the crystalline basement below a thick sedimentary column. Our modelling study is inspired by the borehole geometries and geological setting of the geothermal site at Soultz-sous-Forêts (France) (Gérard et al. (2006)), but our methodology is flexible and can be applied to any other subsurface geology and borehole geometry. Most of the boreholes at Soultz-sous-Forêts are inclined within the target depth range because this increases the chance of intersecting dipping permeable zones. For our study, a borehole that is inclined at 30 °to the vertical was used, with 61 receivers placed at 20 m intervals over the depth range of 3700-4900 m (Lavadera (2013); Place et al. (2011)). Seismic data were simulated from 91 surface source positions straddling a distance of 9000 m and spaced at an interval of 100 m. The velocity model employed as well as the source and receiver geometry are illustrated in Figure 2.1.

2.2.1 Reflection point modelling and constant-velocity medium illumination maps

An advantage of VSP surveying over surface-based seismic measurements is the improved capability of VSPs to image steeply dipping reflectors (Hardage (2000)). With the motivation to study the illumination capabilities of the employed recording geometry under simplified conditions, we carried out an initial investigation to assess the potential reflector coverage (illumination) and computed the reflected wave amplitudes from a given reflector of a particular dip for each subsurface point in a homogeneous medium. We defined our target area to be located below the shallowest receiver. The reflected wave amplitudes for a given dip are calculated for each possible source-receiver pair within
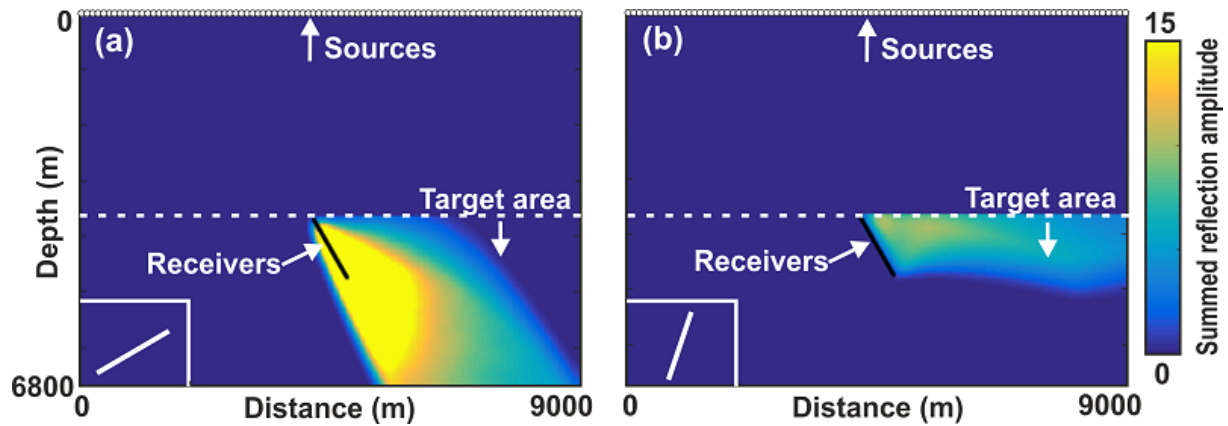
Figure 2.2: (a) Illumination map for fracture zones dipping at 30 °for the given source and receiver
positions in the target area (below the first receiver). (b) As for (a) but for fracture
zones dipping at 70 °. The dip of the fracture zone is indicated in white within the
white square at the bottom left. Note that there are considerably less specular reflection
points for the 70 °dipping fracture zone, hence indicating that it is more challenging to
map steeply dipping than gently dipping interfaces.

the target area. This illumination study was performed using a simple reflection travel time and
raypath modelling algorithm for a constant velocity medium following the approach of Schmelzbach
et al. (2007). Rays were traced for the 91 surface source positions at 100 m spacing over the 9000 m
wide model. We assumed that the reflection amplitudes depend only on spherical wavefront spread-
ing and are proportional to the inverse of the total travel time. The reflection amplitudes were
summed in 20 m x 20 m wide bins to provide a total signal-strength-dependent measure of illumi-
nation. This procedure results in amplitude-dependent illumination maps of the subsurface. Large
illumination values show subsurface areas that can be covered well with the given recording config-
uration. Hence, a higher quality image of a fracture zone with the specific dip can be expected in
these regions because the signal-to-noise ratio will be proportional to the signal level for a constant
noise background. Zero values represent areas of no specular reflection and therefore define blind
zones in this simplified scheme.

Examples of illumination maps for fracture zone dips of 30 °and 70 °(dipping towards the left and
dip measured from the horizontal) are shown in Figure 2.2a and b, respectively. It can be seen that
the given receiver configuration is well suited for imaging 30 °dipping fracture zones around the
borehole as well as below and to the right of the borehole. For a steeply dipping interface, such
as 70 °, the illuminated area shows overall lower amplitude sums compared to the gently dipping
fracture zone, since less reflection points exist for the given configuration. The illuminated area is
considerably smaller and no reflection points below or to the left of the borehole are imaged. Far
offset source positions would be required to obtain an improved subsurface coverage and higher
amplitude sums for steeply dipping interfaces.

For the given source and receiver positions it can be observed that an approximate orthogonal re-
lationship between the borehole and the fracture direction is optimal for imaging. The sparse sub-
surface illumination for the 70 °dipping fracture zone is an indication that it is more challenging to
image steeply dipping fracture zones compared to gently dipping interfaces. Additionally, it can be

observed that fracture zones dipping to the left cannot be imaged to the left of the borehole with the exception of gently dipping interfaces; they can be mapped only if they are located in the near-vicinity of the borehole.

2.2.2 Computation of synthetic VSP data

Reflection point modelling, as shown in Figure 2.2, offers a good preliminary indication of the general feasibility of mapping fracture zones, but strongly simplifying assumptions on the subsurface structure and the nature of wave propagation are made. Furthermore, possible artefacts that may arise during the processing of actual VSP data are not taken into account. To overcome these limitations, we performed a more realistic survey-design study based on acoustic synthetic seismic full waveform modelling with a 2D finite difference scheme (SOFI2D) (Bohlen et al. (2003)) and using the velocity model depicted in Figure 2.1. The background velocities increase continuously with depth, exhibiting a high vertical velocity gradient in the overlying sedimentary section down to a depth of 1.4 km and a much lower vertical velocity gradient in the underlying basement. To simulate a realistic degree of heterogeneity, stochastic velocity fluctuations that show similar characteristics as the sonic log data were superimposed (Goff and Holliger (2012)). A vertically directed source having a dominant frequency of 40 Hz was used in the simulations and the grid spacing set to 1 m.

For the survey-design study, four different fracture zones of different dips and offset positions from the borehole were considered (configurations 1 to 4 in Figure 2.1). The fracture zones, schematically shown in Figure 2.1, were assumed to have a thickness of 40 m and 15% reduced seismic velocity and density compared to the host medium. We used the studies of Juhlin and Palm (2003) and Juhlin and Stephens (2006) as guidelines in assigning velocities to the fracture zones. They observed a seismic velocity reduction of about 15% for fracture zones compared to the granitic host rock. Vertical and horizontal receiver component common-source seismic gathers for all four fracture configurations were simulated for 91 surface source positions at 100 m intervals along the 9,000 m long model. Additionally, Gaussian white noise was added to the resulting waveform data to simulate a realistic signal-to-noise ratio of about 4 based on the average first arrival energy and maximum noise level.

2.2.3 Processing sequence

We applied a seismic processing sequence on the vertical and horizontal component data for imaging the fracture zones, which consisted of geometrical spreading correction, tau-p filtering to separate the direct (downgoing) and reflected (upgoing) wavefields, the application of hand-picked top mute functions to remove any remaining direct wave energy, Kirchhoff depth migration of each recording and stacking the migrated single-source gather images (e.g., Hardage (2000)). An example source gather for fracture zone configuration 2 (indicated by source 14 in Figure 2.1), before and after the tau-p filtering for wavefield separation as well as the corresponding migrated gather, is shown in Figure 2.3. On the migrated image in Figure 2.3c a reflector (R) as well as an artefact (A) can clearly be identified. The black dashed line shows the exact location and extent of the fracture zone, which correlates well with the imaged reflector. The migrated image of the seismic data from this one source position is contaminated by an artefact (A). Furthermore, the location of the fracture zone is ambiguous, since the reflector is imaged as a cone of specific dip around the borehole and therefore
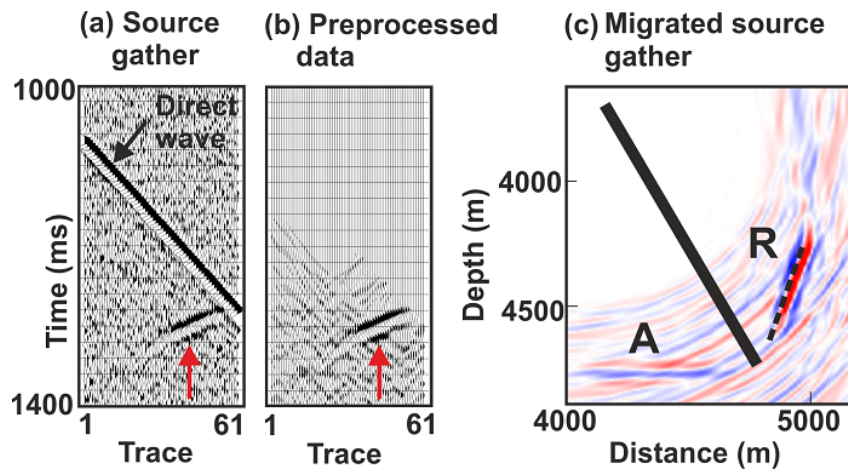
Figure 2.3: Example source gather (x-component) at the position indicated by source 14 in Figure 2.2; (a) before and (b) after pre-processing. A top mute after the first breaks was additionally applied to remove any remaining direct wave energy. The red arrow indicates the fracture zone reflection. (c) Migrated source gather of preprocessed data in (b) with the receiver locations shown in black. R indicates the reflector and A is a migration artefact.

the migration process cannot uniquely determine on which side of the borehole the reflector occurs. To overcome this ambiguity, one could analyse the polarization of the arriving wavefront to limit the image to a certain azimuth (Lüth et al. (2005)) or acquire more source positions to cancel out the artefact and reinforce the image of the fracture zone by constructive interference. Figure 2.4c shows the result of stacking the migrated recordings of all 91 source positions. Most of the artefacts have been effectively suppressed.

2.3 Method to optimize VSP survey design

The overall goal of our survey-design study is to determine the optimal survey layout for a given downhole receiver layout and assuming a particular fracture zone orientation. The working principle of our survey design procedure is illustrated in Figure 2.4 using fracture zone configuration 2 (see also Figure 2.1). First, we constructed a target image (desired optimum image) based on the results obtained when processing the comprehensive dataset (all 91 source gathers; Figure 2.4c). Since this image still contains minor artefacts that could not be removed by the processing, we applied a tapered window and extracted only that part of the migrated image as the reference solution which contained the desired features in the target image (see dashed black line Figure 2.4c enclosing the target). The goodness of any subsequently derived test image (migration result obtained from subsets of the comprehensive dataset) was quantified by the zero-lag 2D crosscorrelation coefficient of the test image with the target (or reference) image.

Apart from 2D crosscorrelation, other approaches such as root-mean-square error (RMSE) and Structural Similarity Index (SSIM) (Wang et al. (2004)) were also tested. The crosscorrelation coefficient and RMSE yielded similar results, whereas SSIM was less stable for noisy data. After careful consideration, the crosscorrelation coefficient was chosen as the measure (or benefit statistic) for the optimization process.
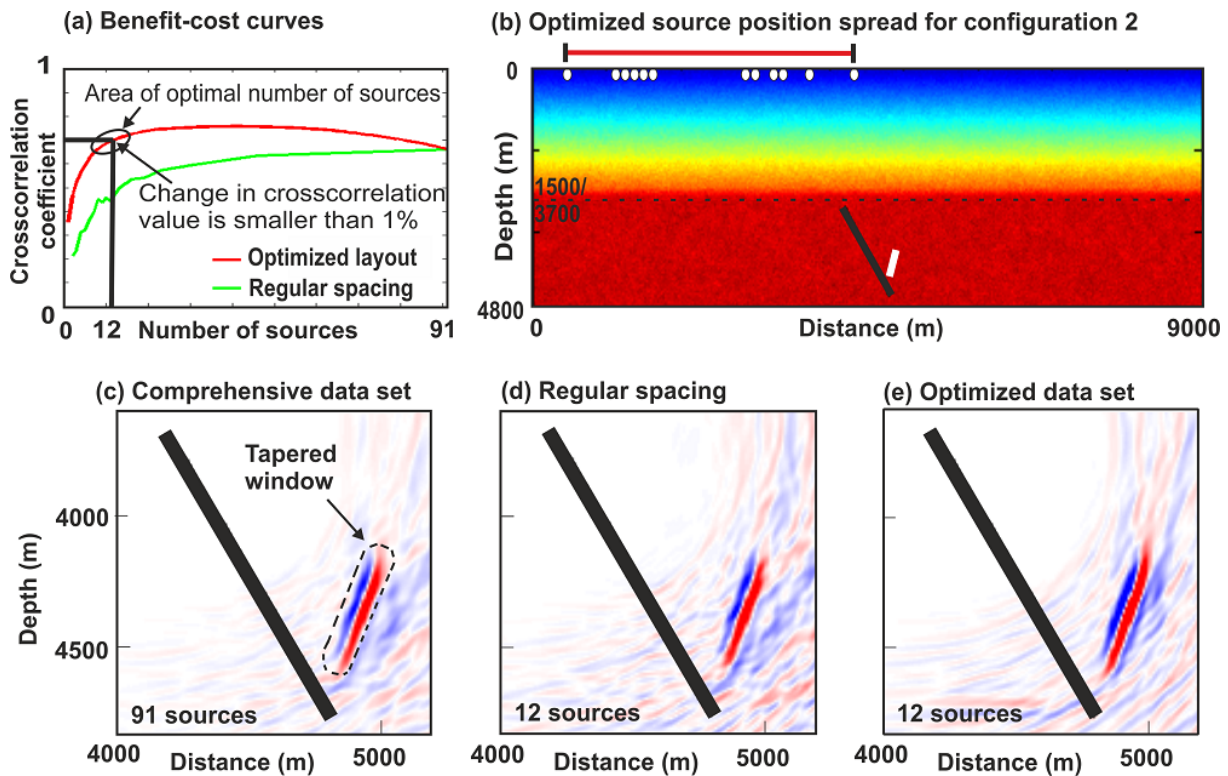
Figure 2.4: Illustration of the optimization procedure using fracture zone configuration 2 (see Figure 2.2). a) Benefit-cost curves for optimized source location design (red) and regularly spaced sources (green). (b) Locations of the optimized source positions (note that only selected depth segments of the full model (see Figure 2.2) are shown, i.e. the depth range between 1500 m and 3700 m was removed). (c) Migrated image obtained using the comprehensive dataset including all 91 sources. (d) Migrated image obtained with 12 regularly spaced sources. (e) Image obtained with 12 optimized sources (see (b) for source locations).

When optimizing the survey geometry for a particular fracture zone orientation and signal-to-noise ratio, 91 test images corresponding to 91 migrated single-source images were produced. These test images were then individually crosscorrelated with the target image (see Figure 2.4c), and the single-source image with the largest crosscorrelation coefficient was selected. Then, the most suitable add-on single-source image was determined by computing all possible stacks of two single-source images (90 possible combinations with the initially selected single-source image) and evaluating the crosscorrelation coefficients with the target image. Further single-source images were subsequently added in an equivalent manner. This allowed benefit-cost curves (benefit corresponding to the crosscorrelation coefficient, cost corresponding to the number of single-sources images) to be constructed. The benefit-cost curve does not reach a value of 1 for the image derived from the complete dataset since it is crosscorrelated with the tapered comprehensive data image.

As shown in Figure 2.4a, the benefit-cost curve rapidly increases when combining only a small number of sources, but flattens out with an ever increasing number of stacked single-source images. When the increase of the crosscorrelation coefficient from one stack to the next becomes smaller than 1%, the resulting stacked images were deemed to no longer improve significantly. Hence this point of diminishing returns defines the optimal selection of single-source images and correspond-

ing source positions. For the example of fracture zone configuration 2, the optimization procedure yielded an optimal subset size of 12 single-source images. The corresponding source positions are shown in Figure 2.4b.

The potency of our optimization method can be demonstrated by comparing the optimized source-point distributions with a regularly spaced source-point distribution, where the distance between consecutive sources is constant for the latter. As shown in Figure 2.4a, the benefit-cost curve corresponding to regularly spaced source positions (green) exhibits considerably lower crosscorrelation coefficients, and furthermore the image obtained with 12 regularly spaced sources with constant offset of 750 m (Figure 2.4d) is clearly inferior to that obtained with the optimized 12 source point image (Figure 2.4e).

We observed that the locations of the selected optimal source positions depend slightly on the realizations of the stochastic velocity fluctuations and the simulated additive noise when we used a different random-number realisation (Goff and Holliger (2012)). However, the spread of the optimized source configurations (horizontal red line in Figure 2.4b) is fairly consistent for different velocity fluctuations / noise realizations. We found that using the optimal number of sources, but with a regular spacing within the optimal source-position spread generally leads to a comparable migrated image with an only slightly lower crosscorrelation value compared to the fully optimized experiment. Hence, we will focus on the spread of the source points instead of the individual source positions in subsequent discussion.

It is also noteworthy that the optimized benefit-cost curve in Figure 2.4a decreases slightly after its maximum is reached at about 42 sources. This indicates that some single-source images in the comprehensive dataset contain no significant signal, but only noise such as migration artefacts. The artefacts mainly result from diffraction hyperbolas that could not be collapsed to their point of origin during the migration. Diffractions are only visible on a few traces on the source gathers and show very little moveout. Hence, the diffraction is not characterized well and artefacts appear after migration. The diffraction artefacts deteriorate not only the quality of the images, but also affect the resulting crosscorrelation with the target image. In other words, more data do not necessarily improve the image quality.

2.4   Results of 2D study

In the following, we summarize the results of applying our optimization procedure to a series of 2D scenarios with different fracture zone geometries (locations, dips and orientations) and varying noise levels.

2.4.1   Different fracture zone dips and distances from the borehole

We have applied our proposed survey design methodology to find optimum source configurations for different fracture zone dips (30°, 50°, 70°, 90°) as well as lateral distances between the midpoint of the fracture zone and the borehole (0 and 300 m). We will limit the presentation of the results to just the four fracture zone configurations shown in Figure 2.1 (dips of 30° and 70°, lateral distances 0 m and 300 m), although our findings are supported by the full suite of fracture models. The results
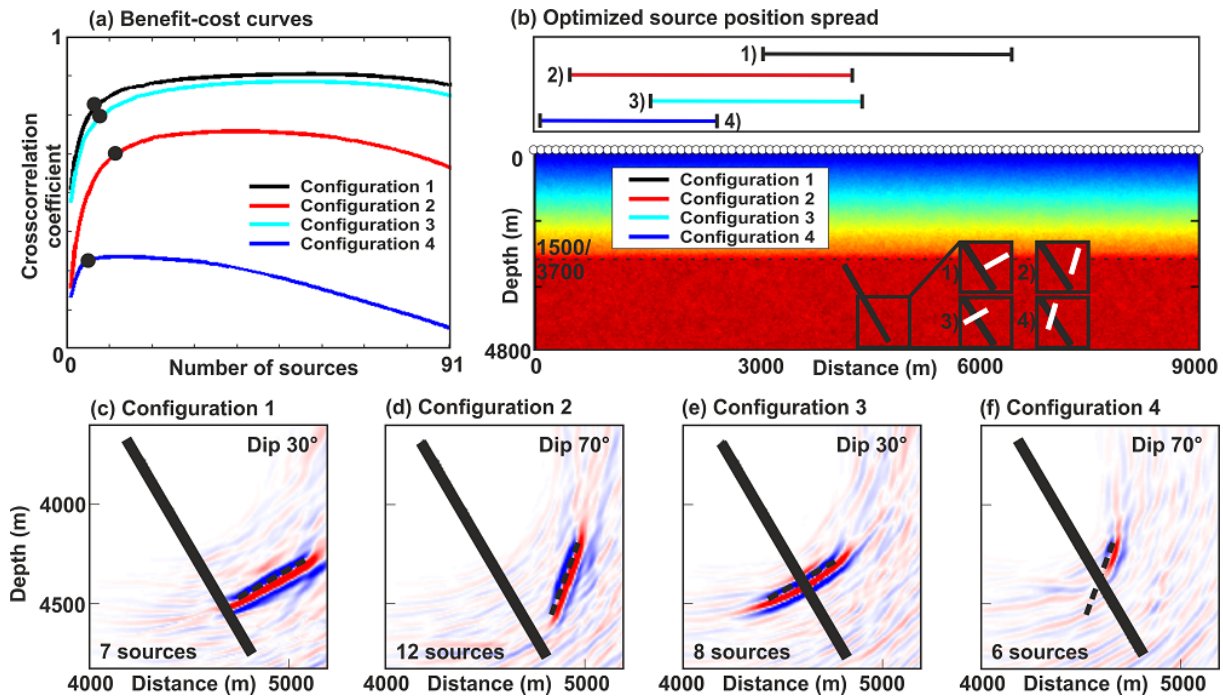
Figure 2.5: (a) Benefit-cost curves for fracture zone configurations 1 to 4 (see Figure 2.2). (b) Spread of the optimized source positions for fracture zone configurations 1 to 4 (note that only selected depth segments of the full model (see Figure 2.2) are shown, i.e. the depth range between 1500 m and 3700 m was removed). (c) to (f) Optimized images for fracture zone configurations 1 to 4, respectively.

are summarized in Figure 2.5. The clearest fracture zone images were obtained for gentle dips (configurations 1 and 3). This is not surprising, considering the higher amplitude values for the shallow gently dipping interfaces in the illumination maps shown in Figure 2.2. For the gentle dips, 7 to 8 sources are required for imaging these fracture zones reliably. The 50° dipping fracture zone can also be imaged reliably; however, more source positions are needed for the fracture zone crossing the borehole.

From the experiment one can see that more source positions are required for imaging steeply dipping targets, such as fracture zone configuration 2, because far offset sources are required that suffer more from amplitude loss due to geometrical spreading. The optimum spread of the sources depends strongly on the position of the fracture zone (Figure 2.5b). Large lateral distances between sources and receivers are required for steeply dipping interfaces, especially for steep fracture zones cross-cutting the borehole (configuration 4). These interfaces represent the most significant challenge for VSP imaging. Only a small segment of the fracture zone can be imaged and hardly any information on the dip can be retrieved (Figure 2.5f). The 90° dipping fracture zone cross-cutting the borehole can basically not be recovered at all. Only far offset source gathers contain reflection energy, whereas the other source gathers predominantly contain diffraction energy. The migration process does not manage to collapse the diffraction hyperbolas, leading to migrated images contaminated by strong artefacts. Therefore, the corresponding benefit-cost curve in Figure 2.5a (dark blue) starts decreasing already after a few sources. The migrated image using the optimal survey layout leads to a low quality

image, indicating that there is little hope to reliably image steeply dipping fracture zones that are crossing the borehole.

2.4.2 Varying signal-to-noise ratios

Different signal-to-noise ratios (S/N) of the data were tested to examine the effect of noise on the shape of the benefit-cost curves and the quality of the migrated images. Benefit-cost curves for different noise levels give indications of how the number of optimal sources must be adapted in order to obtain a migrated image that is comparable in quality to the noise-free image. Figure 2.6 shows an example of different benefit-cost curves for fracture zone configuration 2 with various S/N ratios. The number of required sources increases substantially for noisy data, e.g. 20 source positions for S/N = 2 compared to 10 for S/N = 6. The source position spread moves slightly towards smaller lateral offsets for decreasing S/N, omitting the far offset source positions that suffer more energy loss due to longer travel paths (Figure 2.6b). Hence, we can observe a trade-off between large offsets with higher illumination and near offset with lower noise levels. However, the number of sources seems to have a more pronounced effect on the quality of migrated images than the position of the spread. The migrated images for the different noise levels using the optimal number of sources are shown in Figure 2.6c-f. It can be seen that the final migrated images exhibit a comparable quality.
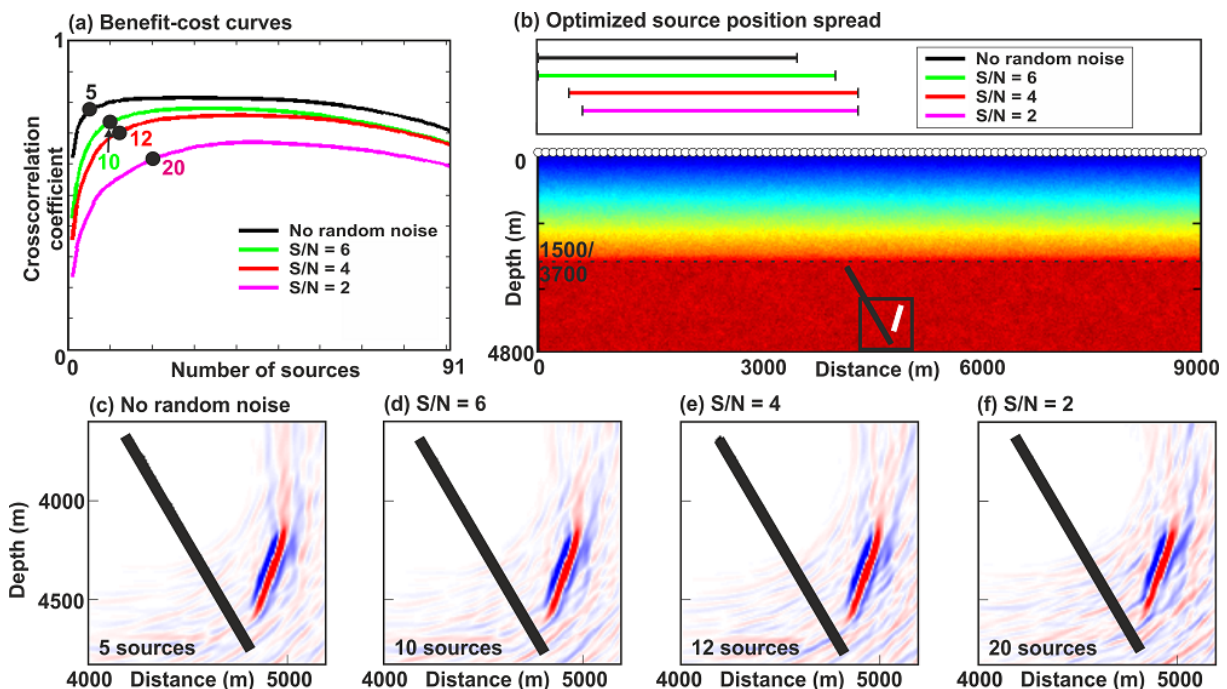
Figure 2.6: (a) Benefit-cost curves for fracture zone configuration 2 using data with different S/N ratios. (b) Spread of the optimized source positions using different S/N ratios (note that only selected depth segments of the full model (see Figure 2.2) are shown, i.e. the depth range between 1500 m and 3700 m was removed). (c) to (f) Optimized images using different S/N ratios. Note that the number of optimal sources increases substantially for decreasing S/N ratio, but comparable image quality is achieved.

2.4.3 Multiple fracture zones

In many realistic scenarios, several fracture zones may be present in the subsurface, such as in the case of Soultz. Therefore, the optimization was tested for the case of multiple interfaces with different dips to investigate if several fracture zones can be imaged reliably. For that reason, the configuration, shown in Figure 2.7a (50 °and 90 °dipping fracture zone with a lateral distance of 300 m from the borehole), was used. First, the optimal source positions based on a single fracture zone dipping with either 50 °or 90 °(Figure 2.7b) were used for the migration. Afterwards, the optimization for imaging both fracture zones together was performed. The corresponding migrated images are shown in Figure 2.7c-e.

It can be observed that the two crossing fracture zones with different dips can be imaged for all three cases. The migrated images in Figure 2.7c and e are comparable in quality and are both superior to the one in 2.7d. Since the latter is optimized only for the 90 °dipping interface, the 50 °dipping interface shows artefacts in that its depth extension is too long. The corresponding source position spread is limited to a very small area that is clearly not enough to image the 50 °dipping fracture zone reliably. The spread for the migrated image in Figure 2.7e lies somewhere in between the two other cases (Figure 2.7b). Generally, we conclude that the source position spread should not be restricted to a small area but rather cover a large distance when multiple fracture zones with different dips may be present.
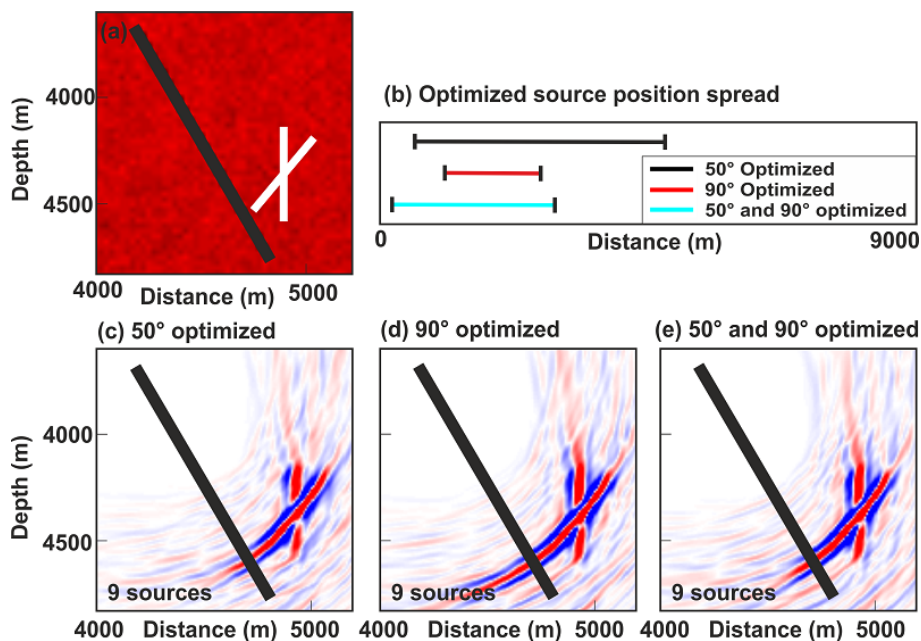
Figure 2.7: (a) Velocity model with two crossing fracture zones plotted in white. (b) Optimized source position spread. (c) to (e) Migrated images optimized for fracture zone dips of 50 °, 90 °(individual) , and 50 °and 90 °combined, respectively. The quality of the migrated image optimized for 90 °in (d) is inferior compared to (c) and (e) due to the narrow source position spread.

2.5   Results of 3D study

2.5.1   Different fracture zone azimuths

As a next step, we extended our survey-design strategy to optimize acquisition geometries for fracture zones located out of the source receiver plane to study 3D effects on 2D imaging. In the previous sections we simulated the 2D case of a fracture zone with a strike perpendicular to the source line, which is the ideal case. However, in reality, for logistical reasons, it might not be possible to acquired data perpendicular to the fracture zone strike. Hence, it is instructive to study how the survey can be optimized for fracture zones having different azimuths in order to minimize à priori known 3D effects.

In a first experiment, we model source recordings for a straight source-point line and different fracture-zone azimuths (0°, 30°, 60°, 90° from the source line), keeping constant the depth and distance of the fracture zone from the borehole. The size of the fracture zone was set to 400 m x 400 m x 40 m. A conceptual model of the survey setup for configuration 1 (azimuth 0°, which represents the ideal setup as in the 2D study) and configuration 2 (azimuth 60°) are presented in Figure 2.8b as a top-view at constant depth and in Figure 2.8c, d as a 3D view. The projected fracture zone strike is indicated by the white box, with the receivers shown in black and the sources in white.

We applied the same processing sequence to the modelled source gathers as in the 2D case, except using a 3D Kirchhoff migration algorithm (Buske (1999)). Since we used a single component migration algorithm, the three component data were rotated such that the energy was maximized in one component. This was achieved by first modeling the experiment with the algorithm described in section 2 to determine the reflected wave arrival direction for each source receiver pair in a constant velocity medium. The amplitudes were then rotated into the theoretical arrival directions. A similar approach was used by Place et al. (2010) and Melanson et al. (2015), where a 3D conceptual model of the subsurface is created by comparing recorded and synthetic data. Such a conceptual model can then be used to determine the direction of the arriving reflection and to orientate the geophones into the principal energy direction.

After 3D migration of the processed and rotated data, two vertical cross sections through the middle of the fracture zone were extracted and analyzed. One is perpendicular to the strike, which corresponds to the length of the fracture zone as in the 2D case (shown in magenta in Figure 2.8e) and one parallel to the strike that describes the width of the fracture zone (shown in green in Figure 2.8e). The images of both cross sections were used during the optimization procedure. The results of the experiment, where the fracture zone has an azimuth of 0° (configuration 1) compared to an azimuth of 60° (configuration 2) are shown in Figure 2.9 for both the comprehensive and the optimized dataset, respectively. For evaluating the quality of the results, the exact length (magenta) and width (green) of the fracture zone are indicated by the dashed lines. It can be observed that the optimized migrated image is of similar quality to the migrated image of the comprehensive dataset.

The fracture zone can be imaged even if the azimuth between the source line and the fracture zone strike is 60°. However, the migrated image clearly is of lower quality than the migrated image for azimuth 0°. The fracture zone is more smeared out at the edges and the dip is slightly too shallow
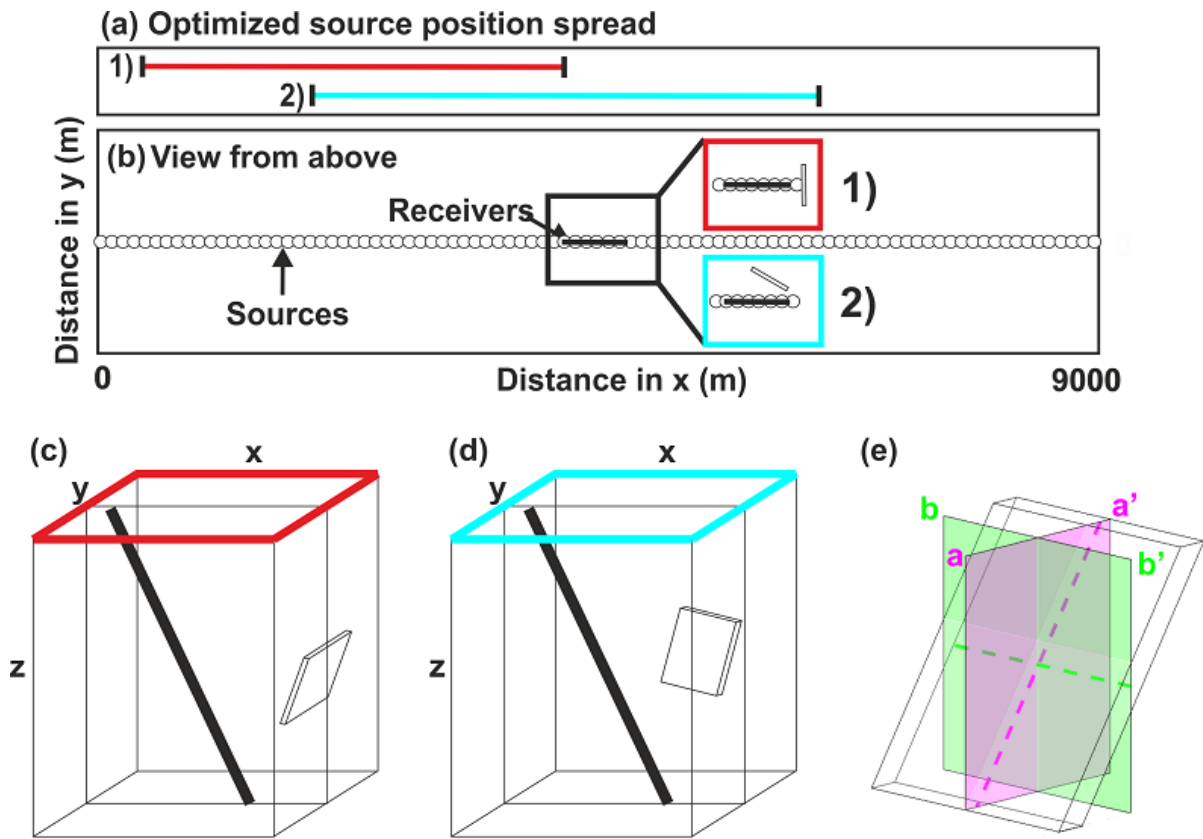
Figure 2.8: (a) Optimized source position spread for configurations 1) and 2) shown in the conceptual models in (b-d). (e) Two cross sections through the middle of the fracture zone that are used for the 3D optimization. The cross section perpendicular to the strike is shown in magenta a-a' and that parallel to the strike in green b-b'. The dashed line in magenta represents the length and the dashed line in green the width of the fracture zone. The migrated images for configurations 1) and 2) are shown in Figure 2.9 for the two perpendicular cross sections.

(compare Figure 2.9a and e, 2.9c and g). In the cross sections shown in Figure 2.9b, d, f, h, the width of the fracture zone is imaged. Comparing the migrated images with the green dashed line (exact width of the fracture zone), it can be seen that the image quality is rather low for both configurations and clearly decreases for increasing azimuth.

The source position spread changes considerably for the two different configurations (Figure 2.8a). The experiment for configuration 2 requires near offset source positions and omits the far offset positions completely, since no reflections occur for far offset shots. When considering all the different azimuths (also 30 °and 90 °which are not displayed in Figure 2.9) the quality of the migrated images decreases for increasing azimuth. Clearly, the best possible image can be obtained with a fracture zone azimuth perpendicular to the source line. The optimal source position spread is highly sensitive to the fracture zone azimuth. Far offset source positions contribute less to the image quality as fracture zone azimuth increases.
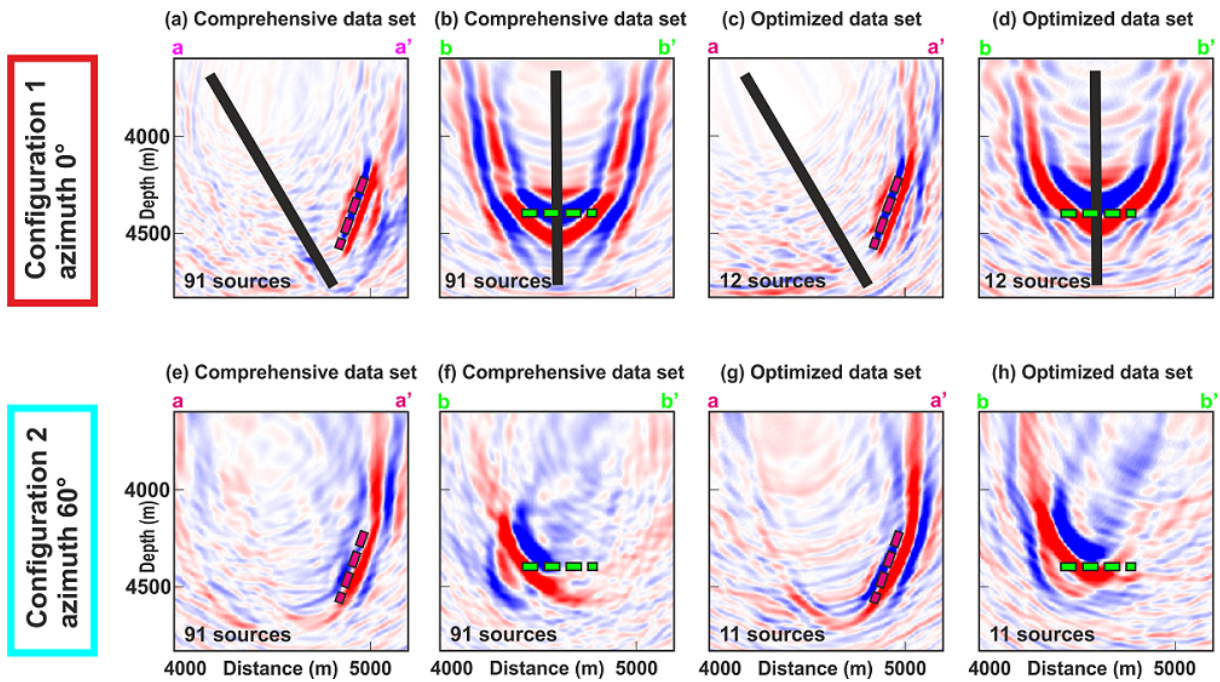
Figure 2.9: Migrated images for configurations 1) and 2) for the comprehensive dataset and the optimized dataset. The two different cross sections that are used for the optimization are illustrated in the conceptual model in Figure 2.8e. The dashed line in magenta represents the length and the dashed line in green the width of the fracture zone. Note the decrease in quality for configuration 2 (e-h) compared to configuration 1 (a-d).

2.5.2 Different source line azimuth

To investigate whether a fracture zone can be better imaged when illuminated from different angles, we simulated a multi-azimuth survey with the 6 source lines as shown in Figure 2.10. The dip of the fracture zone is 70 °and its strike is perpendicular to line L4 (fracture zone is indicated in green in Figure 2.10). In the optimization process we included all source positions from the six different lines L1 to L6 to test which combination of source positions leads to an optimal image.

As can be observed in Figure 2.10, the optimal source positions (red points) lie mostly on line 4 which is perpendicular to the strike of the fracture zone. Only two near offset source positions from line 3 were chosen by the algorithm. Visual inspection of the migrated single source gathers revealed that these two source gathers contain hardly any reflection energy due to the near offsets and are probably included as optimal sources to reduce the artefacts around the fracture zone. Hence, the optimization process favors source positions perpendicular to the fracture zone strike since they contribute most to the image. These results highlight that advanced geological à priori information on the azimuth of potential fracture zones is essential for designing suitable VSP surveys.
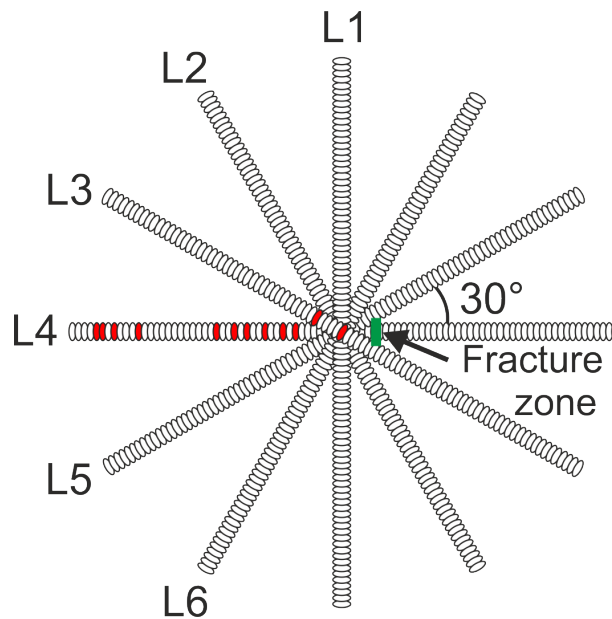
Figure 2.10: Multi-azimuth survey with the optimal source positions (red) and the strike of the
fracture zone (green). Most source positions are located on line 4, indicating that a
narrow azimuth perpendicular to the strike of the fracture zone is favorable to image
a single fracture zone.

2.6 Discussion

The optimized VSP design study was carried out under the acoustic assumption and therefore no
S-waves are present in the data. S-waves and coherent noise (e.g. tube waves) further complicate
the data, however, they could be suppressed largely with f-k or tau-p filtering prior to migration.
Additional complications when dealing with field data are expected with regard to the fracture zone
geometry. The fracture zone was modelled as a band of finite thickness bounded by two plane
interfaces whereas real fracture zones are expected to have a more complex shape, to be rough and
the impedance contrast can deviate from the one that is modelled. Nevertheless, the simple fracture
zone gives a good indication of how well such a structure can be imaged under ideal conditions using
an optimal number of sources and an ideal source spread.

Other complications likely to be encountered in the field are source and receiver coupling variations,
malfunctioning of receivers or skipped source positions. Additionally, the S/N ratio is not known be-
fore a survey. These effects add an element of uncertainty and need to be considered when planning
a survey. Due to the various approximations and simplifications made it is advisable to use a slightly
larger number of sources than that determined by the optimization strategy alone. This provides an
additional factor of safety and diminishes the risk of inferior imaging.

Despite the simplifications, we regard our study as beneficial because it illustrates the limitations and
possibilities for VSP imaging of fracture zones within hardrock basement environments under ideal
conditions. A further advantage of our 3D optimization scheme is that it can easily be adopted to
any acquisition geometry, which allows optimizing crooked-line acquisition and imaging geometries
(e.g., Schmelzbach et al. (2007)). Furthermore, it demonstrates how a VSP experiment can be

optimized with a favorable benefit-cost ratio and how seismic processing can be done to improve the image quality of a fault or fracture.

2.7 Conclusion

In this study a methodology to optimize VSP survey layouts for imaging fracture zones within hardrock basement geothermal reservoirs is presented. Optimal survey layouts in terms of ideal source spread and number of sources are shown for different fracture zone dips and positions. We have shown that the optimal experimental design strongly depends on the dip and location of the fracture zone. Therefore, à priori information on the expected subsurface structures is essential for survey design. For all scenarios considered in this study good results were obtained with a relatively small number of source positions. Adding more shot gathers outside of the optimal spread did not improve the quality of the images, but rather deteriorated the image quality. Therefore, our methodology will be not only useful for designing future field surveys, but also for selecting useful subsets of acquired data for optimum target-oriented processing.

Based on the synthetic data study we found that:

- More source positions and larger offsets are needed as fracture zone dip is increased.

- With decreasing S/N ratio more source positions and smaller offsets are required.

- Source positions should cover a large area when multiple fracture zones with different dips are present.

- Far offset source positions contribute less to the image quality with increasing fracture zone azimuth.

- Several source lines perpendicular to the different fracture zone strikes are ideal for fracture zones with different azimuths.

In this study we have demonstrated the benefits of optimized survey design with 2D and 3D acoustic data. The methodology could further be extended to the more realistic elastic case. This would introduce new challenges in wavefield separation but also add additional value because P-S, S-P and S-S migrated images could be obtained.

Acknowledgment

References

Adam, E., T. Bohlen, and B. Milkereit. 2003. "Vertical seismic profiling at the Bell Allard orebody, Matagami, Quebec". In *Hardrock seismic exploration*, 181–193. Society of Exploration Geophysicists.

Ahmed, K., B. Schwarz, and D. Gajewski. 2015. "Application of the 3D common-reflection-surface stack workflow in a crystalline rock environment". *Geophysical Prospecting* 63 (4): 990–998.

Arnórsson, S. 1995. "Geothermal systems in Iceland: structure and conceptual models—I. High-temperature areas". *Geothermics* 24 (5-6): 561–602.

Barbier, E. 2002. "Geothermal energy technology and current status: an overview". *Renewable and Sustainable Energy Reviews* 6 (1): 3–65.

Bellefleur, G., C. Müller, D. Snyder, and L. Matthews. 2004. "Downhole seismic imaging of a massive sulfide orebody with mode-converted waves, Halfmile Lake, New Brunswick, Canada". *Geophysics* 69 (2): 318–329.

Biasi, G., and L. Preston. 2011. *Regional p-wave tomographic imaging with geothermal application*. GRC Trans. 35,709-711.

Bohlen, T., C. Müller, and B. Milkereit. 2003. "Elastic seismic-wave scattering from massive sulfide orebodies: On the role of composition and shape". In *Hardrock seismic exploration*, 70–89. Society of Exploration Geophysicists.

Brogi, A., A. Lazzarotto, D. Liotta, and G. Ranalli. 2003. "Extensional shear zones as imaged by reflection seismic lines: the Larderello geothermal field (central Italy)". *Tectonophysics* 363 (1): 127–139.

Buske, S. 1999. "Three-dimensional pre-stack Kirchhoff migration of deep seismic reflection data". *Geophysical Journal International* 137 (1): 243–260.

Carr, B., S. Smithson, N. Kareav, A. Ronin, V. Garipov, Y. Kristofferson, P. Digranes, D. Smythe, and C. Gillen. 1996. "Vertical seismic profile results from the Kola Superdeep Borehole, Russia". *Tectonophysics* 264 (1-4): 295–307.

Cosma, C., P. Heikkinen, and J. Keskinen. 2003. "Multiazimuth VSP for rock characterization of deep nuclear waste disposal sites in Finland". In *Hardrock seismic exploration*, 207–226. Society of Exploration Geophysicists.

Cosma, C., O. Olsson, J. Keskinen, and P. Heikkinen. 2001. "Seismic characterization of fracturing at the Äspö Hard Rock Laboratory, Sweden, from the kilometer scale to the meter scale". *International Journal of Rock Mechanics and Mining Sciences* 38 (6): 859–865.

Emsley, S., P. Shiner, N. Enescu, A. Beccacini, and C. Cosma. 2007. "Using VSP surveys to bridge the scale gap between well and seismic data". *Geological Society, London, Special Publications* 270 (1): 83–91.

Geiermann, J., and E. Schill. 2010. "2-D Magnetotellurics at the geothermal site at Soultz-sous-Forêts: Resistivity distribution to about 3000m depth". *Comptes Rendus Geoscience* 342 (7): 587–599.

Gérard, A., A. Genter, T. Kohl, P. Lutz, P. Rose, and F. Rummel. 2006. *The deep EGS (enhanced geothermal system) project at Soultz-sous-Forêts (Alsace, France)*.

Goff, J. A., and K. Holliger. 2012. *Heterogeneity in the crust and upper mantle: Nature, scaling, and seismic properties*. Springer Science & Business Media.

Hardage, B. A. 2000. *Vertical seismic profiling*. Handbook of Geophysical Exploration, Seismic Exploration, 14, Pergamon.

Hloušek, F., O. Hellwig, and S. Buske. 2015. "Three-dimensional focused seismic imaging for geothermal exploration in crystalline rock near Schneeberg, Germany". *Geophysical Prospecting* 63 (4): 999–1014.

Juhlin, C., and H. Palm. 2003. "Experiences from Shallow Reflection Seismics over Granitic Rocks in Sweden". In *Hardrock seismic exploration*, 93–109. Society of Exploration Geophysicists.

Juhlin, C., and M. B. Stephens. 2006. "Gently dipping fracture zones in Paleoproterozoic metagranite, Sweden: Evidence from reflection seismic and cored borehole data and implications for the disposal of nuclear waste". *Journal of Geophysical Research: Solid Earth* 111 (B9).

Lavadera, P. L. 2013. "Traitement des données de sismique de puits acquises en 2007 sur le site de Soultz-sous-Forêts pour la caractérisation de la fracturation du réservoir géothermique". PhD thesis, Université de Strasbourg.

Lüth, S., S. Buske, R. Giese, and A. Goertz. 2005. "Fresnel volume migration of multicomponent data". *Geophysics* 70 (6): S121–S129.

Majer, E., T. V. McEvilly, F. Eastwood, and L. Myer. 1988. "Fracture detection using P-wave and S-wave vertical seismic profiling at The Geysers". *Geophysics* 53 (1): 76–84.

Maurer, H., A. Curtis, and D. E. Boerner. 2010. "Recent advances in optimized geophysical survey design". *Geophysics* 75 (5): 75A177–75A194.

Melanson, D., D. White, C. Samson, G. Bellefleur, E. Schetselaar, and D. Schmitt. 2015. "Mode-converted volcanogenic massive sulphide ore lens reflections in vertical seismic profiles from Flin Flon, Manitoba, Canada". *Geophysical Prospecting* 63 (4): 849–860.

Nakagome, O., T. Uchida, and T. Horikoshi. 1998. "Seismic reflection and VSP in the Kakkonda geothermal field, Japan: Fractured reservoir characterization". *Geothermics* 27 (5): 535–552.

Niitsuma, H., M. Fehler, R. Jones, S. Wilson, J. Albright, A. Green, R. Baria, K. Hayashi, H. Kaieda, K. Tezuka, et al. 1999. "Current status of seismic and borehole measurements for HDR/HWR development". *Geothermics* 28 (4): 475–490.

Perron, G., D. Eaton, B. Elliot, and D. Schmitt. 2003. "Application of downhole seismic imaging to map near-vertical structures: Normétal (Abitibi Greenstone Belt), Québec". In *Hardrock seismic exploration*, 194–206. Society of Exploration Geophysicists.

Place, J., M. Diraison, C. Naville, Y. Géraud, M. Schaming, and C. Dezayes. 2010. "Decoupling of deformation in the Upper Rhine Graben sediments. Seismic reflection and diffraction on 3-component Vertical Seismic Profiling (Soultz-sous-Forêts area)". *Comptes Rendus Geoscience* 342 (7): 575–586.

Place, J., J. Sausse, J.-M. Marthelot, M. Diraison, Y. Géraud, and C. Naville. 2011. "3-D mapping of permeable structures affecting a deep granite basement using isotropic 3C VSP data". *Geophysical Journal International* 186 (1): 245–263.

Rabbel, W., T. Beilecke, T. Bohlen, D. Fischer, A. Frank, J. Hasenclever, G. Borm, J. Kück, K. Bram, G. Druivenga, et al. 2004. "Superdeep vertical seismic profiling at the KTB deep drill hole (Germany): Seismic close-up view of a major thrust zone down to 8.5 km depth". *Journal of Geophysical Research: Solid Earth* 109 (B9).

Salisbury, M. H., C. W. Harvey, and L. Matthews. 2007. "The acoustic properties of ores and host rocks in hardrock terranes". In *Hardrock seismic exploration*, 9–19. Society of Exploration Geophysicists.

Schmelzbach, C., S. Greenhalgh, F. Reiser, J.-F. Girard, F. Bretaudeau, L. Capar, and A. Bitri. 2016. "Advanced seismic processing/imaging techniques and their potential for geothermal exploration". *Interpretation* 4 (4): SR1–SR18.

Schmelzbach, C., H. Horstmeyer, and C. Juhlin. 2007a. "Shallow 3D seismic-reflection imaging of fracture zones in crystalline rock". *Geophysics* 72 (6): B149–B160.

Schmelzbach, C., C. Juhlin, R. Carbonell, and J. F. Simancas. 2007b. "Prestack and poststack migration of crooked-line seismic reflection data: A case study from the South Portuguese Zone fold belt, southwestern Iberia". *Geophysics* 72 (2): B9–B18.

Schreiter, L., F. Hloušek, O. Hellwig, and S. Buske. 2015. "Characterization of seismic reflections from faults in a crystalline environment, Schneeberg, Germany". *Geophysical Prospecting* 63 (4): 1015–1032.

Thomas, R., and R. Schulz. 2007. "Facies differentiation of the Malm by interpretation of reflection seismic profiles and a moving source VSP Experiment". In *Proceedings of the European Geothermal Congress*.

Wang, Z., A. C. Bovik, H. R. Sheikh, and E. P. Simoncelli. 2004. "Image quality assessment: from error visibility to structural similarity". *IEEE transactions on image processing* 13 (4): 600–612.

Wolfgramm, M., J. Bartels, F. Hoffmann, G. Kittl, G. Lenz, P. Seibt, R. Schulz, R. Thomas, and H. Unger. 2007. "Unterhaching geothermal well doublet: structural and hydrodynamic reservoir characteristic; Bavaria (Germany)". In *European Geothermal Congress*.

3

Imaging the high-temperature geothermal field at Krafla using vertical seismic profiling

Contents

Abstract

Geophysical exploration and in particular active-source seismic imaging of geothermal fields is important to assess and optimize the exploitation of natural heat sources for energy production and direct use. The first multi-offset (moving-source) vertical seismic profiling (VSP) experiment over the high-temperature geothermal field in Krafla (Iceland) was carried out in spring 2014 with the aim to test whether VSP is a suitable method to map volcanic stratigraphy, fractures, dykes, steam zones and magmatic bodies at this site and for volcanic environments in general. In this study, we present a workflow for processing the sparse Krafla VSP dataset recorded with receivers in either of two boreholes . The analysis involved first-arrival traveltime inversion and seismic reflection processing. The seismic velocity model obtained by traveltime tomography reveals structural information between the two boreholes and can be linked to an existing geological model, showing that the seismic velocities are mainly controlled by lithology. The zero-offset seismic reflection data were processed into two corridor stacks. Walk-away VSP reflection data were migrated with a novel multicomponent Kirchhoff migration algorithm that includes P- and S-wave isolation to obtain separate PP, PS and SS migrated images. The reflections imaged in the corridor stacks can be linked to the main lithological units known from borehole logging information. Migrated images from the walk-away data reveal reflectors below and to the sides of the two boreholes. Considering à priori information, such as hypocenter locations from earthquake seismology studies, the reflectors can be related to changes in lithology, fault zones, dykes and possibly the top of the Krafla magma chamber. We found that VSP is potentially a useful method to image the key lithological boundaries and volcanic stratigraphy in the complex magmatic environment at Krafla, but à priori information proved to be essential to constrain the processing and interpretation of the sparse array dataset.

3.1 Introduction

Geothermal resources play a major role in the energy supplies of Iceland, both for electricity production and district heating purposes. Iceland is fortuitously located directly on the Mid Atlantic Ridge that marks the plate boundary between the North American and Eurasian plates. This results in very active volcanism and high subsurface temperatures that yield a large potential for geothermal exploitation. Krafla is one of the high temperature areas in Iceland, situated in the neo-volcanic zone near the northern end of the central rift system Figure 3.1. To date, 47 wells have been drilled in the area around the geothermal power plant, which has been operating at 62MW since 1999 (Halldórsdóttir et al. (2010); Guðmundsson and Mortensen (2015)). The first IDDP (Iceland Deep Drilling Project) well was drilled at Krafla close to Víti crater lake in 2009 to produce supercritical fluid to increase the power output (Elders et al. (2014); Friðleifsson et al. (2015)). However, the drilling had to be prematurely stopped at 2100 m depth because magma was unexpectedly encountered in the borehole (Hólmgeirsson et al. (2010); Pálsson et al. (2014)), resulting in a damaged well.

Geophysical exploration of geothermal fields is important to assess and optimize the exploitation of natural heat sources. Seismic reflection surveying is a well-established method to image the subsurface at different scales but it has only been sparingly used in the context of geothermal investigations (Schmelzbach et al. (2016)). So far, only a few surface-based seismic reflection surveys have been acquired in Iceland, all resulting in poor data quality, with very little coherent and interpretable re-

flection signals being recorded (Juhojuntti (2001)). Large-scale active-source upper crustal seismic experiments in northern Iceland revealed the coarse velocity structure of the Krafla caldera (Brands-dóttir et al. (1997); Staples et al. (1997)) and also passive seismic (earthquake) studies were used to constrain the velocity structure of the area (Menke et al. (1998); Tang et al. (2008); Blanck et al. (2011)).

Surface-based seismic reflection imaging in magmatic environments is very challenging. Seismic waves encounter intense scattering while traveling through the highly heterogeneous volcanic rocks, thus leading to data with a low signal-to-noise ratio (e.g. Planke et al. (2000); Salisbury et al. (2007)). A complicating factor is the difficulty of cleanly coupling the seismic radiation into and out of the rock. Additionally, data acquisition in such rough volcanic terrain is logistically complicated and costly. Vertical seismic profiling (VSP; e.g., Hardage (2000); Gaiser (2016)) offers an alternative means to image structures beneath and away from a well in complex volcanic environments. The advantage of VSP over surface-based seismic- reflection surveying is that seismic waves travel shorter paths, since they only pass once through the highly heterogeneous and absorbing shallow subsurface zone. Hence, VSP data suffer less from attenuation and usually contain higher frequencies than surface-based seismic data (e.g. Cosma et al. (2003)). Moreover, with the geophones downhole, the reflected and transmitted waves can be sensed much closer to the target horizons, thus improving detection and recognition of features of interest. However, compared to surface seismic exploration VSP has a limited area of illumination. In VSP surveys, the imaging is restricted to the area in the vicinity of the borehole and more or less to the region in the extended depth position of the borehole, depending on the dip of the reflector (e.g., Reiser et al. (2017)).

VSP surveys have previously been successfully applied to hard rock mineral exploration (Adam et al. (2003); Perron et al. (2003); Bellefleur et al. (2004)), fractured carbonate reservoirs (Emsley et al. (2007)) and potential nuclear waste disposal sites (Cosma et al. (2001), (2003)). There have been a few examples of where VSP surveys have been conducted in a geothermal context (Cameli et al. (1995); Gibson Jr et al. (1995)). In a VSP pilot study of the Geyser steam-bearing geothermal field in northern California, Majer et al. (1988) obtained fracture anisotropy information by analyzing shear wave splitting or birefingence. The fractures are aligned in the fast S wave direction and the time delays between the fast and slow S waves indicate the intensity of fracturing. Nakagome et al. (1998) resolved more detailed structural information on the VSP data than on the surface seismic data and mapped relevant faults and fracture zones in the Kakkonda geothermal field in Japan. Thomas and Schulz (2007) observed a better signal-to-noise ratio on the VSP data in comparison to the surface seismic data and delineated several fault systems in the sedimentary hydrothermal system at Unterhaching. Place et al. (2010), (2011) processed a VSP dataset from the EGS site in Soultz-sous-Forêts and observed reflections (especially P-to-S mode-converted waves) resulting from fracture zones within granitic basement.

All of these studies show the high potential but also the limitations of VSP surveys to characterize geothermal systems in complex environments. In this study, seismic data from the first VSP survey recorded in a high temperature geothermal field in Iceland are analyzed. The applicability and limitations of VSP for mapping the subsurface in the volcanic environment of Krafla were tested. A primary motivation of this investigation was to study if VSP is a suitable method to map volcanic
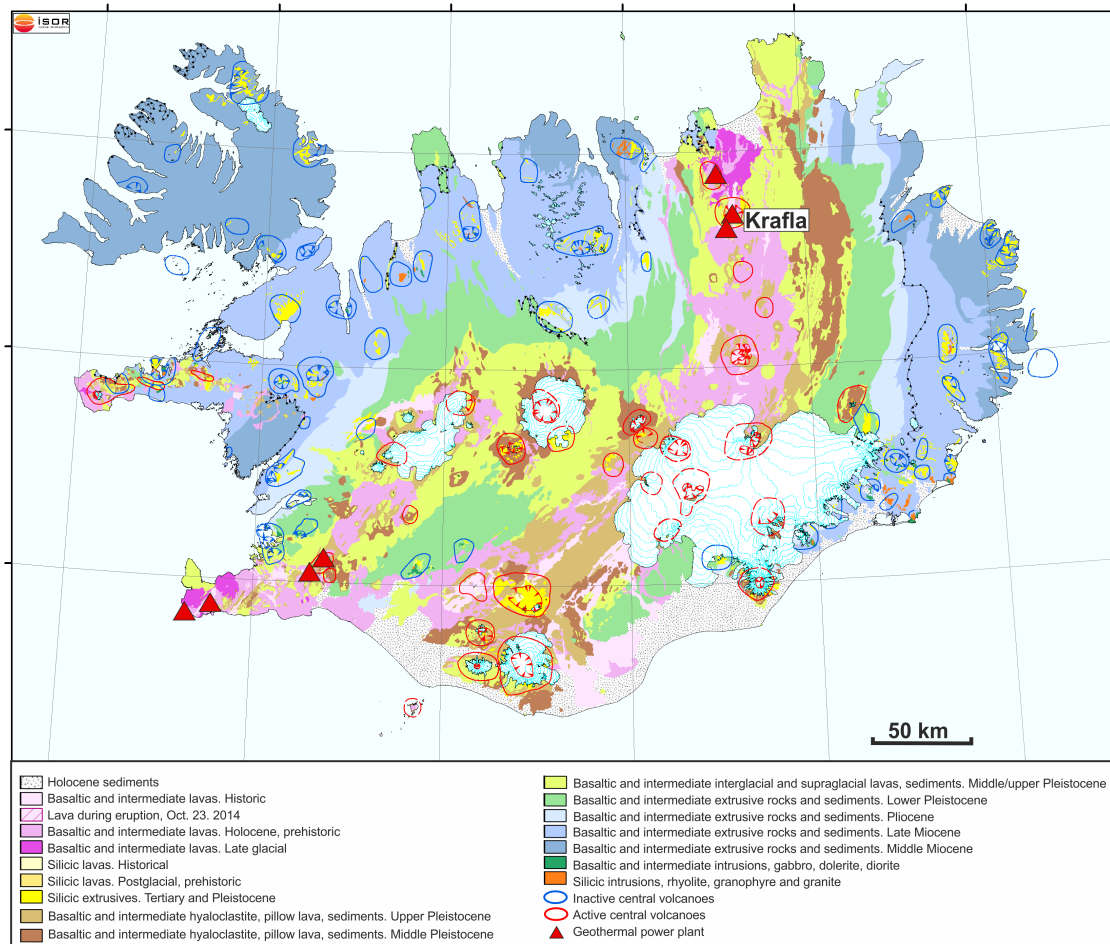
Figure 3.1: Simplified geological map of Iceland, modified after Hjartarson and Sæmundsson (2014). Krafla is situated near the northern end of the central rift system. The rocks are older towards the east and west of the central rift system. Geothermal power plants are shown with red triangles.

stratigraphy and key geological boundaries, such as fractures, dykes, and zones of supercritical fluid and steam. Due to the recent accident and costly drilling into magma at the IDDP well (Elders et al. (2014)) it also needs to be established whether VSP can be used to map magmatic bodies ahead of the borehole to prevent such an incidence in the future.

As will be demonstrated in our paper, VSP data at Krafla do indeed provide useful subsurface information, but due to the inherent spatial resolution limitations associated with the VSP recording geometry and the only moderate signal-to-noise ratio of the data, it is essential that the data analyses are guided and informed by as much à priori information as possible. After a brief description to the test site and the Krafla VSP data set, we demonstrate how zero-offset and walk-away VSP traveltime data can be employed to construct 2D seismic velocity models. Next, we exploit the information content offered by the reflected phases contained in our VSP data and calculate synthetic data to better understand the characteristics of the field data. Besides conventional P wave analyses we also consider S waves and P-to-S converted phases using a novel multicomponent Kirchhoff migration algorithm that takes seismic wavefield polarization information into account. On the basis of these efforts, a refined image of the main geological units at the Krafla test site can be established. We con-

clude our study with a critical review of the benefits and limitations of VSP surveys for geothermal prospecting in volcanic areas.

3.2 Geological setting

Krafla is situated near the northern end of the central rift system (Figure 3.1) and comprises an 8 km x 10 km wide caldera that has been filled with eruptive material since the last interglacial period (Saemundsson (1978), (1991); Brandsdóttir and Menke (1992)). The geology is constrained by interpretation of drill cuttings from multiple boreholes in the area (Ármannsson et al. (1987)). The upper part of the sequence is dominated by hyaloclastites consisting of materials from subglacial eruptions and basalt lava flows. Basaltic intrusions prevail below 1200 m depth followed by gabbroic intrusions (Bodvarsson et al. (1984)). The Krafla region is dominated by an active central volcano and transected by a 100 km long and 4-6 km wide fissure swarm (Saemundsson (1978); Sæmundsson (1991)). Most of the fractures are oriented N to NNE and are steeply dipping (Opheim and Gudmundsson (1989); Hjartardóttir et al. (2012)). Krafla shows periodic volcanic activity at intervals of 250-1000 years. The latest episode, the so-called Krafla fires, lasted from 1975-1984 (Björnsson (1985); Einarsson (1991)). The heat source of the geothermal system originates from a magma chamber at about 3-7 km depth. Several studies confirm the existence of the magma chamber based on the observation of increased S- wave attenuation, lower P wave velocities and the lack of earthquakes (more ductile crust) below 3 km depth (Einarsson (1978); Brandsdottir and Einarsson (1979); Brandsdóttir and Menke (1992); Friðleifsson et al. (2014); Schuler et al. (2015)). The presence of a magma chamber was also indicated by an extensive magneto-telluric survey where low resistivity anomalies rising up to 2.5-5 km depth were observed (Árnason et al. (2007); Friðleifsson et al. (2014)).

3.3 VSP data set

A multi-offset (moving-source) VSP survey was conducted at the high temperature geothermal field at Krafla volcano in Iceland during spring 2014 (Halldórsdóttir et al. (2014); Planke et al. (2016)). The VSP experiment was acquired around two vertical wells K-18 and K-26 that are approximately 2 km apart (Figure 3.2). For each well, a zero-offset experiment was carried out (source locations Ingi, Jon, see Figure 3.2), a number of far-offset source points were recorded for orientation purposes (source location Thorstein, see Figure 3.2, and E-W/N-S walk-away (multi-offset) surveys were also performed (source location Thor 1-11, see Figure 3.2). In this study, we focus on the zero-offset data of well K-18 and K-26 and the E-W walk-away data (shown in red and blue colors in Figure 3.2). In Planke et al. (2016) and Kästner et al. (2018) results from the zero-offset and far-offset VSP data from well K-18 are presented in addition to a seismic source comparison. Millett et al. (2018) provide a detailed volcanic stratigraphy analysis in the borehole of K-18 based on ditch cuttings, sonic log velocities and the zero-offset VSP data, Hersir et al. (2016) provide sonic log data and Árnadóttir, S. (2011) televiewer data from the borehole.

A geophone string (type Sercel SlimWaveTM) with 3C-geophones (15 Hz) at 17 levels with a spacing of 10 m was used. However, since just six caliper arms were available, only data from the six clamped
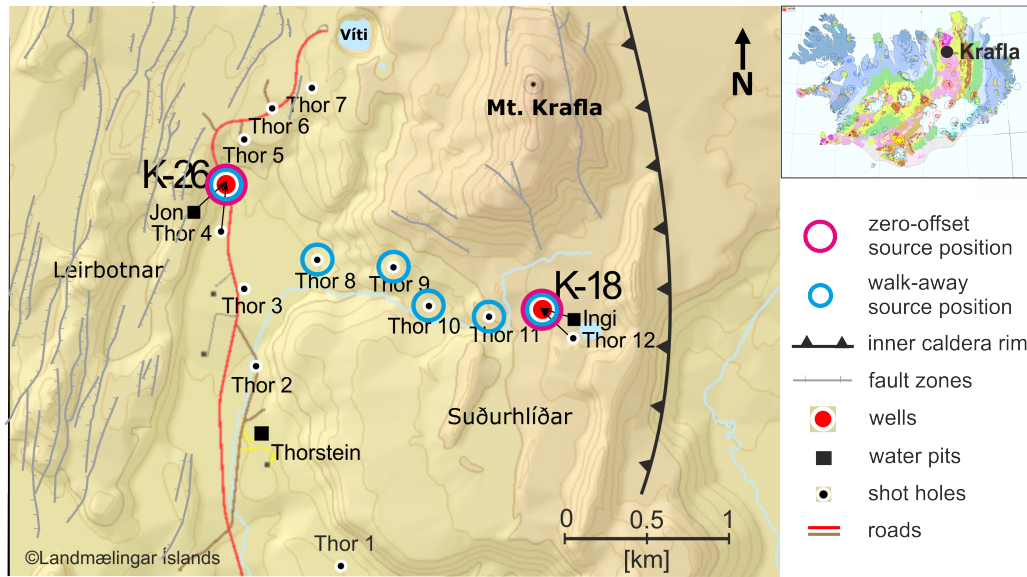
Figure 3.2: Survey layout of the K-18 and K-26 VSP experiment at Krafla with geological features
based on Sæmundsson (1991). The zero-offset experiments are associated with source
locations Ingi and Jon, the far-offset source position with Thorstein and the walk-away
source locations with Thor 1-11 (modified after Halldórsdóttir et al. (2014)). In this
study, we focus on the zero-offset (magenta) and the walk-away data from the E-W
profile (blue).

geophones was of sufficient signal-to-noise ratio (S/N) to be used. Due to the high temperature in
the boreholes, well K-18 needed to be cooled down for several weeks prior to the acquisition and
additionally during the acquisition breaks in the night to maintain the operational temperature of the
geophones. Well K-26 is an injection well and had to be cooled down during the acquisition breaks in
the night. The acquisition parameters for the survey at Krafla are shown in Table 3.1. The zero-offset
and far-offset source positions entailed the deployment of an air gun source (40 m^3 chamber volume
and a working pressure of 130-140 bar) in shallow excavated water pits. For the walk-away source
positions, dynamite charges of 0.5-2 kg were fired in shallow shot holes.

		K-18	**K-26**
	Total well depth	2210 m	2125 m
Zero-offset	receiver station interval	2.5 m	2.5 m
	receiver depth range	10-2180 m	10-1448 m
Far-offset	receiver station interval	10 m	10 m
	receiver depth range	18-2172 m	95-1342 m
Walk-away	receiver station interval	5 m	5 m
	measured receiver depth	1325-1800 m (E-W-line)	915-1150 m (E-W-line)
			1100-1150 m (N-S-line)

Table 3.1: Acquisition parameters for K-18 and K-26 VSP's (after Halldórsdóttir et al. (2014)). Only
the zero-offset and E-W-line walk-away data were used in this study.

3.4 Seismic-data processing and results

3.4.1 First-arrival traveltime inversion of zero-offset data

As a first step, we performed a 1D traveltime inversion using the arrival times of the zero-offset P-wave first arrivals. The zero-offset data are of good quality and the first breaks could be picked reliably on the complete source gather with an accuracy of ~2 ms. The 1D inversion was performed using a starting model with a gradual velocity increase and fixed layer thicknesses of 10 m. Final inversion result velocities for boreholes K-18 and K-26 are shown in Figure 3.3a (red). There are only minor discrepancies between the observed and the predicted travel time data using the final velocity profile (1.5 ms).

To further check the reliability of the inversion results, the resultant model is compared with available sonic log velocities at well K-18 (Hersir et al. (2016) - blue curve in Figure 3.3a). Apart from the generally lower sonic log velocities, which could result from a slightly damaged borehole wall, the velocities correlate well. As the inversion result is rather smooth, we calculated mean velocities for depth intervals obtained from à priori information (geological logs) to introduce impedance contrasts that were used for the synthetic modelling of the zero offset data in subsection 3.4.5. Traveltimes predicted with the resulting model (green line in Figure 3.3a) match the observed travel times equally well as the original (smooth) 1D inversion result (RMS 1.5 ms).
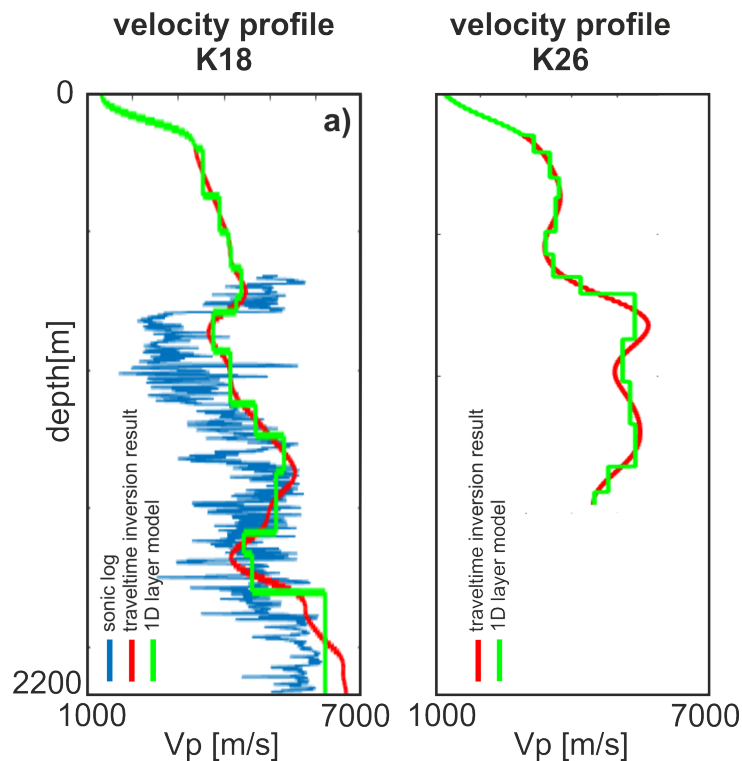
Figure 3.3: Velocity profiles for well a) K-18 and b) K-26. 1D traveltime inversion result is shown in red, mean velocities based on à priori information in green (Planke et al. (2016)) and sonic log velocities in blue (Hersir et al. (2016)). Apart from generally lower sonic log velocities, the measured sonic log and inverted velocities correlate well.

3.4.2   Traveltime inversion of zero-offset and walk-away data

In a next step, we carried out traveltime inversions of the entire VSP data set to investigate the subsurface structure between the boreholes. By forward modelling we found that a 1D model is not sufficient to explain the traveltimes of the walk-away data. Therefore, a 2D traveltime tomography using the zero-offset and walk-away data of both wells was performed. The inversion algorithm is based on a finite-difference Eikonal solver for the forward calculation of traveltimes and raypaths (Podvin and Lecomte (1991)) and an inverse scheme that incorporates damping and smoothing parameters (Lanz et al. (1998)). We used fat ray tomography where the Fresnel volume around the central ray is taken into account, calculated based on source and receiver traveltime fields (Husen and Kissling (2001); Jordi et al. (2016)). With such an approach an increased coverage and more realistic wave propagation could be achieved and helped to better constrain the velocity model of the sparse data set.

Since the ray coverage is limited by the source-receiver geometry, we thoroughly assessed the robustness of the velocity models to variations in the inversion parameters; different initial models and a number of damping and smoothing factor combinations were tested to assess ambiguities of the velocity models. Some results from our analyses are shown in Figure 3.4, where three initial models and two different smoothing factors were tested. The first initial model (gradual increase) starts with 1000 m/s at the surface and has a linear increase of velocity with depth of 2.5 m/s per metre. For the initial model in Figure 3.4d, the 1D inversion results of the zero-offset data sets at the positions of the boreholes were used and the velocities were interpolated between the wells. The last initial model in Figure 3.4g and j is based on the geological model shown in Figure 3.4n (Planke et al. (2016)) that was constructed with the aid of information from drillhole cuttings. The location of the transition between the basalts/hyaloclastites and intrusion-dominated rock was constrained in the starting model based on the geological model (shown with the black line in Figure 3.4n), a gradual velocity increase was used above this interface and a constant velocity below.

We performed the traveltime tomography by searching for the smoothest model that explains the traveltime data within the estimated data uncertainties (Scales et al. (1990); Phillips and Fehler (1991)). The inversion results for the different starting models show similar structures and all result in an RMS data misfit in the range of 5-6 ms, which is compatible with the picking uncertainty of the walk-away data. The models obtained with a low smoothing factor of 2,000 (Figure 3.4b, e, h) result in somewhat smaller RMS values and anomalously high velocity regions are observed (dark red colour). Since such high values are not expected in this area, the smoothing was further increased to suppress these artifacts. The different inversion results with an increased smoothing factor of 4,000 all look alike, independent of the starting model that was used (Figure 3.4). They recover a transition to high velocities around the interface between the basalt/hyaloclastites and the intrusion-dominated rock (black line in Figure 3.4c, f, i). The inversion results from the initial model that includes geological constraints leads to the smoothest velocity model and the lowest RMS value (Figure 3.4j) and, hence, highlights the benefit of including geological information into the starting model.

In Figure 3.4k and l the S-wave inversion results are shown for the initial model that includes geological constraints. The picking uncertainty for the direct S-wave is higher (∼8 ms) than for the P-wave,
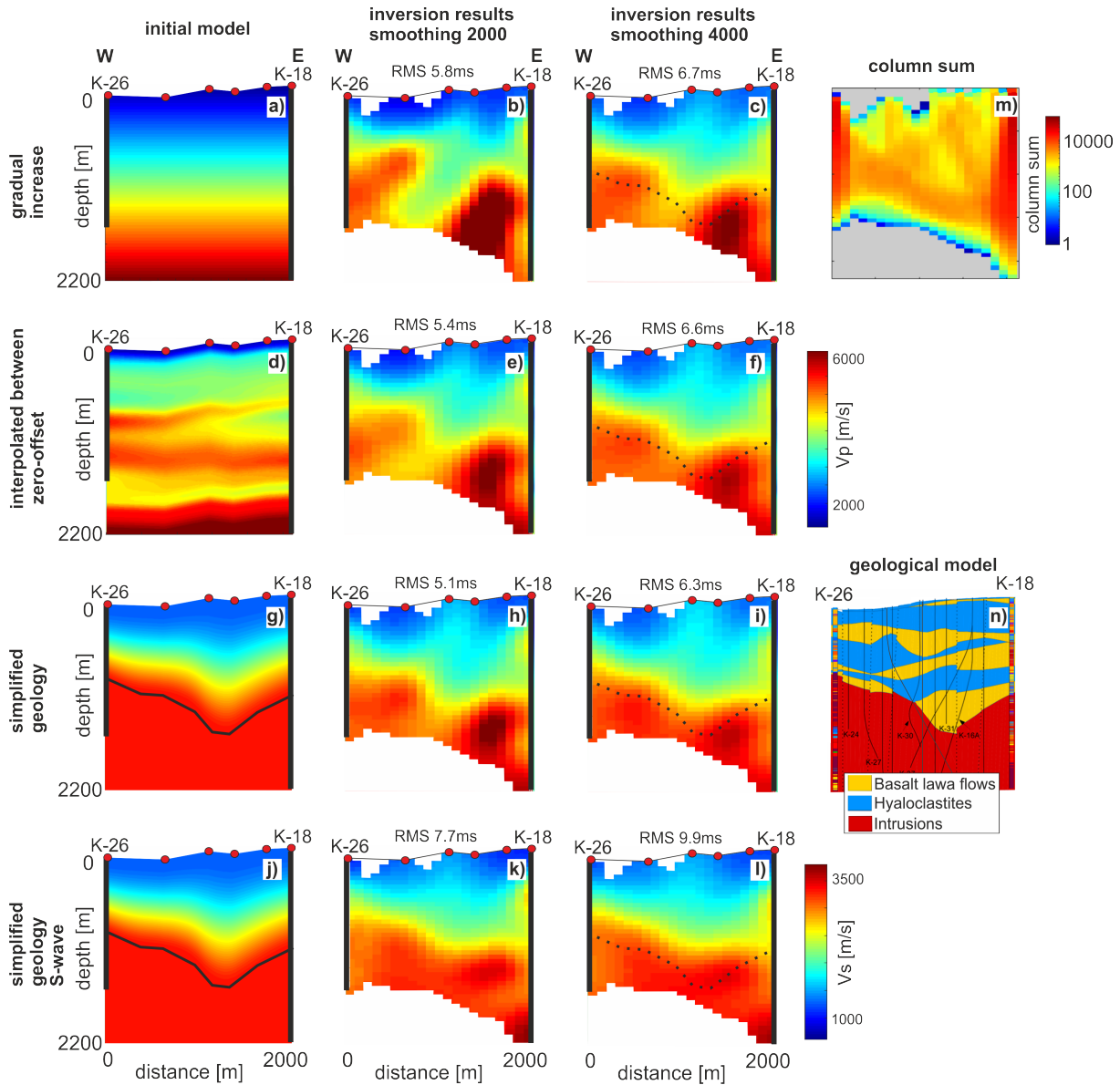
Figure 3.4: Inversion-parameter tests using three different starting models (rows) and two different smoothing factors (columns). Initial and final models for: a-c) an initial model with a gradually increasing velocity, d-f) an initial model based on the zero-offset velocity models, g-i) a two-layer initial model based on simplified geological model, j-l) same as g-i) but using S-wave first arrivals. m) Column sum showing higher values in the vicinity of the borehole and lower values in between due to the limited number of source positions. n) Shows a borehole-based geological model of the area between the boreholes K-26 and K-18 (Planke et al. (2016)). Note that the inversion results with the higher smoothing factor look similar, independent of the starting model. They all resolve the interface between the basalt/hyaloclastites and the intrusion-dominated rock (black dotted line).

which is also represented in the higher RMS values. However, the S-wave inversion results look similar to the P-wave inversion results and also recover the interface between basalt/hyaloclastites. Analysing the Vp/Vs ratio of the inversions results showed large variations in the Vp/Vs ratio within a range of 1.5-2. As the the Vp/Vs ratio in the Icelandic crust is pretty constant with a value of 1.77 (Brandsdóttir et al. (1997)) we judge that the obtained ratios are not sufficiently well constrained, and hence could not be employed for a geological interpretation.

To assess the quality of the final inversion results, the column sums of absolute values of the Jacobian matrix (sensitivities) are displayed in Figure 3.4m. They are a good proxy for the diagonal elements of the model resolution matrix (Meles et al. (2012)). The column sums look very similar for the different inversion results, hence Figure 3.4m is representative for all tomograms. The column sum also serves as an indication of the fat-ray coverage of the subsurface (Jordi et al. (2016)). High values are observed in the vicinity of the boreholes and hence represent areas of high resolution. Due to the limited ray coverage, low values are observed in between the wells and hence a large uncertainty is expected for these regions of the tomogram. The lowest values are seen at the near surface and in greater depth indicating that these areas are not well resolved by the tomography.

3.4.3   Traveltime inversion with geological constraints

Because none of the final tomograms obtained from relatively simple initial models shown in Figure 3.4 resolved the small-scale details of the geological model shown in Figure 3.4n, we assessed whether these structures are compatible with the traveltime data. For that purpose detailed à priori information was introduced in the initial model, and it was tested if the traveltimes can be explained equally well after the inversion. The initial model shown in Figure 3.5a was created according to the conceptual model displayed in Figure 3.4n. The velocities for the different geological units were extracted from petrophysical studies in Iceland (Grab et al. (2017)).

For the inversion, a high damping factor was chosen, such that the inversion algorithm seeks a solution that deviates only slightly from the initial model. The smoothing factor was reduced such that the inversion reached a similar RMS value as the inversion results using no geological constraints
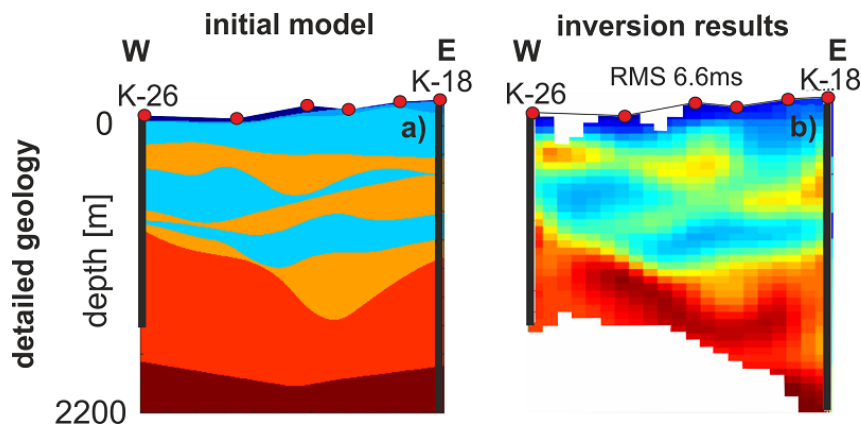
Figure 3.5: a) Initial model that contains detailed geological features based on the geological model in Figure 4n. b) Inversion result that shows similar structural features as the geological model and has an RMS value that corresponds to the picking uncertainty.

(see Figure 3.4c, f). The final tomogram displayed in Figure 3.5b reveals comparable features as the geological initial model with an RMS value similar to the picking accuracy. Hence, this model explains the traveltimes equally well as the model without geological constraints.

3.4.4 Composite model

We used a histogram plot of the velocities in each cell of our final inversion result (Figure 3.5b) to construct a composite model of five main lithological units (Figure 3.6). All model cells of the inversion result were assigned to different bins according to their seismic velocities. The bins were defined based on groupings observed in the histogram plot, velocity ranges for the different geological units presented in a petrophysical study (Grab et al. (2017)), and lithological à priori knowledge (Planke et al. (2016)). Through this process the geophysical model can be converted to a simplified geological model that can be further employed for interpretation and modelling.
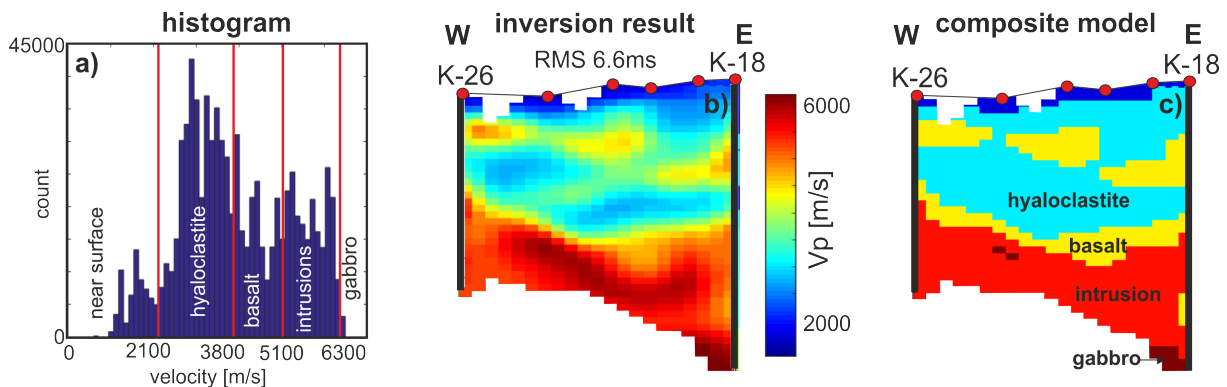
Figure 3.6: a) Histogram plot of the velocities of the inversion result shown in b) (same as Figure 3.5b). The bins are defined based on groups in the histogram plot, petrophysical information and à priori knowledge. c) Inversion result with the assigned bins that show the different geological units.

3.4.5 Reflection seismic processing of the zero-offset data and the resultant 1D model

We used a standard seismic processing flow for the analysis of the vertical and horizontal receiver component data (e.g., Hardage (2000)). The flow consisted of trace editing, first-break picking, geometrical spreading correction ($t^{1.5}$), amplitude balancing (800 ms window), VSP deconvolution, up-/down-going wavefield separation in the F-K domain, bandpass filtering (5–8–60–100 Hz) and F-X deconvolution. A vertical component example of the zero-offset gather from wells K-18 and K-26 before and after processing is shown in Figure 3.7c, d and e, f, respectively. It can be seen that the quality of the K-18 data is generally higher than that of K-26, with clearer reflections observed on the upgoing wavefield. This might be related to the fact that K-26 is an injection well where much higher temperatures are experienced in the well (Planke et al. (2016)).

Since the zero-offset data are well constrained along the borehole, we used the horizontally layered model obtained from the inversion of the zero-offset data (green curve in Figure 3.3) for the first modelling test. Synthetic waveform data were calculated to test the compatibility of the data with a 1D model and to better understand the characteristics of the wavefield (e.g. primary reflections
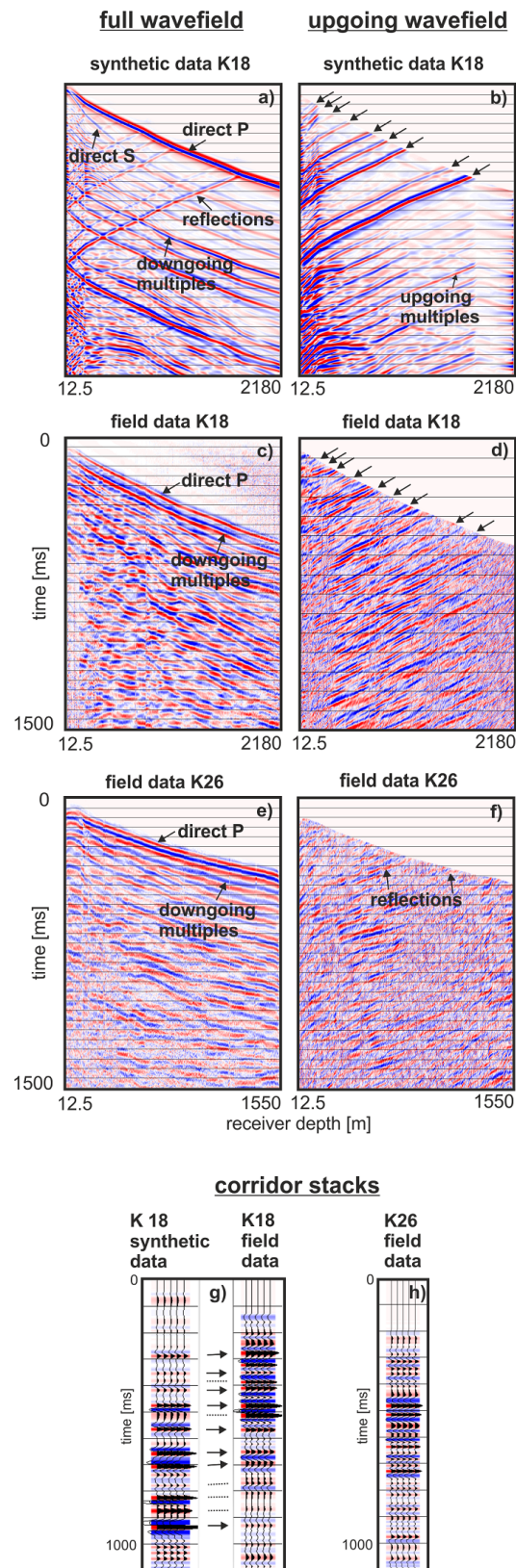
Figure 3.7: Full and upgoing wavefields for the zero-offset source position for a, b) K-18 synthetic data, c, d) K-18 field data, e, f) K-26 field data and g, h) the corresponding corridor stacks. Reflections on the upgoing wavefield occur at the same time in the field and the synthetic data for well K-18 (compare black arrows in b and d). Apart from amplitude differences, the reflections observed in the synthetic and field corridor stacks for well K-18 occur at similar times (black arrows).

and multiples). We used a dominant frequency of 28 Hz based on the analysis of the zero-offset data. Attenuation parameters of the different lithological units were based on Grab et al. (2017). The software SOFI2D (Bohlen et al. (2003)) was used for the simulation and the synthetic waveform data were then processed in the same manner as the field data. The full and the extracted up-going synthetic wavefield for well K-18 are shown in Figure 3.7a and b, respectively. The direct P-wave and several multiples that lead to a reverberatory appearance of the data can be clearly identified in the synthetic wavefield data. The black arrows on the up-going wavefield mark reflections from the different layers. It can be observed that most of the reflections in the synthetic data coincide with reflections in the field data. Hence, the layered 1D model can largely explain the recorded zero-offset data. However, since there are many events present in the data the interpretation is associated with considerable uncertainties.

Differences in (relative) amplitudes between the synthetic and field data are observed at large receiver depths. The reflector from the basement (lowest arrow), for example, is weaker on the field data than on the synthetic data, possibly due to loss of energy because of the scattering nature of the volcanic layers which is not properly accounted for in the numerical modelling. The decrease in amplitude throughout the entire corridor stack is clearly visible on both field corridor stacks in Figure 3.7g and h, where there is very low reflectivity at large depth due to extensive scattering (hence reduced amplitude of the incident wave) over long travel paths. The reflections on the synthetic and field corridor stacks for well K-18 occur at similar times, supporting the validity of the 1D velocity model along the borehole.

3.4.6 Reflection seismic processing and migration of the walk-away data

The walk-away data were processed in the same manner as the zero-offset data. An example source gather for the walk-away source position Thor 11 (~320 m away from well K-18) before and after processing is shown in Figure 3.8a and b, respectively. The direct P-wave, a multiple and several primary reflections (black arrows) are observed in the field data. To better understand the characteristics of the wavefield such as P to S-wave conversions and reflections, synthetic waveform data were calculated for the walk-away source positions. To be consistent with the synthetic calculations of the zero-offset data we again used a dominant frequency of 28 Hz. The 1D velocity model (Figure 3.3b) proved to be insufficient to match the field data since the subsurface is strongly heterogeneous and geological features only have a small lateral extent. Therefore, the velocity model obtained from traveltime tomography with geological constraints (Figure 3.6b) was used for the calculations. Since the velocity model is rather smooth it does not result in clear reflections. It is known that densities also change for the different geological units (Grab et al. (2017)). Therefore, we assigned different density values to the units of the composite model (near surface: 1250 kgm^{-3}, hyaloclastite: 1842 kgm^{-3}, basalt: 2380 kgm^{-3}, gabbro 3288 kgm^{-3} that correspond to minimum and maximum values based on Grab et al. (2017) to introduce impedance contrasts, resulting in reflections while using the model in Figure 3.6b as our input velocities to preserve the same traveltimes. The edges of the different bins were smoothed so that no diffractions were produced due to the blocky shape of the composite model.
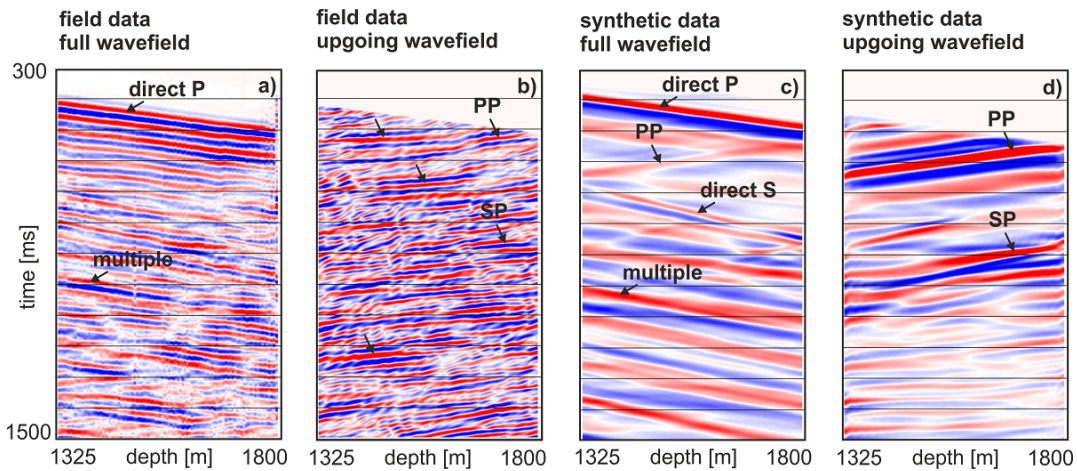
Figure 3.8: Comparison between field (a, b) and synthetic data (c, d) for the full as well as the upgoing wavefield for source position Thor 11. Direct wave, multiples and primary reflected events can be identified on both synthetic and field data and are marked by arrows.

A comparison between the synthetic data and the field data for both the full as well as the upgoing wavefield only recorded by the vertical component for source position Thor 11 (~320 m away from well K-18) is shown in Figure 3.8. Generally, the field data are much more complex than the synthetic data, indicating that the composite model is likely too simplistic and allows us to only explain some of the events observed in the field data (note more reflections in Figure 3.8b than Figure 3.8d indicated with black arrows). The direct P-wave as well as a prominent PP reflection can be identified on both the synthetic and the field data (marked with PP). A prominent downgoing multiple can also be observed on both data sets. In contrast, the direct S-wave and a mode-converted S-to-P wave that results in a prominent SP reflection are much more clearly visible in the synthetic data. An upgoing event can be observed in both the field and the synthetic data at the same arrival time, which might be an SP conversion. The events have a slightly different moveout, which could indicate that the actual reflector has a different dip than the one anticipated. Additionally, a number of events that are only observed on the field data are indicated with black arrows. It remains unclear if these events are reflections or multiples.

To better map the observed reflections to their points of origin, the data were migrated. A multicomponent Kirchhoff prestack depth migration algorithm was used that includes a wavefield separation step to obtain individual PP, PS and SS migrated images (see Appendix for a detailed description of the algorithm). We used the P and S-wave velocity models obtained from the traveltime inversion to compute the traveltimes of PP-, PS-, and SS-reflections. To separate the wavefields at a geophone, the vector formed by the recorded vertical and horizontal components is projected into the direction of the desired P- or S-wave particle motion using the arrival direction computed by ray tracing. Thereby, the recorded amplitudes are rotated either in the direction of propagation for P-wave or perpendicular to it for S-wave imaging.

An overview of all source positions used for the migration, the active receiver layout and individual and stacked migration outputs for the walk-away survey are shown in Figure 3.9. The overall quality of the walk-away data decreases considerably with increasing offset. Due to the small number of

source positions, stacking the individually migrated source gathers does not significantly reduce the amount of smeared-out energy ('migration smiles' or Fraunhoffer arcs) by destructive interference. To assess the quality of the migrated images, we marked the individual migrated reflectors with different colors, depending on whether they were observed on one (yellow) or more than one migrated source gather (blue) or whether a reflector could be observed on several source gathers and more than one migrated mode (green) (PP, PS, SS; Figure 3.9). An example of the analysis of single source migrated images is shown in Figure 3.9a-d. PS migration images from Thor 10 and 11, as well as SS and PP migration images for Thor 10 are shown. It can be seen that the migration of only one source position leads to significant smearing and, hence, ambiguity in the true location of the reflector. However, since we expect either sub-horizontal or steeply dipping interfaces in the investigation area, we restricted the possible reflector locations to either horizontal or steeply dipping interfaces, where slightly higher amplitudes were observed. This approach is subjective and shows that the interpretation is ambiguous with the limited number of source positions and the small aperture of the data. We tried to reduce the ambiguity by introducing the quality scheme and including as much à priori information as possible.

For well K-18, the migrated images of the near-offsets source gathers (Thor 10 and 11) exhibit the highest quality and show similar characteristics (Figure 3.9a, b). Several identical reflections can be observed in the two migrated source gathers as well as for different wave modes (blue and green dashed lines). The summed PP, PS and SS migration images are shown in Figure 3.9f-h). Generally, the PS and the SS migrated images show higher resolution due to the slower S-wave velocities and, hence, smaller wavelengths compared to P-waves. The different migration modes show common features (green dashed lines) as well as complementary information (yellow dashed lines).

The PP, PS and SS migration results for the complete walk-away dataset are shown in Figure 3.9i-k. The flat laying interfaces are generally slightly weaker in amplitude, mostly due to lower quality of the far-offset source recordings. Large horizontal distances between sources and receivers have a favourable geometry to image steeply dipping interfaces in the vicinity of the borehole. Therefore, steeply dipping features appear on the migration images of the full walk-away survey more prominently compared to the near-well source gathers. The positions of the dipping interfaces vary for the different migration modes. This could be due to variable illumination by the different wave modes or due to the lack of velocity constraints in the area that is not covered by travel time tomography (to the east of well K-18 and to the west of K-26).
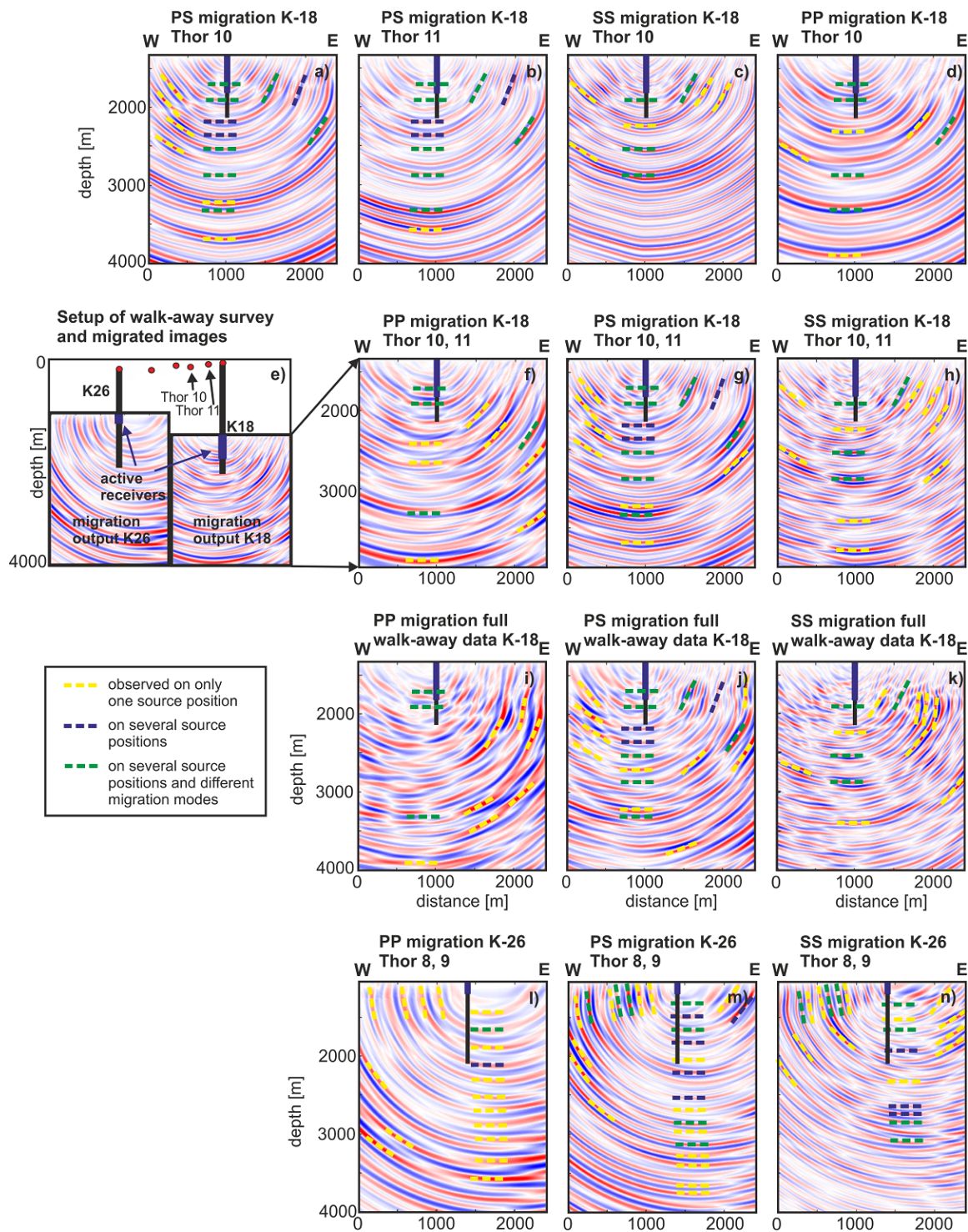
Figure 3.9: a-d) K-18 PS single source migrated images for Thor 11 and 10 and K-18 PP/SS single source migrated images for Thor 11. e) Setup of the source positions, active receiver layout and migration output for the walk-away survey. K-18 PP, PS and SS migrated images are shown for the near-offsets source positions (f-h), for the full walk-away data (i-k) and for K-26 near-offsets (l-n). Reflections that are observed on only a single source position are shown with yellow dashed lines, on several source positions with blue dashed lines and several source positions and different migration modes with green dashed lines. Common events can be identified on the different modes, but also complementary information can be extracted. More steeply dipping interfaces appear on the full walk-away data, since far offset source positions have a favourable geometry to image steeply dipping features.

3.5 Interpretation

The interpretation is organized such that we first analyze the structures in the vicinity of the borehole based on traveltime tomography, corridor stacks and the migrated section along the borehole, then the area between the boreholes is examined taking traveltime tomography into account and finally the structures around and to the sides of the wells are considered based on the migrated walk-away data.

In the following we denote reflectors identified from observations in borehole K-18 with r1, r2, r3, etc., and reflectors identified from observations in K-26 with R1, R2, R3. Identical reflection numbers (e.g., r2 and R2) indicate that these reflections originate from the same feature (reflector).

3.5.1 Structures in the immediate vicinity of the boreholes K-18 and K-26

In Figure 3.10 the composite and the geological model are shown together with the corridor stacks of the zero-offset data for well K-18 and K-26 (Figure 3.10) and the PS migrated sections along a portion of the borehole. We observe that most of the main lithological boundaries coincide with strong reflections (highlighted with red rectangles). The corridor stack of K-18 shows clear reflections for the alternating sequence between the hyaloclastites and basalts (depth of 400 m, 800 m and 950 m). Decreased reflection amplitudes below the depth of 1100 m are probably related to increased scattering and absorption and smaller impedance contrasts within the intrusion-dominated rock.

In K-26 weaker amplitudes are observed down to 500 m and strong reflections from the lower interfaces between hyaloclastites, basalts, and intrusion-dominated rock can clearly be identified (depth of 750 m and 950 m). Interfaces between large-scale structures coincide with reflections observed on
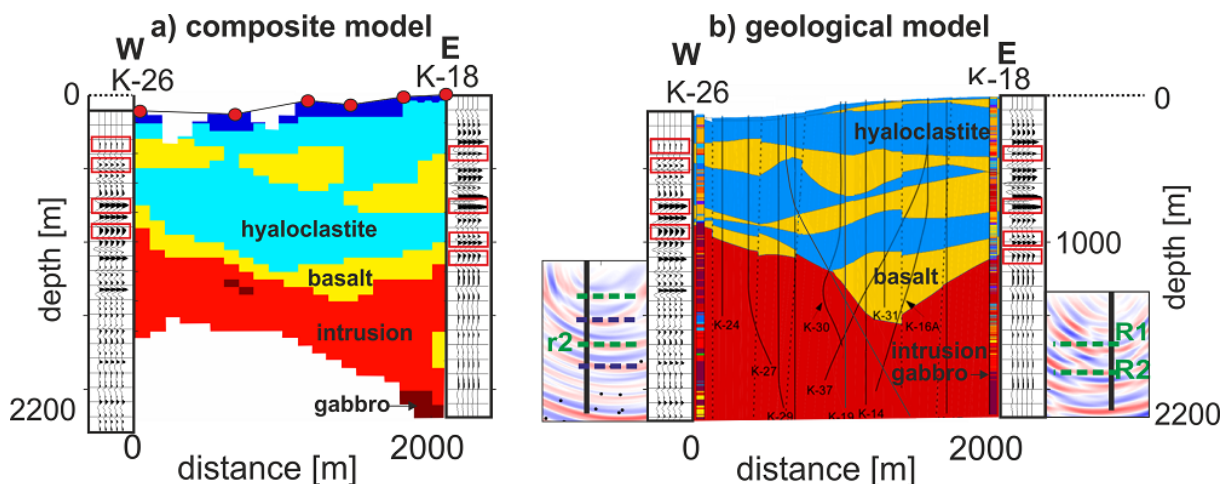
Figure 3.10: The composite and geological model (**planke16**) are shown together with the corridor stack of the zero offset data and the PS migrated section of the walk-away data. The composite and the geological model look similar, indicating that seismic velocities are mainly controlled by geology. Reflections observed on the corridor stacks correlate well with the main lithological units (red rectangles). The reflections on the PS migrated section are consistent with the reflections on the corridor stacks. Refelctors r2/R2 on the migrated images show the transition between intrusion-dominated rock and gabbro.

the corridor stack (red rectangles). The reflection data also reveal internal structures that are related to small scale lithological changes, different degrees of alteration of the rock or small sequences of intrusions (The detailed lithological sequence along the two boreholes can be found in the Appendix; Planke et al. (2016) and the stratigraphic analysis of well K-18 in Millett et al. (2018)).

The reflections observed on the walk-away PS migrated section of the K-26 walk-away data are consistent with the reflections of the corridor stack (Figure 3.10). For the migrated image of K-18 the correlation is less pronounced and the different frequency content makes a direct comparison difficult. However, in both migrated sections a clear reflection is observed for the transition between intrusion-dominated rock and gabbro (r2/R2) at a depth of 1880 m for well K-18 and 1720 m for well K-26 that can also be observed on the corridor stack. Reflector R1 can be related to an altered fracture zone at well K-18 (Planke et al. (2016)). From the borehole information there is no clear indication of the origin of other reflections marked with dashed lines along the borehole of K-26 and hence these reflectors are less certain.

3.5.2   Structures between boreholes K-18 and K-26

The interpretation of the structures between the wells is based on the tomography results with geological à priori information. We would like to emphasize the importance of including à priori information to obtain more structural details and to reduce the ambiguity of the interpretation. The large-scale structures of the geophysically inferred and mapped geological units look similar to the geological model, such as the alternating sequence between hyaloclastites and basalts in the first kilometer and the bowl-shaped interface between the basalt and intrusion-dominated rock in the center of the profile (Figure 3.10). Hence, we can infer that seismic velocities are mainly controlled by lithology at large scales.

Differences between the models are visible on the small scale. The rather thin intermediate basalt layer at ~700 m depth is not recovered by the tomography, the interface between the basalt and intrusion-dominated rock is flatter in the composite model and the transition to the gabbro occurs at greater depth. The differences might result from the resolution limit of the tomography method (Figure 3.4m), but also due to the fact that seismic velocities are not only controlled by lithology, but also other factors, such as porosity, temperature, fractures, micro-cracks, water or gas saturation. These factors can influence the seismic velocity and further add to the complexity of the model.

3.5.3   Large-scale structures around the K-18 and K-26 boreholes from reflection imaging

The PS migration result for the near offsets for well K-18 and K-26 are shown with interpreted reflectors marked by dashed lines (Figure 3.11b). Hypocenter locations of earthquakes that were recorded between November 2015-2016 are shown as black dots (Blanck et al. (2011)). The hypocenters up to a maximum distance of 500 m from the survey line were projected onto the migrated images. To better understand the distribution of the earthquakes in 3D and the locations of geological features (fault zones, caldera rim) a top view of the area is presented in Figure 3.11a. The earthquake hypocenters are mainly located around well K-26, because it is an injection well, where fluids are injected into the surrounding rock.

3.5.4 Structures below the boreholes

The reflectors below the boreholes are generally less reliable and need to be interpreted with more caution, since they cannot be directly linked to borehole data. Other information needs to be considered, such as microseismicity (Blanck et al. (2011)) to relate the reflectors to geological features. The exact locations of the reflectors are less certain with increasing depth because the migration velocities below the borehole are not constrained by the tomography and were extrapolated.

The earthquakes occur mainly around a depth of 2000 m in the area of well K-26 and slightly increase in depth towards the east and west. The majority of the earthquakes are located just above the brittle-ductile transition (BDT) that was located at 2300 m depth based on the seismicity study (Blanck et al. (2011)). The approximate trend of the BDT follows the lower end of the earthquake locations and is shown in Figure 3.11b (light green dashed line). As the depth of earthquakes slightly increases towards the east, the brittle-ductile boundary is expected to be slightly deeper below well K-18 than K-26. Reflectors that might be related to the BDT are marked with r3 for well K-26 and R3 for well K-18 (Figure 3.11b). Reflections from the BDT have been observed in other seismic reflection surveys over geothermal fields. For example, Cameli et al. (1998) related a strong reflection to an active shear zone at the brittle-ductile boundary in southern Tuscany and it is known that seismic velocities strongly decrease at the BDT (Murase and McBirney (1973)). Hence, the BDT might lead to an impedance contrast detectable by seismic reflection if the changes in seismic properties are distinct rather than a smooth transition with depth.

K-18 and K-26 are directly located over a magma chamber that was inferred from the observation of strong S-wave attenuation (Einarsson (1978); Einarsson (1991); Brandsdóttir and Menke (1992)). Based on seismic as well as magnetotelluric studies, the magma chamber is expected to be at around 3 km depth (Einarsson (1978); Árnason et al. (2007); Friðleifsson et al. (2014); Gasperikova et al. (2015)). The well at IDDP-01 (Figure 3.11a) that is located about 800 m to the north of K-26 encountered magma at a depth of 2100 m with temperatures of 900-1000 °C (Friðleifsson et al. (2015)). The large increase in temperature from ~350 °C at the lower end of the wells K-18 and K-26 (Guðmundsson and Mortensen (2015)), to ~760 °C at the brittle-ductile boundary (Fridleifsson and Elders (2005)) and a magma temperature of ~900 °C (Elders et al. (2011)) indicate that the transition occurs over a relatively short distance and hence indicate that the BDT and the top of the magma chamber lie very close together and probably lead to a sharp enough contrast detectable by seismic reflection imaging.

Similar studies have been reported where magma chambers were successfully delineated with seismic reflection imaging (Detrick et al. (1987); Carbotte et al. (2000); Singh et al. (2006)). Seismic velocities decrease with increasing content of partial melt and hence lead to a change in seismic properties (Lees (2007)). Laboratory studies have shown that seismic velocity decreases quite drastically for molten samples with temperatures of > 900 °C (Murase and McBirney (1973)) and hence a reflection from the top of the magma chamber could be feasible. Since the BDT and the top of the magma chamber lie close together, it is unclear whether r3/R3 is related to the former or the latter. On both migrated images, especially for well K-26 it can be seen that there is a section of low reflectivity below r3/R3. This could be an indication that this area might be related to the interior of the magma chamber where low reflectivity is expected.
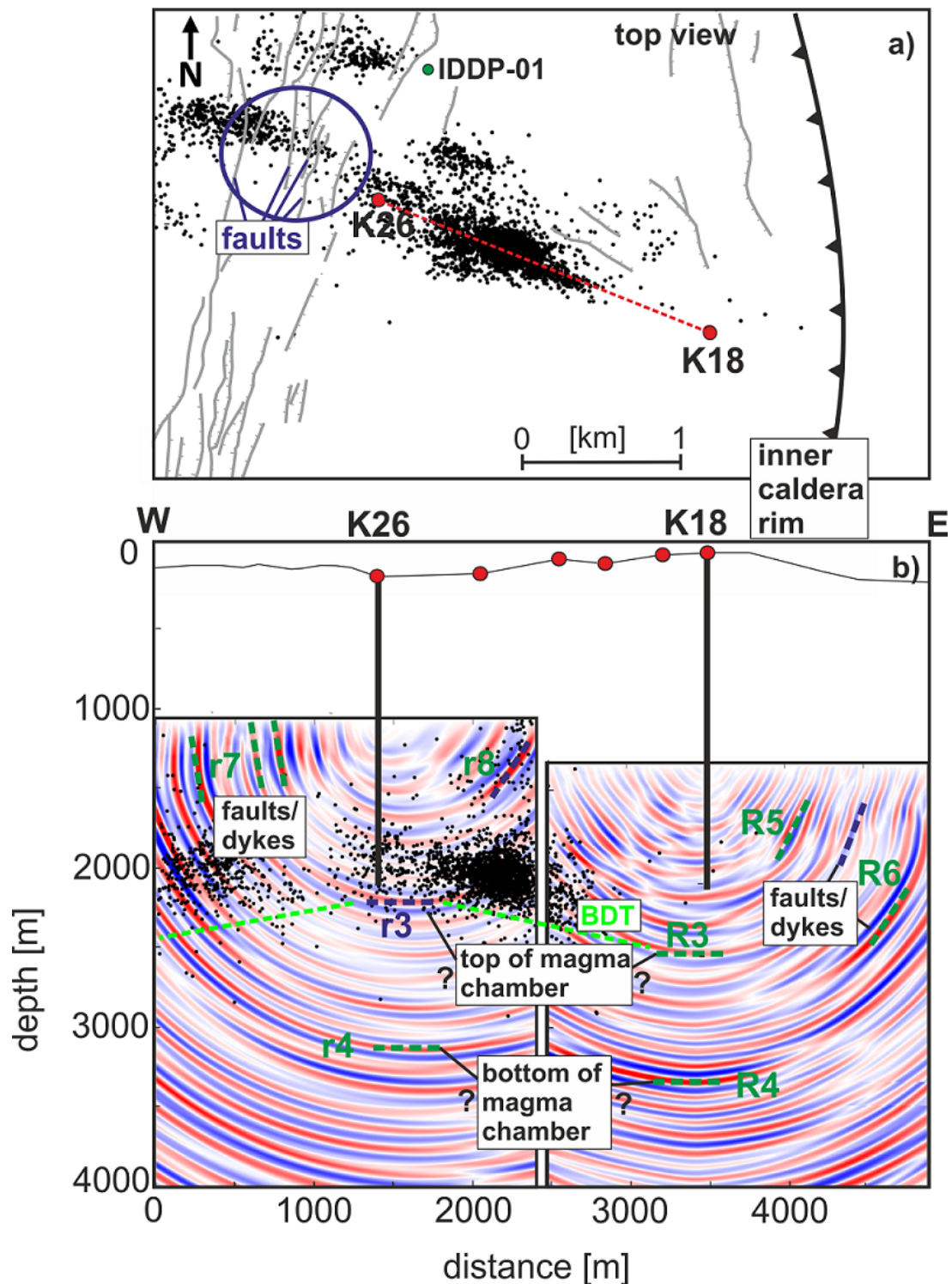
Figure 3.11: a) Top view of simplified geological map (Figure 3.2) with superimposed earthquake hypocenter locations, after Blanck et al. (2011). b) PS migration results of the near-offset source gathers of wells K-26 and K-18 (Figure 3.9e, g) together with projected earthquake locations. The majorities of earthquakes are located at around 2000 m depth. The lower seismicity band indicates a BDT (green dashed line) at around 2300 m. Reflectors r3/R3 could be related to the BDT or the top of the magma chamber due to a zone of low reflectivity below. Reflectors r4/R4 mark the bottom of the low reflectivity zone and could indicate the bottom of the magma chamber. Steeply dipping structures could be related to the inner caldera rim (R5) or fault zones/dykes (R6, r7, r8).

Below the low-reflectivity zone, a strong event is observed at 3350 m depth for well K-18 (R4) and a seismic event of moderate strength at 3250 m depth for well K-26 (r4). Since they mark the bottom of a less reflective zone, they could be related to the bottom of the magma chamber. However, the magma chamber might also be a complex system of dykes, sills and conduits that might not be of a clearly distinct form but rather show broad transitions or several small magma bodies that make the detection with seismic reflection imaging difficult (Donnelly-Nolan (1988); Lees (2007)). The reflections below r3/R3 could then be related to different degree of partial melts or small magma pockets. Another possible interpretation of the reflector is multiple energy that is still present in the data after processing or migration artefacts. Hence, these reflections need to be interpreted with caution.

3.5.5 Structures to the sides of boreholes K-18 and K-26

Steeply dipping reflectors are observed on both migrated images and marked with the labels R5, R6 for well K-18 and r7 and r8 for K-26 (Figure 3.11b). Reflector R5 is about 600 m to the east of well K-18 and could be related to a structure of the inner caldera rim if the dip increases toward the surface. The two dipping reflectors marked with R6 cannot be related to other studies. The high amplitudes of the eastern-most reflector indicate a large impedance contrast that could be associated with a fracture zone or dyke.

Steeply dipping structures are observed on the migrated image to the west of well K-26 and marked as r7 on Figure 3.11b. Several fault zones are observed in this area at the surface (Guðmundsson and Mortensen (2015)) and marked with a blue circle in Figure 3.11a. The fault zones at the surface are steeply dipping and show a strike of N to NNE (Hjartardóttir et al. (2012)). As the strike is perpendicular to the survey line, the acquisition geometry would be favorable to detect reflections from steeply dipping fault zones/ dykes extending down to about 1500 m depth with the VSP experiment. Hence, the reflectors (r7) could be related to the fault zones at the surface. However, the acquisition geometry does not allow for the imaging of such steeply dipping structures below 1500 m depth, hence it is unclear how far down the fault zones extend.

A high amplitude event is observed to the east of well K-26 and marked in the figure as r8. Based on geological à priori information there is no evidence of dykes or fault zones in this area. One possibility of this amplitude event could be an out-of-plane reflection. The reflector r8 coincides with an area of increased seismicity which would favor the interpretation of faults at that location (Figure 3.11b).

3.6 Discussion

3.6.1 Importance of à priori information

The processing and interpretation of the sparse Krafla VSP dataset is very challenging due to limited illumination of the subsurface and low spatial density of receivers to capture the scattered radiation. We tried to address this issue by integrating the results with available geological information that helps to constrain the processing and interpretation as well as limiting the ambiguity of the interpretation.

The velocity structure obtained with traveltime tomography needs to be interpreted with caution because of the limited ray coverage, especially the area between the two wells in the near surface, and the low sensitivity at greater depth (Figure 3.4m). The inversion results obtained with different starting models without including detailed à priori information all are very similar and show the transition between intrusion-dominated rock and gabbro. Therefore, we are confident that travel-time tomography can yield reliable velocity estimates of the large-scale structure (several hundreds of meters) of the area. Mapping detailed lithological units is not possible with the present acquisition geometry without including à priori information. An additional synthetic study would have to be performed to investigate, how many optimally placed source positions would be required to be able to image the lithological units without geological constraints in the starting model.

The construction of the composite model would not be possible without à priori knowledge, hence we emphasize the importance of à priori information. The composite model should not be regarded as a model where physical properties are uniform within the different geological units, but rather it gives plausible bulk velocities that help identify the main lithologies of the system. The bin size that determines the clustering is somewhat subjective. Hence, several plausible composite models are possible. However, by taking à priori information into account we could limit the possibilities and chose the one that is consistent with the geology.

3.6.2   Limited illumination of the subsurface

Stacking of only a few migrated images does not allow completely cancelling migration artefacts by destructive interference. Hence, events observed on the migrated image need to be interpreted with caution. To address this problem we also processed and compared images of converted P- and S-wave images as they illuminate the subsurface regions differently and can yield additional information (Wei et al. (2014)a,b). Even though there was not a specific S-wave source used during the survey, there is significant S-wave energy present in the data. It is unclear where exactly the mode conversion from the predominantly P-wave source signals occurs, but it must be in the upper few meters (e.g. Schmelzbach et al. (2008)), since S-wave energy can be traced back to the uppermost receiver (10 m depth) in the zero offset gathers. Any asymmetry surrounding a P-source will induce S-wave energy. Through analyzing PP, PS and SS migrated images we can extract more information from the multicomponent dataset and can better evaluate the reliability of certain events. Another possibility to obtain more information about the different reflections would be to analyze the polarity of the arrivals which was beyond the scope of this study.

Whereas reflections intersecting the borehole can be verified by geological information based on cutting analysis, the interpretation of deeper events such as the reflection from the BDT or reflections related to the magma chamber is less certain. The P- and S-wave velocities are not constrained away from the borehole and hence the uncertainty of the location increases with increasing depth/distance from the borehole. To better interpret the deeper reflections, we combined results of different geophysical studies, e.g. seismicity and EM studies, to assign reflection events to certain geological interfaces.

3.7 Conclusions

In this study, seismic data from the first VSP experiment in a high temperature geothermal field in Iceland have been analyzed. A workflow was established that enables the construction of a geophysical model of the subsurface based on traveltime inversion and seismic reflection processing. The geophysical model revealed lateral variations in structure between the two boreholes that can directly be linked to the existing geological model. Seismic reflection processing of the walk-away data disclosed reflectors below and to the sides of the boreholes. Based on the study we conclude that:

- VSP is a potentially useful method to image the key lithological boundaries and volcanic stratigraphy in a complex magmatic environment with available à priori information.

- À priori information is essential to constrain sparse VSP datasets, especially for the interpretation of structures that do not intersect the borehole.

- The combined interpretation of PP, PS and SS migrated images helped to assess the reliability of reflections and hence demonstrate the benefit of acquiring seismic data with 3-component geophones.

We observed the following limitations from the experiment:

- The layering sequence between basalts and hyaloclastites on the order of 250 m in the upper 1500 m could not be resolved with traveltime tomography without including à priori information. This demonstrates the resolution limit of the method with the particular acquisition geometry.

- Due to the sparseness of the dataset significant migration artifacts exist, that make interpretation ambiguous in terms of the actual location and dip of the reflectors.

- Due to the 2D geometry of the acquisition, it is not possible to place the reflectors in 3D.

- Reflectors below and to the sides of the boreholes can only be interpreted with caution since velocities are not constrained and possible energy associated with multiples might result in artefacts.

For future surveys we recommend:

- More source points would be favorable to improve illumination and cancel out the artifacts in the migrated images by the process of destructive interference and hence reduce the ambiguity of the interpretation.

- Acquiring more source points at the near-offset range (<1000 m) because the far offset source positions turned out to be of less value due to the low signal-to noise ratios.

- Deploying receivers over a larger depth range.

- Acquiring several source lines to obtain an image in 3D.

- As à priori information was essential in this study we stress the need for interdisciplinary projects in the future where various methods with different capabilities and limitations can be combined to obtain complementary subsurface information.

Acknowledgement

References

Adam, E., T. Bohlen, and B. Milkereit. 2003. "Vertical seismic profiling at the Bell Allard orebody, Matagami, Quebec". In *Hardrock seismic exploration*, 181–193. Society of Exploration Geophysicists.

Ármannsson, H., Á. Gudmundsson, and B. Steingrímsson. 1987. "Exploration and development of the Krafla geothermal area". *Jökull* 37:13–30.

Árnadóttir, S. 2011. *Results of Televiewer Logging in Well K-18 in Krafla High Temperature Area, NE-Iceland*. Reykjavík: Iceland GeoSurvey. ISOR-2014/066.

Árnason, K., V. A.M., and T. Björnsdóttir. 2007. "A study of the Krafla volcano using gravity, micro earthquake and MT data". *Short Course II on Surface Exploration for Geothermal Resources, Kenya*.

Bellefleur, G., C. Müller, D. Snyder, and L. Matthews. 2004. "Downhole seismic imaging of a massive sulfide orebody with mode-converted waves, Halfmile Lake, New Brunswick, Canada". *Geophysics* 69 (2): 318–329.

Björnsson, A. 1985. "Dynamics of crustal rifting in NE Iceland". *Journal of Geophysical Research: Solid Earth* 90 (B12): 10151–10162.

Blanck, H., K. Ágústsson, and K. Gunnarsson. 2011. *Seismic Monitoring in Krafla. November 2015 to November 2016*. Internal report prepared by Iceland GeoSurvey (ÍSOR) for Landsvirkjun. Project no.: 16-0050.

Bodvarsson, G. S., S. M. Benson, O. Sigurdsson, V. Stefansson, and E. T. Eliasson. 1984. "The Krafla geothermal field, Iceland: 1. Analysis of well test data". *Water Resources Research* 20 (11): 1515–1530.

Bohlen, T., C. Müller, and B. Milkereit. 2003. "Elastic seismic-wave scattering from massive sulfide orebodies: On the role of composition and shape". In *Hardrock seismic exploration*, 70–89. Society of Exploration Geophysicists.

Brandsdottir, B., and P. Einarsson. 1979. "Seismic activity associated with the September 1977 deflation of the Krafla central volcano in northeastern Iceland". *Journal of Volcanology and Geothermal Research* 6 (3-4): 197–212.

Brandsdóttir, B., and W. H. Menke. 1992. "Thin low-velocity zone within the krafla caldera, ne-Iceland attributed to a small magma chamber". *Geophysical research letters* 19 (24): 2381–2384.

Brandsdóttir, B., W. Menke, P. Einarsson, R. S. White, and R. K. Staples. 1997. "Färoe-Iceland Ridge Experiment 2. Crustal structure of the Krafla central volcano". *Journal of Geophysical Research: Solid Earth* 102 (B4): 7867–7886.

Cameli, G., F. Batini, I. Dini, J. Lee, R. Gibson Jr, and M. Toksöz. 1995. "Seismic delineation of a geothermal reservoir in the Monteverdi area from VSP data". In *Proceedings of the World Geothermal Congress*, 2:821–826. Florence Italy.

Cameli, G., I. Dini, and D. Liotta. 1998. "Brittle/ductile boundary from seismic reflection lines of southern Tuscany (Northern Apennines, Italy)". *Mem. Soc. Geol. It* 52:153–162.

Carbotte, S. M., A. Solomon, and G. Ponce-Correa. 2000. "Evaluation of morphological indicators of magma supply and segmentation from a seismic reflection study of the East Pacific Rise 15 30'–17 N". *Journal of Geophysical Research: Solid Earth* 105 (B2): 2737–2759.

Cosma, C., P. Heikkinen, and J. Keskinen. 2003. "Multiazimuth VSP for rock characterization of deep nuclear waste disposal sites in Finland". In *Hardrock seismic exploration*, 207–226. Society of Exploration Geophysicists.

Cosma, C., O. Olsson, J. Keskinen, and P. Heikkinen. 2001. "Seismic characterization of fracturing at the Äspö Hard Rock Laboratory, Sweden, from the kilometer scale to the meter scale". *International Journal of Rock Mechanics and Mining Sciences* 38 (6): 859–865.

Detrick, R., P. Buhl, E. Vera, J. Mutter, J. Orcutt, J. Madsen, and T. Brocher. 1987. "Multi-channel seismic imaging of a crustal magma chamber along the East Pacific Rise". *Nature* 326 (6108): 35–41.

Donnelly-Nolan, J. M. 1988. "A magmatic model of Medicine Lake volcano, California". *Journal of Geophysical Research: Solid Earth* 93 (B5): 4412–4420.

Einarsson, P. 1978. "S-wave shadows in the Krafla caldera in NE-Iceland, evidence for a magma chamber in the crust". *Bulletin of Volcanology* 41 (3): 187–195.

Einarsson, P. 1991. "Earthquakes and present-day tectonism in Iceland". *Tectonophysics* 189 (1-4): 261–279.

Elders, W., G. Fridleifsson, and A. Albertsson. 2014. "Drilling into magma and the implications of the Iceland Deep Drilling Project (IDDP) for high-temperature geothermal systems worldwide". *Geothermics* 49:111–118.

Elders, W. A., G. Ó. Friðleifsson, R. A. Zierenberg, E. C. Pope, A. K. Mortensen, Á. Guðmundsson, J. B. Lowenstern, N. E. Marks, L. Owens, D. K. Bird, et al. 2011. "Origin of a rhyolite that intruded a geothermal well while drilling at the Krafla volcano, Iceland". *Geology* 39 (3): 231–234.

Emsley, S., P. Shiner, N. Enescu, A. Beccacini, and C. Cosma. 2007. "Using VSP surveys to bridge the scale gap between well and seismic data". *Geological Society, London, Special Publications* 270 (1): 83–91.

Friðleifsson, G., H. Ármannsson, Á. Guðmundsson, K. Árnason, A. Mortensen, B. Pálsson, and G. Einarsson. 2014. "Site selection for the well IDDP-1 at Krafla". *Geothermics* 49:9–15.

Friðleifsson, G., B. Pálsson, A. Albertsson, B. Stefánsson, E. Gunnlaugsson, J. Ketilsson, and P. Gíslason. 2015. "IDDP-1 drilled into magma—World's first magma-EGS system created". In *World Geothermal Congress*, 19–25.

Fridleifsson, G. O., and W. A. Elders. 2005. "The Iceland Deep Drilling Project: a search for deep unconventional geothermal resources". *Geothermics* 34 (3): 269–285.

Gaiser, J. 2016. *3C Seismic and VSP: Converted waves and vector wavefield applications*. Society of Exploration Geophysicists.

Gasperikova, E., G. K. Rosenkjaer, K. Arnason, G. A. Newman, and N. J. Lindsey. 2015. "Resistivity characterization of the Krafla and Hengill geothermal fields through 3D MT inverse modeling". *Geothermics* 57:246–257.

Gibson Jr, R., J. Lee, M. Toksöz, I. Dini, and G. Cameli. 1995. "Three-dimensional Kirchhoff migration analysis of VSP data from a geothermal field". In *Proceedings of the World Geothermal Congress*, 2:821–826. Florence Italy.

Grab, M., B. Quintal, E. Caspari, H. Maurer, and S. Greenhalgh. 2017. "Numerical modeling of fluid effects on seismic properties of fractured magmatic geothermal reservoirs". *Solid Earth* 8 (1): 255.

Guðmundsson, Á., and A. K. Mortensen. 2015. "Well Locations Consideration of Purpose, Objectives and Achievement with Emphasis on Recent Drilling in the Krafla Geothermal Area". In *Proc. World Geothermal Congress*.

Halldórsdóttir, S., Ö. Erlendsson, G. Hersir, K. Gunnarsson, A. Blischke, H. Helgadóttir, S. Árnadóttir, H. Blanck, F. Kästner, and S. Planke. 2014. *Vertical Seismic Profiling (VSP) Experiment in Krafla, NE-Iceland Field Report – Summary of Operations from May to June 2014*. ISOR-2014/073, 78 pp.

Halldórsdóttir, S., H. Björnsson, A. K. Mortensen, G. Axelsson, and Á. Guðmundsson. 2010. "Temperature model and volumetric assessment of the Krafla geothermal field in N-Iceland". *Proc. World Geotherm. Congr., C*.

Hardage, B. A. 2000. *Vertical seismic profiling*. Handbook of Geophysical Exploration, Seismic Exploration, 14, Pergamon.

Hersir, G., Ö. Erlendsson, H. Ingólfsson, H. Stefánsson, and H. Tryggvason. 2016. *Sonic Logging - A Field Report for Well K-18 in Krafla, NE-Iceland, and Well YT-2 and LA-8 in Eyjafjörður, N-Iceland*. ISOR-2016/028.

Hjartardóttir, Á. R., P. Einarsson, E. Bramham, and T. J. Wright. 2012. "The Krafla fissure swarm, Iceland, and its formation by rifting events". *Bulletin of volcanology* 74 (9): 2139–2153.

Hólmgeirsson, S., A. Gudmundsson, B. Pálsson, H. Bóasson, K. Ingason, and S. Thorhallsson. 2010. "Drilling operations of the first Iceland deep drilling well (IDDP)". In *Proceedings of the World Geothermal Congress 2010*, 10.

Husen, S., and E. Kissling. 2001. "Local earthquake tomography between rays and waves: fat ray tomography". *Physics of the earth and Planetary Interiors* 123 (2): 127–147.

Jordi, C., C. Schmelzbach, and S. Greenhalgh. 2016. "Frequency-dependent traveltime tomography using fat rays: Application to near-surface seismic imaging". *Journal of Applied Geophysics* 131:202–213.

Juhojuntti, N. 2001. "Seismic imaging of deep crustal reflectivity in Sweden and Iceland". PhD thesis, Acta Universitatis Upsaliensis.

Kästner, F., R. Giese, S. Planke, J. Millett, and Ó. Flóvenz. 2018. *Seismic imaging in the Krafla high-temperature geothermal field, NE Iceland, using zero- and far-offset vertical seismic profiling (VSP) data*. Submitted to Journal of Volcanology and Geothermal Research.

Lanz, E., D. E. Boerner, H. Maurer, and A. Green. 1998. "Landfill delineation and characterization using electrical, electromagnetic and magnetic methods". *Journal of Environmental and Engineering Geophysics* 3 (4): 185–196.

Lees, J. 2007. "Seismic tomography of magmatic systems". *Journal of Volcanology and Geothermal Research* 167 (1): 37–56.

Majer, E., T. V. McEvilly, F. Eastwood, and L. Myer. 1988. "Fracture detection using P-wave and S-wave vertical seismic profiling at The Geysers". *Geophysics* 53 (1): 76–84.

Meles, G. A., S. A. Greenhalgh, A. G. Green, H. Maurer, and J. Van der Kruk. 2012. "GPR full-waveform sensitivity and resolution analysis using an FDTD adjoint method". *IEEE Transactions on Geoscience and Remote Sensing* 50 (5): 1881–1896.

Menke, W., M. West, B. Brandsdóttir, and D. Sparks. 1998. "Compressional and shear velocity structure of the lithosphere in northern Iceland". *Bulletin of the Seismological Society of America* 88 (6): 1561–1571.

Millett, J., S. Planke, F. Kästner, A. Blischke, G. Hersir, S. Halldórsdóttir, Ó. Flóvenz, S. Árnadóttir, H. Helgadóttir, S. Vakulenke, S. Buryak, Ö. Elendsson, R. Giese, J. Cavailhes, D. Jerram, Á. Guðmundsson, and E. Júlísson. 2018. *Sub-surface geology and velocity structure of the Krafla high temperature geothermal field, Iceland: Integrated ditch cuttings, wireline and zero offset vertical seismic profile analysis*. Submitted to Journal of Volcanology and Geothermal Research.

Murase, T., and A. McBirney. 1973. "Properties of some common igneous rocks and their melts at high temperatures". *Geological Society of America Bulletin* 84 (11): 3563–3592.

Nakagome, O., T. Uchida, and T. Horikoshi. 1998. "Seismic reflection and VSP in the Kakkonda geothermal field, Japan: Fractured reservoir characterization". *Geothermics* 27 (5): 535–552.

Opheim, J. A., and A. Gudmundsson. 1989. "Formation and geometry of fractures, and related volcanism, of the Krafla fissure swarm, northeast Iceland". *Geological Society of America Bulletin* 101 (12): 1608–1622.

Pálsson, B., S. Hólmgeirsson, Á. Guðmundsson, H. Bóasson, K. Ingason, H. Sverrisson, and S. Thórhallsson. 2014. "Drilling of the well IDDP-1". *Geothermics* 49:23–30.

Perron, G., D. Eaton, B. Elliot, and D. Schmitt. 2003. "Application of downhole seismic imaging to map near-vertical structures: Normétal (Abitibi Greenstone Belt), Québec". In *Hardrock seismic exploration*, 194–206. Society of Exploration Geophysicists.

Phillips, W. S., and M. C. Fehler. 1991. "Traveltime tomography: A comparison of popular methods". *Geophysics* 56 (10): 1639–1649.

Place, J., M. Diraison, C. Naville, Y. Géraud, M. Schaming, and C. Dezayes. 2010. "Decoupling of deformation in the Upper Rhine Graben sediments. Seismic reflection and diffraction on 3-component Vertical Seismic Profiling (Soultz-sous-Forêts area)". *Comptes Rendus Geoscience* 342 (7): 575–586.

Planke, S., S. Halldórsdóttir, G. Hersir, Ö. Elendsson, Ó. Flóvenz, K. Gunnarsson, R. Giese, F. Kästner, E. Júlísson, and J. Millett. 2016.). *Summary Report of WP 4.02: Active Seismic with VSP*. Reykjavík: ÍSOR-2016/049.

Planke, S., P. A. Symonds, E. Alvestad, and J. Skogseid. 2000. "Seismic volcanostratigraphy of large-volume basaltic extrusive complexes on rifted margins". *Journal of Geophysical Research: Solid Earth* 105 (B8): 19335–19351.

Podvin, P., and I. Lecomte. 1991. "Finite difference computation of traveltimes in very contrasted velocity models: a massively parallel approach and its associated tools". *Geophysical Journal International* 105 (1): 271–284.

Reiser, F., C. Schmelzbach, H. Maurer, S. Greenhalgh, and O. Hellwig. 2017. "Optimizing the design of vertical seismic profiling (VSP) for imaging fracture zones over hardrock basement geothermal environments". *Journal of Applied Geophysics* 139:25–35.

Saemundsson, K. 1978. "Fissure swarms and central volcanoes of the neovolcanic zones of Iceland". *Geol. J. Spec* 10:415–432.

Sæmundsson, K. 1991. "Jardfrædi Kröflukerfisins". *Náttúra Myvatns. Hid íslenska Náttúrufrædifélag, Reykjavík*: 24–95.

Salisbury, M. H., C. W. Harvey, and L. Matthews. 2007. "The acoustic properties of ores and host rocks in hardrock terranes". In *Hardrock seismic exploration*, 9–19. Society of Exploration Geophysicists.

Scales, J. A., P. Docherty, and A. Gersztenkorn. 1990. "Regularisation of nonlinear inverse problems: imaging the near-surface weathering layer". *Inverse Problems* 6 (1): 115.

Schmelzbach, C., S. Greenhalgh, F. Reiser, J.-F. Girard, F. Bretaudeau, L. Capar, and A. Bitri. 2016. "Advanced seismic processing/imaging techniques and their potential for geothermal exploration". *Interpretation* 4 (4): SR1–SR18.

Schmelzbach, C., J. F. Simancas, C. Juhlin, and R. Carbonell. 2008. "Seismic reflection imaging over the South Portuguese Zone fold-and-thrust belt, SW Iberia". *Journal of Geophysical Research: Solid Earth* 113 (B8).

Schuler, J., T. Greenfield, R. S. White, S. W. Roecker, B. Brandsdóttir, J. M. Stock, J. Tarasewicz, H. R. Martens, and D. Pugh. 2015. "Seismic imaging of the shallow crust beneath the Krafla central volcano, NE Iceland". *Journal of Geophysical Research: Solid Earth* 120 (10): 7156–7173.

Sinadinovski, C., S. A. Greenhalgh, and I. Mason. 1995. "Three-dimensional reflector imaging of in-mine high frequency crosshole seismic data". *Exploration Geophysics* 26 (3): 325–330.

Singh, S., W. Crawford, H. Carton, T. Seher, V. Combier, M. Cannat, J. Canales, D. Düsünür, J. Escartin, and J. Miranda. 2006. "Discovery of a magma chamber and faults beneath a Mid-Atlantic Ridge hydrothermal field". *Nature* 442 (7106): 1029–1032.

Staples, R. K., R. S. White, B. Brandsdóttir, W. Menke, P. K. Maguire, and J. H. McBride. 1997. "Faeroe-Iceland Ridge Experiment 1. Crustal structure of northeastern Iceland". *Journal of Geophysical Research: Solid Earth* 102 (B4): 7849–7866.

Tang, C., J. A. Rial, and J. M. Lees. 2008. "Seismic imaging of the geothermal field at Krafla, Iceland using shear-wave splitting". *Journal of Volcanology and Geothermal Research* 176 (2): 315–324.

Thomas, R., and R. Schulz. 2007. "Facies differentiation of the Malm by interpretation of reflection seismic profiles and a moving source VSP Experiment". In *Proceedings of the European Geothermal Congress*.

Wei, S., M. V. DeAngelo, and B. A. Hardage. 2014. "Advantages of joint interpretation of PP and P-SV seismic data in geothermal exploration". *Interpretation*.

Weisenberger, T. B., G. Axelsson, A. Arnaldsson, A. Blischke, F. Óskarsson, H. Ármannsson, H. Blanck, H. Helgadóttir, J. Berthet, K. Árnason, K. Ágústsson, S. Gylfadóttir, and V. Guðmundsdóttir. 2015. "Revision of the conceptual model of the Krafla geothermal system".

Appendix A

Multicomponent pre-stack Kirchhoff migration

We adapt a simple multicomponent migration algorithm that was first introduced by (Sinadinovski et al. (1995)) for applications in mine seismology. A reflector in the subsurface can be thought of as a set of closely spaced point scatterers. Since the impulse response of a point scatterer is a diffraction hyperbola with a curvature depending on the velocity of the medium, the probability that a scatterer exists at a specific point in the subsurface can thus be estimated by a summation (integration) of the recorded amplitudes along the diffraction hyperbola. In order to achieve a separation between P- and S-waves we additionally take into account polarisation properties. Here we provide a detailed description of the multicomponent pre-stack Kirchhoff migration that we applied in this paper. Geometrical considerations for the algorithm are given in Figure 3.12.

First, the medium is discretised into a subset of pixels (or voxels in 3D) with Nz pixels in the vertical direction and Nx pixels in the horizontal direction. We then use a raytracer and appropriate P- and S-wave velocity models to calculate the traveltimes from each source position $\boldsymbol{x}_S=(x_S,z_S)$ to each subsurface pixel position $\boldsymbol{x}_P=(x_P,z_P)$ and subsequently from each pixel to each receiver position $\boldsymbol{x}_R=(x_R,z_R)$. As a raytracer, we use a finite-difference solver for the Eikonal equation (Podvin and Lecomte (1991)). This results in traveltime fields $T(\boldsymbol{x}_P,\boldsymbol{x}_S)$, from each source to each pixel, and $T(\boldsymbol{x}_R,\boldsymbol{x}_P)$, from each pixel to each receiver. The total source-to-pixel-to-receiver traveltime t_{i0} is then simply given by:

$$t_{i0} = T(\mathbf{x}_P,\mathbf{x}_S) + T(\mathbf{x}_R,\mathbf{x}_P). \tag{3.1}$$

Now, we estimate the inclination angle θ at which the ray impinges on the receiver. This is easily done by calculating the gradient $g(\boldsymbol{x}_R,\boldsymbol{x}_P)$ of the traveltime field $T(\boldsymbol{x}_R,\boldsymbol{x}_P)$:

$$\mathbf{g}(\mathbf{x}_R,\mathbf{x}_P) = \begin{pmatrix} g_1(\mathbf{x}_R,\mathbf{x}_P) \\ g_2(\mathbf{x}_R,\mathbf{x}_P) \end{pmatrix} = \nabla T(\mathbf{x}_R,\mathbf{x}_P) = \begin{pmatrix} \partial_x T(\mathbf{x}_R,\mathbf{x}_P) \\ \partial_z T(\mathbf{x}_R,\mathbf{x}_P) \end{pmatrix}, \tag{3.2}$$

from which the inclination angle θ is obtained by:

$$\theta = \tan^{-1}\left(\frac{g_1(\mathbf{x}_R,\mathbf{x}_P)}{g_2(\mathbf{x}_R,\mathbf{x}_P)}\right). \tag{3.3}$$

We now compute two quantities $f^P(\boldsymbol{x}_P)$ and $f^{SV}(\boldsymbol{x}_P)$ giving the probabilities that a scatterer exists at pixel location $\boldsymbol{x}_P$ for P-waves and SV-waves, respectively, by summing the recorded amplitudes along
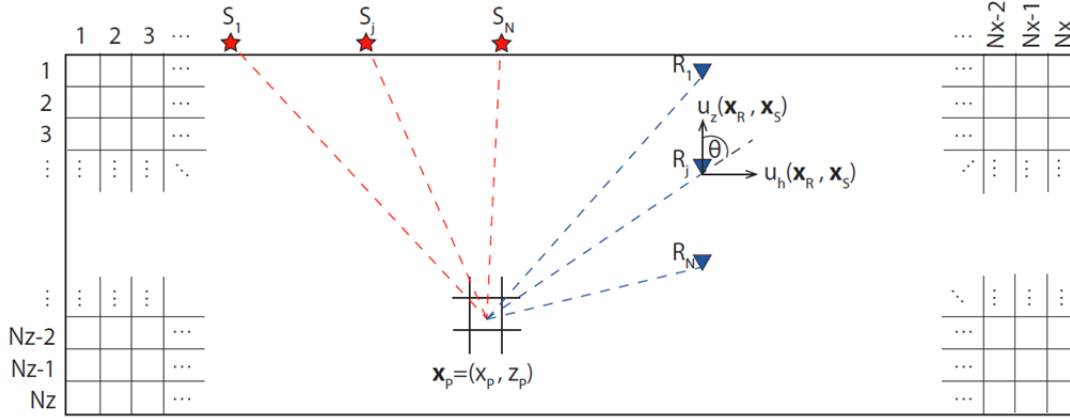
Figure 3.12: Geometry considerations for the multicomponent pre-stack Kirchhoff migration used in this paper.

the diffraction hyperbolas over all sources and all receivers and by taking into account polarisation properties:

$$
\begin{pmatrix} f^P(\mathbf{x}_P) \\ f^{SV}(\mathbf{x}_P) \end{pmatrix} = \sum_{N_S} \sum_{N_R} \sum_{i=i_0}^{i_0+W} \begin{pmatrix} \sin\theta & \cos\theta \\ \cos\theta & -\sin\theta \end{pmatrix} \begin{pmatrix} u_h(\mathbf{x}_R, \mathbf{x}_S, t_i) \\ u_z(\mathbf{x}_R, \mathbf{x}_S, t_i) \end{pmatrix}
\tag{3.4}
$$

Here, $u_h(\mathbf{x}_R,\mathbf{x}_S,t)$ is the horizontal component seismogram recorded at receiver position $\mathbf{x}_R$ as response to a source at position $\mathbf{x}_S$ and $u_z(\mathbf{x}_R,\mathbf{x}_S,t)$ is the vertical component seismogram for the same source–receiver pair. N_S and N_R are the number of sources and receivers, respectively. We additionally include a summation over a time-window of length W to account for the band-limited nature of seismic data. The window length W is chosen to be equal to the dominant period of the data.

In Equation 4, the multicomponent data is projected onto the ray-direction (θ) for P-waves and onto a direction orthogonal to it for SV-waves. This accounts for the different polarisations of the two wave-modes and allows to accurately treat the amplitudes over the whole incidence angle range. If a scatterer is present at the pixel position $\mathbf{x}_P$, amplitudes will add constructively along the diffraction hyperbola, resulting in high values for f^P and f^{SV}. If no scatterer is present, destructive interference will result in small scatterer probabilities f^P and f^{SV}. Finally, the scatterer probabilities are colour-coded and displayed to give the resulting migrated images.

Note that both of the two traveltime fields in Equation 1 can either be computed with a P- or an S-wave velocity model, which allows to image both pure-mode and arbitrarily mode-converted waves.

Appendix B

Lithology of the boreholes K-18 and K-26
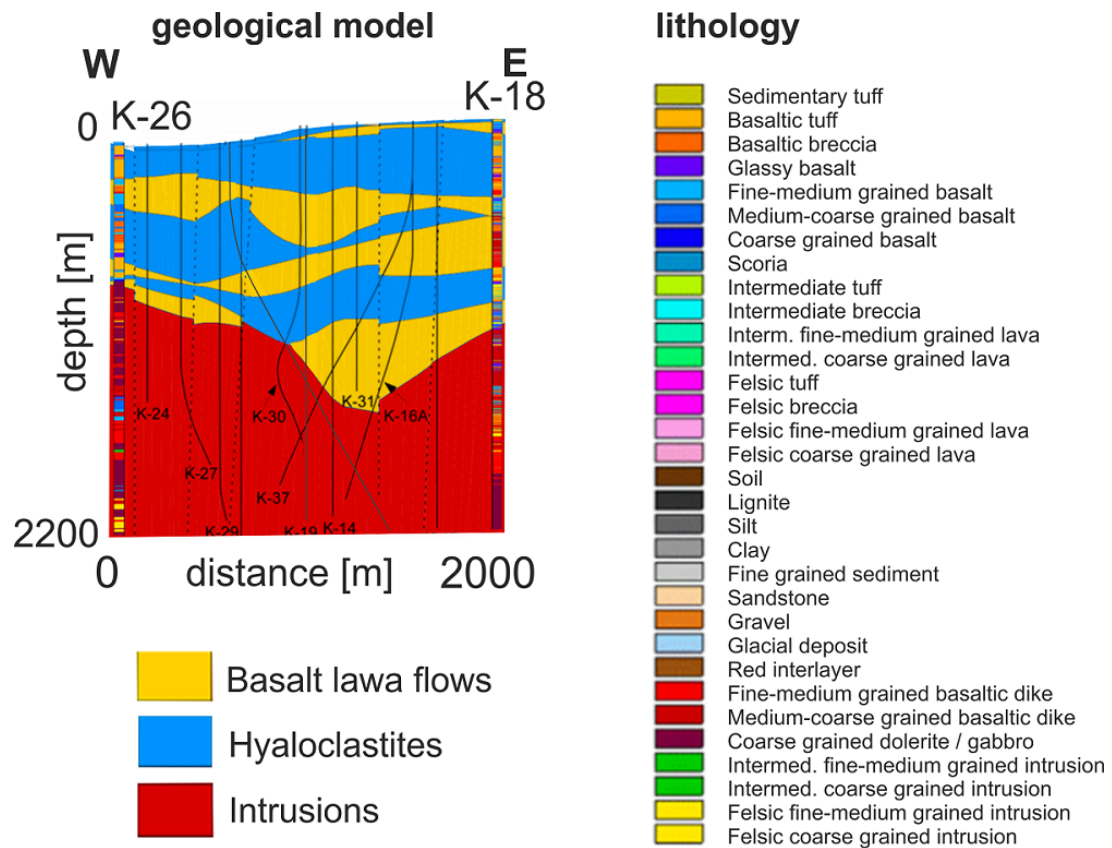
Figure 3.13: Geological model and lithology along the boreholes based on drillhole cuttings (Weisenberger et al. (2015); Planke et al. (2016)).

Full waveform inversion of the VSP data in Thonex

This chapter comprises the application of FWI to a VSP dataset in geothermal environment. Furhter research is required before it can be published.

Abstract

Full waveform inversion (FWI) aims at retrieving subsurface velocity information from the complete seismic wavefield and provides image resolution at wavelength to sub-wavelength scales. Elastic FWI was performed with a VSP dataset acquired in a well in Thonex, Switzerland in the framework of a geothermal exploration project. However, the application of FWI to the walk-above data consisting of 5 source gathers was of limited success. Due to the small receiver coverage for each of the individual source positions, the inversion problem was highly underdetermined leading to a strong trade-off between the source wavelet and the velocity model. In contrast, FWI of the offset VSP-4 source position was more successful, since the receiver array was about three times as long as for the walk-above positions. However, since this subset only contains one source, a reliable inversion of the data was not possible. A larger receiver coverage for the individual walk-above source positions would be necessary to obtain reliable elastic parameters of the subsurface with FWI.

4.1   Introduction

Full waveform inversion (FWI) is a powerful method to image the subsurface at wavelength to sub-wavelength resolution. Compared to conventional seismic methods, FWI utilizes the full wavefield of the seismic records, there is no need to separate different wave types (P-, S-waves, reflections, surface waves, multiples) and hence, the most complete representation of the subsurface is expected. FWI iteratively minimizes the misfit between the observed and predicted waveforms until a subsurface model is found that explains the data within minimal discrepancies.

The FWI technique emerged in the 1980's (Tarantola (1984); Mora (1987)), but was not widely used until recently, when the method gained more popularity due to the increase of computer power and long-offset acquisition geometries (e.g., Plessix (2008); Buske et al. (2009)). FWI was first intro-duced in a time-domain formulation (e.g. Tarantola (1984)) and later developed in the frequency domain (e.g. Pratt and Worthington (1990)). The advantage of FWI in the frequency domain is that the inversion only needs to be performed with a few well-chosen frequencies and hence sub-stantially lower computational costs are experienced, at least for two-dimensional (2D) problems (e.g. Sirgue and Pratt (2004); Maurer et al. (2009)). Additionally, due to the strong non-linearity of the inverse problem, the inversion can be started with low frequencies and higher frequencies can be progressively added as the iterations proceed (Bunks et al. (1995)). This reduces the chance of getting trapped in a local-minimum. Performing the forward calculations in the frequency domain is especially beneficial for multiple sources as the impedance matrix containing the model parameters only needs to be calculated once and the wavefield can then be determined easily as a matrix vector multiplication by simply replacing the source term each time.

Due to the large computational power needed for FWI, most of the studies were performed in 2D using the acoustic approximation (e.g. Pratt and Shipp (1999); Gao et al. (2006); Operto et al. (2006)). However, acoustic FWI results are likely to contain artifacts due to the systematic differ-ences between calculated (acoustic) and field ((visco-)elastic) data (Barnes and Charara (2009)). In particular, in areas with strong velocity discontinuities or large source receiver offsets P- to S-wave conversions can have a significant effect on the waveform amplitudes and, hence, elastic FWI is

more appropriate. The advantage of elastic FWI is that shear-wave velocity and density information can be extracted in addition to the P-wave velocity. Consequently, elastic FWI can be valuable for a wide range of applications, since S-wave information helps to constrain lithology or fluid changes, reservoir parameters and generally enhance resolution due to shorter wavelengths (Barkved et al. (2004)).

FWI applications cover a wide range of topics. Most of the studies are related to surface-based marine reflection profiling or ocean-bottom surveys in hydrocarbon exploration (e.g. Shipp and Singh (2002); Sears et al. (2008); Brossier et al. (2009)), mantle tomography (e.g. Fichtner et al. (2010)) or crustal studies (e.g. Dessa et al. (2004)). At the Ketzin site in Germany, FWI was used to monitor the CO_2 distribution at depth (Zhang et al. (2013)). Examples of synthetic crosswell studies are found in Manukyan et al. (2012) where the information content of multi-component FWI is examined for monitoring nuclear waste repositories and in Barnes et al. (2008) where a FWI method was tested for transversely isotropic media in noisy environments.

Seismic data from vertical seismic profiling (VSP) have sporadically been used for FWI studies. For example, Gao et al. (2006) used acoustic FWI with data from a high-resolution VSP experiment to characterize the near surface of a groundwater contamination site in Utah. Roberts et al. (2008) applied elastic FWI to a VSP dataset in the Gulf of Mexico and obtained elastic parameter models beneath the base of a complex salt structure. Yang et al. (2011) imaged reservoir changes due to the injection of CO_2 by the application of FWI on a time-lapse walkaway VSP data set in Texas. Podgornova et al. (2014) performed anisotropic elastic FWI on a land walkaway VSP dataset in British Columbia and recovered a layered structure of the subsurface that agrees well with sonic data. Owusu et al. (2016) applied anisotropic elastic FWI to walkaway VSP data from the Arabian Gulf and obtained a geologically plausible layered model of the subsurface.

To date, FWI has not been applied in the geothermal context (Schmelzbach et al. (2016)). Hence, it is important to test the potential of imaging geothermal reservoirs with FWI. Here, we studied if FWI can provide a detailed velocity model of the subsurface and can help to better characterize the subsurface at Thonex, Switzerland. After briefly describing the site and the field experiment, we present the first results of elastic FWI with the walk-above VSP dataset (i.e., surface-to-deviated well surveying) acquired in the geothermal well at Thonex and discuss the problems that we encountered with the data set. Next, we present FWI results of an additional source position (VSP-4) that has substantially larger receiver coverage. Finally, we discuss the encountered difficulties and limitations with the dataset from Thonex, and we outline how some of the issues can be approached to further improve the FWI of the Thonex data.

4.2   Site description

Thonex is situated in the region of Geneva in the southwestern part of the Alpine foreland molasse basin. The site is characterized by a thick cover of Mesozoic sediments, primarily carbonate and marl formations and crystalline basement below. In 1993, a geothermal well was drilled in Thonex with the aim to extract water from an aquifer in the Jurassic formation that can be used for district heating purposes (Guglielmetti and Bitri (2017)). A fluid temperature of 70 °C was found in the Upper

Jurassic reef limestones at 1900 m depth that yielded a geothermal gradient of 3.12 °C/100 m. However, the flowrate of 11 m^3/h was below expectations (Guglielmetti and Bitri (2017)). Therefore, a new exploration study was launched with the goals to obtain a detailed velocity model of the area, characterize the carbonate formations, detect fault zones and develop an acquisition approach that can be used for future surveys.

4.3 Data acquisition

The Thonex VSP survey was conducted in a geothermal well that is sub-vertical down to a depth of about 750 m and then deviates at a dip of 20 °-26 ° from the horizontal to a depth of 2600 m. The well was cased down to 1800 m depth, but the geophone cables could not be lowered deeper than 1500 m due to an obstruction in the borehole (Schleifer et al. (2017)). Four offset VSP's (VSP-1-4) and a walk-above VSP with five source positions (WAB-101-105) were acquired (see Figure 4.1). The walk-above survey was planned so that the source positions follow and overlie the direction of the deviated well (Figure 4.2). Every source point covers a predefined interval of 20-28 geophone positions along the well whereas each geophone in that subset records the wave fields from just two source positions, apart from the first and last intervals where only one source position is captured on each of these geophone spreads. The design of the walk-above survey is shown in Figure 4.2. The offset VSP's 1-3 covered the depth interval from 300 m to 1500 m and the VSP-4 an interval from 10 m to 1500 m with a receiver spacing of 10 m (Corubolo et al. (2017)). Two 3-component borehole geophones from Avalon Sciences Ltd were used and a 14-s long source sweep with frequencies between 8 Hz and 120 Hz was created with a Prakla Vibroseis from OGS.

Figure 4.1: Survey layout of the VSP experiment in Thonex. The offset VSP's are marked with VSP-1-4 and the walk-above source positions with WAB-101-105 (modified after Corubolo et al. (2017)).
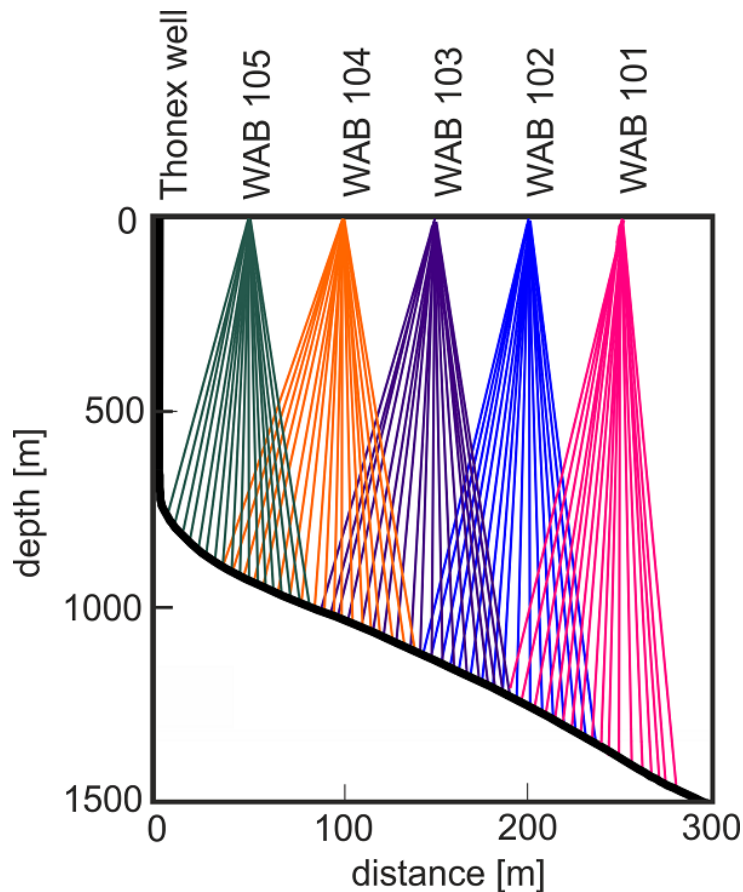
Figure 4.2: Walk-above experiment showing the receiver positions for each source position at the surface. Apart from the first and last interval, all 20-28 receivers in each geophone spread record the wave fields of two different source positions (modified after Gugliel-metti and Bitri (2017)).

4.4 Data examples

The quality of the data is generally good for depths >800 m for VSP1-3 and depths of >500 m for VSP-4. In the shallow borehole intervals, the data quality was generally poor, which was probably due to the condition of the casing, problems in the cement bonding or poor receiver coupling. The walk-above experiment is not affected because the shallowest receiver is located at 830 m depth. A data example of the walk-above source position WAB-103 is shown in Figure 4.3. Clear direct arrivals as well as reflection energy can be identified in the vertical component wave field (Figure 4.3a). The horizontal components were of bad quality, and hence not included in the inversion. The data were processed by OGS for seismic-reflection imaging. The processing sequence consisted of band-pass filtering, first break picking, velocity analysis, wavefield separation, deconvolution, spherical divergence recovering, corridor stack and Kirchhoff migration (Corubolo et al. (2017)). The aligned upgoing wavefield is shown in Figure 4.3b. Clear reflection energy can be observed on the processed source gather.
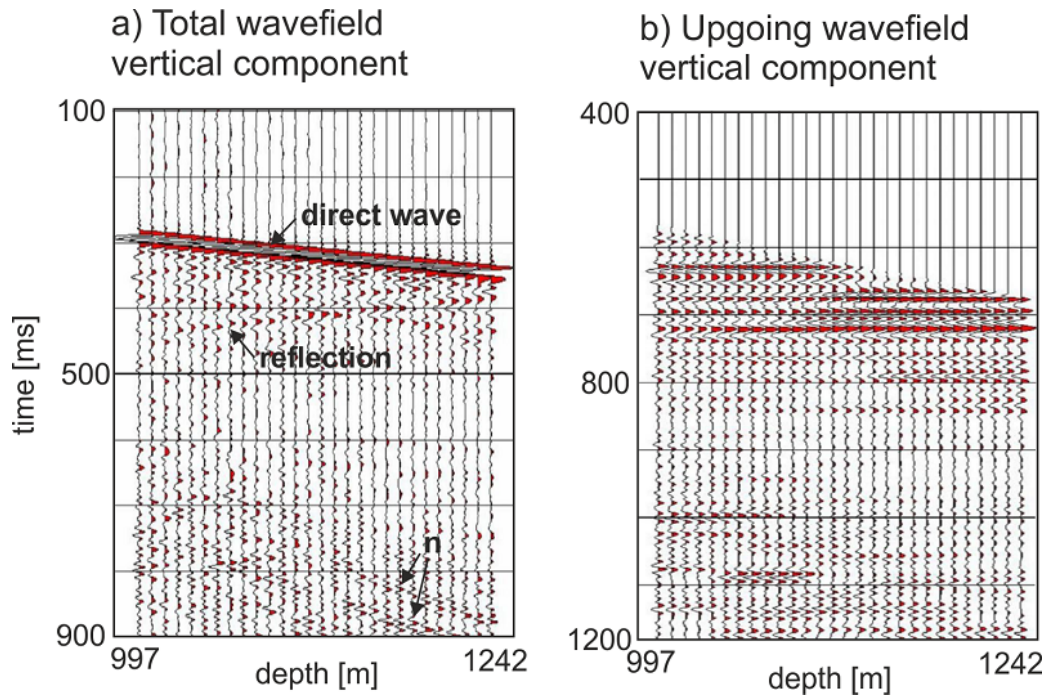
Figure 4.3: Vertical component recording of source position WAB 103 (modified after Corubolo et al. (2017)). a) Total wavefield where clear first arrivals and reflection energy can be identified. Unknown high amplitude events are indicated with n. b) Separated upgoing wavefield with aligned reflections.

4.5   Building the initial model for FWI

It is essential to start the inversion with an initial model that is close to the true subsurface model to prevent the inversion algorithm from getting trapped in a local minimum due to the non-linearity of the FWI problem (Pratt (1999)). The initial model was created based on interval velocities that were calculated using the arrival times of the direct P-wave of the walk-above source positions and VSP-4. The interval velocities of the different source positions were combined and further smoothed (Figure 4.4). The smoothed interval velocities were then used as a 1D initial model for the FWI. The initial S-wave velocity model was obtained assuming a constant Vp/Vs ratio of $\sqrt{3}$ and the initial density model was created using Gardner's velocity-density relation (Gardner et al. (1974)).
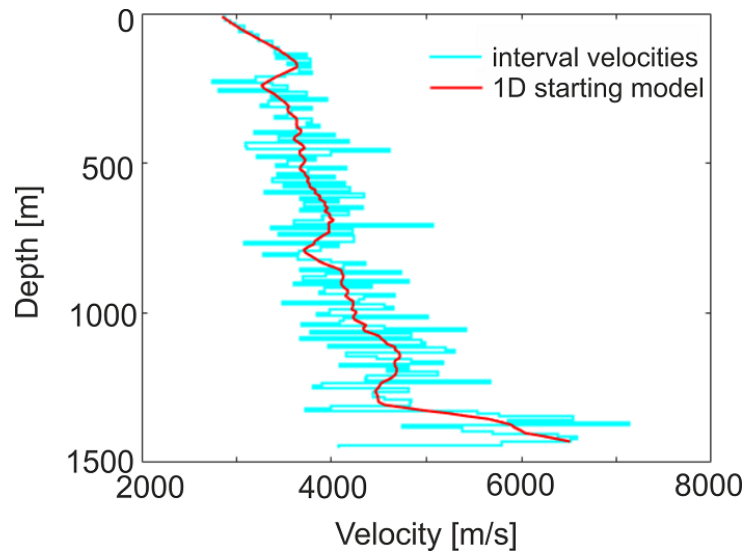
Figure 4.4: Combined interval velocities of the different source positions calculated based on arrival times of the direct P-wave (cyan) and smoothed interval velocities that were used as a 1D starting model for the FWI (red).

4.6 FWI results

FWI was carried out with the vertical component of the walk-above data from Thonex. The goal of the FWI was to find a subsurface model that predicts a wavefield as close as possible to the measured wavefield. The inversion was performed in the frequency domain using frequencies of 10, 20, 30, 40, 50 and 60 Hz. It was shown that it was sufficient to obtain reasonable inversion results when only a few distinct frequencies were considered rather than fitting every time sample of the seismogram during the inversion (Sirgue and Pratt (2004)). Since cycle skipping was not an issue with this dataset, we inverted for all frequencies simultaneously.

The first break times were picked at the onset and the data before the first arrivals were muted. After the first break, an exponential damping was applied to focus on fitting the first wavelets and to ensure a continuous decrease of the influence of later arrivals on the FWI results. With the exponential damping, also the high amplitude events that are observed after 0.6 s (indicated with n in Figure 4.3) could be eliminated. A bandpass filter with corner frequencies of 8 Hz and 65 Hz was applied to the data. The P-wave velocity, S-wave velocity and density were linked by using a cross-gradient coupling term to stabilize the inversion (Manukyan et al. (2017)).

Maurer et al. (2012) showed that the quality of FWI results may deteriorate if proper source and receiver coupling effects are not taken into account. Hence, individual source wavelets and coupling functions are normally estimated. However, since the acquisition geometry of the Thonex VSP data is very sparse, it was not possible to invert for the receiver coupling terms. Only two source positions were recorded by each receiver position, hence more data would be required to properly calculate receiver coupling factors. Different numbers of source wavelets were estimated and the results presented in the following section.

4.6.1 Source wavelet estimation

Source wavelet estimation was performed for either finding a single source wavelet for the entire dataset, or identifying five different source wavelets for each individual source position (WAB-101-105). The corresponding results are shown in Figure 4.5 and Figure 4.6, respectively. The velocity models after 60 iterations with a single source wavelet change only slightly compared to the initial model (Figure 4.5a-d). The velocity and density profiles at a distance of 150 m in Figure 4.5e show that the models become smoother, but generally follow the initial model. The P-wave velocities at shallow depth are slightly lower than the initial model, and also the S-wave velocity shows lower values at about 350 m depth.

Figure 4.5f and g display the time-domain data misfit between the observed and computed seismograms after 60 iterations for two different source positions (WAB-101, WAB-103). It can be seen that the data fit for the initial model is already very good, especially for the first wavelet. At later times the seismograms start to differ. However, there is only a slight improvement of the data fit after 60 iterations. It is clearly visible that there is hardly any change in the later arrivals after the inversion (see source position WAB-101 in Figure 4.5f).

Figure 4.5h and i show the amplitude spectra of the two different source positions. They clearly differ in shape and amplitude, even though the source positions are only about 150 m apart. The differences could originate from dissimilar source and/or receiver coupling factors, and/or near surface effects (Podgornova et al. (2014)). The spectrum of the initial model is quite different comparted to the spectrum of the field data and only slightly improves after the inversion. As the spectra of the different source positions look very different, it is probably not possible to fit the data with only a single source wavelet. Therefore, we repeated the inversion by estimating all five different source wavelets. The corresponding results are shown in Figure 4.6.

The velocity and density models in Figure 4.6a-d show that there is hardly any change between the starting and final models. The 1D profiles clearly reveal that the inversion only makes the model smoother. The seismograms of the field and the calculated data are nearly identical as well as the different amplitude spectra (Figure 4.6). It seems that by considering five different source wavelets, the data can be very well matched. It is not clear whether the good data fit is achieved by a combination of the suitable velocity model and source wavelet estimation, or if the inversion is only controlled by the flexible choice of the source wavelet alone. Therefore, the source wavelets are examined in more detail in Figure 4.7. It can be seen that the single source wavelet (same source wavelet for all source positions), the source wavelet for WAB-101 and that WAB-103 all look quite different. The differences in the first high amplitude cycles could be related to near surface effects. However, at later times the source wavelet should be zero. However, information on the seismogram at later times (e.g. reflections, noise) is just explained by variation of the source wavelet. This can clearly be seen in Figure 4.8, where the seismic source wavelet of WAB-101 (Figure 4.8a) is plotted next to a single trace from the same source position (Figure 4.8b). All the traces look almost identical, thereby indicating that the inversion is controlled by the source wavelet estimation and not by the actual velocity model. This assumption is further tested in the next section.
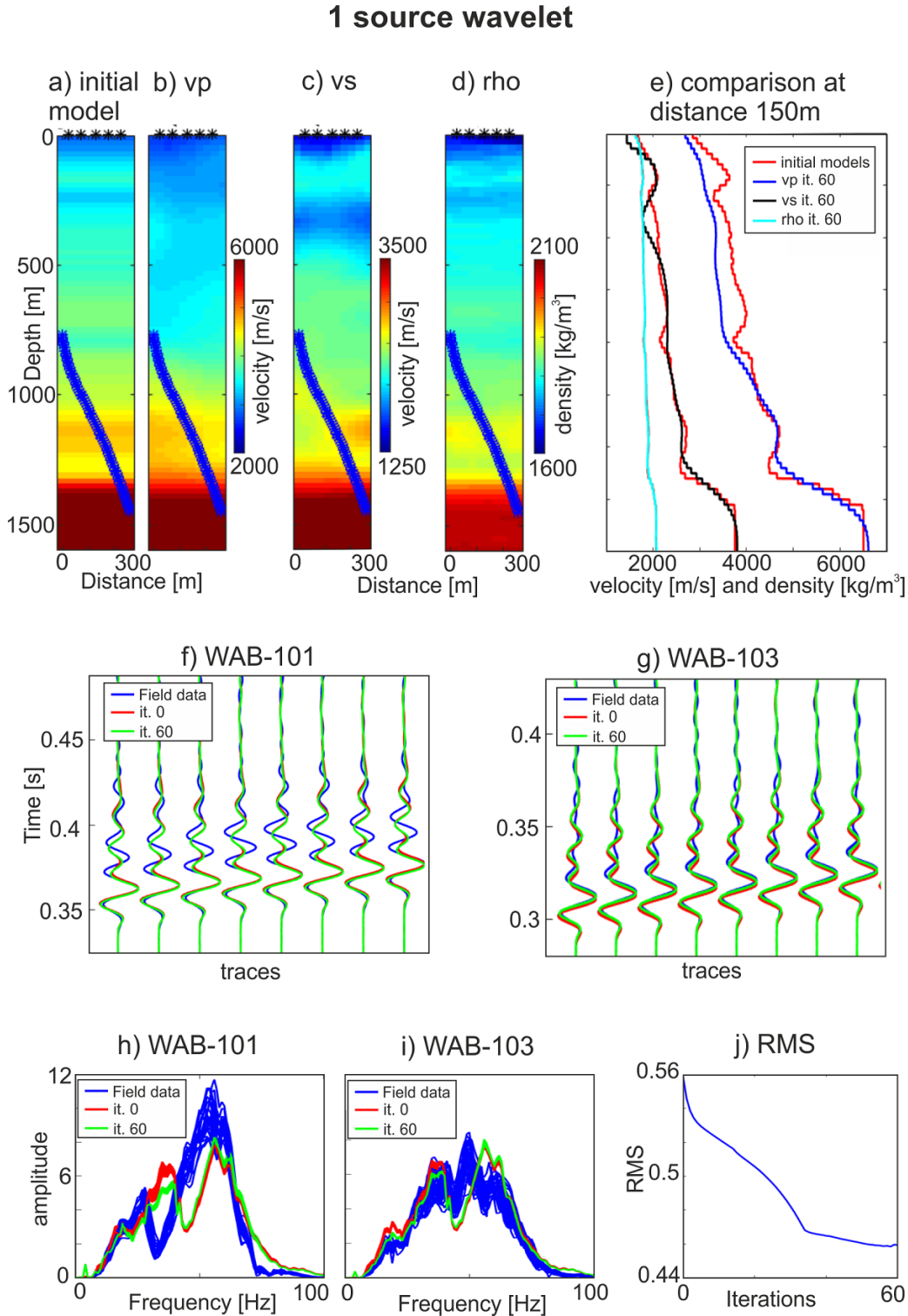
1 source wavelet

Figure 4.5: Inversion results when seeking one single source wavelet for all different source positions. a) Initial velocity model. b-d) Inversion results after 60 iterations. e) Comparison between the initial and final inversion results at a distance of 150 m. f, g) Time domain data misfit for two source positions WAB-101 and WAB-103 and corresponding amplitude spectra in h) and i), respectively. j) RMS data misfit for 60 iterations. The data fit for the initial model is already quite good, and only slight improvements are observed after the inversion. The amplitude spectra for the different sources look very different, hence, suggesting that different source wavelets for each source position should be taken into account.

5 different source wavelets
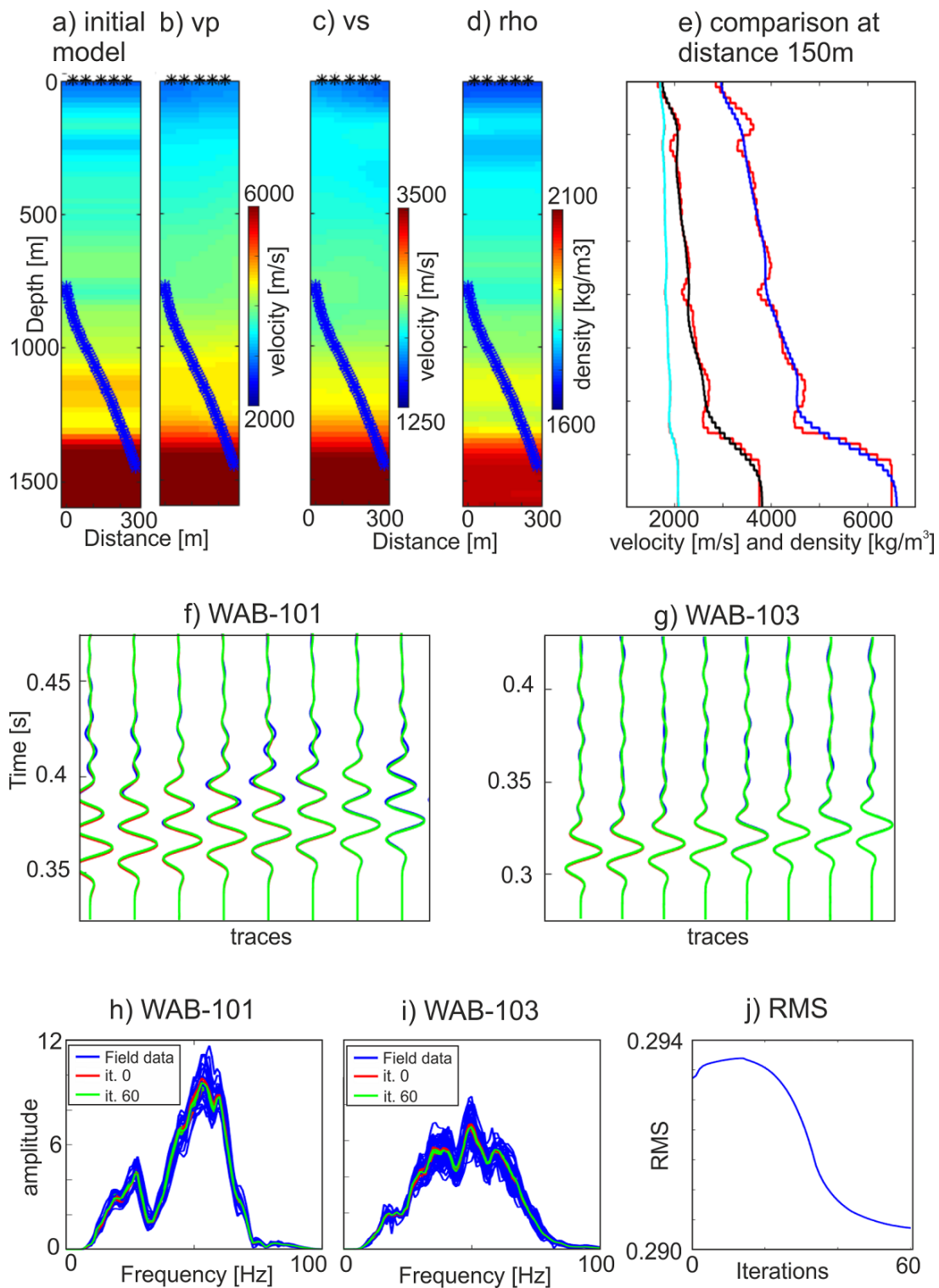
Figure 4.6: Same as Figure 4.5 but for using 5 different source wavelets. The seismograms based on the initial model already match the field data very well. There is hardly any change through the inversion process.
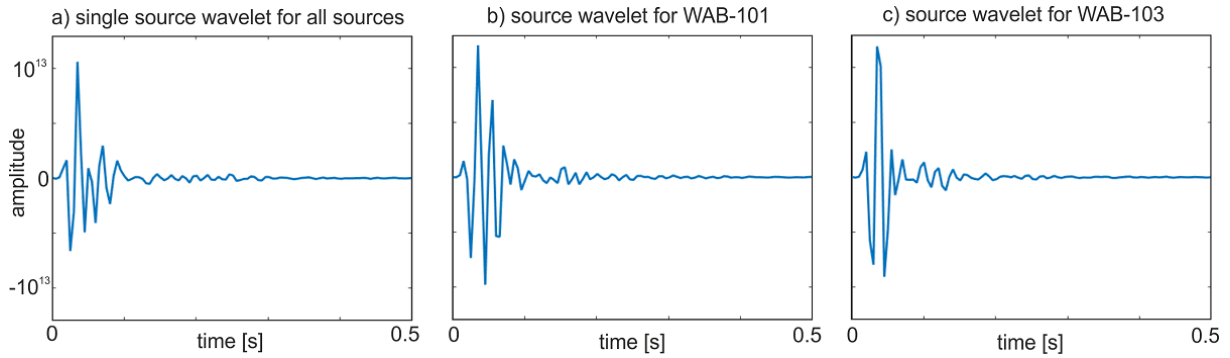
Figure 4.7: Source wavelet signatures for a) single source wavelet inversion (1 source wavelet for all different sources), and results of the individual inversions with b) source wavelet for position WAB-101 and c) WAB-103. The high amplitude differences for the first few cycles could be related to near surface effects. Differences at later times indicate that the source wavelet tries to explain part of the seismogram that should actually be explained by the velocity/density models because the source wavelet should be zero at these later times.
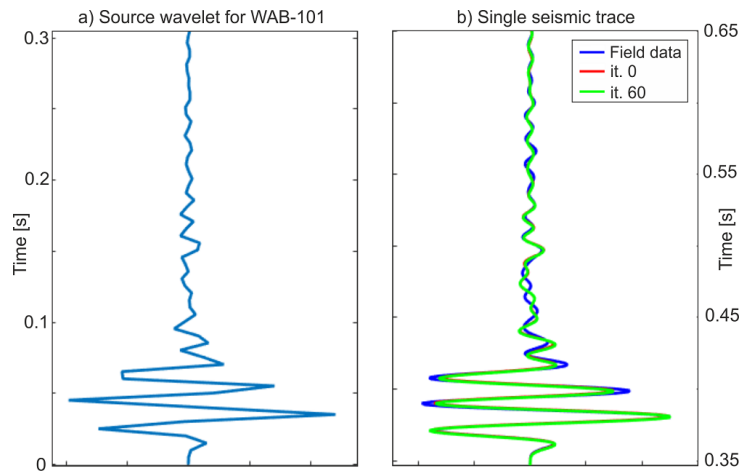
Figure 4.8: Direct comparison between a) the source wavelet and b) a single seismic trace of source position WAB-101. Note that the traces are almost identical, indicating that the inversion is dominated by the source wavelet estimation.

4.6.2 Dependency of the initial model

To test whether the FWI results are mainly controlled by the source wavelet and not by the velocity model, inversions with different initial models were tested. Instead of the interval velocities, we used a constant velocity model down to the first receiver at 830 m depth. As can be seen from the interval velocities in Figure 4.4, the velocity model is clearly not constant within the interval from the surface down to 830 m. Hence, if the inversion was also controlled by the velocity model, it would be expected that the data misfit of the initial model would be large. Additionally, the inversion algorithm would probably get trapped in a local minimum, since the initial model deviates significantly from the true velocity model. However, as shown in Figure 4.9, the data can be matched equally well as before with similar RMS data misfit values. Hence, the correct seismograms can still be created despite a wrong velocity model. We conclude that the inversion is mainly controlled by the source wavelet estimate and the velocity model has a negligible effect. These difficulties probably

5 different source wavelets
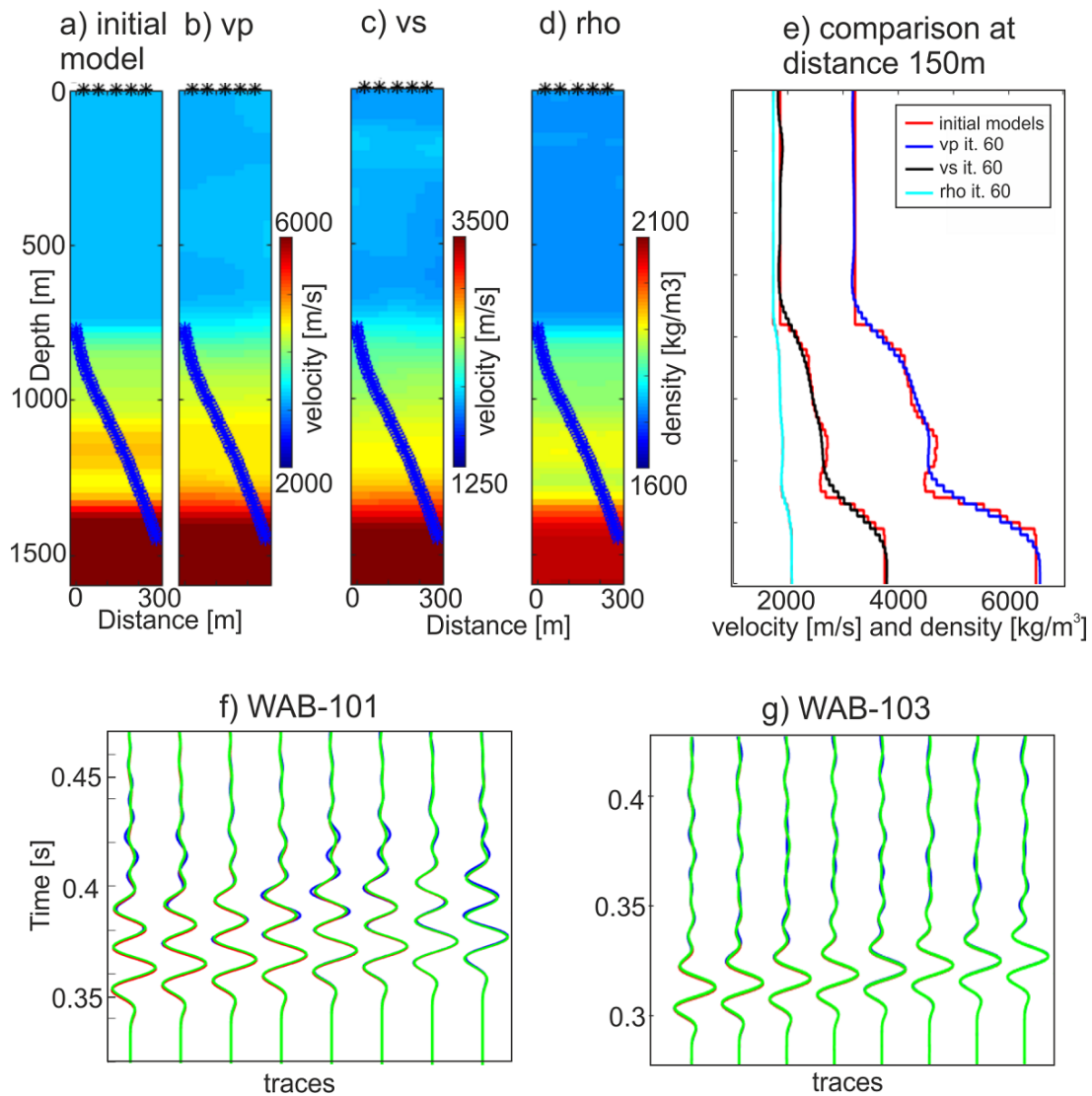
Figure 4.9: Same as Figure 6, but using an initial model with a constant velocity down to the first receiver at 830 m depth. Even with a wrong velocity model, the data fit is very high, indicating that the inversion is controlled by the source wavelet and not by the velocity model.

arise due to the highly underdetermined nature of the inversion problem. Since there are only five source positions with a very small receiver coverage (20-28 receivers per source position) and only two source positions for each receiver the subsurface coverage is very low. It seems that more data would be necessary to better constrain the velocity models.

We also tested different frequencies (only low/high frequencies), but the problem is independent of the choice of frequencies. Additionally, we tried different exponential damping factors after the first break picks to not only focus on the first wavelets but also on later arrivals. But even when the energy after the first arrivals was boosted, the later arrivals could still be explained by the source wavelet.

4.6.3 Including VSP-4

Since the inversion problem of the walk-above data is clearly far too underdetermined, we also included the VSP-4 source position data. VSP-4 is about 550 m away from the well, but in line with the walk-above source positions. VSP-4 has larger receiver coverage since the receivers were deployed from the surface down to 1500 m depth. However, since the data of the first hundred meters were of very low quality, we included only the data between 500-1500 m depth. The results after 45 iterations are shown in Figure 4.10. The velocity models after the inversion deviate slightly from the initial model and 2D structures now appear (Figure 4.10b, c). In Figure 4.10f it can be observed that there is a clear difference between the seismogram of the initial model and the field data (red and green). The source wavelet alone cannot explain the data completely and hence the misfit is reduced by changing the velocity models. After 45 iterations, the data fit is very good, especially for the first few wavelets. At later times the misfit is generally larger.

Including the VSP-4 source gather data in the inversion did not have any effect on the other source positions, as shown before that the inversion only depends on the source wavelet estimation and not
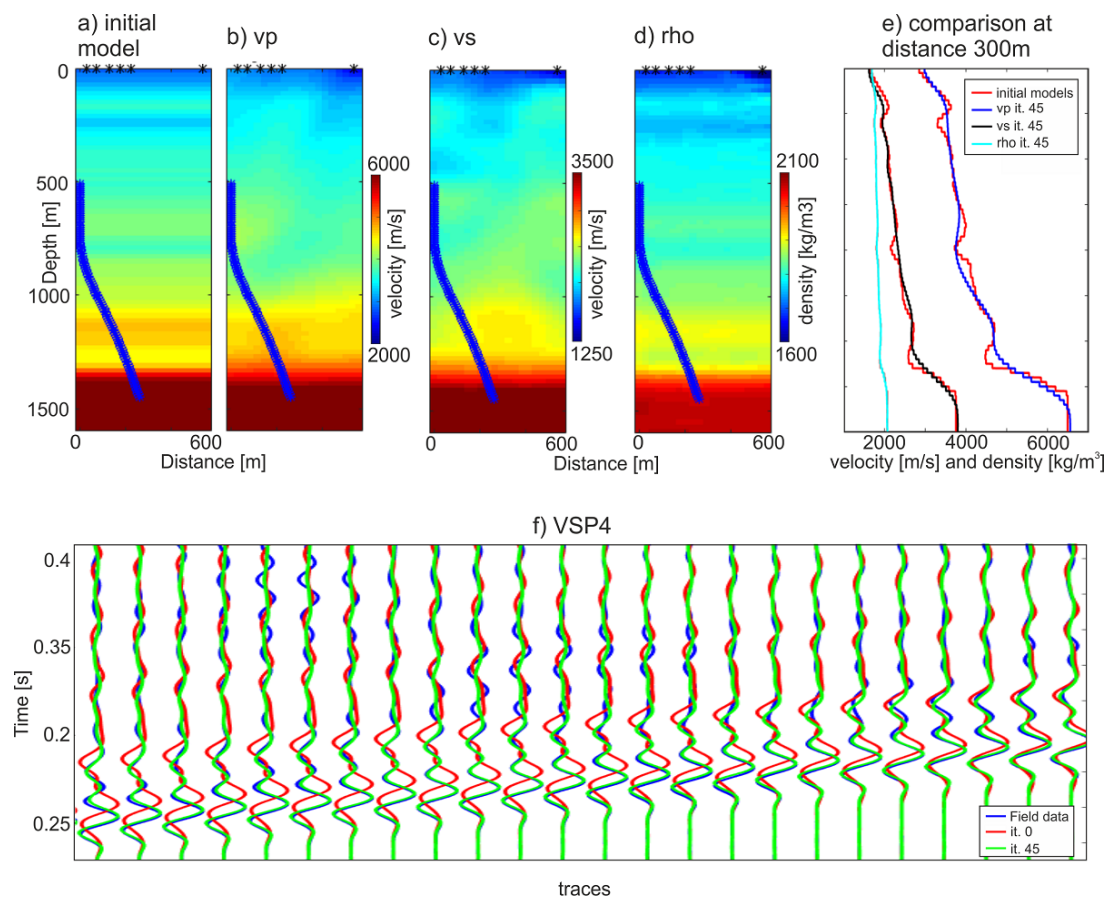
Figure 4.10: Inversion results for VSP-4 using different source wavelets for each source position. a) Initial velocity model. b-d) Inversion results after 45 iterations. e) Comparison between the initial and final inversion results at a distance of 300 m. f) Time domain data misfit for VSP-4. The seismogram of the initial model and the field data do not coincide since the source wavelet alone cannot explain the data. After 45 iterations the data fit is very good and 2D structures appear in the velocity models (a-c).
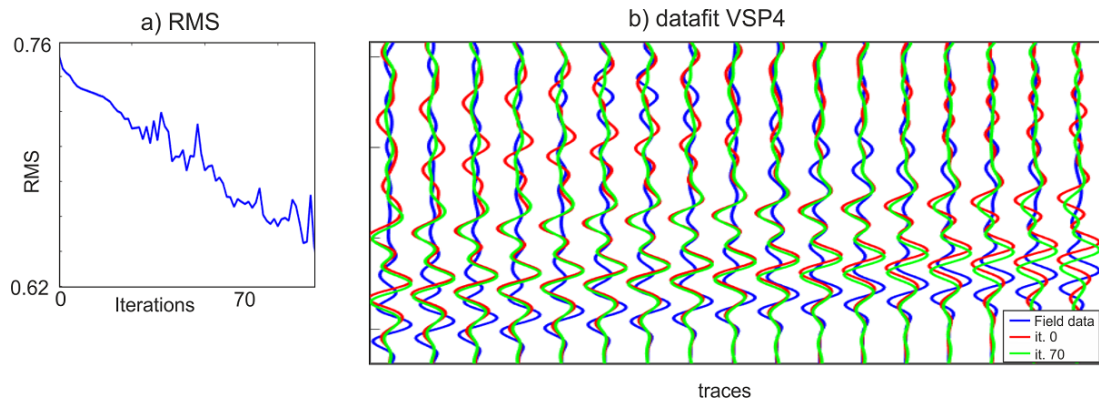
Figure 4.11: RMS values and data misfit for VSP-4 using an initial model with a constant velocity down to the first receiver. The RMS data misfit is not consistently decreasing and the data fit is generally low, indicating that the inversion algorithm is stuck in a local minimum due to an inappropriate initial model.

on the velocity models. Therefore, the velocity models shown in Figure 4.10 need to be interpreted with caution, since the changes are basically only related to one single source position. A larger receiver coverage would be necessary for the walk-above data to contribute to the inversion results.

When the initial model with a constant velocity value down to the first receiver is used for VSP-4, the inversion algorithm has problems in fitting the data. The RMS value is not consistently decreasing (Figure 4.11a) and the data fit after 70 iterations is generally rather poor (Figure 4.11b). It seems that the inversion is trapped in a local minimum due to the non-linearity of the FWI problem. In contrast to the walk-above data, an arbitrary shallow velocity model cannot be used, but a model that is close to the true subsurface model is required to fit the data (as expected for typical FWI problems).

4.7 Conclusion

Elastic FWI of the VSP data at Thonex was applied with limited success. The individual source positions of the walk-above data have very restricted receiver spatial and angular coverage and hence made the application of FWI troublesome due to the highly underdetermined inverse problem. The inversion of the walk-above data was mainly controlled by the source-wavelet determination and independent of the choice of the initial velocity model. An arbitrary velocity model could explain the data with minimal error and hence no information about the subsurface could be retrieved. FWI including the VSP-4 source position was more successful, since the receiver array was about 3 times as long as for the walk-above source position. The source wavelet alone could not explain the data and hence the inversion was also controlled by the velocity model. However, since only one source position had an influence on the velocity models, a reliable interpretation was not possible. We conclude that larger receiver coverage of the individual walk-above source positions would be necessary to obtain reliable elastic parameters of the subsurface with FWI.

4.8 Outlook

A major problem of the FWI of the walk-above data from the Thonex VSP experiment was that the inversion was mainly controlled by the source wavelet. Hence, the solution would be to decrease the influence of the source wavelet. We see the following possibilities:

- Since the source wavelets were very long and hence probably also contain reflection information, the source wavelet would need to be truncated after the first few wavelets. This could be done by first transforming the source wavelet to the time domain, applying e.g. an exponential damping after the first wavelets to zero out later times and then transform the wavelet back into the frequency domain.

- FWI could be tested on the processed data where the direct wave is removed and only the reflected events are present. The inversion would consequently focus more on the reflections that could probably not be explained entirely with the source wavelet due to the different moveout of reflected energy.

References

Barkved, O., B. Bartman, J. Gaiser, R. Van Dok, T. Johns, P. Kristiansen, T. Probert, and M. Thompson. 2004. "The many facets of multicomponent seismic data". *Oilfield Review* 16 (2): 42–56.

Barnes, C., and M. Charara. 2009. "The domain of applicability of acoustic full-waveform inversion for marine seismic data". *Geophysics*.

Barnes, C., M. Charara, and T. Tsuchiya. 2008. "Feasibility study for an anisotropic full waveform inversion of cross-well seismic data". *Geophysical Prospecting* 56 (6): 897–906.

Brossier, R., S. Operto, and J. Virieux. 2009. "Seismic imaging of complex onshore structures by 2D elastic frequency-domain full-waveform inversion". *Geophysics* 74 (6): WCC105–WCC118.

Bunks, C., F. M. Saleck, S. Zaleski, and G. Chavent. 1995. "Multiscale seismic waveform inversion". *Geophysics* 60 (5): 1457–1473.

Buske, S., I. Lecomte, T. Nemeth, S. Operto, and V. Sallares. 2009. *Imaging and inversion—Introduction*. Tech. rep. Society of Exploration Geophysicists.

Corubolo, P., F. Poletto, and B. Farina. 2017. *Processing of VSP and Walkabove VSP data acquired on Thonex-1 well*. Tech. rep. Report OGS 2017 / 48 GEO 12 GEOP Borgo Grotta Gigante TS May 10, 2017.

Dessa, J.-X., S. Operto, S. Kodaira, A. Nakanishi, G. Pascal, J. Virieux, and Y. Kaneda. 2004. "Multiscale seismic imaging of the eastern Nankai trough by full waveform inversion". *Geophysical Research Letters* 31 (18).

Fichtner, A., B. L. Kennett, H. Igel, and H.-P. Bunge. 2010. "Full waveform tomography for radially anisotropic structure: new insights into present and past states of the Australasian upper mantle". *Earth and Planetary Science Letters* 290 (3): 270–280.

Gao, F., A. R. Levander, R. G. Pratt, C. A. Zelt, and G. L. Fradelizio. 2006. "Waveform tomography at a groundwater contamination site: VSP-surface data set". *Geophysics* 71 (1): H1–H11.

Gardner, G., L. Gardner, and A. Gregory. 1974. "Formation velocity and density—The diagnostic basics for stratigraphic traps". *Geophysics* 39 (6): 770–780.

Guglielmetti, L., and A. Bitri. 2017. *THONEX Well VSP Survey*. Tech. rep. Presentation at IMAGE Technical Meeting, Azores, April 2-4 2017.

Manukyan, E., S. Latzel, H. Maurer, S. Marelli, and S. A. Greenhalgh. 2012. "Exploitation of data-information content in elastic-waveform inversions". *Geophysics* 77 (2): R105–R115.

Manukyan, E., H. Maurer, and A. Nuber. 2017. "Improvements to elastic full waveform inversion using cross-gradient constraints". *Geophysics* 83 (2): 1–46.

Maurer, H., S. A. Greenhalgh, E. Manukyan, S. Marelli, and A. G. Green. 2012. "Receiver-coupling effects in seismic waveform inversions". *Geophysics*.

Maurer, H., S. Greenhalgh, and S. Latzel. 2009. "Frequency and spatial sampling strategies for cross-hole seismic waveform spectral inversion experiments". *Geophysics* 74 (6): WCC79–WCC89.

Mora, P. 1987. "Nonlinear two-dimensional elastic inversion of multioffset seismic data". *Geophysics* 52 (9): 1211–1228.

Operto, S., J. Virieux, J.-X. Dessa, and G. Pascal. 2006. "Crustal seismic imaging from multifold ocean bottom seismometer data by frequency domain full waveform tomography: Application to the eastern Nankai trough". *Journal of Geophysical Research: Solid Earth* 111 (B9).

Owusu, J. C., O. Podgornova, M. Charara, S. Leaney, A. Campbell, S. Ali, I. Borodin, L. Nutt, and H. Menkiti. 2016. "Anisotropic elastic full-waveform inversion of walkaway vertical seismic profiling data from the Arabian Gulf". *Geophysical Prospecting* 64 (1): 38–53.

Plessix, R.-E. 2008. "Introduction: Towards a full waveform inversion". *Geophysical Prospecting* 56 (6): 761–763.

Podgornova, O., S. Leaney, M. Charara, and E. von Lunen. 2014. "Elastic Full Waveform Inversion for Land Walkaway VSP Data from British Columbia, Canada". In *76th EAGE Conference and Exhibition 2014*.

Pratt, R. G. 1999. "Seismic waveform inversion in the frequency domain, Part 1: Theory and verification in a physical scale model". *Geophysics* 64 (3): 888–901.

Pratt, R. G., and R. M. Shipp. 1999. "Seismic waveform inversion in the frequency domain, Part 2: Fault delineation in sediments using crosshole data". *Geophysics* 64 (3): 902–914.

Pratt, R. G., and M. Worthington. 1990. "Inverse theory applied to multi-source cross-hole tomography. Part 1: Acoustic wave-equation method". *Geophysical prospecting* 38 (3): 287–310.

Roberts, M. A., S. Singh, and B. E. Hornby. 2008. "Investigation into the use of 2D elastic waveform inversion from look-ahead walk-away VSP surveys". *Geophysical prospecting* 56 (6): 883–895.

Schleifer, A., S. Meneghini, and M. Maffione. 2017. *VSP Survey on Thonex well*. Tech. rep. Acquisition report, Report OGS 2017 / 7 GEO 4 GEOP, Borgo Grotta Gigante TS February 20.

Schmelzbach, C., S. Greenhalgh, F. Reiser, J.-F. Girard, F. Bretaudeau, L. Capar, and A. Bitri. 2016. "Advanced seismic processing/imaging techniques and their potential for geothermal exploration". *Interpretation* 4 (4): SR1–SR18.

Sears, T. J., S. Singh, and P. Barton. 2008. "Elastic full waveform inversion of multi-component OBC seismic data". *Geophysical Prospecting* 56 (6): 843–862.

Shipp, R., and S. Singh. 2002. "Two-dimensional full wavefield inversion of wide-aperture marine seismic streamer data". *Geophysical Journal International* 151 (2): 325–344.

Sirgue, L., and R. G. Pratt. 2004. "Efficient waveform inversion and imaging: A strategy for selecting temporal frequencies". *Geophysics* 69 (1): 231–248.

Tarantola, A. 1984. "Inversion of seismic reflection data in the acoustic approximation". *Geophysics* 49 (8): 1259–1266.

Yang, D., M. Fehler, A. Malcolm, and L. Huang. 2011. "Carbon sequestration monitoring with acoustic double-difference waveform inversion: A case study on SACROC walkaway VSP data". In *SEG Technical Program Expanded Abstracts 2011*, 4273–4277. Society of Exploration Geophysicists.

Zhang, F., C. Juhlin, M. Ivandic, and S. Lüth. 2013. "Application of seismic full waveform inversion to monitor CO2 injection: Modelling and a real data example from the Ketzin site, Germany". *Geophysical Prospecting* 61 (s1): 284–299.

5

Conclusions and outlook

5.1 Summary and conclusion

Seismic exploration methods provide important tools to probe the subsurface and thus investigate potential geothermal sites. They can reduce the risk that is associated with high drilling costs by allowing more intelligent and selective drilling. Moreover, they enable almost continuous coverage of key horizons between wells. Seismic experiments over geothermal reservoirs are generally challenging due to the complex environment and, hence, improved seismic exploration techniques for comprehensive imaging of the subsurface are required. VSP is a valuable method for mapping lithological interfaces and dipping reflectors in complex geological settings in the vicinity of a borehole. In this thesis, the benefits and limitations of applying VSP over geothermal prospects are analyzed and advanced seismic imaging methods for improved subsurface visualization are presented.

Seismic exploration surveys in geothermal projects normally have a small budget. Hence, it is critical to optimally place a preferably low number of source positions for successful imaging of the subsurface. In chapter 2, a method is presented to optimize VSP surveys with a favorable benefit-cost ratio in areas where à priori knowledge is available. Possibilities and limitations of imaging fracture zones within the crystalline basement were analyzed. 2D and 3D acoustic synthetic data were calculated for different fracture zone configurations and processed to pre-stack Kirchhoff depth migrated images. I observed that the optimal source spread and number of sources strongly depend on the dip and location of the fracture zone, which stresses the importance of à priori information for effective survey optimization. More source positions and larger offsets (distance between well head and source position) are required as the fracture zone dip increases. Adding more source positions outside the optimal source-location spread did not improve the quality of the images, but rather deteriorated the image quality in some cases. Therefore, the optimization scheme that is presented is not only useful for designing future VSP survey layouts with a favorable benefit-cost ratio, but also provides a workflow for optimum target-oriented processing.

In chapter 3, a multi-offset VSP field dataset from the high-temperature geothermal field in Krafla, Iceland, was analyzed. The data acquisition was very challenging, especially due to the high subsurface temperatures that required cooling of the boreholes for several weeks prior to the survey. The design of the VSP survey was not optimal in terms of number and location of source positions due to limited financial resources. As a consequence, the recorded data set was very sparse. A workflow was established with a special focus on processing a sparse VSP dataset over a complex volcanic environment. A geophysical model was constructed based on first-arrival traveltime inversion and seismic reflection processing. The application of fat ray tomography turned out to be beneficial for the sparse data sets because the subsurface could be better illuminated and consequently the veloc-

ity models better constrained compared to asymptotic ray based traveltime tomography due to the nature of the fat rays. Since the data were acquired with 3C geophones a multicomponent migration algorithm could be applied to the data. This resulted in individual PP, PS and SS migrated images that helped to assess the reliability of reflections and hence demonstrate the benefit of acquiring seismic data with 3C geophones.

We have found that VSP is a useful method to image the key lithological boundaries, volcanic stratigraphy, fracture zones and dykes in a complex magmatic environment. However, due to the 2D acquisition geometry, it was not possible to orient the reflectors in 3D space. Hence, reflectors below and to the sides of the boreholes cannot be interpreted unambiguously. Although a decrease in reflection amplitudes was observed below the borehole that could indicate the expected magma chamber, it is unclear whether the change in amplitude characteristics is actually related to the presence of the magma chamber. It transpired that à priori knowledge was essential to constrain the analysis of the dataset and was especially useful for the interpretation of the data since significant migration artefacts exist due to the sparseness of the VSP dataset. Furthermore, the interpretation of the Vp/Vs ratio turned out to be difficult, since the velocity models were not sufficiently well constrained to allow a reliable geological interpretation. Based on the results obtained, I formulated strategies for improved data acquisition in the complex magmatic Krafla environment.

In chapter 4, elastic FWI was applied to a multi-offset VSP experiment conducted in a geothermal well in Thonex, Switzerland to test the potential of imaging geothermal reservoirs using FWI. Unfortunately, the application of FWI was of limited success, mainly due to the unsuitable acquisition geometry. The walk-above data set consisted of five individual source positions with very small receiver coverage (20-28 number of receivers) that resulted in a highly under-determined inversion problem. As a result, the inversion was mainly controlled by the source wavelet estimation. Any velocity model could explain the seismic data with minimal error because the data variations were primarily explained by the source wavelet, and hence it was not possible to obtain structural information based on the velocity model. FWI of an additional far-offset source position showed improved results, since the receiver array was about three times longer compared to the walk-above source positions. However, due to the lack of data, no reliable interpretation of the velocity models could be achieved.

5.2   General conclusions regarding the application of VSP for geothermal exploration

I conclude that VSP is a useful method to image the key lithological boundaries, volcanic stratigraphy, fracture zones and dykes in complex magmatic environments. Based on my synthetic-data study, I found that VSP is a suitable method for imaging gently to steeply dipping fracture zones in the vicinity of a well in crystalline basement, but my results emphasize clearly the importance of à priori information both in terms of acquisition and processing. Hence, VSP surveys will be most effective in areas with available geological control so that one can perform an experimental design study before the actual field survey commences. Additionally, à priori information is essential to constrain the processing and the geological interpretation.

VSP experiments in geothermal areas normally have a small number of source positions due to limited financial resources. Acquiring multicomponent data with 3-component geophones is beneficial since P-, S- and mode-converted waves can be identified, separated and analyzed, yielding further information from the seismic records. The additional and complementary information can be essential when interpreting ambiguous migrated images that contain artefacts due to the sparseness and limited aperture of the data set. To incorporate geological information in the processing can also help to better constrain the resultant geophysical models.

The illumination area of a VSP is restricted to the area around the well and hence the subsurface can only be imaged locally- both to the side and ahead of drillhole. Compared to other geophysical methods, VSP provides high-resolution images of structures in the subsurface. The method is thus favorable for finding suitable positions for further wells (e.g. to establish an operational doublet system) or to determine the direction of drilling for deviated wells.

The geology of Krafla consists of different volcanic layering, crystalline basement, dykes and fracture zones. The geological characteristic is usually similar in other magmatic environments and hence the experience gained from the Krafla experiments can be beneficial for future VSP surveys in magmatic environments. Based on the results of the Krafla study I recommend for future VSP studies in magmatic environments:

- Using VSP in areas with available à priori information (e.g. approximate fracture zone direction and dip, location of magma chamber, geological sequence);

- Performing an experimental design study before the field survey;

- Using generally more source positions (>5) and more (>2) near-offset positions (<1000 m) than in the Krafla experiment;

- Using a larger receiver coverage (>200 m) for walk-away experiments;

- Using 3-component geophones to be able to apply multicomponent processing techniques;

As à priori information turned out to be essential, I stress the need for interdisciplinary projects where various methods with different capabilities and limitations can be combined to obtain complementary subsurface information.

5.3 Outlook

5.3.1 Experimental design

Optimized experimental design allows the design of cost-efficient VSP surveys, where geothermal imaging challenges can explicitly be addressed. The study presented in chapter 2 is simplified and performed with the acoustic approximation. The experimental design can further be extended for the elastic case to simulate more realistic conditions. This would involve more challenges since a P- and S-wave separation step would be required and the processing of converted waves is not trivial and cannot be directly transferred from the P-wave processing due to asymmetric ray paths of the converted waves. But it would also provide additional imaging opportunities, because separate P-P,

P-S, S-P and S-S migrated images could be obtained and hence more information could be extracted from the subsurface.

The optimal source positions and number of sources depend on the data analysis method that is used for the optimization and the processing steps involved. We used seismic reflection imaging where migrated images after the application of prestack Kirchhoff depth migration were optimized. The VSP processing can further be improved by the application of Fresnel volume migration that enhances the image quality by limiting the migration operator to the physically defined Fresnel volume of the specular ray paths (Buske et al. (2009)). Moreover, other evaluation methods can be used for the optimization, such as FWI or the analysis of pure S- or converted waves. Combining FWI with optimized experimental design can be of great value since an ideal survey layout can be found as well as the extraction of the data information content maximized (Maurer et al. (2017)).

5.3.2 VSP field surveys

The experimental design study was performed only with synthetic data, hence, a next step would be to prove the concept with an actual field dataset. Since the optimization process requires a large number of source positions, such an experiment would be rather expensive. However, it also provides some benefits in that it allows evaluating the effect of certain simplification and approximations that were made for the synthetic case. Apart from P-waves, also S-, surface- or tube-waves are present in the data and can further add to the complexity of the data. Additionally, the exact position(s) of the fracture zone(s) might not be known, and neither the physical properties nor the exact shape of the fracture zone are necessarily available. It is therefore suggested to perform such an experiment in an area where the geology is well known based on à priori information.

VSP has only been sparingly applied in the context of geothermal exploration. Further research is required to fully understand the benefits and limitations of imaging geothermal reservoirs using VSP. We demonstrated that VSP is a suitable method to image key lithological boundaries and volcanic stratigraphy in complex magmatic environment with available à priori information. However, it is still unclear whether the method can be used to locate steam zones or magma chambers (Grab et al. (2017)). More VSP experiments are required with the focus on target-oriented acquisition and processing. The acquisition layout of the VSP at Krafla was not ideal and hence the presented methodology in chapter 2 can be used for the careful planning of future VSP surveys. We recommend using optimized experimental design to plan target-oriented VSP field acquisitions in complex environments.

The acquisition of VSP data in high temperature geothermal fields is very challenging since boreholes need to be cooled down to maintain the operational temperature of the geophones. Geophones with a high temperature limit are required to decrease the cooling time of the borehole. Additionally, improved geophone orientation of the 3 components is necessary to image reflectors accurately in space. Gimbal-mounted geophones or integrated magnetic compass help to better orient the geophones in space. Alternatively, a far offset source position that is fired after each replacement of the receiver chain can help to properly determine the orientation of the horizontal components.

VSP studies with distributed acoustic sensing (DAS) that use a standard fiber-optic cable instead of geophones have emerged in recent years and show several advantages compared to conventional geophones (Mateeva et al. (2013); Daley et al. (2013); Correa et al. (2017)). DAS cables cover the entire well and hence have a larger receiver coverage, they are less expensive, the cables are thin and can easily be installed permanently in several wells compared to conventional geophones. Hence, they have a high potential for active seismic, passive seismic or ambient noise monitoring. Since optical fibres are well suited for high temperature environments (Reinsch et al. (2013)), DAS cables represent a promising technology for imaging high-temperature geothermal fields where the temperatures are often beyond the operational limit of the geophones (Reinsch et al. (2015)). But it also needs to be investigated how long the cables will remain intact in such high-temperature environments.

Further research of the DAS technology is required to increase the generally low signal-to-noise ratio of DAS cables and to improve the sensitivity in 3 dimensions. DAS cables are so far 1-component and are sensitive to signals traveling along the borehole but lack the broadside sensitivity (Mateeva et al. (2013)). The sensitivity in 3D can be improved by the installation of more than one fibre optic cable or adjusting the shape of the fiber within the cable (Lumens et al. (2013)). Further research is required to be able to obtain directional information from the seismic waveform.

3D reflector imaging is essential in geothermal exploration due to the complex geology. 3D acquisition experiments as well as 3-component geophones have the potential to image structures in 3D space. Multicomponent seismic experiments are still rather rare and further studies are necessary to demonstrate the benefits in geothermal exploration. Focusing on true-amplitude processing can help to obtain more information on reservoir properties such as e.g. fluid saturation by AVO analysis. However, true-amplitude processing in complex environments is very challenging as it is difficult to image structures with low signal-to-noise ratios without the application of pre-stack automatic gain control to equalize amplitudes (Malehmir et al. (2012)). More source positions than in the case of the Krafla VSP are required to increase the S/N by stacking, cancel out migration artefacts and obtain high quality images that also allow the application of advanced imaging methods such as attribute analysis, shear wave birefringence or FWI.

Multicomponent data enable the examination of P-, S- and mode-converted waves. The separation of the different wave types is essential for a reliable analysis of S-waves. Rotational sensors that measure rotational motion in addition to translational motion allow the direct measurement of S-waves in unbounded, isotropic media (Sollberger et al. (2017)). Even though the benefits are large, seismic experiments with rotational motion sensors are rare as there is still a lack of reliable instruments that can accurately measure rotations (Schmelzbach et al. (2017)). Rotational sensors placed in boreholes would measure S-waves only (in a homogeneous medium). A clear isolation of S-waves can be beneficial for the analysis of shear wave splitting that may offer information about fracture orientation and fracture density, an improved imaging in gas bearing zones and the analysis of vp/vs ratios that can yield information about lithology and fluid content. Furthermore, P-waves can have rotational components in anisotropic media (Pham et al. (2010)). Rotational sensors could, therefore, be beneficial for anisotropy studies. Alternatively, geophone arrays can be used to estimate rotational motion by computing horizontal gradients of the recorded seismic translational motion.

Van Renterghem et al. (2017) demonstrates the separation of P-, S- as well as down- and upgoing wavefields on synthetic land and ocean bottom seismic data using spatial gradients. Gradient-based wavfield separation approaches could further be extended to VSP experiments and can contribute to a better separation of P- and S-wave.

5.3.3 FWI

FWI with the VSP data from Thonex was troublesome due to the restricted spatial and angular receiver coverage and hence highly under-determined inverse problem. A major problem was that the inversion was mainly controlled by the source-wavelet determination. It is necessary to decrease the influence of the source wavelets by constraining the source-wavelet during the inversion. This could be achieved by truncating the source wavelet after the first few cycles, as the wavelet was generally very long. For future surveys it is further suggested to determine the source wavelet separately, for example with a few surface geophones close to the source that allow measuring the source wavelet.

Another possibility to decrease the influence of the source wavelet is to pre-process the seismic data and remove the direct wave such that only reflection events are present in the data (e.g., by VSP wavefield separation into an upgoing and downgoing wavefields). Consequently, the source wavelet would play a minor role as the inversion algorithm would be forced to focus on the reflection events that show a different moveout pattern than the direct wave.

The sparseness of the Thonex dataset made the application of FWI difficult. For future surveys it is recommended to increase the receiver coverage for the individual source positions so that the velocity model is better constrained. This would allow obtaining more reliable Vp, Vs and density models. Elastic FWI could then be very beneficial for geothermal exploration, since Vp/Vs ratios could give important information about lithology changes, or porosity and fluid saturation. P- and S-waves are sensitive to temperature changes and could give indications on the spatial extent of high temperature areas.

Another possibility for the application of FWI in the geothermal context is time-lapse monitoring of small changes in the subsurface. Once a baseline velocity model has been constructed, one can invert for the differences between the seismic data at different times to obtain an estimate of the changes in the model. Time-lapse inversion is less dependent on the initial model, because it links directly the differential data to the changes in the model (e.g. Yang et al. (2011)).

The different aspects seem promising and show the potential of applying FWI in geothermal environments. As the application of FWI to geothermal datasets is relatively new and has not yet been fully explored, further studies are required to demonstrate the benefits of FWI on actual field data sets from geothermal sites.

References

Buske, S., S. Gutjahr, and C. Sick. 2009. "Fresnel volume migration of single-component seismic data". *Geophysics* 74 (6): WCA47–WCA55.

Correa, J., A. Egorov, K. Tertyshnikov, A. Bona, R. Pevzner, T. Dean, B. Freifeld, and S. Marshall. 2017. "Analysis of signal to noise and directivity characteristics of DAS VSP at near and far offsets—A CO2CRC Otway Project data example". *The Leading Edge* 36 (12): 994a1–994a7.

Daley, T. M., B. M. Freifeld, J. Ajo-Franklin, S. Dou, R. Pevzner, V. Shulakova, S. Kashikar, D. E. Miller, J. Goetz, J. Henninges, et al. 2013. "Field testing of fiber-optic distributed acoustic sensing (DAS) for subsurface seismic monitoring". *The Leading Edge* 32 (6): 699–706.

Grab, M., B. Quintal, E. Caspari, H. Maurer, and S. Greenhalgh. 2017. "Numerical modeling of fluid effects on seismic properties of fractured magmatic geothermal reservoirs". *Solid Earth* 8 (1): 255.

Lumens, P., A. Franzen, K. Hornman, S. Grandi Karam, G. Hemink, B. Kuvshinov, J. La Follett, B. Wyker, and P. Zwartjes. 2013. "Cable development for distributed geophysical sensing with a field trial in surface seismic". In *Proc. SPIE*, 8794:879435–879435.

Malehmir, A., R. Durrheim, G. Bellefleur, M. Urosevic, C. Juhlin, D. J. White, B. Milkereit, and G. Campbell. 2012. "Seismic methods in mineral exploration and mine planning: A general overview of past and present case histories and a look into the future". *Geophysics* 77 (5): WC173–WC190.

Mateeva, A., J. Lopez, J. Mestayer, P. Wills, B. Cox, D. Kiyashchenko, Z. Yang, W. Berlang, R. Detomo, and S. Grandi. 2013. "Distributed acoustic sensing for reservoir monitoring with VSP". *The Leading Edge*.

Maurer, H., A. Nuber, N. K. Martiartu, F. Reiser, C. Boehm, E. Manukyan, C. Schmelzbach, and A. Fichtner. 2017. "Optimized Experimental Design in the Context of Seismic Full Waveform Inversion and Seismic Waveform Imaging". In *Advances in Geophysics*, 58:1–45. Elsevier.

Pham, N. D., H. Igel, J. de la Puente, M. Käser, and M. A. Schoenberg. 2010. "Rotational motions in homogeneous anisotropic elastic media". *Geophysics* 75 (5): D47–D56.

Reinsch, T., J. Henninges, and R. Ásmundsson. 2013. "Thermal, mechanical and chemical influences on the performance of optical fibres for distributed temperature sensing in a hot geothermal well". *Environmental earth sciences* 70 (8): 3465–3480.

Reinsch, T., J. Henninges, J. Götz, P. Jousset, D. Bruhn, and S. Lüth. 2015. "Distributed Acoustic Sensing Technology for Seismic Exploration in Magmatic Geothermal Areas". In *Proceedings World Geothermal Congress*.

Schmelzbach, C., S. Donner, H. Igel, T. Taufiqurrahman, F. Bernauer, M. Häusler, C. Van Renterghem, J. Wassermann, and J. Robertsson. 2017. *Advances in 6-C seismology: applications of combined translational and rotational motion measurements in global and exploration seismology*. Submitted to Geophysics.

Sollberger, D., S. Greenhalgh, C. Schmelzbach, C. Van Renterghem, and J. Robertsson. 2017. *6-C polarisation analysis using point measurements of translational and rotational ground-motion: Theory and applications*. Submitted to GJI.

Van Renterghem, C., C. Schmelzbach, D. Sollberger, and J. Robertsson. 2017. "Spatial wavefield gradient-based seismic wavefield separation". *Geophysical Journal International*.

Yang, D., M. Fehler, A. Malcolm, and L. Huang. 2011. "Carbon sequestration monitoring with acoustic double-difference waveform inversion: A case study on SACROC walkaway VSP data". In *SEG Technical Program Expanded Abstracts 2011*, 4273–4277. Society of Exploration Geophysicists.

Appendices

A

Advanced seismic processing/imaging techniques and their potential for geothermal exploration

Contents

Abstract

Seismic reflection imaging is a geophysical method that provides greater resolution at depth than other methods and is, therefore, the method of choice for hydrocarbon-reservoir exploration. However, seismic imaging has only sparingly been used to explore and monitor geothermal reservoirs. Yet, detailed images of reservoirs are an essential prerequisite to assess the feasibility of geothermal projects and to reduce the risk associated with expensive drilling programs. The vast experience of hydrocarbon seismic imaging has much to offer in illuminating the route toward improved seismic exploration of geothermal reservoirs - but adaptations to the geothermal problem are required. Specialized seismic acquisition and processing techniques with significant potential for the geothermal case are the use of 3D arrays and multicomponent sensors, coupled with sophisticated processing, including seismic attribute analysis, polarization filtering/migration, converted-wave processing, and the analysis of the diffracted wavefield. Furthermore, full-waveform inversion and S-wave splitting investigations potentially provide quantitative estimates of elastic parameters, from which it may be possible to infer critical geothermal properties, such as porosity and temperature.

A.1   Introduction

Geothermal energy is a promising and increasingly popular sustainable energy source for electricity generation and district heating purposes (Lund et al. (2008)). However, considerable further research and development is necessary to optimize this renewable energy source in terms of the engineering challenges and the geoscientific requirements to identify, locate, and produce geothermal reservoirs. In many places, the high temperatures needed for economical geothermal electricity production are generally found at depths of at least a few kilometers in the earth's crust. Suitable subsurface imaging tools are required to delineate and characterize geothermal reservoirs in sufficient detail at these depths.

Seismic reflection imaging has a greater depth of penetration with reasonable resolution compared with other geophysical methods used to investigate geothermal reservoirs (e.g., gravity, magnetic, electrical resistivity, and electromagnetic surveys; (Barbier (2002)). Seismic reflection investigations map interfaces associated with elastic-property contrasts (i.e., reflecting/ scattering features; Sheriff and Geldart (1995); Yilmaz (2001)) and can provide estimates of physical properties, such as seismic velocities and anisotropy. Potential and diffusive field geophysical techniques such as gravity surveying and electromagnetic imaging provide largescale subsurface volume information (bulk properties). For example, electromagnetic methods have successfully been used in geothermal exploration to image the subsurface electrical resistivity distribution, which is sensitive to fluid content, temperature, and alteration (Munoz (2014)). Passive seismic techniques such as ambient noise tomography and microseismicity studies (Obermann et al. (2015)) have been successfully used to characterize geothermal reservoirs and to monitor changes. However, it is essentially only active (controlled source) seismic methods that can provide the necessary high-resolution fault and fracture characterization at depth necessary for successful well siting.

Oil companies have explored in great detail many sedimentary basins throughout the world; hence, much can be learned from the oil and gas industry in terms of advanced exploration techniques.

For example, fracture zone imaging and characterization is of equal importance to hydrocarbon exploration as it is to geothermal exploration. Key developments in land-seismic acquisition and processing for oil and gas exploration that are relevant to geothermal exploration include 3D and repeated 3D (4D; time-lapse) technology (Lumley (2001); Brown (2004)), multicomponent seismic measurements (Hardage et al. (2011)), advanced and efficient prestack migration schemes (prestack time and depth migration, reverse time migration; (Yilmaz (2001)), seismic attribute and amplitude variation with offset analyses (Luo and Evans (2004); Chopra and Marfurt (2007)), and anisotropy studies (Crampin (1985)).

Enhanced geothermal systems (EGS) have their maximum potential in crystalline basement rock (Tester et al. (2007)) in which temperatures are sufficiently elevated but the permeability is low and in need of artificial stimulation. So far, extensive seismic exploration studies over hard-rock environments (for a comprehensive review, see Eaton et al. (2003) are mainly related to mineral exploration (Milkereit et al. (1994); Drummond et al. (2003); Malehmir et al. (2012)), mapping fracture zones primarily for finding suitable underground repositories for radioactive waste (Green and Mair (1983); Juhlin and Palm (2003); Schmelzbach et al. (2007)), and assorted geologic studies, especially crustal investigations (Clowes et al. (1984); Juhlin et al. (1998); Cook et al. (1999); Schmelzbach et al. (2008)).

There are several key challenges one needs to face in hard-rock seismic exploration (Salisbury et al. (2007); Greenhalgh and Manukyan (2013)): (1) reflection amplitudes are generally weak, leading to low signal-to-noise ratio (S/N) that makes it difficult to image features within crystalline rocks; (2) reflectors are often small, steeply dipping, and laterally discontinuous due to more complex morphology, lithology, and deformation; (3) the high velocities in crystalline basement result in a loss of resolution due to the relatively longer wavelengths; (4) obtaining reliable velocity information in deep basement is problematic without long aperture recordings; and (5) anisotropy can be introduced through fractures and layering, leading to complex wave propagation. Milkereit and Eaton (1998) discuss in detail the seismic challenges that occur in crystalline basement in comparison with sedimentary basins. Low-reflection coefficients make it difficult not only to image large scale structures, such as the Moho discontinuity or major fault structures, but also to obtain a detailed shallow crustal image. Deep crustal studies helped to develop the requisite acquisition and processing techniques for crystalline environments, including metalliferous mining. These large-scale images can also provide valuable information when looking for potential geothermal sites. They can be used as a basis for a more refined study of a promising area and further evaluation of the site.

Although it is used extensively in hydrocarbon exploration and production, seismic reflection imaging has been only rarely used in geothermal exploration to date, with a few notable exceptions (e.g., in the Bavarian Molasse Basin and the Upper Rhine Graben in Germany). However, active-source seismic surveying provides a powerful and essential prerequisite to assess the feasibility of geothermal projects and to reduce the risk associated with expensive drilling programs. Moreover, seismic imaging enables more intelligent and selective drilling. Targets in geothermal exploration are permeable zones of sufficiently high temperature and fluid movement; such zones are mostly controlled by faults and fractures. Hence, the focus in seismic geothermal exploration is mapping deep sedimentary and basement structures, such as faults and fracture zones.

Various sophisticated seismic imaging techniques have been developed for the oil and gas industry as well as for the mining industry, not only for exploration but also for monitoring of reservoirs during production. It needs to be investigated how these techniques can be adapted and applied to geothermal sites to improve the planning and development of geothermal reservoirs. In this paper, we (1) summarize the challenges and current status of geothermal seismic exploration, (2) discuss how geothermal seismic exploration can benefit from experience with seismic methods in hydrocarbon and metalliferous-ore exploration, and (3) review a selection of advanced seismic processing techniques that could potentially be of value for the seismic imaging and evaluation of geothermal reservoirs.

## A.2   Status of geothermal seismic exploration

Permeable fracture zones control the fluid flow in sedimentary and hard-rock geothermal reservoirs and, therefore, need to be considered in the planning of wells. Some examples of seismic reflection investigations in geothermal areas for EGS and hydrothermal systems are described in the following two subsections.

A.2.1   Hydrothermal systems

A geothermal system that contains a naturally occurring permeable layer or layers and a large amount of fluid or vapor that circulates in the subsurface is called a hydrothermal system (Barbier (2002)). Whether the system is economically viable depends on the amount of water or steam that can be extracted and the drilling depth that is necessary to reach the necessary rock temperature. A geothermal reservoir can exist in various depth ranges, depending on surrounding heat sources. High enthalpy systems are mostly related to recent volcanism, show high temperatures at relatively shallow depth and are responsible for most of the electricity production from geothermal areas. Examples for hydrothermal systems in Europe that successfully produce electricity are Lardarello in Italy (Brogi et al. (2005)) and several reservoirs in Iceland (Arnórsson (1995)).

However, moderate-temperature geothermal resources can also be used for electricity production. Deep sedimentary basins that contain an aquifer that enables the fluid to circulate, e.g., the porous sandstone in the North German sedimentary basin (Schellschmidt et al. (2010); Weber et al. (2015)), or faulted reservoirs, e.g., Unterhaching, near Munich, where large fault systems and karstification provide good hydraulic conductivity (Thomas and Schulz (2007); Lüschen et al. (2014)) can be used for electricity generation.

Because hydrothermal systems are naturally occurring, they are limited in geographic location and it is a key challenge to find them. Seismic exploration can be used to image the lateral extent of an aquifer and to characterize the associated fault and fracture systems (Matsushima and Okubo (2003)). Examples of seismic exploration in hydrothermal systems are the study by von von Hartmann et al. (2012) who reprocess a relatively low common-depth-point (CDP) fold (approximately 12) 3D seismic data set acquired in 1985 for hydrocarbon exploration in southern Germany to resolve and characterize Upper Jurassic carbonate platforms that could serve as a geothermal reservoir. Lüschen et al. (2014) study a 3D seismic data set covering an area of approximately $27\,\text{km}^2$ in Unter-
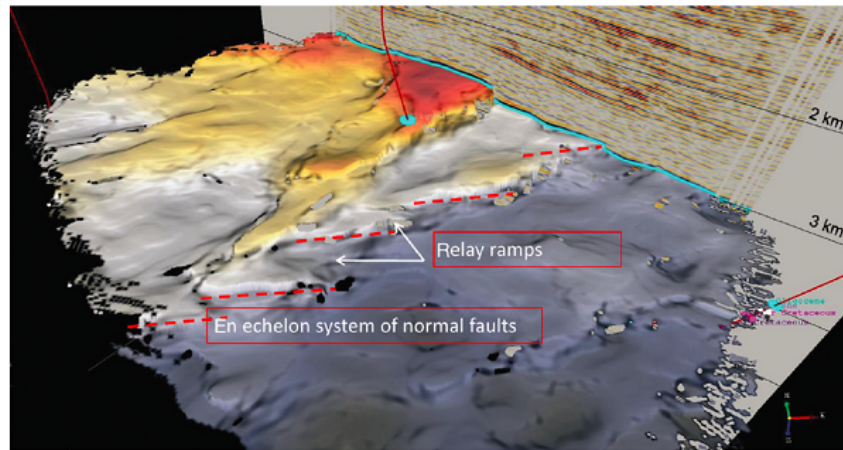
Figure A.1: Mapping key lineaments around the Unterhaching (Munich area, Germany) geothermal site using 3D seismic-reflection imaging. The extent of the Lithothamnion limestone horizon is shown at approximately 3000 m depth; colors ranging from red to dark blue represent differences in depth of approximately 500 m. The Unterhaching Gt2 well is shown in red. Background shows a vertical section through the 3D data cube. Figure reprinted from Lüschen et al. (2014), Copyright (2014), with permission from Elsevier.

haching, Munich, to characterize the Malm sequence that is the target formation for a hydrothermal reservoir (see also Thomas et al. (2010)). The 3D data enabled the mapping of key tectonic features in 3D (Figure A.1) and the analysis of azimuth-dependent reflectivity to obtain indications of the preferred fracture orientations (Figure A.2).

Pussak et al. (2014) process a 3D seismic data set from the Polish Basin to investigate a lower Jurassic horizon that consists of alternating sandstone and claystone layers. The target geothermal reservoir was imaged using a common-reflection-surface (CRS) stack technique (Jäger et al. (2001)) and compared with the results of a conventional normal moveout and dip moveout stack (Yilmaz (2001)). A similar study was conducted by Buness et al. (2014) in the Upper Rhine Graben. It was shown that a CRS stack improved the S/N and is an especially valuable method for sparse data sets because reflections are sampled over several CDP bins instead of just one as in conventional CDP stacking. Amplitude analysis was successfully used to image fault zones.

Deep crustal large-scale seismic images can provide valuable information when looking for potential geothermal sites. An example of imaging the shallow crust for geothermal exploration is given by Brogi et al. (2005) and Riedel et al. (2015). Two deep seismic reflection lines were acquired in southern Tuscany to examine the Lardarello geothermal site. The study helped to understand the tectonic setting, to construct a regional structural model, and to identify a magmatic body that could serve as a current heat source for the Lardarello geothermal site.

A.2.2 Enhanced geothermal systems

EGSs have great potential because they are not limited to specialized geologic environments, such as hydrothermal and magmatic systems. EGSs are an emerging technology, and several research programs have been developed along with pilot plants and the installations have been tested. Ex-
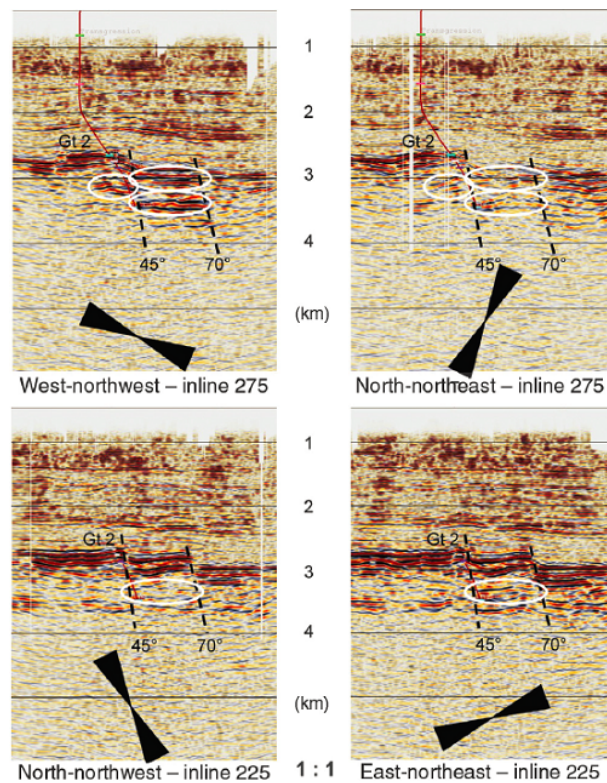
Figure A.2: Azimuth selective processing of the Unterhaching 3D seismic data. The four vertical sections show the processed data for $30\,^{\circ}$ wide source-receiver corridors. Width and orientation of the angle corridors are indicated by the black triangles. Amplitudes are plotted at the same scale. The dashed lines mark the main fault zones and white ellipses mark regions with azimuth-dependent reflectivity. Drill trajectory of well Gt2 is shown in red. Figure reprinted from Lüschen et al. (2014), Copyright (2014), with permission from Elsevier.

amples of EGS can be found worldwide and include Fenton Hill (USA; Duchane and Brown (2002), Soultz-sous-Forêts (France; Genter et al. (2010); Gérard et al. (2006)), Rosemanowes Quarry (UK; Richards et al. (1994)), Hijiori and Ogachi (Japan; Kuriyagawa and Tenma (1999)), Cooper Basin (Australia; Chopra and Wyborn (2003)), and The Geysers (USA; Lipman et al. (1978)).

EGS can be built in many locations worldwide, where a suitable hot rock volume is accessible in the upper few kilometers of the crust (Lund et al. (2008)). These rocks show very low natural permeability, and, hence, the reservoirs need to be artificially fractured to produce a hydraulically conductive subsurface to circulate fluid. Favorable locations for an EGS show a great amount of heat in place and an insulating sedimentary cover layer to retain the heat. Hence, most EGS reservoirs will be located in hard-rock basement rather than in the sedimentary section.

The emphasis of seismic exploration in EGS areas has been on detailed imaging of fault and fracture zones at the top of and within the crystalline basement. Seismic reflection images reveal the subsurface structure and/or stratigraphy and can therefore be used to help establish flow models and find favorable positions for wells. However, there has only been little research on hard-rock seismic reflection imaging in geothermal areas. A few examples are summarized below.

The Rhine Graben is currently one of the main European areas for EGS projects in predominantly crystalline rocks. Sites of planed, active, or ceased geothermal power plants in the Rhine Graben are Soultz-sous-Forêts (France), Landau (Germany), Insheim (Germany), Rittershoffen (France), and Basel (Switzerland). Place et al. (2010) interpret several reprocessed vintage seismic lines in the Soultz-sous-Forêts geothermal site (see also Sausse et al. (2010); Place et al. (2011)). A large number of seismic lines are available due to extensive oil exploration in the area. By focusing on improved static corrections and time migration, some sedimentary reflectors were mapped in greater detail. However, due to the fact that the acquisition parameters (e.g., maximum offset) were originally chosen to image the shallower sediments, the top of the basement and the deeper sediments were not well imaged. Hence, even after reprocessing, structures of geothermal interest within the basement were not recovered.

Recently, Hloušek et al. (2015) and Schreiter et al. (2015) report on the processing and interpretation, respectively, of a 3D survey of approximate areal extent 10×13 km that was conducted in 2012 in western Erzgebirge near the city of Schneeberg, Germany (see also Ahmed et al. (2015); Lüschen et al. (2015)). The aim of the project was to characterize the major fracture zones in the crystalline rock at approximately 4–5 km depth. With expected temperatures of 160–180°, this fracture zone could be used as a natural heat exchanger. An advanced coherency-style prestack depth migration algorithm (Hloušek et al. (2015)) sharpened the image and revealed several fracture zones in 2–5 km depth interval.

Khair et al. (2015) establish a seismic workflow for EGS to characterize faults within deep hot granites. The study site is the Cooper Basin of South Central Australia which is defined by a 3 km thick sediment cover, which serves as a good thermal insulator over a granitic basement. The aim of the project was to image and to identify faults that are most likely to provide the pathways for the circulating fluids.

A.2.3 Vertical seismic profiling at geothermal sites

Vertical seismic profiling (VSP) has been widely used in the oil industry to complement surface seismic data (Hardage (2000)) but its use in geothermal exploration has been somewhat restricted to just checkshot-style surveys for average velocity estimation and converting times to depths. VSPs entail placing receivers downhole and firing into them from surface shots (or other energy sources) at various offsets from the wellhead (including at wellhead, corresponding to zero offset) and different azimuths. VSPs can be applied to identify reflections and trace them to their points of origin in the subsurface, provide information about their orientation and exact location when they intersect the borehole, and tie borehole geology to surface seismic data. They provide the elusive link between synthetic seismograms and actual seismic records. Furthermore, they can be used to image structures away from the well. Because of their many advantages, VSPs can be used for highresolution imaging of lithologic interfaces and dipping features (e.g., fracture zones) in the vicinity of the borehole. Valuable reflectivity, velocity, and anisotropy information can be gained from VSP data. In addition, it is very beneficial for providing a direct linkage between lithology in the borehole and the seismic data, and obtaining accurate velocity values as a function of depth that can be used for the time-depth conversion of surface seismic data.

Cosma et al. (2003) discuss several advantages of VSP over surface seismic data in crystalline rock:

1) Because receivers are placed within the well, traveltimes are shorter, and waves travel only once through the highly attenuating near-surface weathered layer, hence, the signal amplitudes experience less attenuation than in surface seismic data, resulting in generally superior resolution.

2) To map dipping features with surface seismic reflection data, large offsets are required. VSP provides a convenient geometry for mapping gently and steeply dipping interfaces, especially for multioffset and multiazimuth surveys.

3) 3C geophones enable the recording of the full vector wavefield and with polarization analysis, the orientation of reflectors can be retrieved, whereas in surface seismic data, the polarization information is often degraded due to the heterogeneous and lowvelocity near-surface layer.

VSP surveys have successfully been applied in fractured carbonate reservoirs (Emsley et al. (2007)) and in crystalline rock for better understanding of seismic properties in the crust (Carr et al. (1996); Rabbel et al. (2004)), for mineral exploration (Adam et al. (2003); Bellefleur et al. (2004)), and nuclear waste disposal sites (Cosma et al. (2003)).

There have also been a few examples in which VSP has been used to better characterize geothermal sites. Majer et al. (1988) report a VSP pilot study in The Geyser steam-bearing geothermal field in northern California on fracture-induced anisotropy. Nakagome et al. (1998) investigate the Kakkonda geothermal field in Japan and related the weak amplitude zones to increased absorption in fracture zones.

Feighner et al. (1998) identify a coherent reflector that corresponds to a permeable zone responsible for the fluid transport in the Rye Patch geothermal field in Nevada. A VSP and a moving source VSP (MS-VSP) was conducted at Unterhaching in the Munich area to complement surface seismic data (Thomas and Schulz (2007)). It was shown that the VSP had a higher S/N ratio than the surface seismic data and several reflectors could be mapped and fault systems interpreted.

Place et al. (2010), (2011) and Sausse et al. (2010) investigate the geothermal site in Soultz-sous-Forêts in the Upper Rhine Graben with VSP data that was acquired in 1988 and 1993. Diffraction analysis was useful to identify a fault edge and improve the structural interpretation. P-to-S converted wave analysis indicated steeply dipping fracture zones away from the well that control the fluid flow within the granitic basement. An example of the final migrated VSP data is shown in Figure A.3.
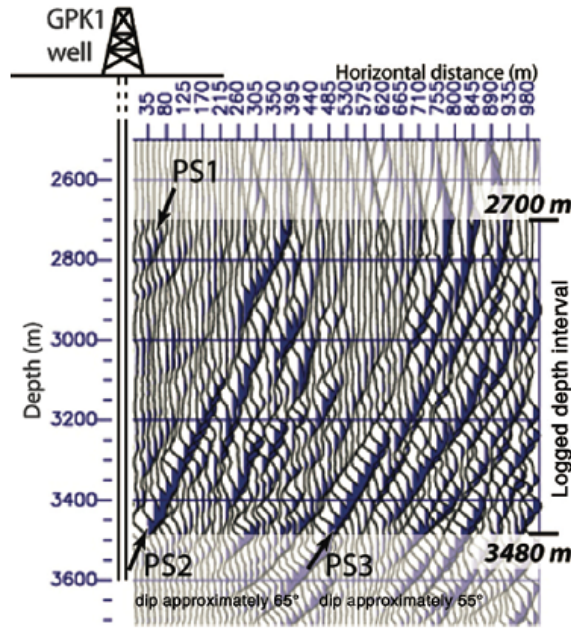
Figure A.3: Migrated image of VSP data from Soultz-sous-Fôrets. Steeply dipping reflectors were mapped using P-S converted reflections. Note that the processing did not allow the positioning of reflectors in 3D. Hence, the image is axially symmetric around borehole GPK1. Figure reproduced from Place et al. (2011) (Figure 6). By permission of Oxford University Press on behalf of The Royal Astronomical Society).

A.3 Review of specialized seismic processing techniques and their potential for geothermal exploration

Over the past few decades, numerous advanced seismic processing techniques have been developed by the oil and gas industry. It remains to be established through detailed testing which of these techniques can be best adapted and profitably applied to geothermal seismic exploration.

A.3.1 Seismic attribute analysis

Seismic attributes are quantities that can be derived from seismic data to extract structural and lithologic information of the subsurface (Chopra and Marfurt (2005), Chopra and Marfurt (2007)). There are different ways of classifying a seismic attribute. Taner et al. (1994) divide attributes into geometric and physical attributes. Geometric attributes are normally used in stratigraphic interpretation and enhance geometric characteristics, such as continuity, unconformities, faults, dip, azimuth, and curvature. Physical attributes have a direct link to physical parameters in the subsurface and are generally used for characterization of lithology and reservoirs. Brown (1996) divides attributes into time, amplitude, frequency, and attenuation attributes, which can be further subdivided into pre- and poststack attributes. Prestack amplitudes contain azimuthal and offset information and can be used to determine fluid content and fracture orientation, whereas poststack seismic amplitudes are analyzed on CDP stacked sections and are more suitable for large amounts of data (Taner (2001)).

A classic set of attributes is derived from the complex trace analysis (e.g., reflection strength/instantaneous amplitude, instantaneous frequency; Taner et al. (1979); Chopra and Marfurt (2005)). Reflection

strength is sensitive to changes in acoustic impedance and can therefore be used to identify different lithology, porosity, hydrocarbons, and thin-bed tuning. High reflection strength is often related to gas accumulation and may be identified through bright spots. Abrupt changes in reflection strength can also indicate faulting. The instantaneous frequency attribute is a useful tool for lithology characterization, identifying increased attenuation, thinbed tuning, and as a fracture zone indicator.

Three-dimensional seismic exploration in the 1990s had a profound impact on seismic attribute analysis. A large number of new attributes were developed, and the extraction of stratigraphic information was expanded to exploitation and reservoir characterization (Chopra and Marfurt (2005)). Dip and azimuth maps became two of the most important attributes for identification of faults and other subtle stratigraphic features. Dip and azimuth are the basis for many geometric attributes, e.g., coherence and curvature. Coherence measures the similarity between waveforms and traces and should be computed along local dip and azimuth of a reflector. Coherent regions indicate a laterally continuous lithology, whereas a low degree of coherency indicates discontinuous events, such as faults and fractures. Figure A.4 illustrates the utility of coherency maps to locate fracture zones.

Applications of attribute analysis in geothermal exploration to enhance the visibility of fracture zones are reported by, for example, von Hartmann et al. (2012) to characterize Upper Jurassic carbonate platforms in southern Germany that could serve as a geothermal reservoir. Different carbonate facies were identified with the help of seismic attribute analysis, such as spectral decomposition. Pussak et al. (2014) extract and analyze root-mean-square (rms) amplitudes, instantaneous frequencies, coherency, and spectral decomposition attributes from a 3D seismic data set to characterize a geothermal reservoir in the Polish Basin with the aim to locate fluid-bearing fracture zones. Seismic attribute analysis is used by Khair et al. (2015) to elucidate deep hot granitic rocks below a thick sedimentary cover at a study site in the Cooper Basin (South Central Australia). The main focus was set on the curvature attribute that enabled the successful imaging of approximately 170 faults that intersect the basement.

A.3.2   Multicomponent (vector) seismic data analysis

The standard practice in land seismic acquisition is to measure the vertical component of the ground motion only. These scalar or 1C data are then processed into P-wave reflectivity or velocity images based on the assumption that the measured 1C records represent mainly P-wave energy (steeply arriving waves polarized in that direction). Multicomponent or vector seismic recordings (measurement with vertical- and horizontalcomponent geophones; 3C geophones) capture the seismic wavefield more completely than 1C techniques and allow, for example, studying S-waves and modeconverted waves (P-S and S-P conversions; Stewart et al. (2002)). The benefits of S-wave and converted-wave exploration are numerous and include "seeing" through gas-bearing sediments, improved fault definition, enhanced near-surface resolution, improved lithologic characterization, subsurface fluid description, and reservoir monitoring (Tatham and McCormack (1991); Stewart et al. (2003)).

Key advantages of multicomponent exploration over 1C data acquisition are the possibility to identify (and separate) the various wave modes based on their polarization properties and to characterize anisotropy by studying S-wave splitting (discussed in detail in the "S-wave birefringence" subsection; Crampin (1981)). Polarization information can be used to determine the direction of different
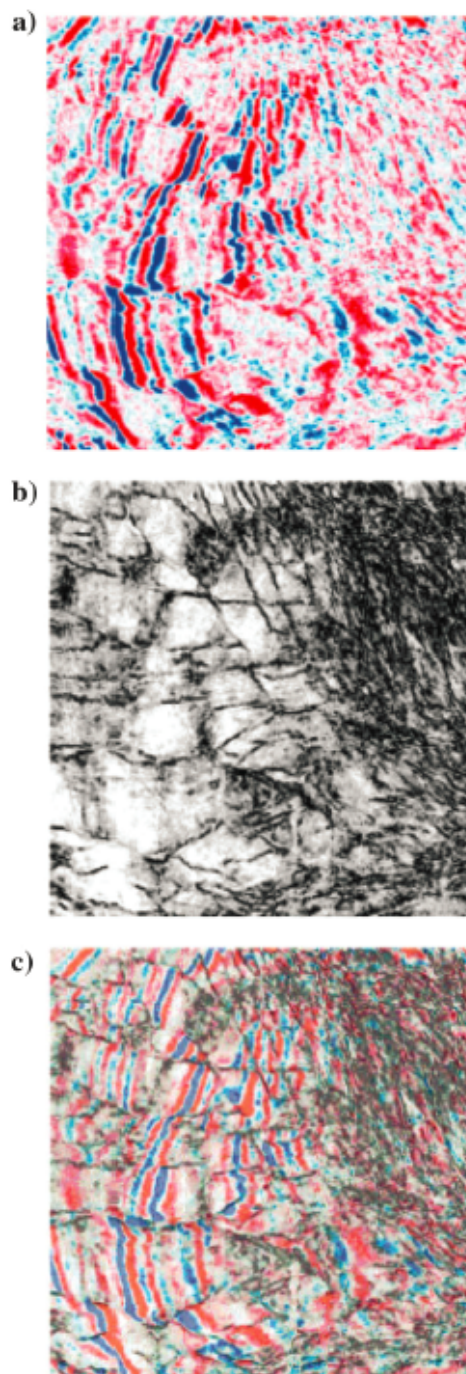
Figure A.4: Illustration of the 3D coherence attribute. Time (horizontal) slices through (a) a 3D seismic data cube and (b) coherence data volume. (c) Overlay of panels (a and b). Note how coherence highlights faults and enhances the interpretation of the intensively fractured region to the right (modified after Chopra and Marfurt (2005).)

arriving wave types (Vidale (1986); Rutty and Greenhalgh (1993)) and to provide the possibility for application of polarization filters to, for example, suppress noise or unwanted modes, such as Rayleigh waves (Özbek (2000)), wavefield separation techniques (Dankbaar (1985); Greenhalgh et al. (1990)), and prestack elastic migration (Chang and McMechan (1994); Zhe and Greenhalgh (1997)). An important motivation of anisotropy studies is the characterization of fracture density and orientation (Crampin, 1985). Fracture characterization is, for example, critical for shale gas production, which is gaining increasing attention in Europe and worldwide (Weijermars et al. (2011)).

Even though land multicomponent seismic exploration gained increased attention during recent years (see, e.g., special sections of The Leading Edge in September 2001, December 2003, and January 2013), it remains a niche play, with, for example, P-S-converted wave analysis still only accounting for approximately 5% of the total seismic processing revenue in the exploration seismic industry (Bansal and Gaiser (2013)). In contrast, multicomponent techniques are well established for vertical-seismic profiling. The reasons why multicomponent seismology has not become a widely adopted approach to exploration are the challenging field logistics (e.g., increased number of channels compared with 1C surveys), the requirement of different processing of converted waves compared with P-waves, and difficulties in interpreting the resultant S-wave images (Stewart et al. (2003)).

Today, converted-wave acquisition and processing (where sources that generate P-waves are used but where the S-wave converted reflections of these waves at the target are recorded on the surface) is in general deemed to be more practical for oil-andgas exploration because S-wave sources are large, expensive, and usually have a considerable environmental impact.

Because in high-enthalpy geothermal systems hot steam can be extracted to generate electricity, it is important to locate steam-bearing fracture zones. Steam introduces higher absorption of the seismic wavefield and also has the effect of decreasing the seismic velocity. Wei et al. (2014)a,b show the benefits of using multicomponent seismic data in the Wister geothermal field, which is a Cenozoic sedimentary basin located in California. The goal of their study was to evaluate potential reservoir units, locate fault, and fracture zones and investigate whether additional value can be gained from multicomponent seismic data. It was shown that V_P/V_S velocity ratios were beneficial to identify and specify different rock types, and that P-SV data were more sensitive to fractures than P-P data, particularly in hot steam-filled sections. Because P-waves get strongly attenuated by gasfilled pores, P-SV images can significantly improve the image quality within and below the gas-filled formation (Figure A.5).

A.3.3 S-wave birefringence

When S-waves encounter an anisotropic medium they show very different characteristics in comparison with P-waves (Tsvankin (2012)). The S-wave splits into fast and slow S-wave components having orthogonal polarizations, which are normal to the wave direction (the same as that of the incident S-wave), whereas the P-wave is less affected by the anisotropy and does not separate (Crampin (1981), (1985); Hardage et al. (2011)). The S-wave splitting can be caused by different anisotropic conditions, such as aligned crystals, stressinduced anisotropy, lithologic anisotropy, structural anisotropy, and crack-induced anisotropy (Crampin and Lovell (1991)). In a fractured medium, the polariza-
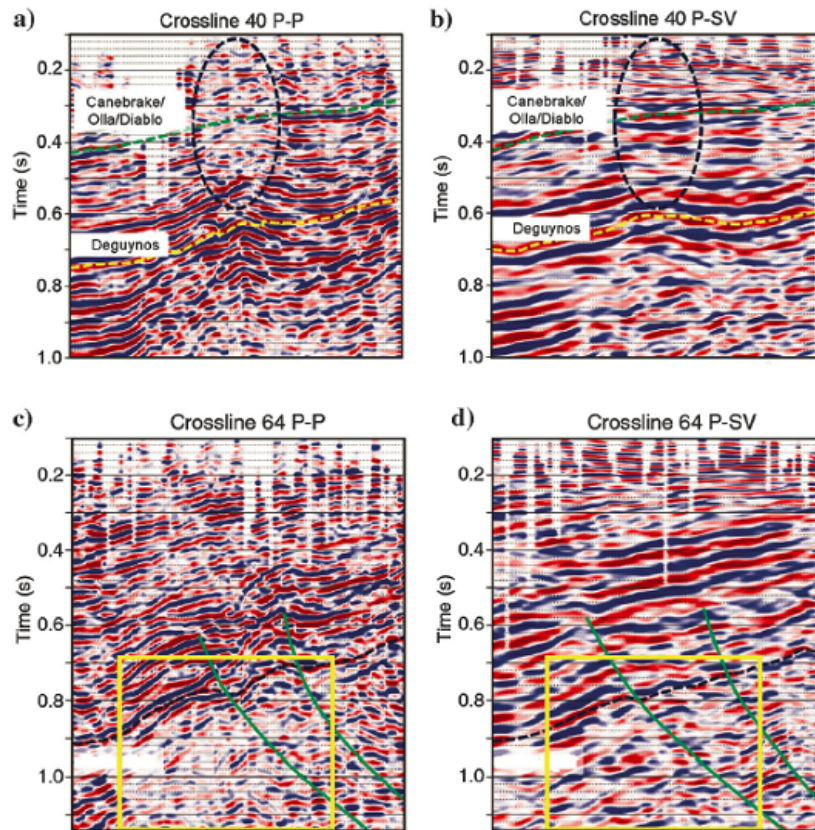
Figure A.5: Seismic section that illustrates (a and b) differences between P-P and P-SV stacks within gas clouds marked by black ovals and (c and d) across a region with low saturation of high-temperature fluid indicated with a yellow rectangle. Note that P-SV data contain more amplitude information within gas clouds and fluid-filled regions compared with P-P data (modified from Wei et al. (2014)b.)

tion of the fast S-wave is oriented parallel to the fracture plane and the slow S-wave shows particle motion perpendicular to the fracture plane. The idea that S-wave splitting can be used for fracture characterization lead to several successful studies in hydrocarbon exploration. It was shown that S-wave birefringence can be used for fracture mapping and that higher anisotropy can be correlated with increased oil production rates (Cliet et al. (1991)).

Because S-waves split whenever they are propagating through an anisotropic medium, the observed polarization can also be induced through the anisotropy of the overburden layer. Yardley and Crampin (1991) suggest the use of VSP surveys to analyze S-wave splitting to avoid the problem of the near-surface layer. It was shown that VSPs are less affected by the surface overburden and that the recorded polarization was dominated by the anisotropy of the rock in the vicinity of the borehole.

The time difference between the fast and slow Swaves is affected by the propagation distance and direction as well as the degree of anisotropy (Li and Mueller (1997)). Because fracture density is mainly responsible for the degree of anisotropy, the time delay can be used to estimate fracture density (Lewis et al. (1991)). The time delay is normally determined by comparing slow and fast S-wave stacked sections. In a study by Hitchings and Potters (2000), a fractured carbonate reservoir is
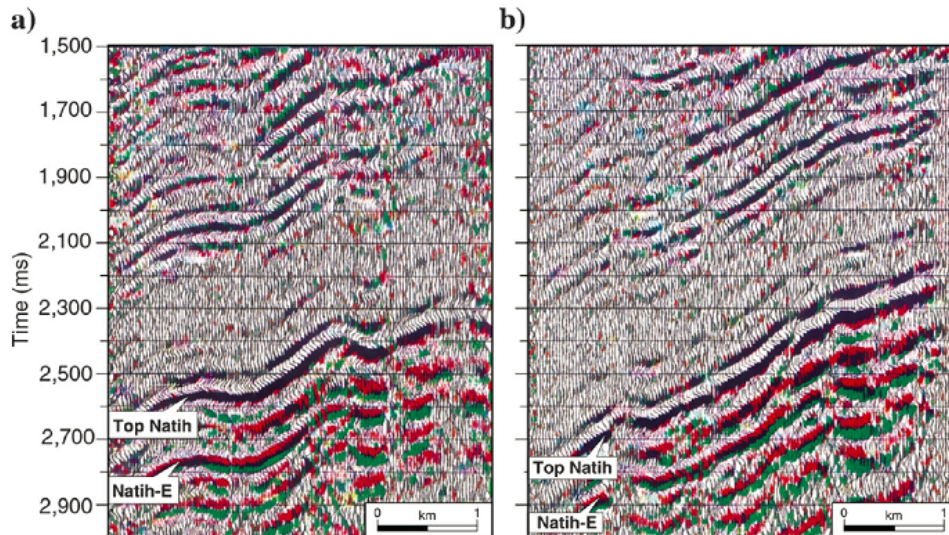
Figure A.6: Processed split S-wave profiles (a and b) over a fractured carbonate reservoir (top and bottom is labeled), after Hitchings and Potters (2000). Red corresponds to the fast S-wave response, green corresponds to the slow S-wave response, and black corresponds to the common response. Time delays within the reservoir increases from left to right, indicating increased fracture density.

examined by analyzing time delays between fast and slow S-waves. Regions with larger time delays indicate increased anisotropy, which corresponded to higher fracture density (Figure A.6).

S-wave splitting in geothermal fields has so far been analyzed by using natural and induced seismic events. Because the time delay between the fast and slow Swave is proportional to the crack density, S-wave birefringence is a valuable tool to characterize fractures in geothermal fields. Case studies in the Coso geothermal field in the Sierra Nevada Range, The Geysers geothermal site near the San Andreas Fault, and the Krafla site in northern Iceland show that polarization and time delay analyses of microearthquakes can be used to detect orientation and fracture density (Rial et al. (2005); Tang et al. (2008)).

Estimating fracture orientation and fracture density as well as understanding the stress state of the subsurface is of great importance in geothermal exploration. The information could be used not only to identify regions with larger hydraulic conductivity, but also to predict directions of hydraulic fracturing. This would provide further constraints on the location and design of geothermal wells. Analyzing fast and slow S-waves on VSP data could therefore provide additional information on fracture orientation and intensity in the subsurface.

A.3.4 Diffraction imaging

For the basement targets of importance in geothermal exploration (e.g., fracture planes, shear zones, fluid pathways, faults) the velocity contrasts are likely to be small, the dips steep, and the surface areas of the reflectors small. This leads to signal amplitudes that are typically one-fifth or less that of reflections from laterally continuous layers encountered in the sedimentary section above. The detection and identification of such small diffraction signatures places severe demands on seismic

field and processing practice. For example, detectability is frequency (wavelength) dependent. The lower the dominant frequency, the harder it is to detect a target feature. The higher the dominant frequency, the greater the wave absorption and the more difficult the field procedures and data processing become.

The ratio of the surface area of the body to the first Fresnel zone determines the horizontal detectable limit. A reflector is considered to be detectable if the ratio exceeds 0.05. For the most part it is expected that the geothermal targets will have a complex shape and spatial dimensions that are comparable with (or smaller than) the Fresnel zone associated with the source frequencies (typically $<50\,\mathrm{Hz}$, but sometimes as high as $90\,\mathrm{Hz}$) used and the target depth (3–5 km). Thus, they fall within the so-called Mie scattering regime, and common tools of the trade such as ray tracing are inappropriate for predicting their seismic expression. Full-wave theoretic modeling is required (e.g., finite-difference modeling; Robertsson and Blanch (2011)). The shape of the reflector itself will exert a first-order control on the Pwave scattering response. Unlike point diffractors, dipping lenticular or ellipsoidal fractures are expected to focus scattered P-waves in the long axis (specular reflection) direction, down dip from the feature (Bohlen et al. (2003)).

It is generally appreciated that with the surface-based CDP (P-wave) reflection technique, steeply dipping, and irregular interfaces are difficult to detect and image. The folded and faulted nature of the host rock in basement terrains means that there is a lack of bed continuity and marker horizons. One obvious approach is to concentrate on the diffracted portion of the wavefield, which can offer superior or even superresolution compared with reflection imaging (Moser and Howard (2008)). The high-resolution (subwavelength) information encoded in diffractions is generally lost during conventional processing. In contrast, diffraction imaging makes it possible to map small-scale discontinuous subsurface objects. Processing techniques to decompose the specular and diffraction (diffuse) energy from the total scattered wavefield have been presented by several researchers in recent years (Landa and Keydar (1998); Khaidukov et al. (2004); Klokov and Fomel (2012)). They are generally based on the ability to decompose the recorded wavefield into continuous full azimuth and dip directivity components in situ at the subsurface points. The technique takes advantage of the kinematic differences of the scattered and reflected seismic energy. Other techniques such as those proposed by Schmelzbach et al. (2008) and Malehmir et al. (2009) use a scheme that measures similarity along diffraction traveltime curves to map the location of point diffractors due to faults/fractures and suspected ore bodies, respectively, in crystalline rocks. This is illustrated in Figure A.7.

A.3.5 Velocity model building

It is standard practice in reflection seismic processing to undertake a semblance- type velocity analysis to identify multiples, estimate interval velocities, and perform a time/depth conversion. Migration velocity analysis to obtain the macro-velocity field is also required for effective imaging, such as post- and prestack migration. The derived interval velocities can also be used for geologic and petrological interpretations, such as discerning rock type, rock condition, and fluid content (Lüschen et al. (2014), (2015)). In the following two sections, we describe two other sophisticated methods for velocity model building — traveltime tomography and full-waveform inversion (FWI).
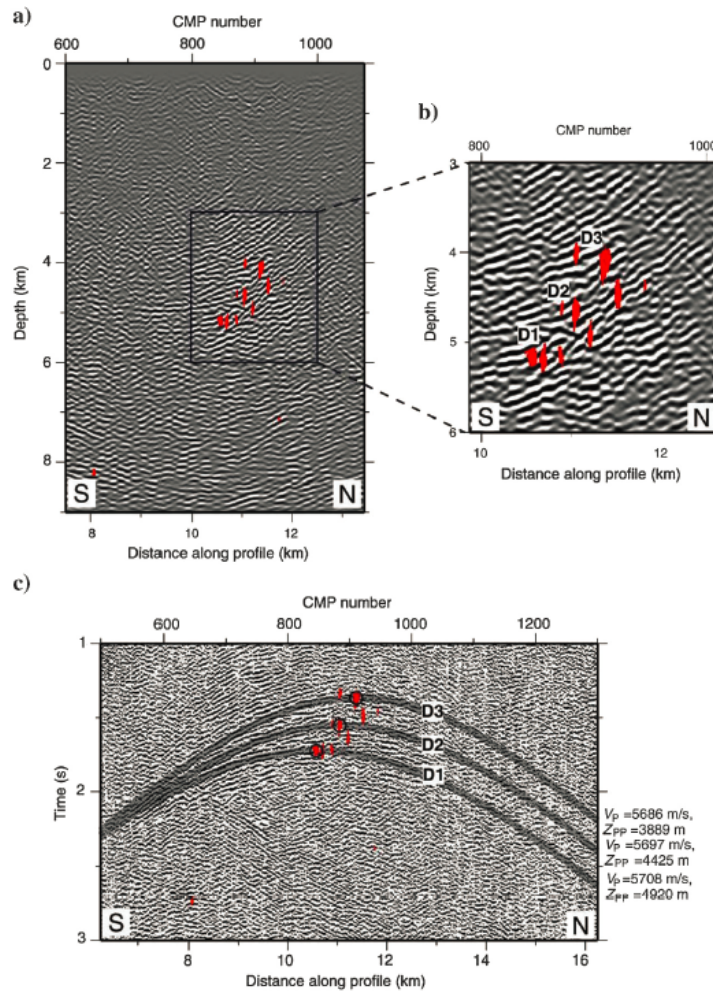
Figure A.7: Diffraction imaging in crystalline rocks. (a) Diffracting elements plotted in red onto migrated and depth-converted 2D seismic section. (b) Close-up view of panel (a). (c) Simulated traveltime curves (gray) for three diffractors shown in red are plotted onto the unmigrated data. Note that the synthetic traveltime curves match reasonably well with the observed diffraction patterns. Figure reprinted from Malehmir et al. (2009), copyright (2009), with permission from Elsevier.

A.3.6 Traveltime tomography

The aim of seismic ray tomography is to find a subsurface velocity model that can explain the first-arrival traveltimes. During the inversion process, the calculated traveltimes are compared with the actual traveltimes, and the velocity model is iteratively modified until the traveltime differences lie within the measurement error (Lanz et al. (1998); Zelt and Barton (1998); Rawlinson and Sambridge (2003)).

Classical ray tomography is based on the high-frequency assumption, which means that the ray is taken to be infinitely thin and not affected by diffraction diffraction and scattering from the surrounding rock. Waveequation tomography was introduced by Pratt and Goulty (1991) and Woodward (1992). Wave-equation tomography is a subset of FWI and does not rely on the high-frequency assumption and should therefore provide higher resolution images. However, the source wavelet

needs to be adequately known for the wavefield calculation and it further assumes the recorded data to be noise free.

Fat ray tomography represents a compromise between classical ray tomography and wave-equation tomography (Vasco et al. (1995); Husen and Kissling (2001); Jordi et al. (2016)). The ray is not assumed to be infinitely thin, but takes the frequency-dependent size of the first Fresnel zone into account for the wave propagation. Scattering within the Fresnel volume results in constructive interference of the seismic signal. Due to a more realistic description of seismic wave propagation, enhanced subsurface imaging is expected. Fat ray tomography is expected to increase the imaging capability in terms of additional subsurface information, improved resolution, and better localization of low-velocity zones due to the more realistic description of the seismic wave propagation. Fat ray tomography can be very beneficial in that it can provide an advanced macro-velocity model for migration, statics analysis, and a suitable starting model for FWI.

Crosshole (borehole-to-borehole) traveltime seismic tomography is often applied to image the velocity structure between wells, with applications including orebody delineation (Greenhalgh et al. (2003)) and hydrocarbon-reservoir monitoring (Spetzler et al. (2008)). If the rocks are anisotropic, the tomography formulation has to be adapted, otherwise the isotropic velocity tomograms can be severely distorted (Pratt et al. (1993)). Several approaches have been proposed to handle anisotropy in crosshole seismic tomography, differing in simplifying assumptions and parameterization of anisotropy (Chapman and Pratt (1992); Zhou et al. (2008)). Vécsey et al. (1998) demonstrate that accounting for anisotropy in crosshole measurements at a potential hot dry rock reservoir to monitor effects of changing fluid pressure greatly enhanced the interpretability of the tomograms.

A.3.7 Full-waveform inversion

FWI is an imaging method that seeks to exploit simultaneously the whole seismic data along each trace to reconstruct high-resolution quantitative images of the characteristic parameters (seismic velocities, density, and attenuation) of large areas of the subsurface. Because the entire seismograms are used for FWI, the most complete representation of the subsurface is expected. Thus, FWI is expected to provide quantitative images with the resolution of migration and diffraction imaging (half of the shortest wavelength expected for favorable illumination). Comprehensive reviews of the method are given by, for example, Virieux and Operto (2009) and Fichtner (2011).

However, the development of FWI has faced several major challenges:

1) The accurate numerical forward modeling of the full 3D viscoelastic wave propagation in a very complex and arbitrary medium including composite features, such as faults, free surface with topography, attenuation and anisotropy is a difficult task, and requires extremely intensive computational facilities.

2) The associated inverse problem is highly nonlinear, in particular for the high frequencies and in the seismic reflection configuration. Indeed, the prior knowledge of the largescale variations of the medium is necessary. This information is given through a reference background (initial) velocity model that can be obtained, for instance, by velocity analysis, or refraction or reflection traveltime tomography.
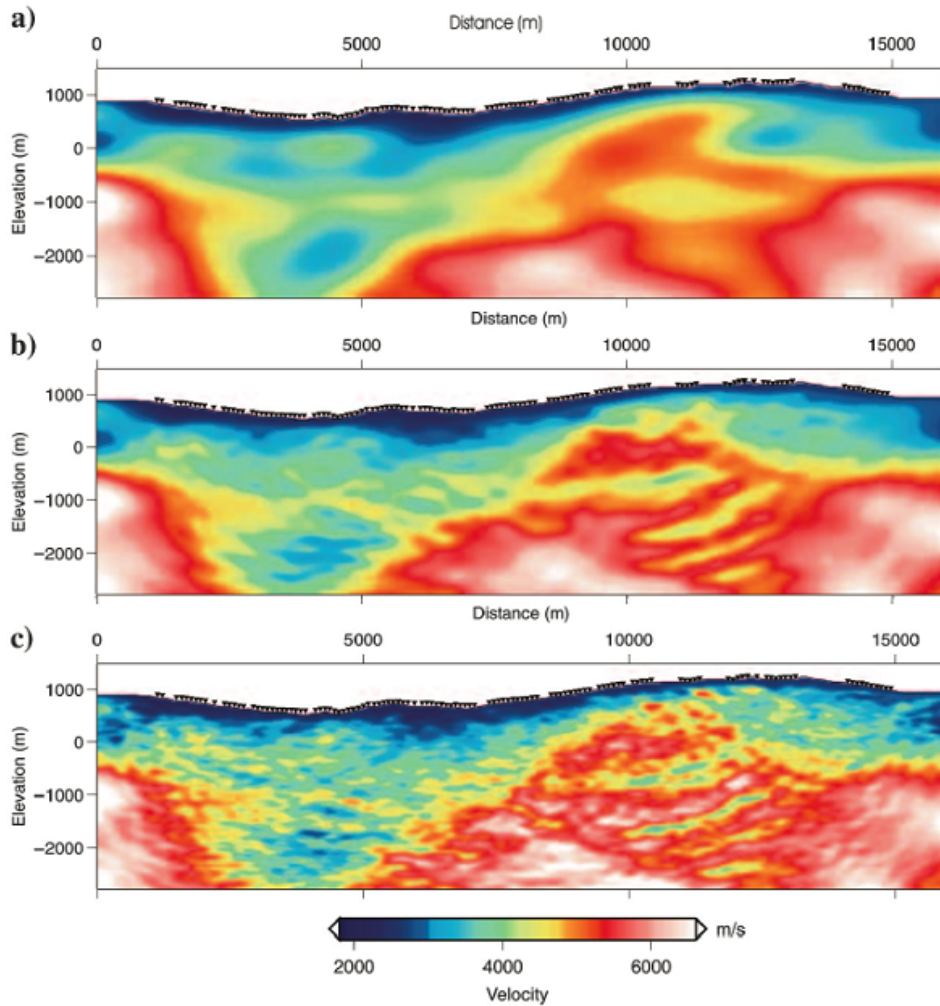
Figure A.8: (a) Velocity model from traveltime tomography. This model was used as a starting model for the full-waveform tomography. (b) Velocity model from full-waveform tomography after the inversion of the 5.4 and (c) 20.06 Hz components. Note the improvement in spatial resolution from panels (a-c). The triangles in panels (a-c) mark the receiver positions involved in the tomography (modified after Operto et al. (2004)).

Due to these difficulties, FWI has been applied in a restricted, sequential, and simplified manner over the past 30 years. Several approaches have been proposed to mitigate the nonlinearity of the inverse problem starting, for example, by inverting first the low-frequency information of the data before progressing to higher frequencies (Sirgue and Pratt (2004); Brossier et al. (2009)).

Initially, FWI was proposed for 2D acoustic data in the time domain (Tarantola (1984); Crase et al. (1990)) and later developed for reasons of computational efficiency in the frequency domain (Pratt (1999); Pratt and Shipp (1999)). Wide-angle refraction data have been used in several studies to build initial models using first-arrival traveltime tomography and then to invert the data using acoustic FWI (Dessa et al. (2004); Operto et al. (2004); Malinowski et al. (2011)). One approach of inverting wide-angle refraction data is early arrivals waveform inversion (EAWI), which provides higher resolution than traveltime tomography but is still restricted to the use of refracted and early arrival reflected and diffracted waves, and thus limited in investigation depth. Figure A.8 shows an example of EAWI illustrating the improved resolution compared with traveltime tomography.
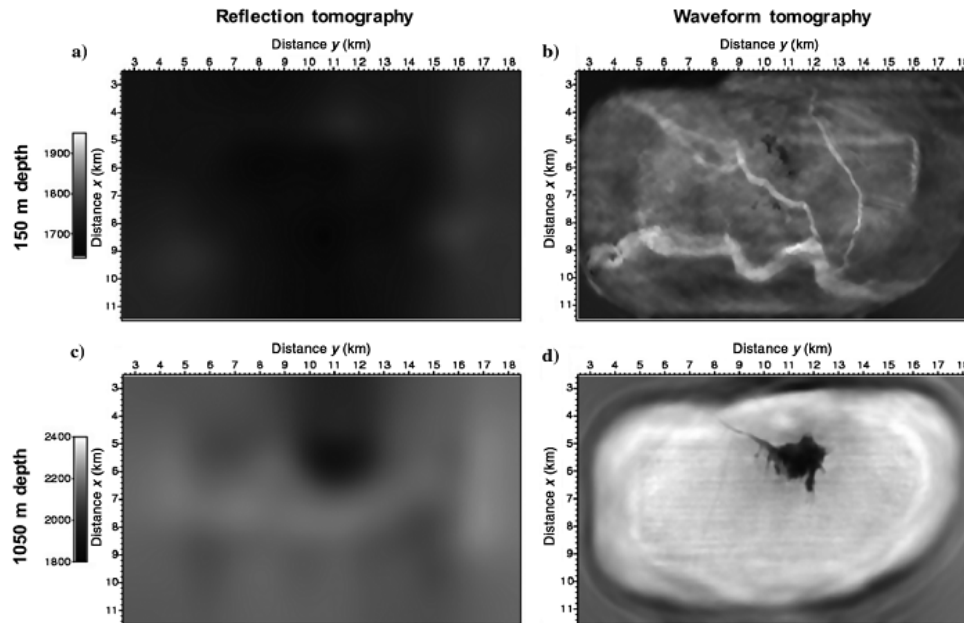
Figure A.9: Example of 3D waveform inversion applied to wide-azimuth ocean-bottom cable data from the Valhall field. Horizontal slices through a 3D velocity model at (a and b) 150 m depth, and (c and d) 1050 m depth for (a and c) the reflection tomography and (b and d) the waveform inversion results (after Sirgue et al. (2009)).

The problem of constructing an accurate initial model is less pronounced in the transmission configuration (crosshole and VSP experiments) because the inverse problem is more linear when using transmitted (forward scattered) waves compared with reflected (back-scattered) waves. Furthermore, traveltime tomography can be used in crosshole surveys to obtain a consistent and accurate initial model, and possibly borehole logs can be used to constrain the inversion. Several studies illustrate the value of FWI for crosshole acquisition geometries (Pratt and Goulty (1991); Manukyan et al. (2012)).

With the evolution and improvement of computing facilities in recent years, 3D inversion has become feasible under the acoustic approximation and has been successfully applied on marine data sets (Sirgue et al. (2009); Figure A.9). Today, 3D time-domain viscoelastic inversion has become feasible in exploration seismics (Vigh et al. (2014); Raknes et al. (2015)), and it is also being progressively applied at the regional and global scale using earthquake sources (Fichtner et al. (2008), Fichtner et al. (2010)). In general, the lithospheric and regional imaging using FWI is easier to solve than FWI of exploration-scale data because accurate background velocity, density, and attenuation models are usually known, and the problem is more linear because the velocity contrasts are smaller and mainly transmitted surface waves are inverted.

Current developments on the exploration-scale seek to combine FWI and wave-equation migration velocity analysis (Symes (2008)). Constant improvements are being made in modeling accuracy and efficiency, for models incorporating anisotropy, attenuation, and high impedance contrasts. Solutions have also been developed to better address the reconstruction of multipleparameters during the inversion (Malinowski et al. (2011); Manukyan et al. (2012); Alkhalifah and Plessix (2014); Vigh et al. (2014)).

To date, FWI has not been used for geothermal exploration. As the exploration depth and surface illumination configurations are similar to oil and gas exploration, application of FWI to geothermal targets can benefit from all the developments made for oil prospecting, but will still be subject to the same difficulties and limitations (cost of forward modeling, construction of an accurate initial model for velocity, density, and attenuation, data preprocessing or transformation when the modeling relies on strong assumptions such as acoustic propagation only). The benefit of using FWI for geothermal exploration is at least an improvement of the structural imaging, for example, when FWIderived velocity information is used for prestack migration. The application of FWI for quantitative imaging is more challenging, and will clearly depend on the ability to build reliable initial velocity and density models. Elastic FWI may provide high-resolution spatial distributions of elastic parameters, which can be linked to intrinsic physical properties, such as porosity and saturation. If the velocity model is well constrained, then it is also possible to expect quantitative estimation of attenuation variations, as shown, for instance, by Hicks and Pratt (2001) and Malinowski et al. (2011). Simultaneous P- and S-wave attenuation imaging potentially provides information on temperature variations and fluid saturation. Temperature increases are known from laboratory investigations and crustal/upper mantle seismic field studies to lower the seismic wave speed and increase the attenuation (Schön (1996)). However, it is often extremely difficult to nigh impossible to isolate small seismic anomalies due to moderate temperature changes from other factors, such as stress, compositional changes, and fluid effects.

Another potential use of FWI in the context of geothermal exploration and production is time-lapse (4D) monitoring of small changes in the subsurface. Once a baseline velocity model has been constructed, the differences between the full seismic data at two or more different times can be inverted to obtain a quantitative estimation of the changes in the model (Raknes and Arntsen (2015)).

A.4 Conclusions

Seismic reflection imaging has a greater depth of penetration combined with reasonable resolution compared with other geophysical methods used to study geothermal reservoirs. Yet, seismic imaging has only sparingly been used for geothermal exploration and it needs to be investigated how established and recently developed seismic data analysis techniques can be adapted and successfully applied to geothermal sites.

EGS will mostly be located in hard rock (basement) rather than the sedimentary rocks. Because the impedance contrasts and reflection coefficients between most crystalline lithologies are smaller than those of sedimentary lithologies, the S/N will be low, making it more difficult to image structures (e.g., fracture zones) in the basement. Moreover, the target reflectors are likely to be rough and of limited spatial extent, further reducing signal amplitudes and exacerbating their detection and delineation. Consequently, particular care must be taken in survey planning, acquisition, and processing to maximize the S/N.

The structures of importance in geothermal exploration in hard-rock environments are expected to be complex in shape and steeply dipping, which means that the reflections will tend to arrive at the surface in unexpected locations. In some cases, borehole measurements (e.g., multicomponent

VSPs) may be better suited to image steeply dipping features than surfacebased surveys. It will be necessary to model surveys beforehand in future seismic experiments to determine optimum locations for sources and receivers, to improve the processing, and to aid with the interpretation of the data. The targets (e.g., fracture zones) are small and will more likely appear as diffractions rather than as reflections on seismic profiles.

Most existing reflection seismic data over potential geothermal fields data were acquired for hydrocarbon exploration purposes, where the survey layout was designed to image the sedimentary column above the crystalline basement. The recording apertures (maximum source-receiver distances) and azimuths are mostly inadequate for imaging steep dips within the basement. Very few successful geothermal-specific seismic reflection surveys have been carried out in the past. Future surveys will require every degree of sophistication that can be brought to bear. The vast experience of oilfield seismic imaging has much to offer in illuminating the route toward improved seismic exploration of geothermal reservoirs — but the geothermal problem is special and comes with its own set of particular considerations. The major technical modifications need to be in the use of 3D arrays and multicomponent sensors, coupled with sophisticated processing, including attribute analysis, polarization filtering/migration, and the separation of diffracted and specular reflected wavefields. For example, attributes like azimuth and dip attributes, coherency, curvature, and spectral decomposition as well as other attributes could be further tested to evaluate the potential for fracture mapping not only in deep sediments but also in crystalline basement. FWI and S-wave splitting investigations can be profitably carried out provided that the data are of sufficient quality and potentially provide quantitative estimates of elastic parameters, from which it may be possible to infer critical reservoir properties, such as porosity and temperature.

A.5 The road ahead via complementary measurements

There are several remaining challenges and areas of active seismic reflection imaging research that may potentially become important to geothermal exploration in the future. A few of them are discussed here. A major challenge in land-seismic acquisition is the impact of the earth's near-surface zone (upper 10s–100s of m) on seismic data recorded on land due to its complexity and heterogeneity. This near-surface impact includes distortions of signals caused by irregular time delays, scattering, and absorption in the near-surface layer(s) and consequent loss of high-frequency information, the generation of coherent surface-related noise (e.g., ground roll, guided waves; Robertsson et al. (1996)), and signal amplitude and phase changes due to rapid lateral near-surface variations. Although many approaches have been developed to, for example, correct for static (time) delays and to remove source-generated noise (Yilmaz (2001)), being able to satisfactorily remove or correct for the distortions caused by the near-surface zone remains a major challenge.

A central goal in geophysical exploration is to build accurate subsurface models that include quantitative estimates of rock properties and fluid content at different scales. Combining complementary geophysical data sets by joint or cooperative inversion and/or interpretation, for example, acquired with different geophysical methods typically reduces ambiguities and facilitates the interpretation. Joint inversion has been used to improve the classification of lithologic zones and to establish petrophysical relationships on different scales (Colombo and De Stefano (2007); Colombo et al. (2014)).

Muñoz et al. (2010) use statistical joint interpretation of electrical resistivity and seismic velocity model to characterize different units at the Groß Schönebeck (Germany) geothermal site in terms of lithology and fracturing.

Microseismic data analysis and interpretation are receiving increasing attention for subsurface exploration and monitoring of hydrocarbon and geothermal reservoirs. If microseismic waveforms are recorded with dense enough receiver layouts, then these data may be analyzed with state-of-the-art seismic imaging and inversion techniques. Reflections identified within the coda of microseismic recordings may be used for imaging of subsurface structures (Schmelzbach et al. (2016)). Considering the usually broad frequency content and the short travel paths between microseismic events and borehole and/or surface-based receivers, the seismic- reflection processing of microseismic waveform recordings is a promising approach for high-resolution subsurface characterization. Reshetnikov et al. (2015) process microseismic waveforms recorded during and after the stimulation of the EGS in Basel, Switzerland, to map a distinct network of reflectors in the vicinity of the injection well.

Acknowledgments

References

Adam, E., T. Bohlen, and B. Milkereit. 2003. "Vertical seismic profiling at the Bell Allard orebody, Matagami, Quebec". In *Hardrock seismic exploration*, 181–193. Society of Exploration Geophysicists.

Ahmed, K., B. Schwarz, and D. Gajewski. 2015. "Application of the 3D common-reflection-surface stack workflow in a crystalline rock environment". *Geophysical Prospecting* 63 (4): 990–998.

Alkhalifah, T., and R.-É. Plessix. 2014. "A recipe for practical full-waveform inversion in anisotropic media: An analytical parameter resolution study". *Geophysics*.

Arnórsson, S. 1995. "Geothermal systems in Iceland: structure and conceptual models—I. High-temperature areas". *Geothermics* 24 (5-6): 561–602.

Bansal, R., and J. Gaiser. 2013. "An introduction to this special section: Applications and challenges in shear-wave exploration". *The Leading Edge* 32 (1): 12–12.

Barbier, E. 2002. "Geothermal energy technology and current status: an overview". *Renewable and Sustainable Energy Reviews* 6 (1): 3–65.

Bellefleur, G., C. Müller, D. Snyder, and L. Matthews. 2004. "Downhole seismic imaging of a massive sulfide orebody with mode-converted waves, Halfmile Lake, New Brunswick, Canada". *Geophysics* 69 (2): 318–329.

Bohlen, T., C. Müller, and B. Milkereit. 2003. "Elastic seismic-wave scattering from massive sulfide orebodies: On the role of composition and shape". In *Hardrock seismic exploration*, 70–89. Society of Exploration Geophysicists.

Brogi, A., A. Lazzarotto, D. Liotta, G. Ranalli, C. W. Group, et al. 2005. "Crustal structures in the geothermal areas of southern Tuscany (Italy): insights from the CROP 18 deep seismic reflection lines". *Journal of Volcanology and Geothermal Research* 148 (1): 60–80.

Brossier, R., S. Operto, and J. Virieux. 2009. "Seismic imaging of complex onshore structures by 2D elastic frequency-domain full-waveform inversion". *Geophysics* 74 (6): WCC105–WCC118.

Brown, A. 2004. *Interpretation of three-dimensional seismic data*. AAPG Memoir 42.

– . 1996. "Seismic attributes and their classification". *The leading edge* 15 (10): 1090–1090.

Buness, H. A., H. Hartmann, H.-M. Rumpel, C. M. Krawczyk, and R. Schulz. 2014. "Fault imaging in sparsely sampled 3D seismic data using common-reflection-surface processing and attribute analysis–a study in the Upper Rhine Graben". *Geophysical Prospecting* 62 (3): 443–452.

Carr, B., S. Smithson, N. Kareav, A. Ronin, V. Garipov, Y. Kristofferson, P. Digranes, D. Smythe, and C. Gillen. 1996. "Vertical seismic profile results from the Kola Superdeep Borehole, Russia". *Tectonophysics* 264 (1-4): 295–307.

Chang, W.-F., and G. A. McMechan. 1994. "3-D elastic prestack, reverse-time depth migration". *Geophysics* 59 (4): 597–609.

Chapman, C. t., and R. Pratt. 1992. "Traveltime tomography in anisotropic media—I. Theory". *Geophysical Journal International* 109 (1): 1–19.

Chopra, P., and D. Wyborn. 2003. "Australia's first hot dry rock geothermal energy extraction project is up and running in granite beneath the Cooper Basin, NE South Australia". In *Proceedings of the Ishihara Symposium: Granites and Associated Metallogenesis*, vol. 43.

Chopra, S., and K. Marfurt. 2005. "Seismic attributes—A historical perspective". *Geophysics* 70 (5): 3SO–28SO.

Chopra, S., and K. J. Marfurt. 2007. *Seismic attributes for prospect identification and reservoir characterization*. Society of Exploration Geophysicists / European Association of Geoscientists / Engineers.

Cliet, C., L. Brodov, A. Tikhonov, D. Marin, and D. Michon. 1991. "Anisotropy survey for reservoir definition". *Geophysical Journal International* 107 (3): 417–427.

Clowes, R., A. Green, C. Yorath, E. Kanasewich, G. West, and G. Garland. 1984. "LITHOPROBE—a national program for studying the third dimension of geology". *Journal of the Canadian Society of Exploration Geophysicists* 20:23–39.

Colombo, D., and M. De Stefano. 2007. "Geophysical modeling via simultaneous joint inversion of seismic, gravity, and electromagnetic data: Application to prestack depth imaging". *The Leading Edge* 26 (3): 326–331.

Colombo, D., G. McNeice, N. Raterman, M. Zinger, D. Rovetta, and E. Sandoval Curiel. 2014. "Exploration beyond seismic: The role of electromagnetics and gravity gradiometry in deep water subsalt plays of the Red Sea". *Interpretation* 2 (3): SH33–SH53.

Cook, F. A., A. J. Velden, K. W. Hall, and B. J. Roberts. 1999. "Frozen subduction in Canada's Northwest Territories: Lithoprobe deep lithospheric reflection profiling of the western Canadian Shield". *Tectonics* 18 (1): 1–24.

Cosma, C., P. Heikkinen, and J. Keskinen. 2003. "Multiazimuth VSP for rock characterization of deep nuclear waste disposal sites in Finland". In *Hardrock seismic exploration*, 207–226. Society of Exploration Geophysicists.

Crampin, S. 1985. "Evaluation of anisotropy by shear-wave splitting". *Geophysics* 50 (1): 142–152.

Crampin, S. 1981. "A review of wave motion in anisotropic and cracked elastic-media". *Wave motion* 3 (4): 343–391.

Crampin, S., and J. H. Lovell. 1991. "A decade of shear-wave splitting in the Earth's crust: what does it mean? what use can we make of it? and what should we do next?" *Geophysical Journal International* 107 (3): 387–407.

Crase, E., A. Pica, M. Noble, J. McDonald, and A. Tarantola. 1990. "Robust elastic nonlinear waveform inversion: Application to real data". *Geophysics* 55 (5): 527–538.

Dankbaar, J. 1985. "Separation of P-and S-waves". *Geophysical Prospecting* 33 (7): 970–986.

Dessa, J.-X., S. Operto, S. Kodaira, A. Nakanishi, G. Pascal, J. Virieux, and Y. Kaneda. 2004. "Multiscale seismic imaging of the eastern Nankai trough by full waveform inversion". *Geophysical Research Letters* 31 (18).

Drummond, B., A. Owen, J. Jackson, B. Goleby, and S. Sheard. 2003. "Seismic-Reflection imaging of the environment around the Mount Isa Orebodies, Northern Australia: A case study". In *Hardrock seismic exploration*, 127–138. Society of Exploration Geophysicists.

Duchane, D., and D. Brown. 2002. "Hot dry rock (HDR) geothermal energy research and development at Fenton Hill, New Mexico". *Geo-Heat Centre Quarterly Bulletin* 23 (4): 13–19.

Eaton, D. W., B. Milkereit, and M. H. Salisbury. 2003. *Hardrock seismic exploration*. Society of Exploration Geophysicists.

Emsley, S., P. Shiner, N. Enescu, A. Beccacini, and C. Cosma. 2007. "Using VSP surveys to bridge the scale gap between well and seismic data". *Geological Society, London, Special Publications* 270 (1): 83–91.

Feighner, M., T. Daley, and E. Majer. 1998. *Results of vertical seismic profiling at Well 46-28, Rye Patch Geothermal Field, Pershing County, Nevada*. Tech. rep. Lawrence Berkeley National Lab., Berkeley, CA (US).

Fichtner, A., B. Kennett, H. Igel, and H. Bunge. 2008. "Theoretical background for continental-and global-scale full-waveform inversion in the time–frequency domain". *Geophysical Journal International* 175 (2): 665–685.

Fichtner, A. 2011. "Introduction to Iterative Non-linear Minimisation". In *Full Seismic Waveform Modelling and Inversion*, 113–140. Springer.

Fichtner, A., B. L. Kennett, H. Igel, and H.-P. Bunge. 2010. "Full waveform tomography for radially anisotropic structure: new insights into present and past states of the Australasian upper mantle". *Earth and Planetary Science Letters* 290 (3): 270–280.

Genter, A., K. Evans, N. Cuenot, D. Fritsch, and B. Sanjuan. 2010. "Contribution of the exploration of deep crystalline fractured reservoir of Soultz to the knowledge of enhanced geothermal systems (EGS)". *Comptes Rendus Geoscience* 342 (7): 502–516.

Gérard, A., A. Genter, T. Kohl, P. Lutz, P. Rose, and F. Rummel. 2006. *The deep EGS (enhanced geothermal system) project at Soultz-sous-Forêts (Alsace, France)*.

Green, A., and J. Mair. 1983. "Subhorizontal fractures in a granitic pluton: Their detection and implications for radioactive waste disposal". *Geophysics* 48 (11): 1428–1449.

Greenhalgh, S., I. Mason, E. Lucas, D. Pant, and R. Eames. 1990. "Controlled direction reception filtering of P-and S-waves in τ-p space". *Geophysical Journal International* 100 (2): 221–234.

Greenhalgh, S., and E. Manukyan. 2013. "Seismic reflection for hardrock mineral exploration: Lessons from numerical modeling". *Journal of Environmental and Engineering Geophysics* 18 (4).

Greenhalgh, S., B. Zhou, and S. Cao. 2003. "A crosswell seismic experiment for nickel sulphide exploration". *Journal of Applied Geophysics* 53 (2): 77–89.

Hardage, B. A. 2000. *Vertical seismic profiling*. Handbook of Geophysical Exploration, Seismic Exploration, 14, Pergamon.

Hardage, B. A., M. V. DeAngelo, P. E. Murray, and D. Sava. 2011. *Multicomponent seismic technology*. Society of Exploration Geophysicists.

Hicks, G. J., and R. G. Pratt. 2001. "Reflection waveform inversion using local descent methods: Estimating attenuation and velocity over a gas-sand deposit". *Geophysics* 66 (2): 598–612.

Hitchings, V. H., and H. Potters. 2000. "Production and geologic implications of the Natih 9-C, 3-D seismic survey". *The Leading Edge* 19 (10): 1117–1124.

Hloušek, F., O. Hellwig, and S. Buske. 2015a. "Improved structural characterization of the Earth's crust at the German Continental Deep Drilling Site using advanced seismic imaging techniques". *Journal of Geophysical Research: Solid Earth* 120 (10): 6943–6959.

Hloušek, F., O. Hellwig, and S. Buske. 2015b. "Three-dimensional focused seismic imaging for geothermal exploration in crystalline rock near Schneeberg, Germany". *Geophysical Prospecting* 63 (4): 999–1014.

Husen, S., and E. Kissling. 2001. "Local earthquake tomography between rays and waves: fat ray tomography". *Physics of the earth and Planetary Interiors* 123 (2): 127–147.

Jäger, R., J. Mann, G. Höcht, and P. Hubral. 2001. "Common-reflection-surface stack: Image and attributes". *Geophysics* 66 (1): 97–109.

Jordi, C., C. Schmelzbach, and S. Greenhalgh. 2016. "Frequency-dependent traveltime tomography using fat rays: Application to near-surface seismic imaging". *Journal of Applied Geophysics* 131:202–213.

Juhlin, C., M. Friberg, H. Echtler, T. Hismatulin, A. Rybalka, A. Green, and J. Ansorge. 1998. "Crustal structure of the Middle Urals: Results from the (ESRU) Europrobe seismic reflection profiling in the Urals experiments". *Tectonics* 17 (5): 710–725.

Juhlin, C., and H. Palm. 2003. "Experiences from Shallow Reflection Seismics over Granitic Rocks in Sweden". In *Hardrock seismic exploration*, 93–109. Society of Exploration Geophysicists.

Khaidukov, V., E. Landa, and T. J. Moser. 2004. "Diffraction imaging by focusing-defocusing: An outlook on seismic superresolution". *Geophysics* 69 (6): 1478–1490.

Khair, H. A., D. Cooke, and M. Hand. 2015. "Seismic mapping and geomechanical analyses of faults within deep hot granites, a workflow for enhanced geothermal system projects". *Geothermics* 53:46–56.

Klokov, A., and S. Fomel. 2012. "Separation and imaging of seismic diffractions using migrated dip-angle gathers". *Geophysics* 77 (6): S131–S143.

Kuriyagawa, M., and N. Tenma. 1999. "Development of hot dry rock technology at the Hijiori test site". *Geothermics* 28 (4): 627–636.

Landa, E., and S. Keydar. 1998. "Seismic monitoring of diffraction images for detection of local heterogeneities". *Geophysics* 63 (3): 1093–1100.

Lanz, E., D. E. Boerner, H. Maurer, and A. Green. 1998. "Landfill delineation and characterization using electrical, electromagnetic and magnetic methods". *Journal of Environmental and Engineering Geophysics* 3 (4): 185–196.

Lewis, C., T. L. Davis, and C. Vuillermoz. 1991. "Three-dimensional multicomponent imaging of reservoir heterogeneity, Silo Field, Wyoming". *Geophysics* 56 (12): 2048–2056.

Li, X.-Y., and M. C. Mueller. 1997. "Case studies of multicomponent seismic data for fracture characterization: Austin Chalk examples". In *Carbonate seismology*, 337–372. Society of Exploration Geophysicists.

Lipman, S., C. Strobel, and M. Gulati. 1978. "Reservoir performance of The Geysers field". *Geothermics* 7 (2-4): 209–219.

Lumley, D. 2001. "Time-lapse seismic reservoir monitoring". *Geophysics* 66 (1): 50–53.

Lund, J. W., L. Bjelm, G. Bloomquist, and A. K. Mortensen. 2008. "Characteristics, development and utilization of geothermal resources-a Nordic perspective". *Episodes* 31 (1): 140–147.

Luo, M., and B. J. Evans. 2004. "An amplitude-based multiazimuthal approach to mapping fractures using P-wave 3D seismic data". *Geophysics* 69 (3): 690–698.

Lüschen, E., S. Görne, H. Hartmann, R. Thomas, and R. Schulz. 2015. "3D seismic survey for geothermal exploration in crystalline rocks in Saxony, Germany". *Geophysical Prospecting* 63 (4): 975–989.

Lüschen, E., M. Wolfgramm, T. Fritzer, M. Dussel, R. Thomas, and R. Schulz. 2014. "3D seismic survey explores geothermal targets for reservoir characterization at Unterhaching, Munich, Germany". *Geothermics* 50:167–179.

Majer, E., T. V. McEvilly, F. Eastwood, and L. Myer. 1988. "Fracture detection using P-wave and S-wave vertical seismic profiling at The Geysers". *Geophysics* 53 (1): 76–84.

Malehmir, A., C. Juhlin, C. Wijns, M. Urosevic, P. Valasti, and E. Koivisto. 2012. "3D reflection seismic imaging for open-pit mine planning and deep exploration in the Kevitsa Ni-Cu-PGE deposit, northern Finland". *Geophysics*.

Malehmir, A., C. Schmelzbach, E. Bongajum, G. Bellefleur, C. Juhlin, and A. Tryggvason. 2009. "3D constraints on a possible deep> 2.5 km massive sulphide mineralization from 2D crooked-line seismic reflection data in the Kristineberg mining area, northern Sweden". *Tectonophysics* 479 (3): 223–240.

Malinowski, M., S. Operto, and A. Ribodetti. 2011. "High-resolution seismic attenuation imaging from wide-aperture onshore data by visco-acoustic frequency-domain full-waveform inversion". *Geophysical Journal International* 186 (3): 1179–1204.

Manukyan, E., S. Latzel, H. Maurer, S. Marelli, and S. A. Greenhalgh. 2012. "Exploitation of data-information content in elastic-waveform inversions". *Geophysics* 77 (2): R105–R115.

Matsushima, J., and Y. Okubo. 2003. "Rheological implications of the strong seismic reflector in the Kakkonda geothermal field, Japan". *Tectonophysics* 371 (1): 141–152.

Milkereit, B., and D. Eaton. 1998. "Imaging and interpreting the shallow crystalline crust". *Tectonophysics* 286 (1): 5–18.

Milkereit, B., A. Green, J. Wu, D. White, and E. Adam. 1994. "Integrated seismic and borehole geophysical study of the Sudbury Igneous Complex". *Geophysical Research Letters* 21 (10): 931–934.

Moser, T., and C. Howard. 2008. "Diffraction imaging in depth". *Geophysical Prospecting* 56 (5): 627–641.

Munoz, G. 2014. "Exploring for geothermal resources with electromagnetic methods". *Surveys in geophysics* 35 (1): 101–122.

Muñoz, G., K. Bauer, I. Moeck, A. Schulze, and O. Ritter. 2010. "Exploring the Groß Schönebeck (Germany) geothermal site using a statistical joint interpretation of magnetotelluric and seismic tomography models". *Geothermics* 39 (1): 35–45.

Nakagome, O., T. Uchida, and T. Horikoshi. 1998. "Seismic reflection and VSP in the Kakkonda geothermal field, Japan: Fractured reservoir characterization". *Geothermics* 27 (5): 535–552.

Obermann, A., T. Kraft, E. Larose, and S. Wiemer. 2015. "Potential of ambient seismic noise techniques to monitor the St. Gallen geothermal site (Switzerland)". *Journal of Geophysical Research: Solid Earth* 120 (6): 4301–4316.

Operto, S., C. Ravaut, L. Improta, J. Virieux, A. Herrero, and P. Dell'Aversana. 2004. "Quantitative imaging of complex structures from dense wide-aperture seismic data by multiscale traveltime and waveform inversions: a case study". *Geophysical prospecting* 52 (6): 625–651.

Özbek, A. 2000. "Multichannel adaptive interference cancelling". In *SEG Technical Program Expanded Abstracts 2000*, 2088–2091. Society of Exploration Geophysicists.

Place, J., M. Diraison, C. Naville, Y. Géraud, M. Schaming, and C. Dezayes. 2010. "Decoupling of deformation in the Upper Rhine Graben sediments. Seismic reflection and diffraction on 3-component Vertical Seismic Profiling (Soultz-sous-Forêts area)". *Comptes Rendus Geoscience* 342 (7): 575–586.

Place, J., J. Sausse, J.-M. Marthelot, M. Diraison, Y. Géraud, and C. Naville. 2011. "3-D mapping of permeable structures affecting a deep granite basement using isotropic 3C VSP data". *Geophysical Journal International* 186 (1): 245–263.

Pratt, R. G. 1999. "Seismic waveform inversion in the frequency domain, Part 1: Theory and verification in a physical scale model". *Geophysics* 64 (3): 888–901.

Pratt, R. G., and N. R. Goulty. 1991. "Combining wave-equation imaging with traveltime tomography to form high-resolution images from crosshole data". *Geophysics* 56 (2): 208–224.

Pratt, R. G., and R. M. Shipp. 1999. "Seismic waveform inversion in the frequency domain, Part 2: Fault delineation in sediments using crosshole data". *Geophysics* 64 (3): 902–914.

Pratt, R., W. McGaughey, and C. Chapman. 1993. "Anisotropic velocity tomography: A case study in a near-surface rock mass". *Geophysics* 58 (12): 1748–1763.

Pussak, M., K. Bauer, M. Stiller, and W. Bujakowski. 2014. "Improved 3D seismic attribute mapping by CRS stacking instead of NMO stacking: Application to a geothermal reservoir in the Polish Basin". *Journal of Applied Geophysics* 103:186–198.

Rabbel, W., T. Beilecke, T. Bohlen, D. Fischer, A. Frank, J. Hasenclever, G. Borm, J. Kück, K. Bram, G. Druivenga, et al. 2004. "Superdeep vertical seismic profiling at the KTB deep drill hole (Germany): Seismic close-up view of a major thrust zone down to 8.5 km depth". *Journal of Geophysical Research: Solid Earth* 109 (B9).

Raknes, E. B., and B. Arntsen. 2015. "A numerical study of 3D elastic time-lapse full-waveform inversion using multicomponent seismic data". *Geophysics* 80 (6): R303–R315.

Raknes, E. B., B. Arntsen, and W. Weibull. 2015. "Three-dimensional elastic full waveform inversion using seismic data from the Sleipner area". *Geophysical Journal International* 202 (3): 1877–1894.

Rawlinson, N., and M. Sambridge. 2003. "Seismic traveltime tomography of the crust and lithosphere". *Advances in Geophysics* 46:81–199.

Reshetnikov, A., J. Kummerow, H. Asanuma, M. Häring, and S. A. Shapiro. 2015. "Microseismic reflection imaging and its application to the Basel geothermal reservoir". *Geophysics* 80 (6): WC39–WC49.

Rial, J. A., M. Elkibbi, and M. Yang. 2005. "Shear-wave splitting as a tool for the characterization of geothermal fractured reservoirs: Lessons learned". *Geothermics* 34 (3): 365–385.

Richards, H., R. Parker, A. Green, R. Jones, J. Nicholls, D. Nicol, M. Randall, S. Richards, R. Stewart, and J. Willis-Richards. 1994. "The performance and characteristics of the experimental hot dry rock geothermal reservoir at Rosemanowes, Cornwall (1985–1988)". *Geothermics* 23 (2): 73–109.

Riedel, M., C. Dutsch, C. Alexandrakis, I. Dini, S. Ciuffi, and S. Buske. 2015. "Seismic depth imaging of a geothermal system in Southern Tuscany". *Geophysical Prospecting* 63 (4): 957–974.

Robertsson, J., K. Holliger, and A. Green. 1996. "Source-generated noise in shallow seismic data". *European Journal of Environmental Geophysics* 1:107–124.

Robertsson, J. O., and J. O. Blanch. 2011. "Numerical methods, finite difference". In *Encyclopedia of solid earth geophysics*, 883–892. Springer.

Rutty, M., and S. Greenhalgh. 1993. "The correlation of seismic events on multicomponent data in the presence of coherent noise". *Geophysical Journal International* 113 (2): 343–358.

Salisbury, M. H., C. W. Harvey, and L. Matthews. 2007. "The acoustic properties of ores and host rocks in hardrock terranes". In *Hardrock seismic exploration*, 9–19. Society of Exploration Geophysicists.

Sausse, J., C. Dezayes, L. Dorbath, A. Genter, and J. Place. 2010. "3D model of fracture zones at Soultz-sous-Forêts based on geological data, image logs, induced microseismicity and vertical seismic profiles". *Comptes Rendus Geoscience* 342 (7): 531–545.

Schellschmidt, R., B. Sanner, S. Pester, and R. Schulz. 2010. "Geothermal energy use in Germany In: Proceedings of the World Geothermal Congress". *Bali, Indonesia*.

Schmelzbach, C., J. Kummerow, P. Wigger, A. Reshetnikov, P. Salazar, and S. Shapiro. 2016. "Microseismic reflection imaging of the Central Andean crust". *Geophysical Journal International* 204 (2): 1396–1404.

Schmelzbach, C., C. Juhlin, R. Carbonell, and J. F. Simancas. 2007. "Prestack and poststack migration of crooked-line seismic reflection data: A case study from the South Portuguese Zone fold belt, southwestern Iberia". *Geophysics* 72 (2): B9–B18.

Schmelzbach, C., J. F. Simancas, C. Juhlin, and R. Carbonell. 2008a. "Seismic reflection imaging over the South Portuguese Zone fold-and-thrust belt, SW Iberia". *Journal of Geophysical Research: Solid Earth* 113 (B8).

Schmelzbach, C., C. Zelt, C. Juhlin, and R. Carbonell. 2008b. "P-and SV-velocity structure of the South Portuguese Zone fold-and-thrust belt, SW Iberia, from traveltime tomography". *Geophysical Journal International* 175 (2): 689–712.

Schön, J. H. 1996. *Physical properties of rocks: Fundamentals and principles of petrophysics*. Vol. 65. Elsevier.

Schreiter, L., F. Hloušek, O. Hellwig, and S. Buske. 2015. "Characterization of seismic reflections from faults in a crystalline environment, Schneeberg, Germany". *Geophysical Prospecting* 63 (4): 1015–1032.

Sheriff, R. E., and L. P. Geldart. 1995. *Exploration seismology*. Cambridge university press.

Sirgue, L., O. Barkved, J. Van Gestel, O. Askim, and J. Kommedal. 2009. "3D waveform inversion on Valhall wide-azimuth OBC". In *71st EAGE Conference and Exhibition incorporating SPE EUROPEC 2009*.

Sirgue, L., and R. G. Pratt. 2004. "Efficient waveform inversion and imaging: A strategy for selecting temporal frequencies". *Geophysics* 69 (1): 231–248.

Spetzler, J., Z. Xue, H. Saito, and O. Nishizawa. 2008. "Case story: time-lapse seismic crosswell monitoring of CO2 injected in an onshore sandstone aquifer". *Geophysical Journal International* 172 (1): 214–225.

Stewart, R. R., J. E. Gaiser, R. J. Brown, and D. C. Lawton. 2003. "Converted-wave seismic exploration: Applications". *Geophysics* 68 (1): 40–57.

Stewart, R., J. E. Gaiser, R. J. Brown, and D. C. Lawton. 2002. "Converted-wave seismic exploration: Methods". *Geophysics* 67 (5): 1348–1363.

Symes, W. W. 2008. "Migration velocity analysis and waveform inversion". *Geophysical prospecting* 56 (6): 765–790.

Taner, M. T. 2001. "Seismic attributes". *CSEG recorder* 26 (7): 48–56.

Taner, M. T., F. Koehler, and R. Sheriff. 1979. "Complex seismic trace analysis". *Geophysics* 44 (6): 1041–1063.

Taner, M. T., J. S. Schuelke, R. O'Doherty, and E. Baysal. 1994. "Seismic attributes revisited". In *SEG Technical Program Expanded Abstracts 1994*, 1104–1106. Society of Exploration Geophysicists.

Tang, C., J. A. Rial, and J. M. Lees. 2008. "Seismic imaging of the geothermal field at Krafla, Iceland using shear-wave splitting". *Journal of Volcanology and Geothermal Research* 176 (2): 315–324.

Tarantola, A. 1984. "Inversion of seismic reflection data in the acoustic approximation". *Geophysics* 49 (8): 1259–1266.

Tatham, R. H., and M. D. McCormack. 1991. *Multicomponent seismology in petroleum exploration*. Society of Exploration Geophysicists.

Tester, J. W., B. J. Anderson, A. S. Batchelor, D. D. Blackwell, R. DiPippo, E. M. Drake, J. Garnish, B. Livesay, M. C. Moore, K. Nichols, et al. 2007. "Impact of enhanced geothermal systems on US energy supply in the twenty-first century". *Philosophical Transactions of the Royal Society of London A: Mathematical, Physical and Engineering Sciences* 365 (1853): 1057–1094.

Thomas, R., and R. Schulz. 2007. "Facies differentiation of the Malm by interpretation of reflection seismic profiles and a moving source VSP Experiment". In *Proceedings of the European Geothermal Congress*.

Thomas, R., E. Lueschen, and R. Schulz. 2010. "Seismic reflection exploration of Karst phenomena of a geothermal reservoir in Southern Germany". In *Proceedings of the World Geothermal Congress*.

Tsvankin, I. 2012. *Seismic signatures and analysis of reflection data in anisotropic media*. Society of Exploration Geophysicists.

Vasco, D. W., J. E. Peterson Jr, and E. L. Majer. 1995. "Beyond ray tomography: Wavepaths and Fresnel volumes". *Geophysics* 60 (6): 1790–1804.

Vécsey, G., K. Holliger, R. Pratt, B. Dyer, and A. Green. 1998. "Anisotropic seismic tomography of a potential hot dry rock reservoir before and during induced pressurization". *Geophysical research letters* 25 (11): 1991–1994.

Vidale, J. E. 1986. "Complex polarization analysis of particle motion". *Bulletin of the Seismological society of America* 76 (5): 1393–1405.

Vigh, D., K. Jiao, D. Watts, and D. Sun. 2014. "Elastic full-waveform inversion application using multicomponent measurements of seismic data collection". *Geophysics*.

Virieux, J., and S. Operto. 2009. "An overview of full-waveform inversion in exploration geophysics". *Geophysics* 74 (6): WCC1–WCC26.

Von Hartmann, H., H. Buness, C. M. Krawczyk, and R. Schulz. 2012. "3-D seismic analysis of a carbonate platform in the Molasse Basin-reef distribution and internal separation with seismic attributes". *Tectonophysics* 572:16–25.

Weber, J., B. Ganz, R. Schellschmidt, B. Sanner, and R. Schulz. 2015. "Geothermal energy use in Germany". In *Proceedings of the World Geothermal Congress*.

Wei, S., M. DeAngelo, and B. Hardage. 2014a. "Interpretation of multicomponent seismic data across Wister geothermal field, Imperial Valley, California". *Interpretation*.

Wei, S., M. V. DeAngelo, and B. A. Hardage. 2014b. "Advantages of joint interpretation of PP and P-SV seismic data in geothermal exploration". *Interpretation*.

Weijermars, R., G. Drijkoningen, T. Heimovaara, E. Rudolph, G. J. Weltje, and K. Wolf. 2011. "Unconventional gas research initiative for clean energy transition in Europe". *Journal of Natural Gas Science and Engineering* 3 (2): 402–412.

Woodward, M. J. 1992. "Wave-equation tomography". *Geophysics* 57 (1): 15–26.

Yilmaz, O. 2001. "Seismic data analysis: Processing, inversion, and interpretation of seismic data: SEG".

Zelt, C. A., and P. J. Barton. 1998. "Three-dimensional seismic refraction tomography: A comparison of two methods applied to data from the Faeroe Basin". *Journal of Geophysical Research: Solid Earth* 103 (B4): 7187–7210.

Zhe, J., and S. A. Greenhalgh. 1997. "Prestack multicomponent migration". *Geophysics* 62 (2): 598–613.

Zhou, B., S. Greenhalgh, and A. Green. 2008. "Nonlinear traveltime inversion scheme for crosshole seismic tomography in tilted transversely isotropic media". *Geophysics*.

B

Vertical seismic profiling (VSP) survey optimization for imaging fracture zones over geothermal areas

Contents

Summary

A primary focus of geothermal seismic imaging is to map dipping faults and fracture zones that control the permeability and fluid flow. We simulated and processed acoustic synthetic data to optimize VSP survey layouts for mapping moderately to steeply dipping fracture zones over geothermal reservoirs. The geophysical models were based on the geothermal site at Soultz-sous-Forêts (France). It was found that fracture zones located at a borehole offset distance of about 300 m can be imaged accurately for a range of the different dips. Only 8 to 12 source positions were required for obtaining very good results. Adding further sources did not necessarily improve the results, but rather resulted in image distortions. Generally, large offsets between sources and the borehole are required for imaging steeply dipping interfaces. When such features cross-cut the borehole, they are particularly difficult to image.

B.1   Introduction

Geothermal energy is a promising sustainable energy resource, but has not yet reached its full potential. Compared to oil and gas exploration, controlled-source seismic surveying for geothermal purposes has only been applied sporadically. Hence, it is of great significance to further explore the potential of seismic imaging and to test how seismic techniques need to be adapted to image relevant structures over geothermal areas. Enhanced geothermal systems have their maximum potential in crystalline rock at depths of a few km where temperatures are sufficiently high. A fracture network is created to circulate hot fluid that can be extracted for electricity production. The primary focus in hardrock geothermal exploration is to map fracture zones, which control permeability and fluid flow. These are often steeply dipping structures that are particularly challenging to image with surface seismic exploration techniques. Vertical seismic profiling (VSP) may offer the means for imaging steeply dipping structures such as fracture zones. It can provide important information on structures around the well and can help decide where to place additional wells in order to achieve a functioning circulation between wells. We performed a synthetic modelling and processing study with the aim to optimize the survey design of VSP experiments as well as to optimize the processing in terms of selecting a favourable data subset for the migration (imaging) of reflection data from fracture zones of a certain dip.

Our modelling study is based on the geological situation at the geothermal site at Soultz-sous-Forêts (France) (Gérard et al. (2006)). Here, the velocities increase continuously with depth, exhibiting a high gradient in the sediments down to a depth of 1.4 km and a much lower gradient in the underlying basement (Figure B.1a). To simulate a realistic degree of heterogeneity, stochastic velocity fluctuations are superimposed. Most of the boreholes at the site are inclined since this increases the chance of intersecting dipping permeable zones in a certain depth range. For our modelling study a borehole inclined at 30°to the vertical with 61 receivers placed at 20 m intervals over the depth range 3700-4900 m was used. Recordings were simulated for 91 surface source positions at 100 m spacing over the 9000 m wide model. Different dips and positions of fracture zones were considered (configurations 1 to 4 in Figure B.1).
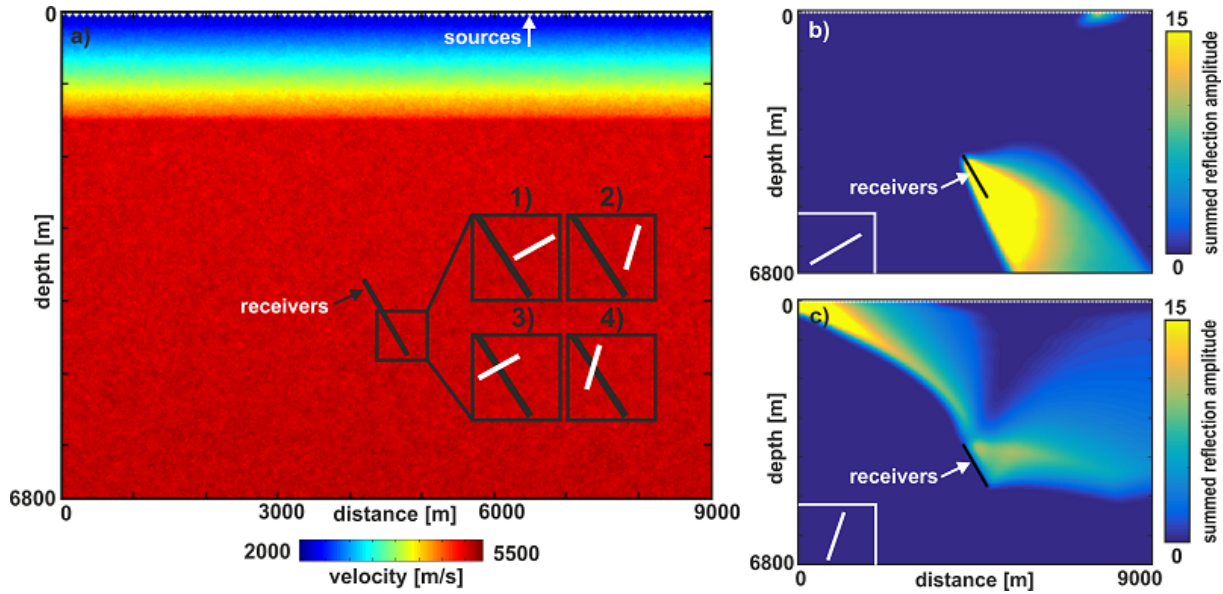
Figure B.1: a) Velocity model with receivers (black) and 91 source positions at the surface (white). Insets indicate the different fracture zone configurations (white) used in this study. b) Illumination map for fracture zones dipping at 30°(configurations 1 and 3 in Figure B.1a). c) Illumination map for fracture zones dipping at 70°(configurations 2 and 4 in Figure B.1a).

## B.2 Reflection point modelling

As a preliminary investigation of reflector coverage (illumination) we computed the reflected wave amplitudes from a given interface of specified dip for each point in the model and each possible source-receiver pair (Schmelzbach et al. (2007)). This feasibility study was performed using a constant velocity medium. We assumed that the reflection amplitudes depend on spherical spreading only and are proportional to the inverse of the total travel time. The reflection amplitudes were then summed in 20 m x 20 m wide bins. This procedure results in amplitude-dependent illumination maps of the subsurface. Large amplitude values show subsurface areas that can be covered well with the given recording configuration. Hence, a higher quality image of a fracture zone with the specific dip can be expected in this region because the signal-to-noise ratio will be proportional to the signal level. Zero values represent areas of no specular reflections and therefore define blind zones.

Examples of illumination maps for fracture zone dip of 30°and 70°(dipping towards the left) are shown in Figure B.1b and c, respectively. It can be seen that the given receiver configuration is well suited for imaging 30°dipping fracture zones around the borehole as well as slightly below and to the right of the borehole. For a steeply dipping interface, such as 70°, there are considerably less specular reflection points around the borehole and no reflection points below or to the left of it. This is an indication that it is more challenging to image steeply dipping fracture zones compared to gently dipping interfaces. Additionally, it can be observed that fracture zones dipping to the left cannot be imaged to the left of the borehole with the exception of gently dipping interfaces; they can be mapped only if they are located in the near-vicinity of the borehole or if weak diffractions are exploited.

B.3 Optimized VSP survey design

For a detailed analysis under more realistic conditions acoustic synthetic seismic wavefield modelling was performed using the velocity model in Figure B.1a and employing a 2D finite difference scheme (SOFI2D) Bohlen et al. (2003). The fracture zones, schematically shown in Figure B.1a, were assumed to have a thickness of 40 m and 15% reduced seismic velocity and density compared to the background. Common-source gathers for all fracture configurations were simulated for all 91 source positions. Additionally, random noise was added to the resulting waveform data to simulate a realistic signal-to-noise ratio of about 4. Subsequently, we applied a seismic processing sequence for imaging the fracture zones consisting of geometrical spreading correction, tau-p filtering to separate the direct and reflected waves, Kirchhoff depth migration of each recording and stacking single-source images. As an example, the resulting image for fracture zone configuration 2 is shown in Figure B.2c. Clearly, the fracture zone can be imaged reliably using all 91 source positions (comprehensive data set), but it would be interesting to see if comparable results could be obtained with a small subset of source gathers. For that purpose, we established a suitable survey design procedure that is illustrated using fracture zone configuration 2 (Figure B.2). First, we constructed a target image based on the results from the comprehensive data set (Figure B.2c). Since this image still contains minor artefacts that could not be removed by the processing, we applied a tapered window, such that only the desired features remained in the target image (see dashed black line Figure B.2c enclosing the target). The goodness of a test image (subsurface image obtained with subsets from the comprehensive data set) was quantified by the coefficient obtained from a 2D crosscorrelation of the test image with the target image. Initially, 91 test images corresponding to 91 migrated single-source images were produced. These test images were then crosscorrelated with the target image, and the single-source image with the largest crosscorrelation coefficient was selected. Then, the most suitable add-on single-source image was determined by computing all possible stacks of two single-source images (90 possible combinations with the initially selected single-source image) and evaluating the crosscorrelation coefficients with the target image. Further single-source images were subsequently added in an equivalent manner. This allowed benefit-cost curves (benefit = crosscorrelation coefficient, cost = number of single-sources images) to be constructed. As shown in Figure B.2a, the benefit-cost curve strongly increases initially, when adding only a small number of sources, but flattens after combining a certain number of single-source images. When the increase of the crosscorrelation coefficient becomes smaller than 1%, the resulting stacked images no longer improve significantly, and hence this point was chosen as the optimal number of single-sources images. For fracture zone configuration 2, this yielded an optimal subset size of 12 single-source images. The corresponding source positions are shown in Figure B.2b. The performance of our optimization method can be demonstrated by comparing optimized source distributions with regularly spaced distributions. As shown in Figure B.2a, the corresponding benefit-cost curve exhibits considerably lower cross-correlation coefficients, and the image obtained with 12 regularly spaced sources (Figure B.2d) is inferior to that with the optimized image (Figure B.2e). It is important to note that the optimal number of sources, identified with our method, is an approximate value rather than an exact measure. Likewise, the exact locations of the source positions change with different stochastic fluctuations of the velocities and different realizations of the simulated data noise. However, the spread of the optimized source configurations (horizontal green line in Figure B.2b) is fairly consistent.
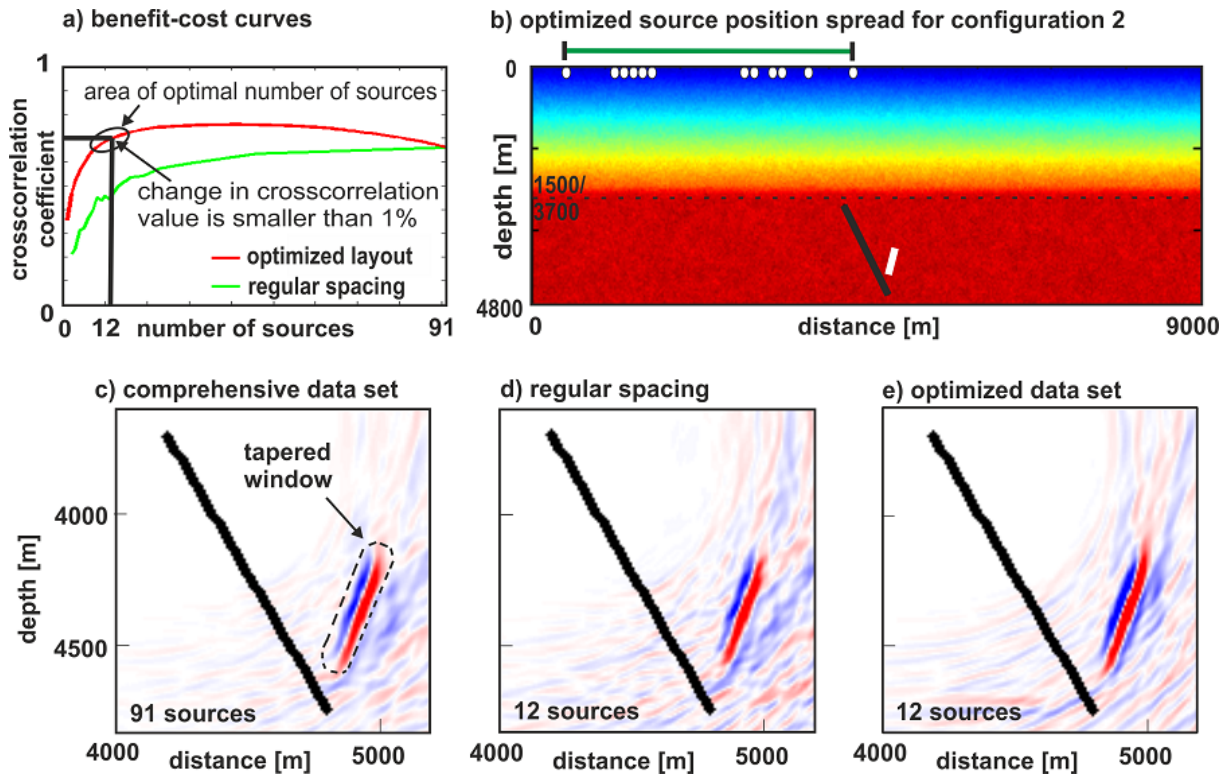
Figure B.2: Illustration of the optimized survey design procedure using fracture zone configuration 2 (see Figure B.1a). a) Benefit-cost curves for optimized design (red) and regularly spaced sources (green). b) Spread of the optimized source positions (note that only selected depth segments of the full model (see Figure B.1a) are shown, i.e. the depth range between 1500 and 3700 m was removed). c) Image obtained with the comprehensive data set including all 91 sources. d) Image obtained with 12 regularly spaced sources. e) Image obtained with 12 optimized sources (see panel b).

Hence, we will focus on the spread instead of the individual source positions. It is also noteworthy that the optimized benefit-cost curve in Figure B.2a decreases slightly after the maximum is reached. This indicates that some single-source images in the comprehensive data set contain no reflections, but only migration artefacts. This decreases not only the quality of the images, but also affects the resulting crosscorrelation with the target image. In other words, more data does not necessarily improve the image quality!

B.4 Results

We have applied the survey design methodology to all four fracture zone configurations shown in Figure B.1. The results are summarized in Figure B.3. Not surprisingly, best results were obtained for shallow dips (configurations 1 and 3). Only 7 to 8 sources are required for imaging these fracture zones reliably. The spread of the sources depends strongly on the position of the fracture zones (Figure B.3b). As already shown in Figure B.2, more sources are required for obtaining an optimal image for the steeply dipping fracture zone configuration 2. Steeply dipping fracture zones crosscutting the receiver array (configuration 4) represent the biggest challenge for VSP imaging. Most shot records include more diffractions than reflections. Therefore, the corresponding benefit-cost curve
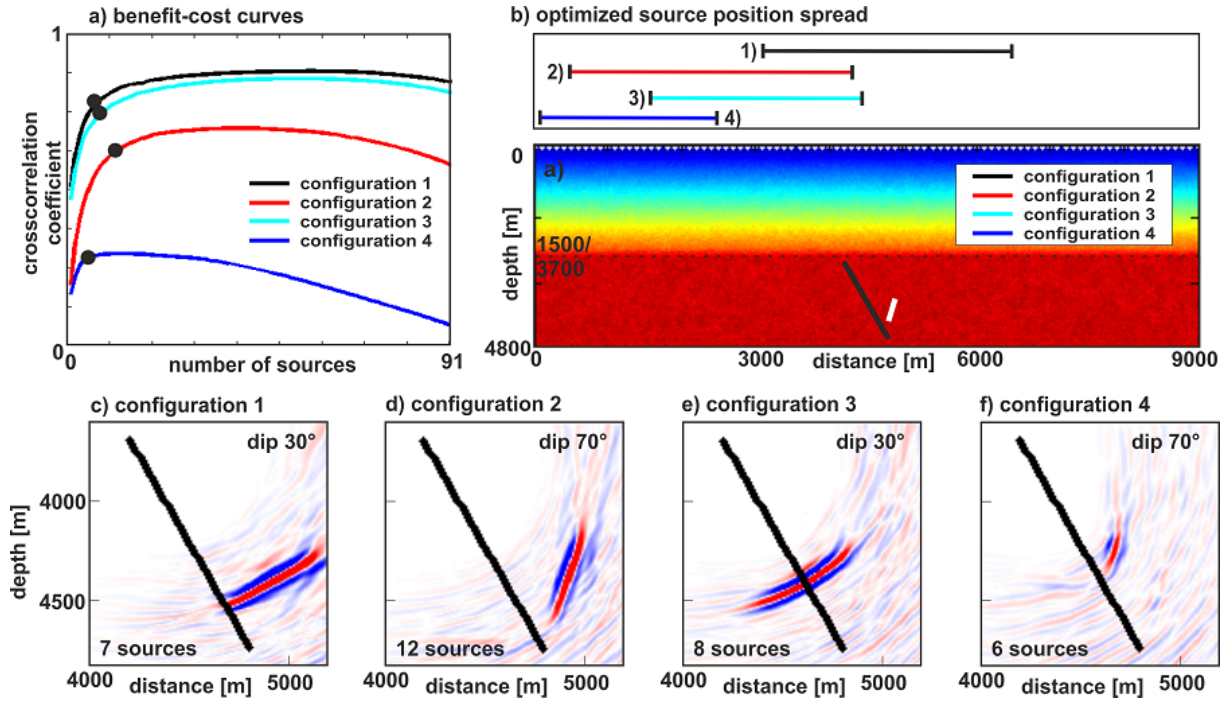
Figure B.3: a) Benefit-cost curves for fracture zone configurations 1 to 4. b) Spread of the optimized source positions for fracture zone configurations 1 to 4 (note that only selected depth segments of the full model (see Figure B.1a) are shown, i.e. the depth range between 1500 and 3700 m was removed). c) to f): Optimized images for fracture zone configurations 1 to 4.

in Figure B.3a starts decreasing already after a few shots, thereby indicating that there is little hope to image such structures reliably.

B.5   Conclusions

We have developed a novel strategy for optimizing VSP survey layouts suitable for mapping fracture zones over hardrock basement geothermal environments. The ideal survey layout strongly depends on the dip and location of the fracture zone. Therefore, à priori information on the expected subsurface structures is essential for survey design. For all scenarios considered in this study good results could be obtained with a relatively small number of source positions. Adding more data did not improve the quality of the images, but rather deteriorated the image quality. Therefore, our methodology will be not only useful for designing future field surveys, but also for selecting useful subsets of acquired data for optimum target-oriented processing. In this study we have demonstrated the benefits of optimized survey design with 2D acoustic data. Extending the methodology to the more realistic elastic 3D case is conceptually straightforward (although computationally very demanding). However, we expect the benefits of an optimized 3D design to be particularly high, because it will be likely not possible to acquire a comprehensive 3D field data set.

References

Bohlen, T., C. Müller, and B. Milkereit. 2003. "Elastic seismic-wave scattering from massive sulfide orebodies: On the role of composition and shape". In *Hardrock seismic exploration*, 70–89. Society of Exploration Geophysicists.

Gérard, A., A. Genter, T. Kohl, P. Lutz, P. Rose, and F. Rummel. 2006. *The deep EGS (enhanced geothermal system) project at Soultz-sous-Forêts (Alsace, France)*.

Schmelzbach, C., H. Horstmeyer, and C. Juhlin. 2007. "Shallow 3D seismic-reflection imaging of fracture zones in crystalline rock". *Geophysics* 72 (6): B149–B160.

C

Testing Vertical Seismic Profiling (VSP) as a subsurface mapping method at the Krafla volcanic geothermal field in Iceland

Contents

Summary

Vertical seismic profiling (VSP) was tested for mapping volcanic stratigraphy, fractures, dykes, fluid and steam in the geothermal area of Krafla in Iceland. Seismic imaging in magmatic environments is very challenging, largely due to the intense scattering of seismic waves traveling through the highly heterogeneous volcanic rocks. VSP offers means to image structures beneath and away from the well in complex volcanic environments. The VSP survey at Krafla was carried out in two wells, for each of which a zero offset, a far offset and a walk-away experiment were recorded. The zero offset data is of good quality, with the observed reflections corresponding to stratigraphic boundaries that can be explained by a simple 1D velocity model. The corridor stacks of the synthetic and field data look similar to each other, apart from a constant time shift and amplitude differences. High scattering in the subsurface leads to low amplitude reflections from deeper horizons. The walk-away data shows little coherent reflectivity. Furthermore, a complex 2D velocity model involving heterogeneities in the horizontal as well as vertical directions will be required to explain the observed seismograms.

C.1   Introduction

Geothermal resources play a major role in the energy supplies of Iceland, for example for electricity production and district heating systems, because Iceland is fortuitously located directly on the Mid Atlantic Ridge resulting in very active volcanism. Geophysical exploration of geothermal fields is important to assess and optimize the exploitation of natural heat sources. Reflection seismic surveying is a well-known method to image the subsurface but it has only been sparingly used in the context of geothermal exploration (Schmelzbach et al. (2016)). Additionally, seismic imaging in magmatic environments is very challenging, largely due to the intense scattering of seismic waves traveling through the highly heterogeneous volcanic rocks and the often complicated data acquisition in rough volcanic terrain. So far, only a few surface-based seismic reflection surveys have been acquired in Iceland, with essentially all resulting in very little coherent and interpretable reflections being recorded (Juhojuntti (2001)).

Vertical seismic profiling (VSP) offers an alternative means to image structures beneath and away from the well in complex volcanic environments. The advantage of VSP over surface-based reflection seismic surveying is that seismic waves travel shorter paths and pass only once through the highly heterogeneous and absorbing shallow subsurface zone, hence suffering less from attenuation (e.g. Cosma et al. (2003)). Moreover, with the geophones downhole, the reflected and transmitted waves can be sensed much closer to the target horizons, thus improving detection and recognition. VSP has already been applied successfully to map relevant features like faults and fracture zones in the geothermal context such as in Kakkonda geothermal field in Japan (Nakagome et al. (1998)).

In this study, the applicability and limitations of VSP for mapping the subsurface in the volcanic environment of the Krafla geothermal system in Iceland is tested on data from the first VSP acquired in Iceland. A primary motivation of this investigation was to study if VSP is a suitable method to map volcanic stratigraphy and key geological boundaries, such as fractures, dykes, and zones of supercritical fluid and steam. Due to the recent disastrous and costly drilling into magma at the

IDDP well (Elders et al. (2014)) it also needs to be investigated whether VSP can be used to map magmatic bodies ahead of the borehole.

C.2 VSP data acquisition

The VSP survey was conducted at the high temperature geothermal field at Krafla volcano, Iceland in the summer 2014. Krafla is situated near the northern end of the central rift system (Figure C.1) and comprises an 8 km x 10 km wide caldera of a central volcano. More than 30 boreholes have been drilled in the area around a geothermal power plant that has produced at a capacity of 60 MW since 1999. The VSP experiment was conducted around two wells (K-18, K-26). For each well, a zero-offset experiment was carried out (INGI, JON in Figure C.1), a number of far-offset source points were recorded for orientation purposes (Thorstein on Figure C.1), and E-W/N-S walk-away surveys were also performed (Thor 1-11 on Figure C.1; Table C.1). The zero-offset and far-offset source positions entailed the deployment of an air gun source in shallow excavated water pits. For the walk-away source positions, dynamite charges were fired in shallow shot holes.
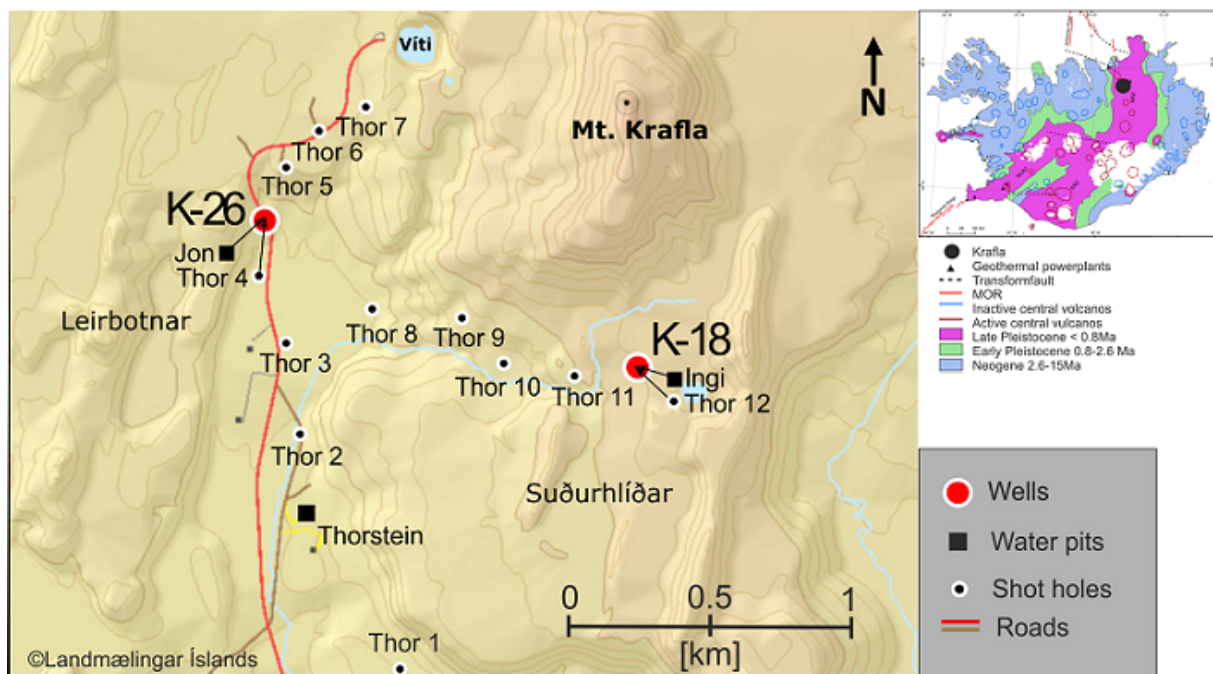
Figure C.1: Survey layout of the K-18 and K-26 VSP surveys at Krafla. The zero-offset experiments are associated with Ingi and Jon, the far-offset source positions with Thorstein and the walk-away source locations with Thor 1-11. In the upper right diagram is a simplified geological map of Iceland showing the location of Krafla (modified after Hersir et al., 2016).

		K-18	K-26
Zero-offset	receiver station interval	2.5m	2.5m
	receiver depths	10-2180m	10-1448m
Far-offset	receiver station interval	10m	10m
	receiver depths	18-2172m	95-1342m
Walk-away	receiver station interval	5m	5m
	measured receiver depth	1325-1800 (E-W-line)	915-1150m (E-W-line)
			1100-1150m (N-S-line)

Table C.1: Acquisition parameters for K-18 and K-26 VSP's.

C.3   VSP data processing

A standard seismic processing flow was sufficient for analysis of the vertical and horizontal receiver component data from the zero-offset source experiments. It consisted of trace editing, first break picking, geometrical spreading correction, VSP deconvolution, up-/down-going wavefield separation in the F-K domain, bandpass filtering and F-X deconvolution. An example of the vertical component zero-offset gather (Ingi) and horizontal component walkaway gather (Thor 10) before and after the processing are shown in Figure C.2a, f, and b, g, respectively. The first break picks for the down-going P waves were used to build a simplified 1D compressional wave velocity model (Figure C.2e for layers that were defined based on drillhole cuttings (Hersir et al. (2016)). For appraising the suitability of the 1D velocity model shown in Figure C.2e, synthetic waveform data were calculated for this simplified model using a 2D finite difference scheme (SOFI2D; Bohlen et al. (2003)), and then processed in the same manner as the field data. The full (downgoing plus upgoing waves) plus the extracted up-going synthetic wavefields for both source positions are shown in Figure C.2c, d and h, i, respectively. They can be compared with the corresponding field records.

C.4   Results

On the full wavefield records, the direct P-wave can be clearly identified as well as several multiples that result in a reverbatory appearance of the data. On the zero offset synthetic data, clear reflections from the different layers can be observed in the upgoing wavefield (black arrows in Figure C.2d). The arrows at these specific depths are also shown in the field data. It can be seen that most of the arrows coincide with reflections observed in the field data. Hence, our layered 1D model explains the zero offset data fairly well. However, the upper part of the synthetic model seems too simplistic because more reflections are observed here in the field data. There is a clear difference between the amplitudes for larger receiver depths. The reflection from the basement is not as prominent on the field data as it is on the synthetic data, which is explained by the scattering nature of the volcanic layers (and hence loss of energy) which is not properly accounted for in the numerical modeling.

The walk away data are generally of lower quality than the zero offset data (Figure C.2f to i). The reflections are less prominent and hence cannot be identified with the same level of confidence, especially the lowermost reflection from the basement. The upper reflection is of higher amplitude and more coherent than the lower reflection. The synthetic calculations show a PS mode conversion in addition to the pure mode PP reflection. On the field data it is not clear whether a PP or a PS reflection is present. Further analysis, such as polarization filtering for separation of P- and S-
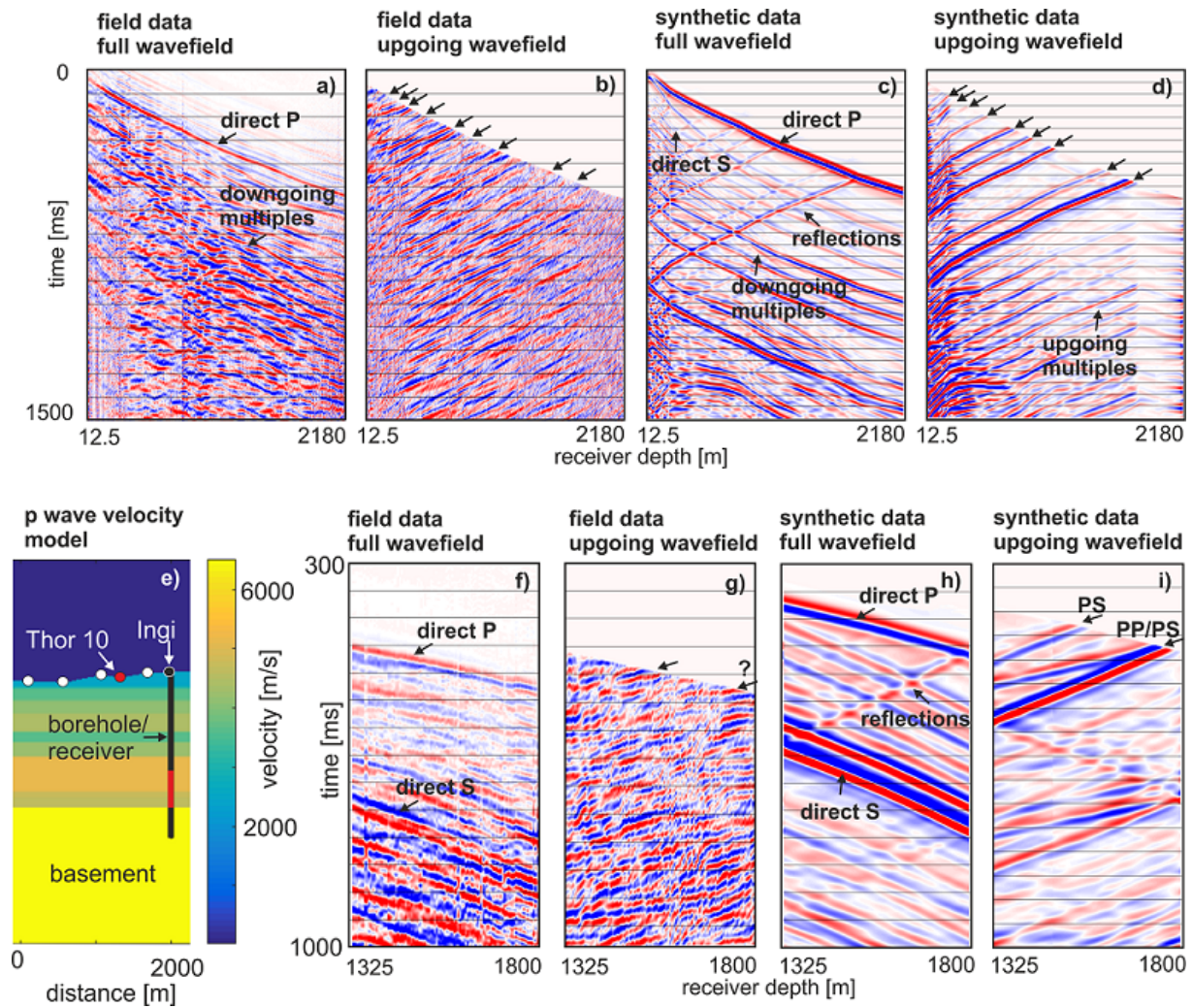
Figure C.2: Field and synthetic data for zero offset source position Ingi (a-d) and walk away source position Thor 10 (f-i). d) Simplified 1D P-wave velocity model that was used for the calculation of the synthetic data. Note that most of the reflections observed on the synthetic data can also be identified on the field data. All gathers are trace normalized, except g) where AGC was applied for display purposes.

waves, will be necessary to further examine the S-wave energy. The different arrival times of the direct P-wave for the field data and the synthetic data from source position Thor 10 indicate that the subsurface is strongly heterogeneous and geological features only have a small lateral extent. An additional explanation could be the presence of a low velocity near- surface layer that has not been taken into account for the synthetic modelling.

The zero-offset synthetic and field data were further processed to corridor stack stage (Figure C.3). Apart from a fixed time shift of about 40ms and amplitude differences, the reflections appearing in both corridor stacks occur at similar times. Discrepancies arise mainly at larger depths, where there is little reflectivity due to extensive scattering (hence reduced amplitude of the incident wave) over long travel paths. The time shift is an indication that the velocity model still needs to be improved. However, the reflections from the different layers can be identified clearly.
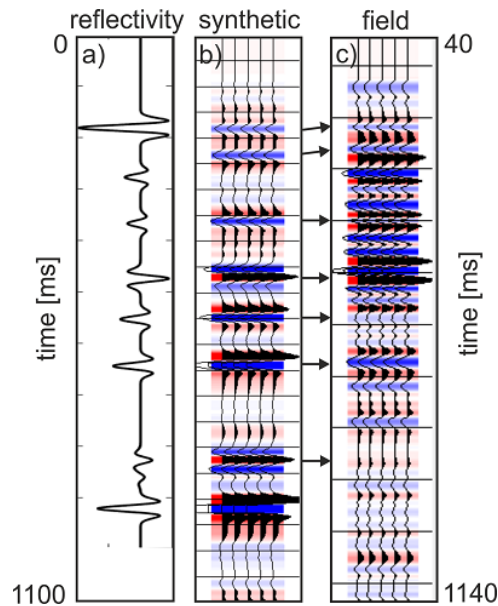
Figure C.3: a) Reflectivity of the synthetic model in Figure C.2e. Corridor stack of the synthetic
data b) and field data c). Apart from a constant time shift and amplitude differences,
the reflections seen in the two corridor stacks occur at similar times (black arrows).

C.5 Conclusions and Outook

In this study, VSP data from the Krafla volcanic area in Iceland have been processed to assess the
applicability of VSP for mapping the subsurface in such hydrothermal environments. The zero offset
experiment seems to be a suitable method to map key geologic boundaries. Many reflections are
observed and can be explained with a simple 1D velocity model. A high degree of seismic scattering
in the subsurface is evident from the greatly reduced amplitudes of the deeper reflections. For the
walkaway experiment, the 1D velocity model assumption is inadequate because it does not explain
the data sufficiently well. The velocity model needs to be improved to take lateral heterogeneities
into account as well and a possible low velocity near-surface layer. Since there is a substantial
amount of S wave energy present in the field data, the potential of S-wave imaging needs to be
further investigated.

Acknowledgment

References

Bohlen, T., C. Müller, and B. Milkereit. 2003. "Elastic seismic-wave scattering from massive sulfide
orebodies: On the role of composition and shape". In *Hardrock seismic exploration*, 70–89. Society
of Exploration Geophysicists.

Cosma, C., P. Heikkinen, and J. Keskinen. 2003. "Multiazimuth VSP for rock characterization of deep nuclear waste disposal sites in Finland". In *Hardrock seismic exploration*, 207–226. Society of Exploration Geophysicists.

Elders, W., G. Fridleifsson, and A. Albertsson. 2014. "Drilling into magma and the implications of the Iceland Deep Drilling Project (IDDP) for high-temperature geothermal systems worldwide". *Geothermics* 49:111–118.

Hersir, G., Ö. Erlendsson, H. Ingólfsson, H. Stefánsson, and H. Tryggvason. 2016. *Sonic Logging - A Field Report for Well K-18 in Krafla, NE-Iceland, and Well YT-2 and LA-8 in Eyjafjörður, N-Iceland.* ISOR-2016/028.

Juhojuntti, N. 2001. "Seismic imaging of deep crustal reflectivity in Sweden and Iceland". PhD thesis, Acta Universitatis Upsaliensis.

Nakagome, O., T. Uchida, and T. Horikoshi. 1998. "Seismic reflection and VSP in the Kakkonda geothermal field, Japan: Fractured reservoir characterization". *Geothermics* 27 (5): 535–552.

Schmelzbach, C., S. Greenhalgh, F. Reiser, J.-F. Girard, F. Bretaudeau, L. Capar, and A. Bitri. 2016. "Advanced seismic processing/imaging techniques and their potential for geothermal exploration". *Interpretation* 4 (4): SR1–SR18.

Acknowledgments

I would like to express my gratitude to all the people who were involved in my PhD thesis and contributed to the completion of the thesis. First, I would like to thank my supervisor Hansruedi for his continuous support and guidance throughout my PhD. I highly appreciated the very challenging outdoor activities we made together, such as all the climbing, ski and mountain bike tours. I am very grateful for the supervision of Cedric who provided friendly, patient and helpful support throughout. Thank you for your valuable suggestions and you were always there when times became difficult. I probably would have given up if it wasn't for your optimism, encouraging words and constant support. Furthermore, I would like to thank Stewart, who is probably the smartest person in the whole geophysical universe. You were always available for questions and discussions even after you left ETH. I appreciated your technical inputs, insightful comments and I learned a lot about scientific writing from you. I would like to thank Lars, Johan and Stöff for examining my PhD thesis and chairing the PhD defense.

I thank the IMAGE consortium and the Swiss National Science Foundation for financing my PhD thesis. I am grateful for the productive collaboration within the IMAGE project. Thank you Gylfi, Ólafur, Sæunn, Sverre, Felix, Rudi, Chrystel, Jean-François, and Luca for your help in gaining access to field data and for the many interesting discussions.

Special thanks to Edgar for the support in the last months. My PhD would have lasted longer without your help. Thank you Heinrich for the technical support and the constructive comments related to seismic processing. Many thanks to Monika, Elisabeth, Sabine and Sigrid for taking care of all the administrational aspects, André for helping with all logistical problems and Christoph for dealing with the technical issues.

I am deeply grateful to the whole EEG group for the wonderful time I spent at ETH, the enjoyable lunch breaks, the fun outdoor activities and the nice atmosphere. Special thanks to the people I shared the office with: André, Cédéric, Claudio, Constantin, David, Eric, Kaspar, Lisbeth, Marlies and Peter. I appreciated the entertaining breaks, you often made me laugh and I could always count on you when I needed your support.

Last but not least, I would like to express my gratitude to my family and friends for their love, encouragement and constant support.

Curriculum Vitae

Personal

Full Name	Fabienne Reiser
Date of Birth	March 20, 1985
Place of Birth	Zurich, Switzerland
Citizenship	Swiss

Education

Since 2013	PhD Student at the Department of Earth Sciences, ETH Zurich
2010 – 2012	M.Sc. in Geophysics, ETH Zurich
2005 – 2010	B.Sc. in Earth Sciences, ETH Zurich

Professional Experience

Aptil 2012 – Sept.2012	Internship, Nagra, Wettingen, Switzerland
Sept. 2010 – Dec. 2012	Internship, ETH Zurich, Switzerland
July 2010 –Aug. 2010	Norges geologiske undersøkelse (NGU) Trondheim, Norway
Aug. 2009 –Dec. 2009	Norges geologiske undersøkelse (NGU) Trondheim, Norway

Journal articles

2018

F. Reiser, C. Schmelzbach, D. Sollberber, H. Maurer, S. Greenhalgh, S. Planke, F. Kästner, Ó. Flóvenz, R. Giese, S. Halldórsdóttir, G.P. Hersir (2018): Imaging the high-temperature geothermal field at Krafla using vertical seismic profiling. *Submitted to Journal of Volcanology and Geothermal Research*.

2017

H. Maurer, A. Nuber, N.K. Mariartu, **F. Reiser**, C. Boehm, E. Manukyan, C. Schmelzbach, A. Fichtner (2017): Optimized Experimental Design in the Context of Seismic Full Waveform Inversion and Seismic Waveform Imaging. *Advances in Geophysics*, 58, 25–35, https://doi.org/10.1016/bs.agph.2017.10.001.

C. Schmelzbach, S. Greenhalgh, **F. Reiser**, J.F. Girard, F. Bretaudeau, L. Capar, A. Bitri (2017): Advanced seismic processing/imaging techniques and their potential for geothermal exploration. *Interpretation*, 4, SR1–SR18, https://doi.org/10.1190/INT-2016-0017.1.

F. Reiser, C. Schmelzbach, H. Maurer, S. Greenhalgh, O. Hellwig (2017): Optimizing the design of vertical seismic profiling (VSP) for imaging fracture zones over hardrock basement geothermal environments. *Journal of Applied Geophysics*, 139, 25–35, https://doi.org/10.1016/j.jappgeo.2017.02.023.

2014

F. Reiser, J.E. Podgorski, C. Schmelzbach, H. Horstmeyer, A.G. Green, T. Kalscheuer, H. Maurer, W.K.H. Kinzelbach, G. Tshoso, O. Ntibinyane (2014): Constraining helicopter electromagnetic models of the Okavango Delta with seismic-refraction and seismic-reflection data. *Geophysics*, 79, B123–B134, https://doi.org/10.1190/geo2013-0278.1.

2013

T. Kalscheuer, M. Bastani, S. Donohue, L. Persson, A.A. Pfaffhuber, **F. Reiser**, Z. Ren (2013): Delineation of a quick clay zone at Smørgrav, Norway, with electromagnetic methods under geotechnical constraints. *Journal of Applied Geophysics*, 92, 121–136, https://doi.org/10.1016/j.jappgeo.2013.02.006.

Expanded abstracts

F. Reiser, C. Schmelzbach, H. Maurer, S. Greenhalgh, S. Planke, G.P. Hersir, S. Halldórsdóttir, R. Giese, F. Kästner (2017): Vertical Seismic Profiling (VSP) Survey Optimization for Imaging Fracture Zones over Geothermal Areas. *In 79th EAGE Conference and Exhibition 2017*.

F. Reiser, C. Schmelzbach, H. Maurer, S. Greenhalgh (2016): Vertical Seismic Profiling (VSP) Survey Optimization for Imaging Fracture Zones over Geothermal Areas. *In 78th EAGE Conference and Exhibition 2016*.

C. Schmelzbach, **F. Reiser**, D. Sollberger, L. Rabenstein, H. Horstmeyer, E. Sutter, H. Maurer, J. Robertsson, S. Greenhalgh (2014): Multi-method geophysical imaging of a Quaternary valley in northern Switzerland. *84th Annual International Meeting, Society of Exploration Geophysicists*.

A.G. Green, J.E. Podgorski, **F. Reiser**, P. Meier, C. Schmelzbach, T. Kalscheuer, L. Rabenstein, H. Horstmeyer, H. Maurer, S. Greenhalgh, W.K.H. Kinzelbach, E. Auken, G. Tshoso (2013): Results of recent ground-based geophysical surveys in the Okavango Delta. *SAGA 13th biennial conference*.